Advances in coronary CT angiography and PET perfusion imaging for the detection of coronary artery disease

Bom, Michiel Jeroen

2022

document version
Publisher's PDF, also known as Version of record

Advances in Coronary CT Angiography and PET Perfusion Imaging for the Detection of Coronary Artery Disease

Michiel J. Bom

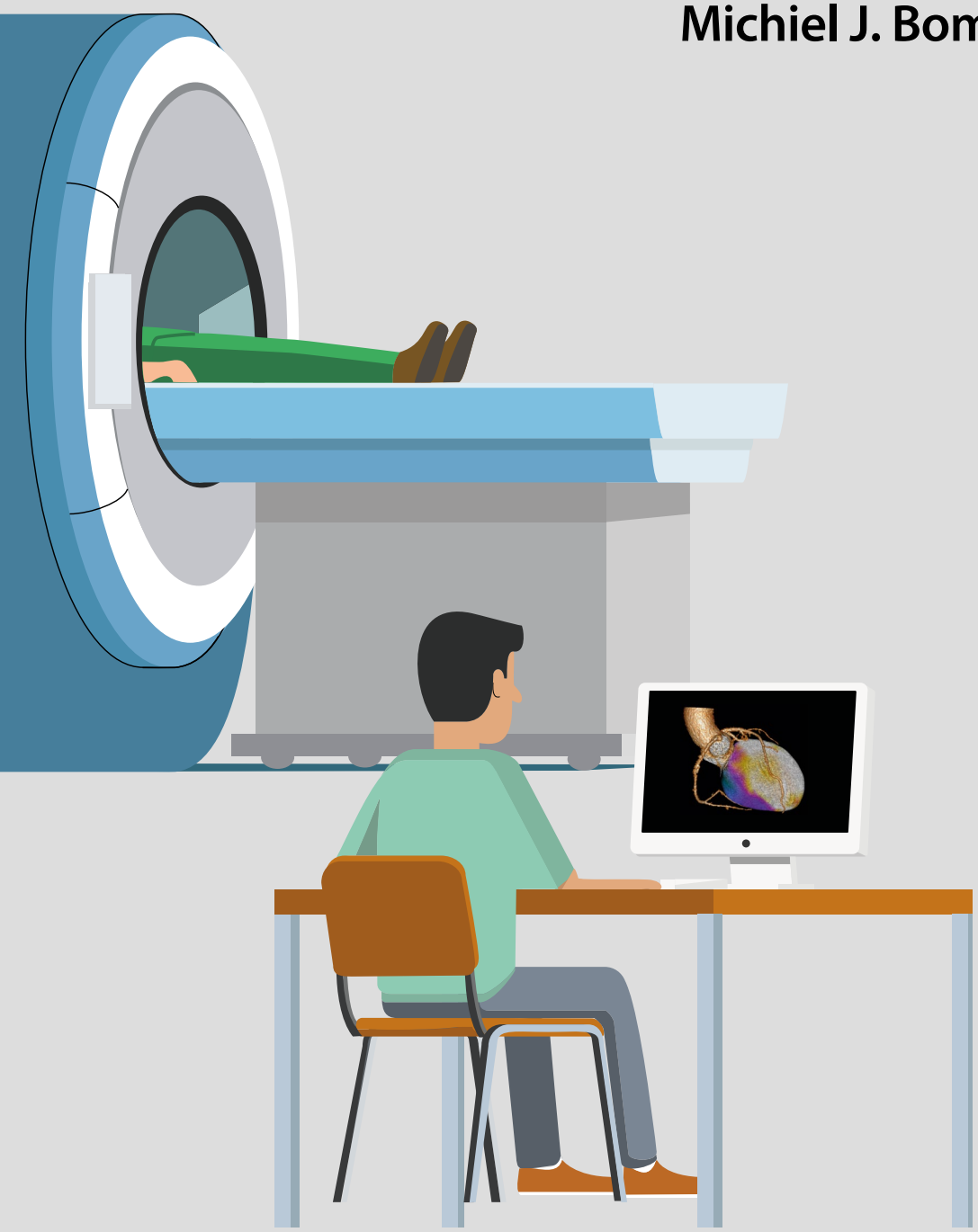

Advances in Coronary CT Angiography and PET Perfusion Imaging for the Detection of Coronary Artery Disease

Michiel J. Bom

Advances in Coronary CT Angiography and PET Perfusion Imaging for the Detection of Coronary Artery Disease

ISBN	978-94-6423-552-4
Cover design	M.J. Bom
Lay-out & design	M.J. Bom
Printing	ProefschriftMaken | proefschriftmaken.nl

Financial support by the Dutch Heart Foundation for the publication of this thesis is gratefully acknowledged.

Additional financial support by Castor, ChipSoft, Guerbet, Olink Proteomics, Heartflow, and VU University Amsterdam is gratefully acknowledged.

VRIJE UNIVERSITEIT

Advances in Coronary CT Angiography and PET Perfusion Imaging for the Detection of Coronary Artery Disease

ACADEMISCH PROEFSCHRIFT

ter verkrijging van de graad Doctor aan
de Vrije Universiteit Amsterdam,
op gezag van de rector magnificus
prof.dr. C.M. van Praag,
in het openbaar te verdedigen
ten overstaan van de promotiecommissie
van de Faculteit der Geneeskunde
op vrijdag 18 februari 2022 om 13.45 uur
in een bijeenkomst van de universiteit,
De Boelelaan 1105

door

Michiel Jeroen Bom

geboren te Almelo

promotoren:	prof.dr. P. Knaapen prof.dr. A.C. van Rossum
copromotor:	dr. I. Danad
promotiecommissie:	prof.dr. S.A.J. Chamuleau prof.dr. J. Knuuti prof.dr. N. van Royen prof.dr. J.W. Jukema prof.dr. C. van Kuijk dr. P.G.H.M. Raijmakers

Table of contents

Chapter 1

General introduction and outline of the thesis

General introduction

Ischemic heart disease caused by coronary artery disease (CAD) remains a leading cause of morbidity and mortality worldwide.(1,2) The assessment and management of patients with suspected CAD is primarily focused on the detection and treatment of hemodynamically obstructive coronary stenoses. This includes an initial diagnostic work-up which typically involves a clinical evaluation estimating the probability of disease followed by a non-invasive imaging test.(3) A myriad of non-invasive imaging modalities are available for this purpose and can be roughly divided into two groups, i.e. anatomical testing with coronary computed tomography angiography (CCTA) or functional testing using exercise testing or myocardial perfusion imaging.

Coronary computed tomography angiography

CCTA is a widely available non-invasive imaging tool that pertains the visualization of coronary stenoses with excellent accuracy for invasive coronary angiography (ICA).(4) However, the visual assessment of stenosis severity using either CCTA or ICA has been shown to hold limited value for the identification of the physiological significance of a coronary stenosis. This is clearly illustrated by the fact that revascularization based on stenosis severity does not improve prognosis.(5) Invasively measured fractional flow reserve (FFR) is currently considered the gold standard for hemodynamic significance of coronary stenoses, given the superiority of FFR-guided revascularization to revascularization based on coronary angiography alone. Despite the excellent sensitivity and negative predictive value of stenosis grading using CCTA, specificity for FFR-defined hemodynamically significant CAD has been shown to be moderate at best.(4) In an attempt to increase diagnostic performance, several novel CCTA indices have been proposed, such as transluminal attenuation gradient (TAG), CT-derived fractional flow reserve (FFR_{CT}), subtended myocardial mass (V_{sub}) and various qualitative and quantitative atherosclerotic plaque measures (Figure 1).(6-15) These novel indices hold great promise and further studies are needed to evaluate their diagnostic and prognostic potential. In addition to the use of CCTA for the diagnostic work-up of patients with suspected CAD, recent advances in FFR_{CT} technology have enabled the simulation of blood flow after virtual removal of a stenosis, hereby predicting the hemodynamic effects of stenting using standard CCTA data.(16,17)

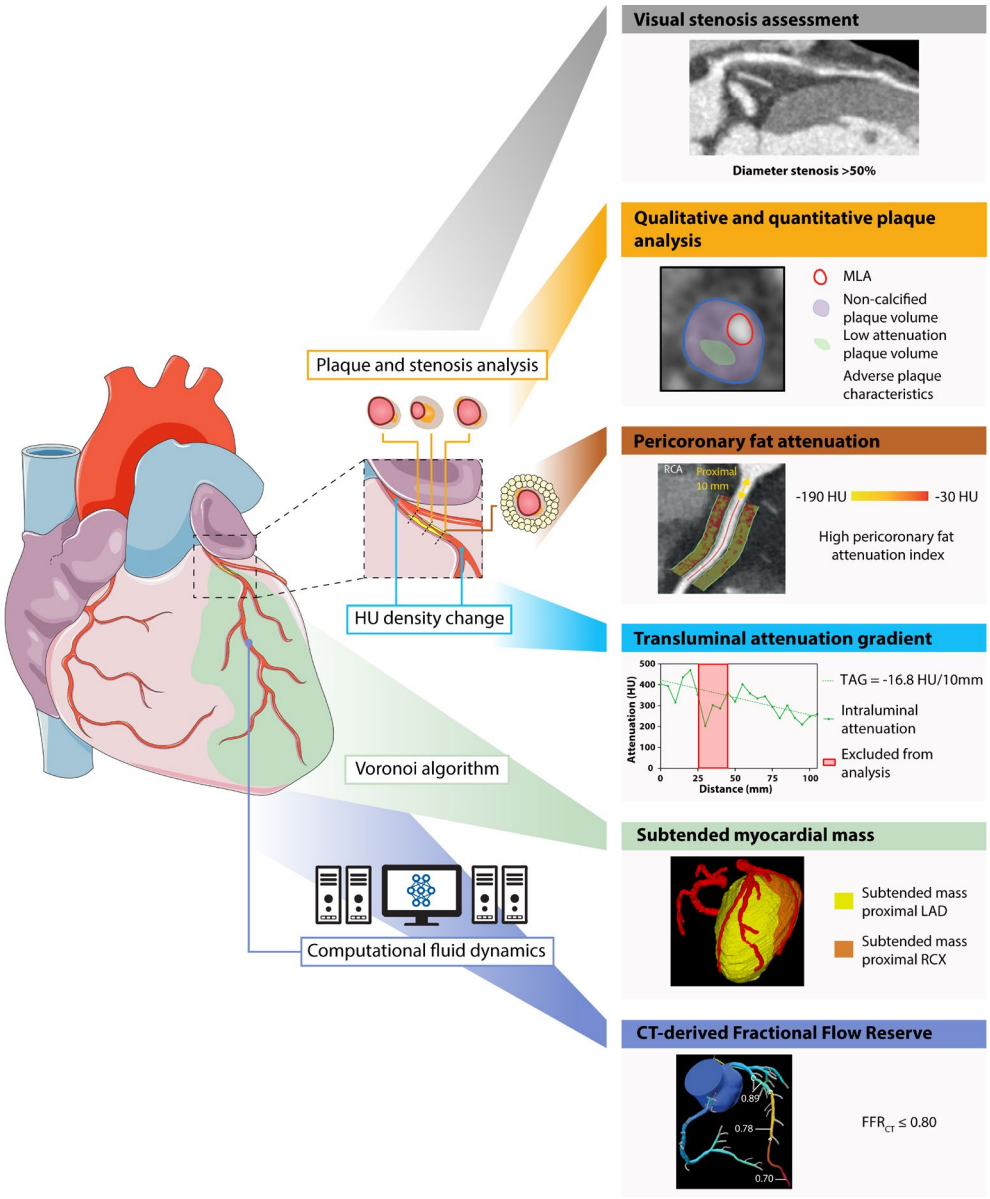

Figure 1. Comprehensive CCTA assessment
Conventional interpretation of CCTA typically involves visual assessment of stenosis grade, in which a diameter stenosis of >50% defines a positive CCTA result. Additionaly, several novel CT indices have been proposed to increase the diagnostic and prognostic performance of CCTA. Among these indices are qualitative and quantitative measures of stenosis (minimal lumen area, MLA) and plaque (plaque volumes and characteristics), transluminal attenuation gradient (TAG) which is a measure of change in CT attenuation density along the course of the vessel, pericoronary fat attenuation index which is a measure of pericoronary fat inflammation and subtended myocardial mass which is calculated using the Voronoi algoritm. Lastly, CT-derived fractional reserve (FFR$_{CT}$) has been proposed to hold great value for the diagnosis of patients with suspected CAD.

The non-invasive prediction of the potential physiological benefit of stenting might be useful for PCI planning and lesion selection.

Positron emission tomography perfusion imaging

Contrary to anatomical testing, functional testing with myocardial perfusion imaging is used to ascertain the physiological consequence of CAD on myocardial perfusion. Among these myocardial perfusion imaging modalities, positron emission tomography (PET) has been shown to hold great promise for the detection of myocardial ischemia.(18) PET perfusion imaging is a radionucleide imaging technique that enables absolute quantification of myocardial blood flow. Several PET tracers have been validated for use in clinical practice, i.e. $[^{15}O]H_2O$, $^{13}NH_3$ and ^{82}Rb. Among these tracers, $[^{15}O]H_2O$ is considered the optimal tracer for quantification of absolute MBF, given the linear relationship between accumulation / clearance of the tracer and myocardial perfusion.(19) The clinical applicability of $[^{15}O]H_2O$ PET perfusion imaging has been confirmed by several studies reporting excellent diagnostic accuracy of $[^{15}O]H_2O$ PET derived MBF for FFR-defined hemodynamically obstructive CAD.(18,20) Over the last decade, several different approaches have been used in PET perfusion imaging analysis (Figure 2). Some have proposed to use global perfusion for the left ventricle as a whole, others have advocated the use of regional perfusion values. Additionally, the longitudinal flow gradient has also been proposed to yield incremental diagnostic value to absolute MBF.(21,22) Further investigation into these different parameters are warranted to ascertain the diagnostic and prognostic potential of $[^{15}O]H_2O$ PET perfusion imaging.

Hybrid imaging

In addition to the use of either CCTA or PET perfusion imaging alone, recent technological advances have enabled the introduction of hybrid imaging. The anatomical information on presence and location of coronary stenosis from CCTA may be synergistic to the functional assessment of myocardial perfusion obtained from PET. Initial studies on the diagnostic performance of hybrid PET/CT however have shown conflicting results.(20,23-25) Future studies are warranted to establish the diagnostic and prognostic value of hybrid imaging.

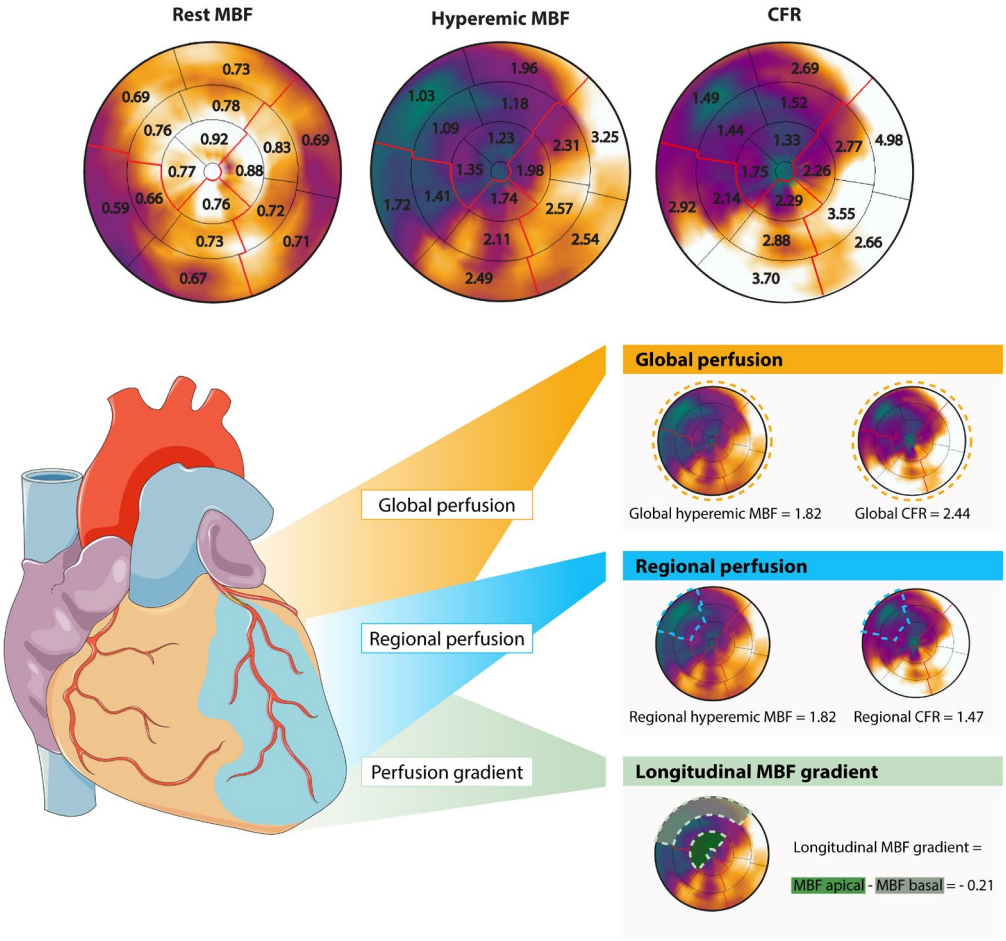

Figure 2. Assessment of quantitative [^{15}O]H_2O perfusion imaging
In [^{15}O]H_2O PET perfusion imaging, absolute myocardial bloodflow (MBF) is quantified during rest and during hyperemic condititions induced by adenosine stress. Absolute MBF values are expressed as mL/min/g and calculated for the 17 segments of the LV defined by the standard AHA model as illustrated in the polarmaps (top panel). In addition to rest and hyperemic MBF, coronary flow reserve (CFR) is calculated as the ratio between hyperaemic and resting MBF. Global perfusion values are subsequently calculated for the left ventricle as a whole and regional perfusion values are defined by the two adjacent segments with the lowest MBF values. Lastly, the longitidunal MBF gradient has been proposed as a promosing PET perfusion index for the diagnosis of hemodynamically obstructive coronary artery disease. The longitudinal MBF gradient is defined as a abnormal decrease in hyperemic MBF from the base to the apex of the left ventricle.

Outline of the thesis

The aim of this thesis was to improve the diagnostic work-up of patients with suspected CAD through the investigation of advances in CCTA (**Part I**), [^{15}O]H_2O PET perfusion imaging (**Part II**) and hybrid imaging (**Part III**).

Part I Coronary Computed Tomography Angiography

Chapter 2 investigates the reclassification of patients using CCTA and the implications of CCTA results on patient management in a cohort of 1560 patients with a low-to-intermediate pre-test probability of obstructive CAD. In **Chapter 3**, the incremental diagnostic value of CCTA-derived transluminal attenuation gradient for the identification of ischemia as defined by both the invasive reference standard FFR and the noninvasive reference standard quantitative PET perfusion is evaluated. Additionally, the influence of coronary luminal dimension on these contrast enhancement-based flow estimations is investigated. **Chapter 4** reports on the discriminative performance of the HEART-score to determine CCTA-derived coronary artery disease and prognosis in patients referred for CCTA after emergency department presentation. **Chapter 5** investigates the diagnostic value of contemporary on-site CCTA assessment using qualitative and quantitative stenosis and plaque measures combined with subtended myocardial mass. Additionally, the incremental diagnostic value of remotely performed CT-derived FFR (FFR_{CT}) analysis to on-site CCTA assessment is evaluated. In **Chapter 6**, the predictive ability of targeted proteomics for coronary plaque morphology is investigated. For this purpose, plasma levels of 358 proteins were used to generate machine learning models for the presence of CCTA-defined high-risk plaques or the complete absence of coronary atherosclerosis. **Chapter 7** addresses the incremental prognostic performance of coronary artery calcium scoring and CCTA in a single-center cohort of 1551 patients with suspected CAD and low to intermediate pre-test probability of obstructive CAD. In **Chapter 8**, the prognostic performance of a novel post-processing tool in CCTA analysis, allowing visualization of pericoronary fat inflammation, is investigated. In a retrospective cohort of patients with suspected CAD, the incremental prognostic performance of pericoronary fat inflammation to comprehensive CCTA plaque assessment is evaluated. **Chapter 9** provides data on the ability of the novel FFR_{CT} planner tool for predicting the hemodynamic benefits of PCI

in a cohort of patients with FFR measurements before and after PCI.

Part II [^{15}O]H_2O Positron Emission Tomography

Chapter 10 describes the use of the PET-derived longitudinal flow gradient in the diagnosis of hemodynamically obstructive CAD. Additionally the influence of lesion location on the relationship between PET the longitudinal flow parameters and FFR is investigated. In **Chapter 11**, the results of a retrospective cohort study investigating the prognostic value of [^{15}O]H_2O PET derived global and regional myocardial perfusion are presented.

Part III Hybrid Imaging

Chapter 12 gives a detailed overview of the detection and treatment of vulnerable coronary plaques, i.e. plaques with a high susceptibility to rupture. Various invasive and non-invasive imaging modalities, including PET and CT, and their ability to identify vulnerable plaques are discussed. Furthermore, the chapter elaborates on the potential of both systemic therapy using lipid-lowering and anti-inflammatory drugs and local therapy using preventive stenting. In **Chapter 13**, the impact of using CCTA derived coronary anatomy to improve diagnostic performance of [^{15}O]H_2O PET is investigated. For this purpose, myocardial blood flow is calculated from PET perfusion using standard segmentation according to the AHA model and using individualized segmentation, in which CCTA is used to assign coronary arteries to PET perfusion territories. **Chapter 14** details a retrospective cohort study on the prognostic value of hybrid PET/CT, combining PET-derived myocardial blood flow with CCTA-derived stenosis severity and high-risk plaque morphology.

References

1. Writing Group M, Mozaffarian D, Benjamin EJ, et al. Executive Summary: Heart Disease and Stroke Statistics--2016 Update: A Report From the American Heart Association. Circulation. 2016;133:447-54.
2. Townsend N, Wilson L, Bhatnagar P, Wickramasinghe K, Rayner M, Nichols M. Cardiovascular disease in Europe: epidemiological update 2016. Eur Heart J. 2016;37:3232-45.
3. Knuuti J, Wijns W, Saraste A, et al. 2019 ESC Guidelines for the diagnosis and manage-

ment of chronic coronary syndromes. Eur Heart J. 2020;41:407-77.
4. Meijboom WB, Meijs MF, Schuijf JD, et al. Diagnostic accuracy of 64-slice computed tomography coronary angiography: a prospective, multicenter, multivendor study. J Am Coll Cardiol. 2008;52:2135-44.
5. van Nunen LX, Zimmermann FM, Tonino PA, et al. Fractional flow reserve versus angiography for guidance of PCI in patients with multivessel coronary artery disease (FAME): 5-year follow-up of a randomised controlled trial. Lancet. 2015;386:1853-60.
6. Nakazato R, Shalev A, Doh JH, et al. Aggregate plaque volume by coronary computed tomography angiography is superior and incremental to luminal narrowing for diagnosis of ischemic lesions of intermediate stenosis severity. J Am Coll Cardiol. 2013;62:460-7.
7. Park HB, Heo R, Hartaigh B, et al. Atherosclerotic plaque characteristics by CT angiography identify coronary lesions that cause ischemia: a direct comparison to fractional flow reserve. JACC Cardiovasc Imaging. 2015;8:1-10.
8. Gaur S, Ovrehus KA, Dey D, et al. Coronary plaque quantification and fractional flow reserve by coronary computed tomography angiography identify ischaemia-causing lesions. Eur Heart J. 2016;37:1220-7.
9. Driessen RS, Stuijfzand WJ, Raijmakers PG, et al. Effect of Plaque Burden and Morphology on Myocardial Blood Flow and Fractional Flow Reserve. J Am Coll Cardiol. 2018;71:499-509.
10. Yang DH, Kang SJ, Koo HJ, et al. Incremental Value of Subtended Myocardial Mass for Identifying FFR-Verified Ischemia Using Quantitative CT Angiography: Comparison With Quantitative Coronary Angiography and CT-FFR. JACC Cardiovasc Imaging. 2019;12:707-17.
11. Driessen RS, Danad I, Stuijfzand WJ, et al. Comparison of Coronary Computed Tomography Angiography, Fractional Flow Reserve, and Perfusion Imaging for Ischemia Diagnosis. J Am Coll Cardiol. 2019;73:161-73.
12. Norgaard BL, Leipsic J, Gaur S, et al. Diagnostic performance of noninvasive fractional flow reserve derived from coronary computed tomography angiography in suspected coronary artery disease: the NXT trial (Analysis of Coronary Blood Flow Using CT Angiography: Next Steps). J Am Coll Cardiol. 2014;63:1145-55.
13. Min JK, Leipsic J, Pencina MJ, et al. Diagnostic accuracy of fractional flow reserve from anatomic CT angiography. JAMA. 2012;308:1237-45.
14. Stuijfzand WJ, Danad I, Raijmakers PG, et al. Additional value of transluminal attenuation gradient in CT angiography to predict hemodynamic significance of coronary artery stenosis. JACC Cardiovasc Imaging. 2014;7:374-86.

15. Choi JH, Koo BK, Yoon YE, et al. Diagnostic performance of intracoronary gradient-based methods by coronary computed tomography angiography for the evaluation of physiologically significant coronary artery stenoses: a validation study with fractional flow reserve. Eur Heart J Cardiovasc Imaging. 2012;13:1001-7.
16. Kim KH, Doh JH, Koo BK, et al. A novel noninvasive technology for treatment planning using virtual coronary stenting and computed tomography-derived computed fractional flow reserve. JACC Cardiovasc Interv. 2014;7:72-8.
17. Ihdayhid AR, White A, Ko B. Assessment of Serial Coronary Stenoses With Noninvasive Computed Tomography-Derived Fractional Flow Reserve and Treatment Planning Using a Novel Virtual Stenting Application. JACC Cardiovasc Interv. 2017;10:e223-e5.
18. Danad I, Uusitalo V, Kero T, et al. Quantitative assessment of myocardial perfusion in the detection of significant coronary artery disease: cutoff values and diagnostic accuracy of quantitative [(15)O]H2O PET imaging. J Am Coll Cardiol. 2014;64:1464-75.
19. Driessen RS, Raijmakers PG, Stuijfzand WJ, Knaapen P. Myocardial perfusion imaging with PET. Int J Cardiovasc Imaging. 2017;33:1021-31.
20. Danad I, Raijmakers PG, Driessen RS, et al. Comparison of Coronary CT Angiography, SPECT, PET, and Hybrid Imaging for Diagnosis of Ischemic Heart Disease Determined by Fractional Flow Reserve. JAMA Cardiol. 2017;2:1100-7.
21. Valenta I, Antoniou A, Marashdeh W, et al. PET-measured longitudinal flow gradient correlates with invasive fractional flow reserve in CAD patients. Eur Heart J Cardiovasc Imaging. 2017;18:538-48.
22. Valenta I, Quercioli A, Schindler TH. Diagnostic value of PET-measured longitudinal flow gradient for the identification of coronary artery disease. JACC Cardiovasc Imaging. 2014;7:387-96.
23. Kajander S, Joutsiniemi E, Saraste M, et al. Cardiac positron emission tomography/computed tomography imaging accurately detects anatomically and functionally significant coronary artery disease. Circulation. 2010;122:603-13.
24. Thomassen A, Petersen H, Johansen A, et al. Quantitative myocardial perfusion by O-15-water PET: individualized vs. standardized vascular territories. Eur Heart J Cardiovasc Imaging. 2015;16:970-6.
25. Liga R, Vontobel J, Rovai D, et al. Multicentre multi-device hybrid imaging study of coronary artery disease: results from the EValuation of INtegrated Cardiac Imaging for the Detection and Characterization of Ischaemic Heart Disease (EVINCI) hybrid imaging population. Eur Heart J Cardiovasc Imaging. 2016;17:951-60.

PART I

Coronary Computed Tomography Angiography

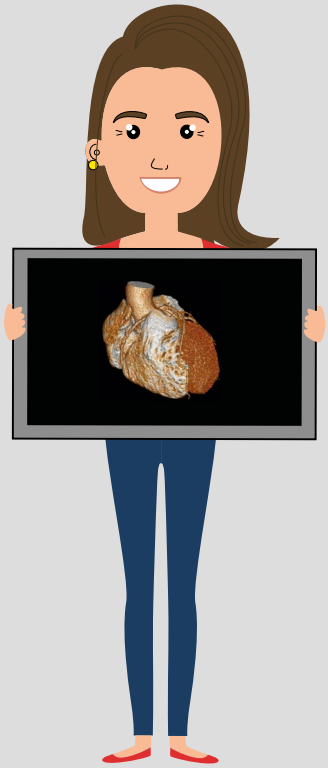

Chapter 2

Diagnostic and Therapeutic Usefulness of Coronary Computed Tomography Angiography in Out-Clinic Patients Referred for Chest Pain

Michiel J. Bom, Petrus M. van der Zee, Jan H. Cornel,
Friso M. van der Zant, and Remco J.J. Knol

Am J Cardiol. 2015;116(1):30-6

Abstract

Coronary computed tomography angiography (CCTA) is widely used to exclude coronary artery disease (CAD) in patients with low to intermediate pre-test probability (PTP) of obstructive CAD. The aim of our study was to investigate the reclassification by CCTA and the implications of CCTA results on management because limited studies exist on these subjects; 1560 patients with chest pain without a history of CAD and with low or intermediate PTP of CAD referred for CCTA from the out-patient clinic were prospectively included. PTP was defined by the Duke Clinical Score as either low (<15%), low-intermediate (15 to 50%) or high-intermediate (50 to 85%). Distribution of CCTA results among the categories of PTP of CAD and the influence of CCTA results on management were analysed. CCTA revealed obstructive CAD in 7%, 15%, and 23% of cases, in patients with low, low-intermediate, and high-intermediate PTP of CAD, respectively; 855 of 1031 (83%) patients with intermediate PTP of CAD showed no obstructive CAD on CCTA and were consequently reclassified. Management changes after CCTA occurred in 689 (44%) patients. In 633 (41%) patients, medication was altered and 135 (9%) were referred for invasive coronary angiography. Treatment with statin was initiated in 442 (28%) and stopped in 71 (5%) patients. Aspirin was initiated in 192 (12%) and stopped in 139 (9%) patients. In conclusion, in a routine clinical cohort, CCTA resulted in reclassification in most patients. Furthermore, our study suggests that the Duke Clinical Score overestimates the probability of obstructive CAD compared with CCTA findings. Finally, CCTA results have implications on patient management, with medication changes in 41% of patients.

Introduction

Ischemic heart disease due to coronary artery disease (CAD) remains the most important cause of death worldwide.(1) The guidelines on stable CAD recommend a stepwise approach in symptomatic patients with considered stable coronary artery disease.(2,3) The process starts with the clinical assessment of the probability of obstructive coronary artery disease, the pre-test probability (PTP). Risk scores such as the Duke Clinical Score are used to estimate the PTP.(4,5) Non-invasive testing, such as coronary computed tomographic angiography (CCTA), is advised in patients with suspected CAD.(2,6) CCTA has great diagnostic performance, with a high negative predictive value.(7,8) However it is less accurate in patients with a high PTP of CAD, because of overestimation of disease in these patients.(9,10) Thus the appropriate use criteria advise to use CCTA only in patients with low or intermediate PTP.(11) In these patients CCTA is widely used to reclassify patients by excluding or diagnosing obstructive coronary artery disease. The implications of CCTA results on patient management, however, are not clear.(12-16) Therefore, the aim of this study was to describe to what extent CCTA leads to reclassification and which impact CCTA results have on patient management in out-clinic patients with chronic chest pain and low to intermediate PTP of obstructive CAD.

Methods

From December 13, 2011 and August 26, 2014 all patient with chronic chest pain with low or intermediate PTP of CAD referred for CCTA from the outpatient clinic were prospectively included after a diagnostic work up. None of the patients had a prior history of CAD. Baseline characteristics included were prospectively entered in a database: age, gender, and cardiovascular risk factors. The PTP was calculated using the Duke Clinical Score.(17) According to the ESC guidelines for stable CAD, patients with an intermediate PTP (15-85%) were divided into two groups: low-intermediate (15-50%) and high-intermediate (50-85%).(2) Baseline and post-CCTA medication use were documented in the database. Referral for perfusion scan, ICA and revascularization were ascertained from procedural reports. All patients gave written informed consent for usage of their data.

Patient preparation, image acquisition, and image analysis were performed as stated below and as previously described by Krul et al.(18)

Metformin was stopped in patients with an estimated glomerular filtration rate of <60 mL/min. If resting heart rate was above 60 bpm 100mg atenolol was administered orally 1 hour prior to CCTA. When the heart rate remained above 60 bpm additional metoprolol intravenously could be administered in steps of 5mg to a maximum of 30mg. Patients were given two doses nitroglycerin sublingually of 0.4mg prior to CCTA.

All scans were performed with a 2x64 slice flying focal spot, effectively 2x128–slice (Somatom Definition Flash; Siemens Medical Systems, Erlangen, Germany). A 10–15 mL test bolus containing non-ionic low-osmolar iodinated radiocontrast (ultravist 370) was injected, followed by a flush of 40 mL saline, both at a flow rate of 5-6 mL/s. The time point of maximal contrast enhancement in the ascending aorta at the level of the pulmonary trunk was recorded, and an additional delay of 5 s was added to define the optimal time point for acquisition of coronary artery data. A dual-head injector then injected 48–75 mL contrast depending on kV used for the high-pitch flash scan and 75 mL in case of prospective or retrospectively triggered scan, followed by 45 mL 30/70% contrast/saline solution at a flow rate of 6 mL/s. The tube voltage (80, 100, or 120 kV) and tube current were determined automatically by the scanning system based on body geometry.(19) The delivered radiation dose was also generated automatically by the scanner software and represented as dose length product (DLP). The effective dose of the scan was calculated by multiplying the DLP with the k-factor of 0.014 mSv x (mGy x cm)$^{-1}$, which is generally used for effective dose estimation in cardiac CT studies. The total dose of topogram, testbolus, CaSc and CCTA was used to estimate the effective radiation dose for each patient. All scans were read in consensus by a CBCCT accredited nuclear medicine physician and a cardiologist experienced in the interpretation of CCTA. In case of disagreement a third opinion was decisive. For CAC-score, coronary calcifications were defined as dense lesions in coronary arteries with densities >130 Hounsfield units. Calcifications were manually assigned to coronary arteries and added to the Agatston score for each patient.(20)

Structures >1 mm^2 within and/or adjacent to the coronary artery lumen, which could

be clearly distinguished from the vessel lumen, were scored as a coronary plaque. (21) Coronary plaques were scored per coronary segment. Each coronary plaque was quantified for stenosis by visual estimation.

Obstructive CAD was defined as a lumen stenosis in any of the major coronary vessels of >50%, either left main artery (LM), left anterior descending artery (LAD), circumflex artery or right coronary artery. Normal coronary arteries were defined as CAC-score=0 and no coronary plaque. Non-obstructive CAD was defined as CAC-score>0 and/or any plaque that did not meet the criteria for obstructive CAD. In obstructive coronary artery disease the extent of CAD was recorded, either 1-vessel, 2-vessel or 3-vessel CAD. High-risk anatomic features were defined as LM stenosis >50%, >50% stenosis in the proximal LAD or 3-vessel CAD with >50% stenosis.

Statistical analysis was performed using SPSS software (version 22.0.0, IBM). Continuous variables are presented as mean ± SD and categorical variables as frequencies with percentages. Variables were compared with a chi-square test for categorical variables and by applying an analysis of variance (ANOVA) or an unpaired student t-test for continuous variables as appropriate. Continuous variables were tested for normal distribution.

The presence of coronary artery disease at CCTA was evaluated in the different categories of the Duke Clinical Score, respectively low, low-intermediate, and high-intermediate, using descriptive statistics. Descriptive statistics were also used to evaluate the management changes in patients with normal coronary arteries, patients with non-obstructive CAD and patients with obstructive CAD. Changes in patient management consisted of two different types of changes: changes in cardiac medication and/or referral for invasive coronary angiography (ICA). Cardiac medication changes between the baseline situation and after CCTA were defined as discontinuation or addition of aspirin or statin. The referral for perfusion scans, either $^{13}NH_3$ positron emission tomography or single photon emission computed tomography, was evaluated in patients with obstructive CAD and patients with obstructive CAD and high risk anatomic features. Referral for ICA was defined as the occurrence of ICA in the first 60 days after CCTA. As in previous studies this 60-day landmark was used to differentiate between CCTA-driven ICA and long term revascularization which is considered to

be indicative for the prognosis.(22) Acute revascularizations in myocardial infarction patients were also considered non CCTA-driven. The 60-day landmark was also used for perfusion scans.

Results

The baseline characteristics of the total study population (n=1560) and the baseline characteristics in the different categories of the PTP are summarized in table 1. Cardiac risk factors and baseline medication use were more frequent in higher PTP categories.

The CCTA results are shown in table 2. In 48 patients CCTA showed obstructive CAD with high-risk anatomic features. Two patients with left main CAD on CCTA also had three-vessel disease. The effective radiation delivered to the entire group was 2.4±2.0 mSv (DLP 174±142; mean±SD). The high-pitch flash scans (n=1130) resulted in an effective dose of 1.6±0.7 mSv (DLP 114±47), the prospectively triggered scans (n=395) in 4.5±2.45 mSv (DLP 322±176) and the retrospectively triggered scans (n=35) in 6.5±2.8 mSv (DLP 463±196).

CCTA led to reclassification in 894 patients (57%), of which 39/529 (7%) of the low PTP category were reclassified as having obstructive CAD, whereas 855/1031 (83%) of the low-intermediate and high-intermediate PTP category without obstructive CAD were reclassified as having no obstructive CAD. The reclassification is illustrated in figure 1.

The alteration in patient management after CCTA is shown in table 3 and figure 2. Presence of obstructive CAD, as well as non-obstructive CAD, was associated with medication changes and referral for ICA ($p<0.001$). Patient management was changed in 689 (44%) patients after CCTA. Alteration of baseline medication after CCTA occurred in 633 (41%) patients. Treatment with statin was initiated in 442 (28%) patients and stopped in 71 (5%) patients. In 192 (12%) patients treatment with aspirin was initiated and in 139 (9%) aspirin was stopped after CCTA. Of all patients with normal coronary arteries, aspirin was discontinued in 105 patients after CCTA (16%).

A total number of 135 (9%) patients were referred for ICA. Nineteen (3%) patients with non-obstructive CAD at CCTA, 116 (54%) patients with obstructive CAD at

Table 1. Baseline characteristics

Demographics	Total (n=1560)	Pre-test probability			p-value#
		Low (n=529)	Low-intermediate (n=764)	High-intermediate (n=267)	
Age (years)	57.9 ± 10.2	54.9 ± 10.1	58.6 ± 10.2	62.1 ± 8.8	<0.001
Women	971 (62.2%)	462 (87.3%)	424 (55.5%)	85 (31.8%)	<0.001
BMI (kg/m2)	26.6 ± 4.5	26.5 ± 5.1	26.7 ± 4.3	26.8 ± 3.8	0.58
Cardiac risk factors					
Diabetes Mellitus	122 (7.8%)	24 (4.5%)	64 (8.4%)	34 (12.8%)	0.001
Hba1c (n=53) *	6.8 ± 1.6				
Hypertension	464 (29.7%)	134 (25.3%)	244 (31.9%)	86 (32.2%)	0.024
Hyperlipidemia	396 (25.4%)	114 (21.6%)	208 (27.2%)	74 (27.7%)	0.044
Family history of CAD∞	738 (47.4%)	258 (48.9%)	362 (47.4%)	118 (44.2%)	0.46
Smoker	279 (17.9%)	77 (14.6%)	152 (19.9%)	50 (18.7%)	0.045
eGFR<60	44 (2.8%)	15 (2.8%)	24 (3.1%)	5 (1.9%)	0.56
Baseline medication					
Aspirin	501 (32.1%)	131 (24.8%)	243 (31.8%)	127 (47.6%)	<0.001
Statin	534 (34.2%)	122 (23.1%)	277 (36.3%)	135 (50.6%)	<0.001
Beta-blocker	606 (38.8%)	166 (35.2%)	286 (37.4%)	134 (50.2%)	<0.001
ACE-i / ARB	392 (25.1%)	108 (20.4%)	203 (26.6%)	81 (30.3%)	0.004
Calciumchannel blocker	96 (6.2%)	32 (6.0%)	50 (6.5%)	14 (5.2%)	0.74
Nitrate	49 (3.1%)	6 (1.1%)	24 (3.1%)	19 (7.1%)	<0.001
Acenocoumarol	38 (2.4%)	9 (1.7%)	17 (2.2%)	12 (4.5%)	0.047

eGFR = estimated glomerular filtration rate; ACE-i / ARB = ACE-inhibitor / Angiotensin receptor blocker. * Hba1C was documented in 53 patients; ∞ in 2 patients family history of CAD was missing;.# =p-value for distribution of baseline characteristics among the different categories of the pre-test probability.

CCTA and 28 (58%) patients with obstructive CAD and high risk anatomic were referred for ICA. Ninety-four (71%) patients who received ICA were subsequently revascularized by either PCI or CABG. Six (2.8%) patients with obstructive CAD and 2 (4.2%) patients with obstructive CAD with high-risk anatomic features at CCTA were referred for a perfusion scan within 60 days. Both perfusion scans in the patients with high-risk anatomic features showed no signs of ischemia. One patient without CAD at CCTA was referred for a perfusion scan because of low CCTA image quality.

Table 2. CCTA data

Variable	Total (n=1560)	Pre-test probability		
		Low PTP (n=529)	Low-intermediate PTP (n=764)	High-intermediate PTP (n=267)
Calcium (Agatston score)				
0	744 (47.7%)	336 (63.5%)	334 (43.7%)	74 (27.7%)
0.1-100	501 (32.1%)	127 (24.0%)	268 (35.1%)	106 (39.7%)
100-400	216 (13.8%)	54 (10.2%)	113 (14.8%)	49 (18.4%)
>400	99 (6.3%)	12 (2.3%)	49 (6.4%)	38 (14.2%)
CCTA results				
Normal coronary arteries	659 (42.2%)	308 (58.2%)	294 (38.5%)	57 (21.3%)
Non-obstructive CAD	686 (44.0%)	182 (34.4%)	354 (46.3%)	150 (56.2%)
Number of coronary arteries narrowed (>50%)	215 (13.8%)	39 (7.4%)	116 (15.2%)	60 (22.5%)
1	165 (10.6%)	31 (5.9%)	94 (12.3%)	39 (14.6%)
2	34 (2.2%)	6 (1.1%)	13 (1.7%)	15 (5,6%)
3	13 (0.8%)	1 (0.2%)	7 (0.9%)	5 (1.9%)
Left main	4 (0.3%)	1 (0.2%)	2 (0.3%)	1 (0.4%)
High risk narrowings*	48 (3.1%)	5 (0.9%)	30 (3.9%)	13 (4.9%)

CCTA = coronary computed tomography angiography; CAD = coronary artery disease; PTP = pre-test probability. * high risk narrowings were defined as left main, 3-vessel and/or proximal LAD disease

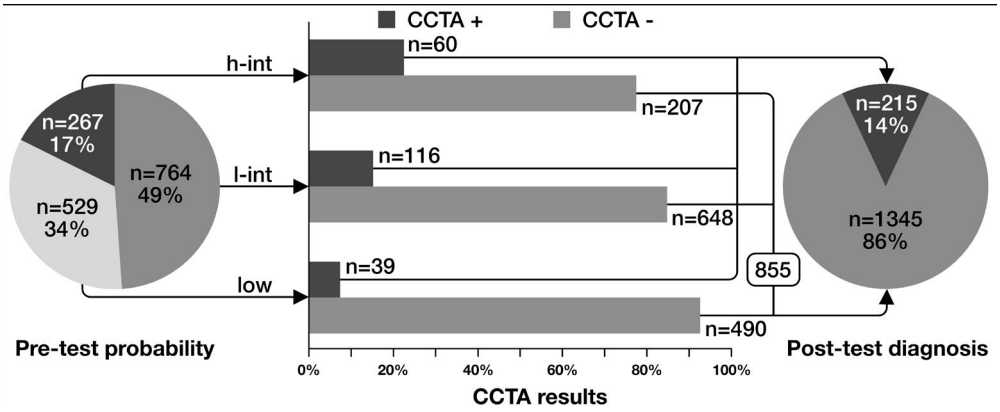

Figure 1. Reclassification from PTP of obstructive CAD to post-test diagnosis.
CCTA + = obstructive coronary artery disease at CCTA; CCTA - = no obstructive coronary artery disease at CCTA; l-int = low-intermediate; h-int = high-intermediate.

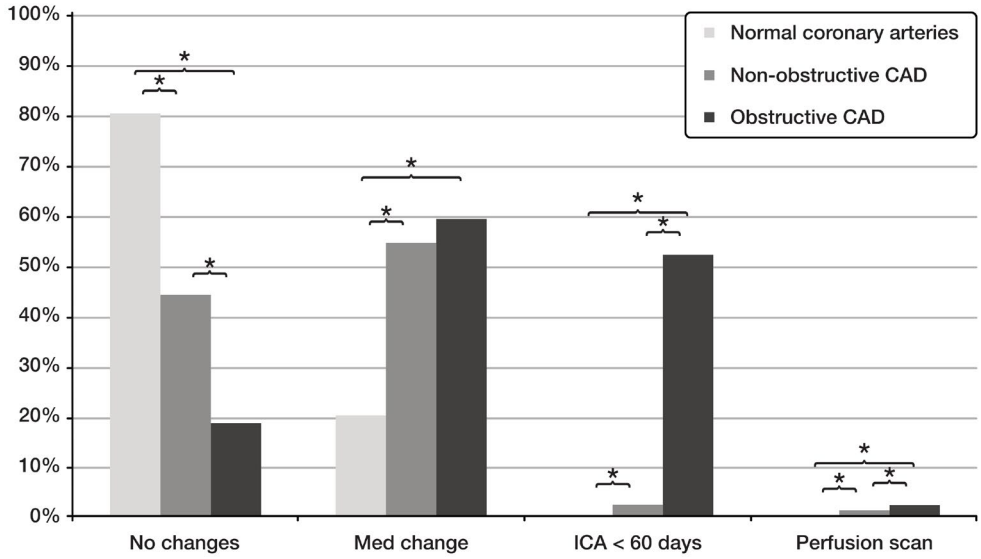

Figure 2. CCTA results and changes in patient management.
Med change = changes in medication. * significant difference between groups with p value <0.01.

Table 3. Pre- and post-test medication

	Aspirin			Statin		
CCTA results	**Pre-test**	**Post-test**	**Change**	**Pre-test**	**Post-test**	**Change**
Normal coronary arteries	174 (26.4%)	72 (10.9%)	111 (16.8%)	178 (27.0%)	121 (18.4%)	76 (11.5%)
Non-obstructive CAD	238 (34.7%)	306 (44.5%)	136 (19.8%)	251 (36.6%)	565 (82.4%)	334 (48.7%)
Obstructive CAD	89 (41.4%)	166 (77.2%)	84 (39.1%)	105 (48.8%)	203 (94.4%)	103 (47.9%)
Overall	501 (32.1%)	544 (34.8%)	331 (21.2%)	534 (34.2%)	889 (57.0%)	513 (32.9%)

CCTA = coronary computed tomography angiography; CAD = coronary artery disease

Discussion

This is the first study to report on the reclassification and management changes after CCTA in out-clinic symptomatic patients with chronic chest pain and a low to intermediate pre-test likelihood of obstructive coronary artery disease, in whom the added value of CCTA is expected to be highest and in whom CCTA is considered appropriate.(11) In this routine clinical cohort CCTA led to reclassification in the majority of patients. 83% of patients with intermediate PTP of CAD had no obstructive CAD on CCTA and were consequently reclassified. Furthermore, CCTA results had implications on patient management in a large amount of patients. Patient management was changed in 44% of patients after CCTA. Baseline medication was altered in 41% of patients and ICA was performed in 9% of patients. Changes in patient management, both medication changes and referral for ICA, correlated with the presence of CAD at CCTA.

In a recent study by Hadamitzky et al. reclassification of patients with intermediate PTP was slightly less frequent than in our study; 71% of patients with an intermediate PTP were reclassified by CCTA as low risk.(23) This can be partly explained by the fact that 28% of patients in the study by Hadamitzky et al. were asymptomatic, whereas our patients were symptomatic. Meijboom et al. reported a lower reclassification rate: 52% of intermediate PTP patients were reclassified as having no obstructive CAD at CCTA.(10) The broader definition of intermediate PTP in our study might account for this

discrepancy, since Meijboom et al. considered intermediate 30-70%.

Several risk scores have been developed to estimate the PTP of obstructive CAD, such as the Duke Clinical Score, the Diamond and Forrester Method and the Morise Score.(4,24,25) Jensen et al showed the Diamond and Forrester Method and the Duke Clinical Score to be superior to the Morise Score in predicting the PTP.(5) A recent study reported that the Duke Clinical Score is a better predictor of obstructive CAD on CCTA than the Diamond and Forrester Method.(26) Despite its superiority to other risk scores, our study suggests that the Duke Clinical Score overestimates the probability of obstructive CAD compared to the findings on CCTA. In patients with low-intermediate (15-50%) and high-intermediate (50-85%) PTP the amount of patients with obstructive CAD on CCTA was lower than expected. The overestimation of obstructive CAD by the Duke Clinical Score as compared to CCTA findings has also been recently described by Genders et al.(27)

Cheezum et al. retrospectively studied pre- and post-CCTA prescription patterns of aspirin and statin in 1125 patients without prior history of CAD.(12) Change in aspirin treatment was similar to that in our study. However change in statin treatment was more frequent, with change in approximately 60% of patients. This may be due to the different definition of change in therapy. Cheezum et al. considered alteration of dosage also a change in therapy, greatly influencing the number of changes in therapy. Recently, Uretsky et al reported lower post-test medication changes (aspirin and statin); approximately in 25% of patients.(15) Pre-test medication use in their cohort however was more frequent, which can partly explain the fewer changes in therapy. Low-dose aspirin in patients with stable coronary artery disease is a Class IA recommendation in the guidelines.(2,3) As in our study, all previous studies however showed suboptimal post-CCTA aspirin use, ranging 71-95%.(12,16,28) Although overestimation of CAD is a known limitation of CCTA,(9,10) awareness among physician should be raised to improve prescription rate of aspirin in patients with obstructive CAD.

The guidelines advise referral for ICA in patients with high risk anatomic features at CCTA.(2,3) In accordance to our study, Hachamovtich et al. showed a suboptimal referral rate for ICA in these patients of approximately 60%.(28) Since overestimation of CAD is an important limitation of CCTA,(9,10) clinicians may be withheld from

referral for ICA. However, only 4% of patients with diagnostic uncertainty (i.e. obstructive lesions of high risk on CCTA without further ICA) received ischemia detection for alternative risk stratification. A multinational observational study by Min et al. showed worse prognosis in patients with CAD with high-risk anatomic features at CCTA treated with medical treatment only rather than referral for ICA and consecutive revascularization.(29) Referral for ICA seems preferable over medical treatment only in patients with high-risk anatomic features.

Our study shows that CCTA is a non-invasive imaging tool with an important impact on the daily clinical practice of patients with chronic chest pain and low to intermediate PTP, with reclassification in the majority of patients and alteration in management in nearly half of patients. Currently, relatively low radiation doses, with a mean 2.4 mSv in our cohort, further support the appropiateness of the CCTA strategy in low to intermediate risk chronic chest pain patiens.

Several limitations must be taken into account. This study describes implications of CCTA results on management, however no information about follow-up was obtained. Limited studies report on the prognostic impact of management changes after CCTA. The study by Cheezum et al.(12) was underpowered for all endpoints, in the study by Uretsky et al.(15) no adverse events occurred and the study by Hulten and co-workers (13) was underpowered for most endpoints but showed a reduction of adverse events by statin therapy in patients with extensive non-obstructive CAD. Further research is warranted to evaluate the prognostic impact of therapy changes after CCTA. Finally, the single center design of our study allows for a real-world evaluation, however it may limit the extrapolation to other clinics.

References

1. World Health Organization. The top 10 causes of death. 2014, May; Available at: http://www.who.int/mediacentre/factsheets/fs310/en.
2. Montalescot G, Sechtem U, Achenbach S, et al. 2013 ESC guidelines on the management of stable coronary artery disease: the Task Force on the management of stable coronary artery disease of the European Society of Cardiology. Eur Heart J 2013;34:2949-3003.
3. Fihn SD, Gardin JM, Abrams J, et al. 2012 ACCF/AHA/ACP/AATS/PCNA/SCAI/STS Guideline for the diagnosis and management of patients with stable ischemic heart

disease: a report of the American College of Cardiology Foundation/American Heart Association Task Force on Practice Guidelines, and the American College of Physicians, American Association for Thoracic Surgery, Preventive Cardiovascular Nurses Association, Society for Cardiovascular Angiography and Interventions, and Society of Thoracic Surgeons. J Am Coll Cardiol 2012;60:e44-e164.

4. Pryor DB, Harrell FE, Lee KL, et al. Am J Med 1983;75:771-780.
5. Jensen JM, Voss M, Hansen VB, et al. Risk stratification of patients suspected of coronary artery disease: comparison of five different models. Atherosclerosis 2012;220:557-562.
6. Taylor AJ, Cerqueira M, Hodgson JM, et al. ACCF/SCCT/ACR/AHA/ASE/ASNC/NASCI/SCAI/SCMR 2010 appropriate use criteria for cardiac computed tomography. A report of the American College of Cardiology Foundation Appropriate Use Criteria Task Force, the Society of Cardiovascular Computed Tomography, the American College of Radiology, the American Heart Association, the American Society of Echocardiography, the American Society of Nuclear Cardiology, the North American Society for Cardiovascular Imaging, the Society for Cardiovascular Angiography and Interventions, and the Society for Cardiovascular Magnetic Resonance. J Am Coll Cardiol 2010;56:1864-1894.
7. Paech DC, Weston AR. A systematic review of the clinical effectiveness of 64-slice or higher computed tomography angiography as an alternative to invasive coronary angiography in the investigation of suspected coronary artery disease. BMC Cardiovasc Disord 2011;11:32-2261-11-32.
8. Chow BJ, Abraham A, Wells GA, et al. Diagnostic accuracy and impact of computed tomographic coronary angiography on utilization of invasive coronary angiography. Circ Cardiovasc Imaging 2009;2:16-23.
9. Budoff MJ, Dowe D, Jollis JG, et al. Diagnostic performance of 64-multidetector row coronary computed tomographic angiography for evaluation of coronary artery stenosis in individuals without known coronary artery disease: results from the prospective multicenter ACCURACY (Assessment by Coronary Computed Tomographic Angiography of Individuals Undergoing Invasive Coronary Angiography) trial. J Am Coll Cardiol 2008;52:1724-1732.
10. Meijboom WB, van Mieghem CA, Mollet NR, et al. 64-Slice Computed Tomography Coronary Angiography in Patients with High, Intermediate, Or Low Pretest Probability of Significant Coronary Artery Disease. J Am Coll Cardiol 2007;50:1469-1475.
11. Taylor AJ, Cerqueira M, Hodgson JM, et al. ACCF/SCCT/ACR/AHA/ASE/ASNC/NASCI/SCAI/SCMR 2010 appropriate use criteria for cardiac computed tomography. A report of the American College of Cardiology Foundation Appropriate Use Criteria

Task Force, the Society of Cardiovascular Computed Tomography, the American College of Radiology, the American Heart Association, the American Society of Echocardiography, the American Society of Nuclear Cardiology, the North American Society for Cardiovascular Imaging, the Society for Cardiovascular Angiography and Interventions, and the Society for Cardiovascular Magnetic Resonance. J Am Coll Cardiol 2010;56:1864-1894.

12. Cheezum MK, Hulten EA, Smith RM, et al. Changes in preventive medical therapies and CV risk factors after CT angiography. JACC Cardiovasc Imaging 2013;6:574-581.
13. Hulten E, Bittencourt MS, Singh A, et al. Coronary artery disease detected by coronary computed tomographic angiography is associated with intensification of preventive medical therapy and lower low-density lipoprotein cholesterol. Circ Cardiovasc Imaging 2014;7:629-38.
14. LaBounty TM, Devereux RB, Lin FY, Weinsaft JW, Min JK. Impact of coronary computed tomographic angiography findings on the medical treatment and control of coronary artery disease and its risk factors. Am J Cardiol 2009;104:873-877.
15. Uretsky S, Rozanski A, Supariwala A, et al. Clinical outcomes following a strategy of optimized medical management and selective "downstream" procedures following coronary computed tomography angiography. Int J Cardiol 2013;165:468-473.
16. Ovrehus KA, Botker HE, Jensen JM, Munkholm H, Johnsen SP, Norgaard BL. Influence of coronary computed tomographic angiography on patient treatment and prognosis in patients with suspected stable angina pectoris. Am J Cardiol 2011;107:1473-1479.
17. Bayliss J. Duke Clinical Score: Prediction of Coronary Heart Disease in a Patient with Chest Pain. April 2, 2009; Available at: http://www.zunis.org/DukeChestPain-CADPredictor.htm.
18. Krul MM, Bogaard K, Knol RJ, et al. Coronary artery disease in patients with atypical chest pain with and without diabetes mellitus assessed with coronary CT angiography. BMJ Open Diabetes Res Care 2014;2:e000004.
19. Lee KH, Lee JM, Moon SK, et al. Attenuation-based automatic tube voltage selection and tube current modulation for dose reduction at contrast-enhanced liver CT. Radiology 2012;265:437-47.
20. Agatston AS, Janowitz WR, Hildner FJ, Zusmer NR, Viamonte MJ, Detrano R. Quantification of coronary artery calcium using ultrafast computed tomography. J Am Coll Cardiol 1990;15:827-32.
21. Leber AW, Knez A, Becker A, et al. Accuracy of multidetector spiral computed tomography in identifying and differentiating the composition of coronary atherosclerotic plaques: a comparative study with intracoronary ultrasound. J Am Coll Cardiol 2004;43:1241-7.

22. Hou ZH, Lu B, Gao Y, et al. Prognostic value of coronary CT angiography and calcium score for major adverse cardiac events in outpatients. JACC Cardiovasc Imaging 2012;5:990-999.
23. Hadamitzky M, Distler R, Meyer T, et al. Prognostic value of coronary computed tomographic angiography in comparison with calcium scoring and clinical risk scores. Circ Cardiovasc Imaging 2011;4:16-23.
24. Diamond GA, Forester JS. Analysis of probability as an aid in the clinical diagnosis of coronary-artery disease. N Engl J Med 1979;300:1350 –1358.
25. Morise AP, Haddad WJ, Beckner D. Development and validation of a clinical score to estimate the probability of coronary artery disease in men and women presenting with suspected coronary disease. Am J Med 1997;102:350-356.
26. Wasfy MM, Brady TJ, Abbara S, et al. Comparison of the Diamond-Forrester method and Duke Clinical Score to predict obstructive coronary artery disease by computed tomographic angiography. Am J Cardiol 2012;109:998-1004.
27. Genders TS, Steyerberg EW, Hunink MG, et al. Prediction model to estimate presence of coronary artery disease: retrospective pooled analysis of existing cohorts. BMJ 2012;344:e3485.
28. Hachamovitch R, Nutter B, Shaw LJ, et al. Patient management after noninvasive cardiac imaging results from SPARC (Study of myocardial perfusion and coronary anatomy imaging roles in coronary artery disease). J Am Coll Cardiol 2012;59:462-74.
29. Min JK, Berman DS, Dunning A, et al. All-cause mortality benefit of coronary revascularization vs. medical therapy in patients without known coronary artery disease undergoing coronary computed tomographic angiography: results from CONFIRM (COronary CT Angiography EvaluatioN For Clinical Outcomes: An InteRnational Multicenter Registry). Eur Heart J 2012;33:3088-3097.

Chapter 3

Diagnostic Value of Transluminal Attenuation Gradient for the Presence of Ischemia as Defined by Fractional Flow Reserve and Quantitative Positron Emission Tomography

Michiel J. Bom, Roel S. Driessen, Wynand J. Stuijfzand, Pieter G. Raijmakers, Cornelis C. Van Kuijk, Adriaan A. Lammertsma, Albert C. van Rossum, Niels van Royen, Juhani Knuuti, Maija Mäki, Koen Nieman, James K. Min, Jonathon A. Leipsic, Ibrahim Danad, and Paul Knaapen

JACC Cardiovasc Imaging. 2019;12(2):323-333

Abstract

Objectives: The aim of this study was to investigate the incremental diagnostic value of transluminal attenuation gradient (TAG), TAG with corrected contrast opacification (TAG-CCO), and transluminal diameter gradient (TDG) over coronary computed tomography (CCTA) derived diameter stenosis alone for the identification of ischemia as defined by both the invasive reference standard fractional flow reserve (FFR) and the non-invasive reference standard quantitative positron emission tomography (PET).

Background: In addition to anatomical information obtained by CCTA, several functional CT-parameters have been proposed to more accurately identify hemodynamically significant lesions, e.g. TAG, TAG-CCO, and more recently TDG. However, clinical validation studies have reported conflicting results and a recent study has suggested that TAG may be affected by changes in vessel diameter.

Methods: Patients with suspect coronary artery disease underwent CCTA and [^{15}O]H_2O PET followed by invasive coronary angiography with FFR of all major coronary arteries. TAG, TAG-CCO, and TDG were assessed and the incremental diagnostic value of these parameters over CCTA-derived diameter stenosis alone for ischemia as defined by PET (hyperemic MBF ≤2.30 ml/min/g) and FFR (≤0.80) was determined.

Results: A total of 557 (91.9%) coronary arteries of 201 patients were included for analysis. TAG, TAG-CCO, and TDG did not discriminate between vessels with or without ischemia as defined by either PET or FFR. Furthermore, these parameters did not have incremental diagnostic accuracy over CCTA alone for the presence of ischemia as defined by PET and FFR. There was a significant correlation between TDG and TAG ($r=0.47$, $p<0.001$) and between TDG and TAG-CCO ($r=0.37$, $p<0.001$).

Conclusions: TAG, TAG-CCO, and TDG do not provide incremental diagnostic value over CCTA alone for the presence of ischemia as defined by [^{15}O]H_2O PET and/or FFR. The lack of diagnostic value of contrast enhancement based flow estimations appears related to coronary luminal dimension variability.

Introduction

Coronary computed tomography angiography (CCTA) is a widely available tool for non-invasive assessment of patients with suspected coronary artery disease (CAD) with a high sensitivity and negative predictive value.(1) However, CCTA has relatively low specificity for the detection of hemodynamically significant coronary stenoses. In an attempt to increase specificity, several CT-techniques have been proposed, e.g. CT perfusion imaging, CT-derived fractional flow reserve (CT-FFR), and transluminal attenuation gradient (TAG).(2-4) Unlike CT perfusion imaging and CT-FFR, which require additional radiation or elaborate off-site post-processing with dedicated software, TAG analysis of intracoronary luminal attenuation is available from standard CCTA data. TAG is based on the concept that in the presence of a significant coronary stenosis, the luminal attenuation will decrease more rapidly. To correct for the time-dependent perturbation of coronary contrast delivery associated with imaging of multiple heart beats, TAG with corrected coronary opacification (TAG-CCO) has been proposed.(5) Studies on the diagnostic value of TAG and TAG-CCO to identify FFR-positive lesions have yielded conflicting results.(3,4,6-9) Moreover, limited data exists on the comparison of TAG and TAG-CCO with quantitative PET perfusion, which is considered the non-invasive gold standard for myocardial perfusion. Recently, correlation between luminal diameter decrease along the course of the coronary artery, expressed as transluminal diameter gradient (TDG), and TAG has been suggested as an explanation for the lack of diagnostic value of TAG.(10) The aim of this study was therefore to assess the diagnostic accuracy of TDG, TAG, and TAG-CCO for the presence of ischemia. Results were tested against the invasive (FFR) and non-invasive reference standard ($[^{15}O]H_2O$ positron emission tomography (PET)). Additionally, the potential correlation of TAG and TDG was explored.

Methods

Study population

The current report is a substudy of the PACIFIC trial and details regarding the study design are described previously.(11) In brief, 208 patients with suspected CAD underwent CCTA, single photon emission computed tomography, and $[^{15}O]H_2O$ PET imaging, followed by invasive coronary angiography (ICA) with FFR measurement

in all major coronary vessels. For the current analysis patients with both CCTA and PET imaging were included (n=201). Vessels with a chronic total occlusion (CTO) were excluded from analysis due to inability to measure distal attenuation. In case of a significant left main stenosis (≥50%), LAD and LCx were excluded from analysis because of inability to measure proximal attenuation (figure 1). The study protocol was approved by the Medical Ethics Committee of the VU University Medical Center and written informed consent was obtained.

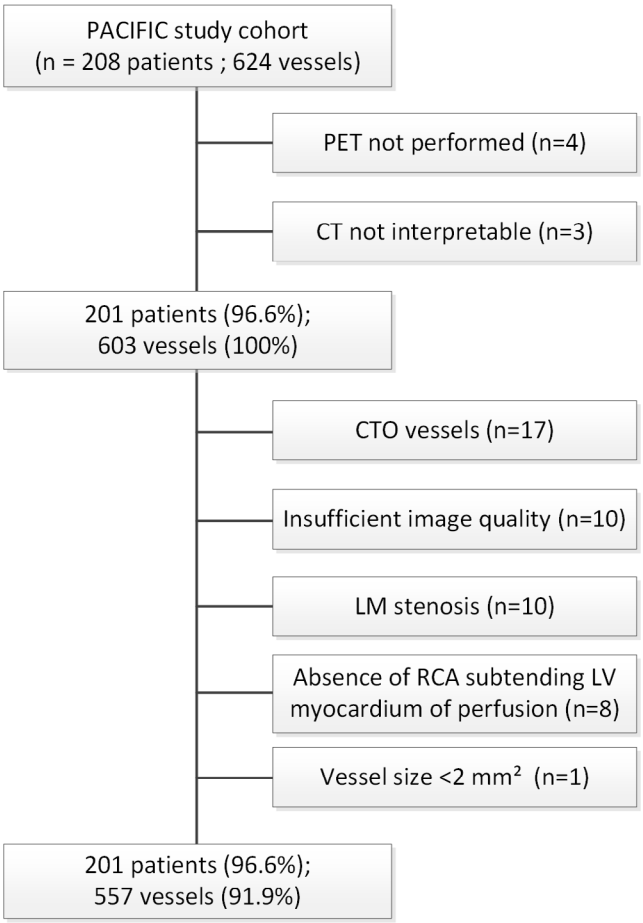

Figure 1. Flowchart of study population
CT = computed tomography; CTO = chronic total occlusion; LM = left main; PET = positron emission tomography; RV-branch = right ventricle branch

CCTA acquisition

Patient preparation and image acquisition were performed as described previously.(11) In short, patients underwent CCTA on a 256-slice CT-scanner (Brilliance iCT, Philips Healthcare, Best, the Netherlands) with a collimation of 128 x 0.625 mm and a tube rotation time of 270 ms. A tube current between 200 and 360 mAs at 120 kV, adjusting primarily the mAs based on body habitus. Axial scanning was performed with prospective ECG-gating (Step & Shoot Cardiac, Philips Healthcare) at 75% of the R-R interval. A bolus of 100 mL iobitidol (Xenetix 350) was injected intravenously (5,7 $mL \cdot s^{-1}$) followed by a 50 mL saline flush. The scan was triggered using an automatic bolus tracking technique, with a region of interest placed in the descending thoracic aorta with a threshold of 150 Hounsfield Units (HU).

$[^{15}O]H_2O$ positron emission tomography

Patients were scanned on a hybrid PET/CT device (Gemini TF 64, Philips Healthcare) following intravenous injection of 370 MBq of $[^{15}O]H_2O$. Scans were acquired under resting conditions and during vasodilator stress by intravenous infusion of adenosine (140 $\mu g \cdot kg^{-1} \cdot min^{-1}$). Patients were instructed not to consume products containing caffeine or xanthine 24 hours prior to the scan. Scanning protocol, image acquisition and quantification of myocardial blood flow (MBF) have been described in detail previously.(12)

Invasive coronary angiography and FFR

ICA and FFR measurements were performed as described previously.(11) In brief, all major coronary arteries were routinely interrogated by FFR except for occluded or subtotal lesions ≥90%. Maximal hyperemia was induced by infusion of intracoronary (150 μg) or intravenous (140 $\mu g \cdot kg^{-1} \cdot min^{-1}$) adenosine. An FFR of ≤0.80 was considered hemodynamically significant. In case of a missing FFR, subtotal stenoses of ≥ 90% were deemed significant, whereas lesions with stenosis of ≤30% (obtained with QCA) were deemed non-significant.

CCTA analysis

Obstructive CAD was defined as a stenosis in any of the major coronary vessels of ≥50%, either left main artery, LAD, LCx, or RCA. Grading of the CCTA images was

based on an intention-to-diagnose basis with non-interpreSupplementary Table egments considered positive for obstructive CAD. Analysis of stenosis grade was performed by independent blinded core laboratories (Departments of Radiology, St. Paul's Hospital, Vancouver, Canada and Weill Cornell Medical College, Dalio Institute of Cardiovascular Imaging, New York-Presbyterian Hospital, New York).

TAG analysis was performed as described previously,(4,5) with the use of CT Comprehensive Cardiac Analysis (Philips Healthcare), and as depicted in figure 2. The centerline was reconstructed for each major coronary artery. Cross-sectional images perpendicular to the centerline were used for TAG analysis. A circular region of interest of 1.0 mm^2 was manually positioned at 5 mm intervals from the ostium to distal where the vessel's cross-sectional area fell below 2.0 mm^2. TAG was expressed as the change in HU per 10 mm length of coronary artery, defined as the linear regression coefficient between intraluminal radiological attenuation and length from the ostium. To correct for time dependent perturbation of contrast delivery associated with imaging over several heart cycles, the TAG-CCO was calculated. Each coronary attenuation measurement was normalized to the attenuation of the descending aorta of the corresponding cycle by dividing the coronary attenuation by the aortic attenuation. In accordance with TAG, the lumen diameter was measured in cross-sectional images at 5 mm-intervals (figure 2). TDG was defined as the linear regression coefficient between the diameter and length from the ostium and expressed as the change in diameter per 10 mm length.(10) Attenuation and diameter measurements at the level of stenosis and/or calcification were excluded from TAG and TDG analysis.

PET analysis

PET scans were analyzed by an independent blinded core laboratory (Turku University Hospital and University of Turku, Finland). Ischemia was defined by a perfusion defect of at least two adjacent myocardial segments with hyperemic MBF ≤2.30 $mL \cdot min^{-1} \cdot g^{-1}$. (12) Standard segmentation was used to assign coronary arteries to vascular territories on parametric MBF images.(13)

Statistical analyses

Statistical analyses were performed using the SPSS software package (version 20.0.0,

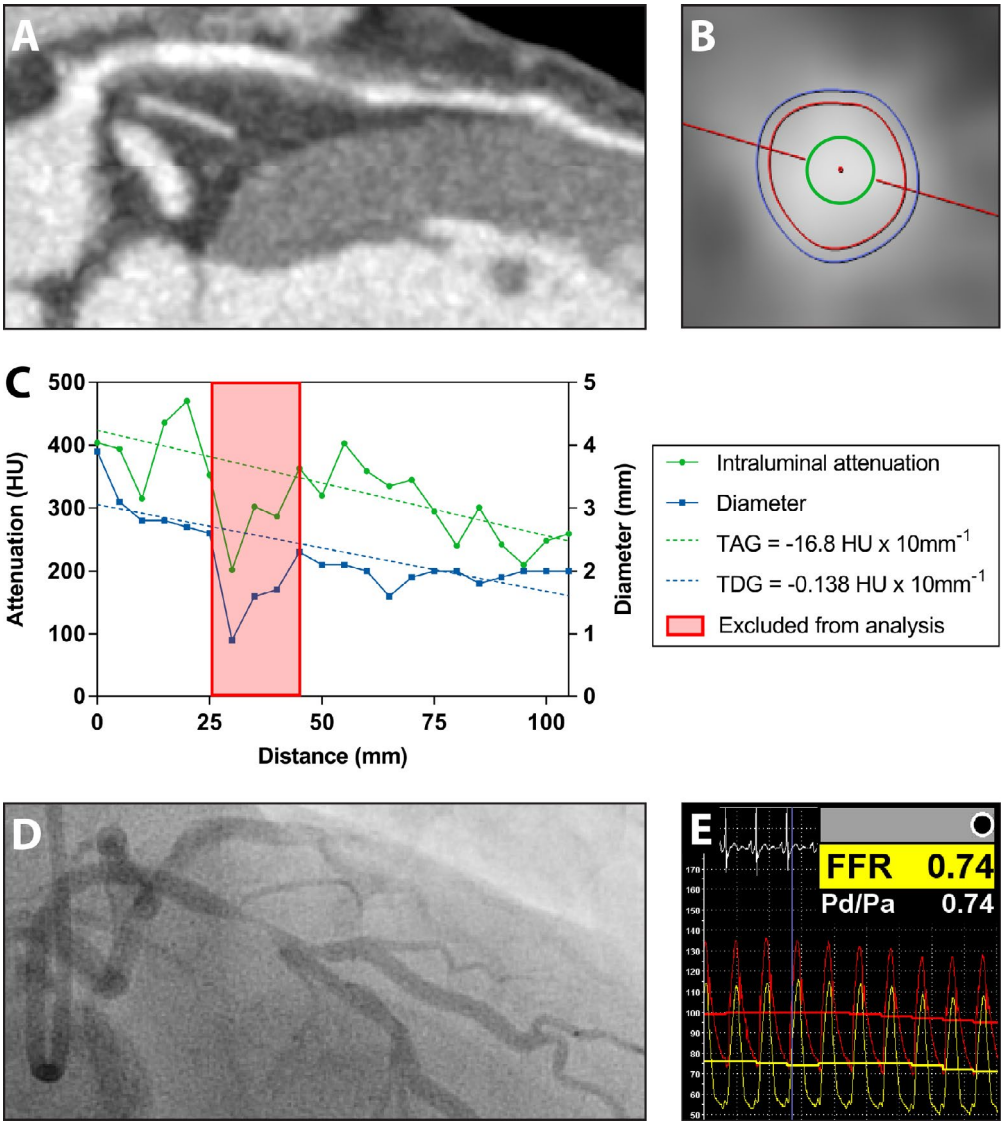

Figure 2. Example of TAG and TDG analysis
CCTA shows a >50% stenosis in the proximal LAD (A). The coronary luminal diameter (red circle) and attenuation (green circle) are measured in cross-sectional CT images (B) at 5-mm intervals from the ostium to distal. TAG and TDG analysis (C) show a gradual decrease of luminal attenuation and diameter, resulting in a negative TAG and TDG. Measurements at the level of stenosis were excluded from analysis (red box). The presence of a hemodynamically significant stenosis in the proximal LAD is confirmed by invasive coronary angiography (D) and FFR (E).
CCTA = coronary computed tomography angiography; HU = Hounsfield units; FFR = fractional flow reserve; TAG = transluminal attenuation gradient; TDG = transluminal diameter gradient

IBM SPSS Statistics). Continuous variables were tested for normal distribution. Normal distributed continuous variables are presented as mean ± SD. Non-normal distributed variables are presented as median with interquartile range. Categorical variables are presented as frequencies with percentages. Continuous variables of TAG, TAG-CCO and TDG were compared between groups using Generalized Estimating Equations in order to account for multiple observations within patients. Models included a main effect for the grouping variables and an exchangeable correlation structure was used. Spearman's correlation was used to measure association between TDG and TAG and between TDG and TAG-CCO. The incremental value of TAG, TAG-CCO and TDG to CCTA-derived diameter stenosis ≥50% for the presence of ischemia as defined by both PET and FFR was determined by comparing the respective areas under the receiver-operating characteristic (ROC) curve using the method of DeLong. A p-value <0.05 was considered statistically significant.

Results

Study population

A total of 201 (96.6%) patients with interpretable CCTA and PET images were included for analysis. Of these patients, 13 vessels were excluded because of inadequate CCTA image quality to allow for TAG analysis. An additional 10 vessels were excluded due to significant left main stenosis, 17 vessels due to CTO and 1 vessel because of vessel size <2 mm^2. Furthermore, the RCA was excluded in 8 patients because of a left dominant coronary anatomy in which the RCA did not subtend LV myocardium. Ultimately, 557 (91.9%) coronary arteries of 201 patients were included for analysis (figure 1). Baseline characteristics are listed in table 1.

CCTA and PET

In 115 (57.2%) patients, CCTA showed obstructive CAD in 206 (33.8%) vessels. PET imaging showed reduced stress MBF, in 93 (46.3%) patients and in 190 (34.1%) vascular territories.

ICA and FFR

QCA analysis showed a ≥50% stenosis at ICA in 88 (43.8%) patients and in 126 (22.6%)

Table 1. Baseline characteristics

Demographics	N = 201
Age, yrs	58 ± 9
Male	129 (64%)
Body mass index	27 ± 4
Cardiovascular risk factors – no (%)	
Diabetes Mellitus type II	32 (16%)
Hypertension	94 (47%)
Hyperlipidaemia	79 (39%)
Current tobacco use	40 (20%)
History of tobacco use	99 (49%)
Family history of CAD	103 (51%)
Type of chest-pain – no (%)	
Typical angina	71 (35%)
Atypical angina	75 (37%)
Non-specific chest discomfort	55 (27%)

Values are mean ± SD or n (%). CAD = coronary artery disease.

vessels. A total of 518 (93.0%) arteries were interrogated with FFR. Of 39 (7.0%) vessels in which FFR was not performed, 36 (6.5%) had a diameter stenosis of >90% and these vessels were thus deemed hemodynamically significant. In 3 (0.5%) vessels FFR assessment was not possible due to severe tortuosity of the vessel. However, none of these vessels had a lesion with a diameter stenosis >30% and these vessels were deemed non-obstructed. A total of 83 (41.3%) patients had one or more hemodynamically significant lesions. In these patients, the number of vessels with hemodynamically significant CAD was 125 (22.4%).

Transluminal attenuation gradient

An overview of TAG, TAG-CCO, and TDG values stratified by PET results is depicted in table 2. Mean values of TAG, TAG-CCO, and TDG were not significantly different between both groups of PET results (p=0.38, p=0.59, and p=0.35 respectively). In the subgroup of vessels with significant stenosis at CCTA, there was also no significant difference in TAG, TAG-CCO and TDG values between vessels with and without PET-defined ischemia (p=0.72, p=0.39, and p=0.39 respectively). Table 3 shows mean TAG, TAG-CCO, and TDG values stratified by FFR. Although mean TAG and TAG-

Table 2. TAG and TDG analysis on a per vessel basis stratified by PET results

	Total	Hyperemic MBF > 2.30	Hyperemic MBF ≤ 2.30	p-value*
All vessels	**N=557**	**N=367**	**N=190**	
TAG, HU x 10mm^{-1}	-9.88 ± 10.9	-10.2 ± 10.8	-9.20 ± 11.2	0.38
TAG-CCO, HU x 10mm^{-1}	-0.0301 ± 0.0359	-0.0310 ± 0.0331	-0.0285 ± 0.0408	0.59
TDG, mm x 10mm^{-1}	-0.217 ± 0.140	-0.221 ± 0.148	-0.209 ± 0.123	0.35
CCTA DS ≥50%	**N=171**	**N=68**	**N=103**	
TAG, HU x 10mm^{-1}	-10.8 ± 12.4	-10.5 ± 11.1	-11.1 ± 13.2	0.72
TAG-CCO, HU x 10mm^{-1}	-0.0332 ± 0.0398	-0.0299 ± 0.0281	-0.0353 ± 0.0459	0.39
TDG, mm x 10mm^{-1}	-0.210 ± 0.115	-0.199 ± 0.0857	-0.217 ± 0.131	0.39

Values are mean ± SD or n (%). * p-value for difference between hyperemic MBF groups. HU = hounsfield units; MBF = myocardial blood flow; TAG = transluminal attenuation gradient; TAG-CCO = transluminal attenuation gradient corrected contrast opacification; TDG = transluminal diameter gradient

Table 3. TAG and TDG analysis on a per vessel basis stratified by FFR results

	Total	FFR >0.80	FFR ≤0.80	p-value*
All vessels	**N=557**	**N=125**	**N=432**	
TAG, HU x 10mm^{-1}	-9.88 ± 10.9	-9.65 ± 10.7	-10.7 ± 11.8	0.37
TAG-CCO, HU x 10mm^{-1}	-0.030 ± 0.036	-0.0287 ± 0.0340	-0.0350 ± 0.0415	0.17
TDG, mm x 10mm^{-1}	-0.217 ± 0.140	-0.219 ± 0.149	-0.210 ± 0.103	0.47
CCTA DS ≥50%	**N=171**	**N=86**	**N=85**	
TAG, HU x 10mm^{-1}	-10.8 ± 12.4	-9.71 ± 11.4	-12.0 ± 13.3	0.33
TAG-CCO, HU x 10mm^{-1}	-0.0332 ± 0.0398	-0.0270 ± 0.0321	-0.0394 ± 0.0456	0.08
TDG, mm x 10mm^{-1}	-0.210 ± 0.115	-0.199 ± 0.0857	-0.217 ± 0.131	0.39

Values are mean ± SD or n (%). * p-value for difference between hyperemic MBF groups. FFR = fractional flow reserve; other abbreviations as in Table 2.

CCO were slightly lower in vessels with a positive FFR than those with a negative FFR, these changes were not statistically significant (p=0.37 and p=0.17 respectively). Accordingly, in vessels with a significant stenosis at CCTA no statistically significant differences in TAG, TAG-CCO and TDG were noted between FFR groups (p=0.33, p=0.08, and p=0.76 respectively).

Incremental diagnostic value of TAG, TAG-CCO and TDG for presence of ischemia

The results of ROC analyses on the incremental value of TAG parameters to CCTA-derived diameter stenosis alone for the presence of ischemia, as defined by PET and FFR, are illustrated in figure 3. TAG, TAG-CCO, and TDG did not significantly increase the area under the curve (AUC) for the presence of ischemia as defined by PET or FFR. However, there was a non-significant trend for a minor increase in AUC for the addition of both TAG and TAG-CCO to CCTA-derived diameter stenosis alone for the presence of ischemia as defined by PET perfusion (p=0.053 and p=0.08 respectively).

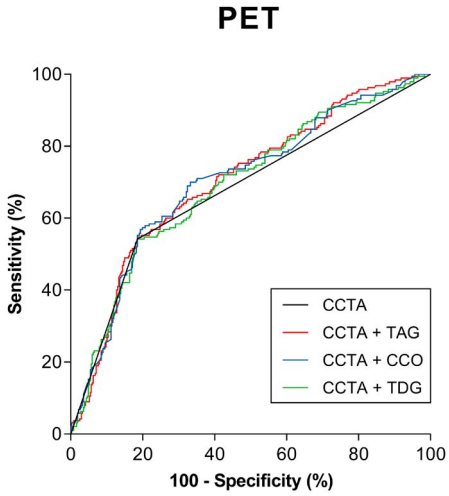

Test	AUC	(95% CI)	p-value *
CCTA	0.68	(0.64 - 0.72)	-
CCTA + TAG	0.70	(0.67 - 0.74)	0.053
CCTA + CCO	0.70	(0.66 - 0.74)	0.08
CCTA + TDG	0.69	(0.65 - 0.73)	0.27

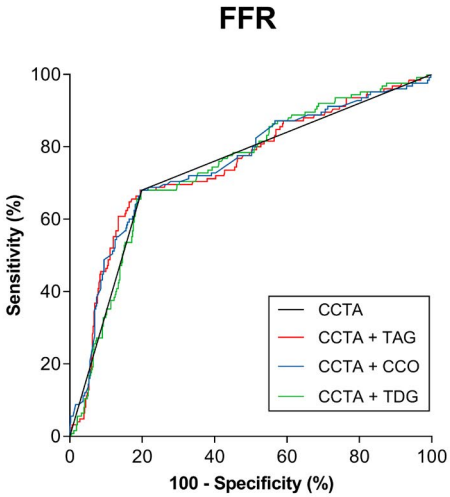

Test	AUC	(95% CI)	p-value *
CCTA	0.74	(0.68 - 0.79)	-
CCTA + TAG	0.75	(0.70 - 0.80)	0.52
CCTA + CCO	0.75	(0.70 - 0.80)	0.38
CCTA + TDG	0.74	(0.69 - 0.79)	0.87

Figure 3. Diagnostic value of CCTA alone versus CCTA with TAG, TAG-CCO and TDG for the presence of ischemia.
Receiver-operating characteristic curve analysis with area under the curve (AUC) for the diagnogstic value of CCTA-derived diameter stenosis (≥50%) alone versus CCTA with TAG, TAG with corrected contrast opacification (TAG-CCO), and TDG for the presence of ischemia as defined by PET (left column) and FFR (right column). * p-value for difference with CCTA alone. CI = confidence interval; PET = positron emission tomography; other abbreviations as in figure 2

Correlation of TAG parameters with TDG

The correlation between TAG parameters (TAG and TAG-CCO) and TDG is shown in figure 4. There was a significant correlation between both TAG and TDG (r=0.472; p<0.001) and between TAG-CCO and TDG (r=0.376; p<0.001).

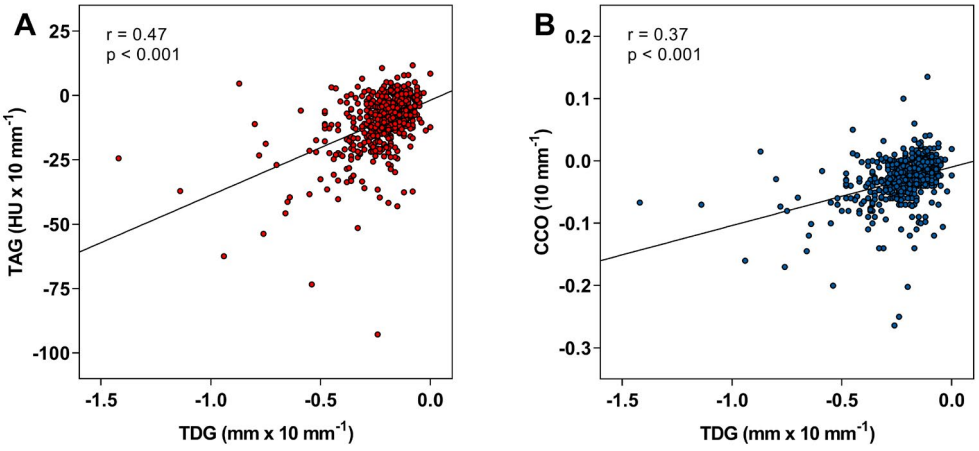

Figure 4. Correlation between TAG and TDG and TAG-CCO and TDG.
Both TAG (A) and TAG-CCO (B) were significantly correlated with TDG. Abbreviations as in figure 2

Discussion

Our study is the first to assess the diagnostic potential of TAG, TAG-CCO and TDG for the presence of ischemia as defined by both the non-invasive gold standard [^{15}O]H_2O PET and the invasive gold standard FFR. Results show that neither TAG, TAG-CCO nor TDG provide incremental diagnostic value over CCTA-derived diameter stenosis alone for the identification of hemodynamically significant lesions defined by either PET or FFR. Furthermore, the change in coronary artery diameter, defined by TDG, correlated with both TAG and TAG-CCO, which implies TAG may be influenced by decreased attenuation because of decrease in diameter.

Diagnostic value of TAG for the presence of FFR-defined ischemia

Previous studies on the diagnostic value of TAG for the identification of FFR positive lesions have shown conflicting results.(6,7,9) An overview of these studies is represented in table 4. Choi et al. retrospectively studied the diagnostic performance of TAG and

Table 4. Overview of studies on the diagnostic value of transluminal attenuation gradient (TAG) and corrected contrast opacification (CCO)

Study	Number of patients (vessels)	CT acquisition	Reference standard	Parameter	AUC	Incremental to CCTA alone
Choi et al. (7)	63 (97)	64-slice, retrospective gating	FFR ≤0.80	CCTA	0.73	-
				CCTA + TAG	0.81	Yes
				CCTA + CCO	0.78	No
Yoon et al. (9)	53 (82)	64-slice, retrospective gating	FFR ≤0.80	CCTA	0.73	-
				TAG	0.63	N/A
Stuijfzand et al. (6)	85 (253)	256-slice, prospective gating	FFR ≤0.80	CCTA	0.85	-
				CCTA + TAG	0.87	No
				CCTA + TAG-CCO	0.88	No
Wang et al. (14)	32 (32)	1st gen DSCT, retrospective gating; 2nd gen DSCT, prospective gating	FFR ≤0.80	CCO	0.85	Yes
				TAG	0.68	No
Wong et al. (4)	54 (78)	320-slice, prospective gating	FFR ≤0.80	CCTA	0.79	-
				CCTA + TAG	0.88	Yes
Ko et al. (15)	61 (82)	320-slice, prospective gating	FFR ≤0.80	CCTA	0.69	-
				CCTA + TAG	0.72	No
Benz et al. (16)	39 (69)	64 or 256 slice, prospective gating	NH_3 PET: RFR <0.69	CCO	0.71	N/A
Present study	201 (557)	256-slice, prospective gating	FFR ≤0.80	CCTA	0.74	-
				CCTA + TAG	0.75	No
				CCTA + TAG-CCO	0.75	No
			$[^{15}O]H_2O$ PET: stress MBF ≤2.30	CCTA	0.68	-
				CCTA + TAG	0.70	No
				CCTA + TAG-CCO	0.70	No

AUC = area under the curve; CCTA = coronary computed tomography angiography derived diameter stenosis ≥50%; DSCT = dual-source CT; gen = generation; N/A = analysis on incremental value of TAG/CCO to CCTA-derived diameter stenosis alone not performed; other abbreviations as in Table 2.

CCO compared with CCTA alone in 65 patients with a 64-row CCTA.(7) The authors reported superior diagnostic accuracy of TAG over CCTA alone, with AUCs of 0.81 and 0.73 respectively. Subsequently, Yoon et al. showed that TAG could significantly predict the presence of FFR-positive vessels (AUC=0.63), however the diagnostic performance of TAG was not significantly different to that of CCTA diameter stenosis.(9) More recently, our group prospectively investigated the value of TAG over CCTA alone in 85 patients using a 256-slice CT.(6) There was no incremental diagnostic value of TAG for the presence of hemodynamically obstructed vessels and in contrast to the aforementioned studies, TAG was not able to discriminate between vessels with or without hemodynamically significant lesions. The present study is the largest study to date and results are in line with our previous work. TAG values were numerically lower in the FFR ≤0.80 group, however this was not statistically significant. Furthermore, TAG did not improve diagnostic accuracy over CCTA alone for the presence of hemodynamically obstructed vessels. When comparing the incremental value of TAG in the various studies, one must take notice of the large heterogeneity in the diagnostic value of CCTA alone, with an AUC ranging from 0.73 to 0.85.(6,7,9) The relatively low diagnostic value of CCTA alone in the present study might be partly explained by the use of the intention-to-diagnose analysis. Despite the low diagnostic value of CCTA alone and although TAG was only performed in selected patients in which TAG is deemed feasible, TAG did not provide incremental diagnostic accuracy over CCTA alone.

Temporal uniformity in TAG analysis

According to its theoretical framework, TAG is dependent on temporal uniformity of image acquisition. Scanners with very wide detector arrays or dual source CT-scanners with a high-pitch spiral scan mode can image the entire heart in a single heartbeat. Most studies on TAG, including the present study, have used 64- to 256-slice CT-scanners in axial scan mode, which require several heart cycles to acquire all images. To correct for this temporal non-uniformity CCO was introduced, in which the intraluminal attenuation is normalized to the attenuation of the descending aorta of the corresponding cycle. Like TAG, reports on the diagnostic value of CCO have shown conflicting results.(6,7,14) Wang et al. have retrospectively evaluated the diagnostic value of CCO in 32 patients (and 32 vessels) and reported good diagnostic performance

of CCO with an AUC of 0.85 for the identification of FFR-positive lesions.(14) The aforementioned study by Choi et al., however, did not show incremental value of CCO over CCTA alone for the presence of FFR-positive lesions.(7) In an effort to optimize results, our group has previously reported on the diagnostic value of TAG-CCO, in which CCO is calculated using linear regression of CCO values along the coronary artery, as is done with TAG. Although lower TAG-CCO values were found in vessels with a positive FFR than in those with a negative FFR, TAG-CCO did not improve diagnostic accuracy over CCTA alone.(6) In line with these results, the present study showed no incremental value of TAG-CCO over CCTA alone for the identification of hemodynamically obstructed vessels. Limited studies have reported on the diagnostic value of TAG obtained in a single heart beat with a 320-slice CT (TAG-320). Wong et al. reported that in a cohort of 54 patients, TAG-320 had incremental value over CCTA alone for detection of significant FFR.(4) Recently, Ko et al. investigated the diagnostic value of TAG-320 for the presence of significant FFR in a substudy of the NXT trial.(15) TAG-320 was found to add no incremental value when added to CCTA, with AUCs of 0.69 and 0.75 respectively. Future studies are warranted to elucidate the diagnostic value of TAG-320.

Diagnostic value of TAG and CCO for the presence of PET-defined ischemia

To date, no studies have reported on the diagnostic value of TAG in comparison with the non-invasive gold standard for myocardial perfusion, quantitative PET perfusion. For CCO, only one small retrospective study with 39 patients (and 69 vessels) has evaluated its diagnostic value for the presence of ischemia, as defined by relative flow reserve measured using $[^{13}N]NH_3$ PET.(16) CCO decrease was significantly correlated with PET-defined ischemia (r = -0.48). In the present study hyperemic MBF measured with $[^{15}O]H_2O$ PET was used as a reference standard. Since $[^{15}O]H_2O$ is metabolically inert and freely diffusible across myocyte membranes, it is considered the optimal tracer for quantification of MBF.(17) Hyperemic MBF was used as reference standard, because it is reported to have the highest diagnostic accuracy in quantitative PET perfusion.(12) In the present study, neither TAG nor TAG-CCO were able to discriminate between vessels with and without $[^{15}O]H_2O$ PET-defined ischemia. Furthermore, in line with the lack of diagnostic value for FFR-positive lesions, TAG and TAG-CCO did not

significantly increase the diagnostic value of CCTA alone for the identification of PET-defined ischemia (AUCs of 0.70, 0.70, and 0.68 respectively).

Recently, Park et al. have shown in a combined vessel phantom, animal and clinical study that intraluminal attenuation is affected by the diameter of the vessel.(10) For their clinical investigation, TAG and TDG were calculated in 62 patients (and 152 vessels). In line with the present findings, TAG was significantly correlated with TDG (r=0.580), implying that TAG might be related to decrease of attenuation due to decrease in luminal diameter. This might partly explain the lack of diagnostic value of TAG. The diminution of attenuation in smaller vessels might be caused by the partial volume averaging effect, in which several objects are encompassed on the same CT-voxel due to the limited spatial resolution.(18) Park et al. however proposed the point-spread function as a possible mechanism.(10) The point spread function is the response of an imaging system to a point source. Widening of the point-spread function and subsequent image blurring occurs more often in smaller objects.(19) Therefore, CT density is underestimated in smaller objects such as coronary arteries.(20) In TAG analysis, this might result in decreased attenuation along the course of the vessel.

Park et al. further reported that TDG was able to discriminate between vessels with and without a significant stenosis at ICA, whereas TAG was not. The authors therefore proposed TDG as a potential functional CT parameter. In the present study however, TDG had no incremental value to CCTA alone for the identification of the presence of ischemia.

Another limitation in TAG analysis is the fact that TAG is measured in a resting state and thus can only represent resting coronary flow. Since resting flow is known to remain stable up to the point of sub-total occlusion,(21) it is not unanticipated that TAG is unable to identify hemodynamically obstructed coronary arteries. To overcome this issue, a recent study has evaluated the use of TAG during pharmacological stress.(22) In a cohort of 27 patients, the authors found that stress TAG after intravenous adenosine infusion was associated with added radiation exposure and inferior image quality without improving diagnostic accuracy.

Limitations

The present study has several limitations. Firstly, the presence of a CTO with large collateral circulation is reported to result in increased flow in the supplying donor artery.(23) While 17 CTO vessels were excluded from analysis, supplying donor arteries were not. Theoretically, the presence of a CTO might have influenced TAG and TAG-CCO measurements in these donor arteries. However, our results did not change when donor arteries where excluded from analysis (data not shown). Secondly, some assumptions were made in case of missing FFR measurements (39 vessels, 7.0%). Although previous reports have shown that FFR is positive in the vast majority of cases with a >90% stenosis and negative in all most all cases with <30% stenosis, minor influence of these assumptions on our study results may have occurred.(24) Thirdly, image acquisition, contrast injection, scan-trigger protocol and CT-scanner type are known to affect contrast enhancement of CCTA and might have affected our results.(25) As mentioned previously, novel CT-scanners with single heart-beat imaging might be better suited for the measurement of TAG parameters. Lastly, since standard segmentation according to the American Heart Association was used to assign coronary arteries to PET perfusion territories,(13) some mismatch between coronary arteries and their corresponding vascular territories may have occurred. Prior studies have therefore used an individualized approach in which angiography is used to assign coronary arteries to perfusion territories.(12) However, the clinical impact of this individualized approach is dispuSupplementary Table ince similar results are reported with the use of the individualized approach and the standard segmentation.(26)

Conclusion

This study shows that neither TAG, TAG-CCO nor TDG provide incremental diagnostic value for the presence of ischemia as defined by both the non-invasive gold standard [^{15}O]H_2O PET perfusion imaging and the invasive gold standard FFR. Since TAG was significantly correlated with TDG, the lack of diagnostic value of TAG may be a result of interrelation with differences in coronary luminal diameter.

References

1. Meijboom WB, Meijs MF, Schuijf JD, et al. Diagnostic accuracy of 64-slice computed

tomography coronary angiography: a prospective, multicenter, multivendor study. J Am Coll Cardiol. 2008;52:2135-44.

2. Koo BK, Erglis A, Doh JH, et al. Diagnosis of ischemia-causing coronary stenoses by noninvasive fractional flow reserve computed from coronary computed tomographic angiograms. Results from the prospective multicenter DISCOVER-FLOW (Diagnosis of Ischemia-Causing Stenoses Obtained Via Noninvasive Fractional Flow Reserve) study. J Am Coll Cardiol. 2011;58:1989-97.
3. Wong DT, Ko BS, Cameron JD, et al. Comparison of diagnostic accuracy of combined assessment using adenosine stress computed tomography perfusion + computed tomography angiography with transluminal attenuation gradient + computed tomography angiography against invasive fractional flow reserve. J Am Coll Cardiol. 2014;63:1904-12.
4. Wong DT, Ko BS, Cameron JD, et al. Transluminal attenuation gradient in coronary computed tomography angiography is a novel noninvasive approach to the identification of functionally significant coronary artery stenosis: a comparison with fractional flow reserve. J Am Coll Cardiol. 2013;61:1271-9.
5. Choi JH, Min JK, Labounty TM, et al. Intracoronary transluminal attenuation gradient in coronary CT angiography for determining coronary artery stenosis. JACC Cardiovasc Imaging. 2011;4:1149-57.
6. Stuijfzand WJ, Danad I, Raijmakers PG, et al. Additional value of transluminal attenuation gradient in CT angiography to predict hemodynamic significance of coronary artery stenosis. JACC Cardiovasc Imaging. 2014;7:374-86.
7. Choi JH, Koo BK, Yoon YE, et al. Diagnostic performance of intracoronary gradient-based methods by coronary computed tomography angiography for the evaluation of physiologically significant coronary artery stenoses: a validation study with fractional flow reserve. Eur Heart J Cardiovasc Imaging. 2012;13:1001-7.
8. Chow BJ, Kass M, Gagne O, et al. Can differences in corrected coronary opacification measured with computed tomography predict resting coronary artery flow? J Am Coll Cardiol. 2011;57:1280-8.
9. Yoon YE, Choi JH, Kim JH, et al. Noninvasive diagnosis of ischemia-causing coronary stenosis using CT angiography: diagnostic value of transluminal attenuation gradient and fractional flow reserve computed from coronary CT angiography compared to invasively measured fractional flow reserve. JACC Cardiovasc Imaging. 2012;5:1088-96.
10. Park EA, Lee W, Park SJ, Kim YK, Hwang HY. Influence of Coronary Artery Diameter on Intracoronary Transluminal Attenuation Gradient During CT Angiography. JACC Cardiovasc Imaging. 2016;9:1074-83.

11. Danad I, Raijmakers PG, Driessen RS, et al. Comparison of Coronary CT Angiography, SPECT, PET, and Hybrid Imaging for Diagnosis of Ischemic Heart Disease Determined by Fractional Flow Reserve. JAMA Cardiol. 2017.
12. Danad I, Uusitalo V, Kero T, et al. Quantitative assessment of myocardial perfusion in the detection of significant coronary artery disease: cutoff values and diagnostic accuracy of quantitative [(15)O]H2O PET imaging. J Am Coll Cardiol. 2014;64:1464-75.
13. Cerqueira MD, Weissman NJ, Dilsizian V, et al. Standardized myocardial segmentation and nomenclature for tomographic imaging of the heart. A statement for healthcare professionals from the Cardiac Imaging Committee of the Council on Clinical Cardiology of the American Heart Association. Circulation. 2002;105:539-42.
14. Wang R, Renker M, Schoepf UJ, et al. Diagnostic value of quantitative stenosis predictors with coronary CT angiography compared to invasive fractional flow reserve. Eur J Radiol. 2015;84:1509-15.
15. Ko BS, Wong DT, Norgaard BL, et al. Diagnostic Performance of Transluminal Attenuation Gradient and Noninvasive Fractional Flow Reserve Derived from 320-Detector Row CT Angiography to Diagnose Hemodynamically Significant Coronary Stenosis: An NXT Substudy. Radiology. 2016;279:75-83.
16. Benz DC, Grani C, Ferro P, et al. Corrected coronary opacification decrease from coronary computed tomography angiography: Validation with quantitative 13N-ammonia positron emission tomography. J Nucl Cardiol. 2017.
17. Driessen RS, Raijmakers PG, Stuijfzand WJ, Knaapen P. Myocardial perfusion imaging with PET. Int J Cardiovasc Imaging. 2017;33:1021-31.
18. Machida H, Tanaka I, Fukui R, et al. Current and Novel Imaging Techniques in Coronary CT. Radiographics. 2015;35:991-1010.
19. Rollano-Hijarrubia E, Stokking R, van der Meer F, Niessen WJ. Imaging of small high-density structures in CT A phantom study. Acad Radiol. 2006;13:893-908.
20. Paul NS, Blobel J, Kashani H, Rice M, Ursani A. Quantification of arterial plaque and lumen density with MDCT. Med Phys. 2010;37:4227-37.
21. Gould KL, Lipscomb K. Effects of coronary stenoses on coronary flow reserve and resistance. Am J Cardiol. 1974;34:48-55.
22. Ko BS, Seneviratne S, Cameron JD, et al. Rest and stress transluminal attenuation gradient and contrast opacification difference for detection of hemodynamically significant stenoses in patients with suspected coronary artery disease. Int J Cardiovasc Imaging. 2016;32:1131-41.
23. Ladwiniec A, Cunnington MS, Rossington J, et al. Collateral donor artery physiology

and the influence of a chronic total occlusion on fractional flow reserve. Circ Cardiovasc Interv. 2015;8.

24. Tonino PA, Fearon WF, De Bruyne B, et al. Angiographic versus functional severity of coronary artery stenoses in the FAME study fractional flow reserve versus angiography in multivessel evaluation. J Am Coll Cardiol. 2010;55:2816-21.
25. Bae KT. Intravenous contrast medium administration and scan timing at CT: considerations and approaches. Radiology. 2010;256:32-61.
26. Thomassen A, Petersen H, Johansen A, et al. Quantitative myocardial perfusion by O-15-water PET: individualized vs. standardized vascular territories. Eur Heart J Cardiovasc Imaging. 2015;16:970-6.

Chapter 4

Discriminative Power of the HEART Score for Obstructive Coronary Artery Disease in Acute Chest Pain Patients Referred for CCTA

Michiel J. Bom*, Adriana Q. Kolff*, Remco J. J. Knol,
Friso M. van de Zant, Petrus M. van der Zee, and Jan H. Cornel

* Both authors contributed equally

Crit Pathw Cardiol. 2016;15(1):6-10

Abstract

Objective: To investigate the ability of the HEART score to predict the presence of obstructive coronary artery disease (CAD) determined by coronary computed tomography angiography (CCTA) and its ability to predict the occurrence of major adverse cardiac events (MACE) in patients referred for CCTA after emergency department (ED) presentation.

Methods: From December 2011 to August 2014, 710 ED patients with chest pain who underwent CCTA within 30 days were included. The HEART score was retrospectively calculated and patients were followed for MACE, comprised of death, myocardial infarction, and revascularization. Association of CAD at CCTA in the different categories of the HEART score was analyzed using $\chi 2$ test. The performance of the HEART score in discriminating between those with and without obstructive CAD was evaluated by receiver operating characteristics. Kaplan–Meier analysis was used to assess MACE-free survival stratified by HEART score categories.

Results: During median follow-up of 826 days (interquartile range: 563–1056), MACE occurred in 46 (6.5%) patients; 3 (0.4%) myocardial infarction, 8 (1.1%) death, and 36 (5.1%) revascularizations. A low HEART score was a significant predictor for MACE -free survival ($P = 0.010$). CCTA revealed obstructive CAD in 11.7% of patients, with no significant difference between patients with a low and intermediate/high HEART score, respectively 10.7% and 13.2% ($P = 0.29$). The ability of the HEART score to identify obstructive CAD was poor with an AUC of the receiver operating characteristics curve of 0.53.

Conclusion: The HEART score does not adequately identify patients with obstructive CAD at CCTA. It does however predict occurrence of MACE in medium-term follow-up. Excluding patients from additional testing based solely on a low HEART score may lead to suboptimal patient management. CCTA had important implications on patient management and may be a more appropriate tool to further stratify risk in ED chest pain patients.

Introduction

Chest pain is the main symptom of patients visiting the cardiac emergency department (ED). In less than half of these visits, the symptoms are caused by cardiac disease. (1) However, prior studies estimate that between 2% and 5% of chest pain patient presenting to the ED who are discharged develop myocardial infarction within 30 days.(2) Different prediction models have been developed in search of a cost-effective and safe way to stratify patient risk for major adverse cardiac events (MACE). The traditional clinical risk scores (TIMI, GRACE, Sanchis, Goldman score) perform poorly in the low–intermediate risk population in their ability to predict the occurrence of MACE and the presence of obstructive coronary artery disease (CAD).(3,4) The recently developed HEART score stratifies patients in low (0-3 points), intermediate (3-6 points), and high risk (7-10 points) based on patient history, age, cardiac risk factors, EKG, and troponin value (Fig. 1). The Dutch prospective validation study by Backus et al (5) showed a high negative predictive value of a low HEART score, with occurrence of MACE in 1.7% of cases within 6 weeks days of ED visit. A recent cohort study by Mahler et al6 even suggests that due to the very high negative predictive value one could safely refrain from additional diagnostic testing in patient with a low HEART score. Recent studies have demonstrated that coronary computed tomography angiography (CCTA) is a useful tool in low to intermediate risk ED patients for the identification of obstructive CAD and to identify patients at increased risk of MACE. (7–10) This study was devised to evaluate if a low HEART score predicts a true low risk ED population in whom additional testing will not lead to medical or invasive interventions and can thus be omitted. To examine this, the ability of a low HEART score to predict the presence of CAD at CCTA and the ability to predict the occurrence of MACE were evaluated.

Methods

Patient selection

From December 14, 2011 to August 19, 2014, 713 consecutive patients who presented to the cardiac ED of the Medical Centre Alkmaar and subsequently underwent CCTA were prospectively included. All CCTA's were performed either during clinical observation or within 30 days following ED presentation.

Prospectively collected data included patient characteristics, cardiovascular risk profile, medication changes (changes in statin and aspirin treatment), and CCTA results. By means of retrospective chart examination, a HEART score was retrospectively calculated for all patients. The local scientific board approved the analysis and all patients signed an informed consent statement for usage of their data.

HEART score

The HEART score was retrospectively calculated in all patients as described by Backus et al.(5) A low HEART score was defined as a total score of 0-3, an intermediate HEART score 4-6, and a high HEART score 7-10 (Fig. 1). The definition of the different composites of the HEART score will be briefly discussed.

		Points	
History	Highly suspicious	2	
	Moderately suspicious	1	
	Slightly suspicious	0	
EKG	Significant ST-deviation	2	
	Non specific repolarization disturbance / LBTB /PM	1	
	Normal	0	
Age	>65 years	2	
	> 45 an d <65 years	1	
	< 45 years	0	
Risk factors[1]	≥ 3 risk factors	2	
	1 or 2 risk factors	1	
	No risk factors known	0	
Troponin	> 3x normal limit	2	
	> 1 and < 3x normal limit	1	
	≤ 1x normal limit	0	
TOTAL			

[1] Risk factors: hyperlipidaemia, hypertension, cigarette smoking, diabetes Mellitus, obesity, positive family history

Figure 1. HEART score calculation for chest pain patients

History

Chest pain typical for coronary ischemia was graded 2 points, partly typical complaints 1 point, and nonspecific chest pain 0 points, following ESC guidelines in traditional clinical classification of chest pain.(11)

Electrocardiogram

The electrocardiogram was reviewed according to the Minnesota criteria.(3,5)

Risk Factors

Cardiac risk factors were noted prospectively for all patients (hypercholesterolemia, hypertension, diabetes mellitus, cigarette smoking, BMI > 30, and positive family history for premature CAD). Two points were awarded to those with >3 risk factors or known atherosclerotic disease, 1 point in the case of 1-2 risk factors, and 0 points if no risk factors were recorded.

Troponin

Troponin value was assessed by measuring by high sensitive troponin-I, with cut-off value >0.05 μg/L (Beckman high sensitive troponin-I). Serial troponin values were obtained according to ESC guidelines with a second value at least 3 hours after presentation if presenting within 6 hours of chest pain complaints.(11) For calculation of the HEART score, a troponin >0.15 μg/L (>3× normal limit) was awarded 2 points, 0.05-0.14 μg/L was awarded 1 point, and <0.05 μg/L was awarded 0 point.

Follow-up

Patients were followed for the occurrence of MACE, defined as death, myocardial infarction and/or revascularization, either coronary artery bypass graft or percutaneous coronary intervention. A commonly used 60-day landmark was used to differentiate between CCTA-driven invasive coronary angiography and late revascularization which is considered to be indicative for the prognostic value of CCTA.(12) In case patients experienced more than 1 event, the first event was chosen.

Information on myocardial infarction and revascularization was obtained from the electronic medical records. Information on mortality was obtained from the municipal personal records database.

CCTA acquisition

Patient preparation, CCTA acquisition, interpretation, and radiation dose calculation was done as extensively described in the descriptive study by Bogaard et al.(13) and

will only be briefly discussed in this study. Coronary artery calcium scoring (CACS) and CCTA were acquired with Somaton Definition Flash CT scanner (2 × 128 slices, Siemens Medical Systems, Erlangen, Germany). All scans were read in consensus by a certification board of cardiovascular computed tomography accredited nuclear medicine physician and a cardiologist experienced in the interpretation of CCTA. In case of disagreement, a third opinion was decisive. Each coronary segment was scored for the presence of plaques and calcium. A CACS was obtained in best diastolic phase with a tube voltage of 120 kV, 3 mm slice thickness. The dataset was filtered using a B35f medium reconstruction kernel. Areas with Hounsfield units of >130 were considered to contain calcium, and were manually assigned to coronary arteries. Obstructive CAD was defined as a lumen stenosis in any of the major coronary vessels of >50%, either left main artery, left anterior descending artery, circumflex artery, or right coronary artery. Normal coronary arteries were defined as CAC score of 0 and no coronary plaque. Nonobstructive CAD was defined as CAC score >0 and/or any plaque that did not meet the criteria for obstructive CAD. In obstructive CAD, the extent of CAD was recorded, 1-, 2-, or 3-vessel CAD.

Statistics

Statistical Package for Social Sciences version 22.0.0 (IBM SPSS, Chicago, IL) was used for statistical analysis. Continuous variables are presented as mean ± SD and categorical variables as frequencies with percentages. Continuous variables were tested for normal distribution. Variables were compared with a $\chi 2$ test for categorical variables and by applying an analysis of variance or an unpaired student t test for continuous variables as appropriate. Presence of CAD at CCTA in the HEART score was analyzed using $\chi 2$ test. To further evaluate the performance of the HEART score to differentiate between those with and without obstructive CAD, a receiver operating characteristics curve was plotted and the area under the curve was calculated. Kaplan–Meier analysis was used to assess MACE-free survival stratified by HEART score categories.

Results

Baseline characteristics

Initially, 713 patients were included in the database for follow-up. Three (0.4%) patients

were lost to follow-up, leaving a total number of 710 studied patients. An overview of the baseline characteristics of the total study population and of the different HEART score categories are shown in Table 1. Because of the low number of patients with high HEART score (n = 5), the intermediate and high HEART -score patients were grouped together. The presence of different risk factors and typical symptoms were more frequent and baseline cardiac medication use was less frequent in patients with a low HEART score compared with patients with intermediate/high HEART score.

Table 1. Baseline characteristics

	Low HEART-score (n=393)	Intermediate/high HEART score (n=317)	p-value
Demographics			
Age	52.6±9.8	59.3±10.5	<0.001
Women	238 (60.6%)	223 (63.7%)	0.39
Body Mass Index	26.5±4.6	28.0±4.5	<0.001
Diabetes	23 (5.9%)	44 (13.9%)	0.001
Hypertension	93 (23.7%)	169 (53.3%)	<0.001
Hyperlipidemia	76 (19.3%)	121 (38.2%)	<0.001
Family history of CAD	200 (50.9%)	183 (57.7%)	0.069
Smoking	127 (32.3%)	96 (30.3%)	0.56
eGFR<60	6 (1.5%)	20 (6.3%)	0.001
Clinical symptoms			
Non-anginal chestpain	219 (55.7%)	57 (18.0%)	<0.001
Atypical angina	153 (38.9%)	154 (48.6%)	0.010
Typical angina	21 (5.3%)	106 (33.4%)	<0.001
Baseline medication			
Aspirin	144 (36.6%)	196 (61.8%)	<0.001
Statin	153 (38.9%)	211 (66.6%)	<0.001
Beta-blocker	147 (37.4%)	222 (70.0%)	<0.001
ACE-i / ARB	75 (19.1%)	113 (35.6%)	<0.001
Calcium channel blocker	17 (4.3%)	24 (7.6%)	0.065
Nitrate	4 (1.0%)	17 (5.4%)	0.001
Acenocoumarol	8 (2.0%)	14 (4.4%)	0.069

eGFR = estimated glomerular filtration rate; ACE-i / ARB = ACE-inhibitor / angiotensin receptor blocker

Follow-up

During a median follow-up of 826 days (interquartile range: 563-1056), MACE occurred in 46 (6.5%) patients. Three (0.4%) patients had a myocardial infarction and 8 (1.1%) patients died. Thirty-six (5.1%) patients were revascularized during follow-up, of which 30 (4.2%) underwent percutaneous coronary intervention and 6 (0.8%) underwent coronary artery bypass graft. Of all revascularizations, 2 (5.6%) were acute revascularizations in myocardial infarction patients and 28 (77.8%) were CCTA-driven, performed within 60 days after CCTA. Patients with a low HEART score had a significantly better MACE-free survival than patients with an intermediate to high HEART score (Kaplan–Meier p = 0.010; Fig. 2).

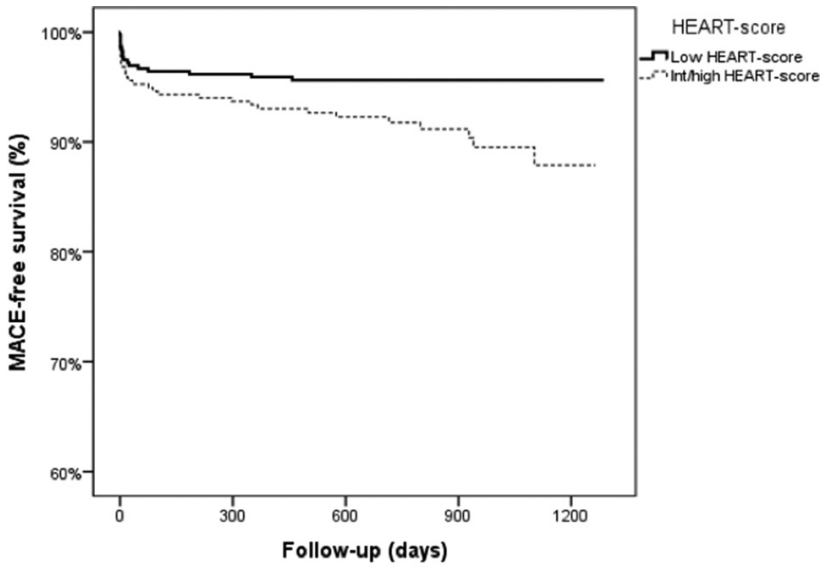

Follow-up (days)	0	300	600	900	1200
Low HEART-score	392	377	282	167	23
Int/high HEART-score	316	297	222	117	26

Figure 2. MACE-free survival in patients with low and intermediate/high HEART score

CCTA results and management

CCTA showed normal coronary arteries in 332 (45.4%) patients, nonobstructive CAD in 305 (43.0%) patients, and obstructive CAD in 83 (11.7%) patients. Based on

CCTA results, medication changes occurred in 300 (42.3%) patients of the total study population (Table 2).

Table 2. Pre- and post-test medication stratified by CCTA results

	Statin			Aspirin		
CCTA results	**Pre-test**	**Post-test**	**Change**	**Pre-test**	**Post-test**	**Change**
Normal coronary arteries	148 (46.0%)	65 (20.2%)	94 (29.2%)	154 (47.8%)	38 (11.8%)	119 (36.9%)
Non-obstructive CAD	172 (56.4%)	253 (83.0%)	104 (34.1%)	148 (48.5%)	155 (50.8%)	63 (20.7%)
Obstructive CAD	44 (53.0%)	76 (91.6%)	35 (42.2%)	38 (45.8%)	68 (81.9%)	30 (36.1%)
Overall	364 (51.3%)	394 (55.5%)	233 (32.8%)	340 (47.9%)	261 (36.8%)	212 (29.9%)

CCTA = coronary computed tomography angiography; CAD = coronary artery disease

CCTA results and HEART score

Table 3 shows CCTA results stratified by the different HEART score categories. Patients with a low HEART score had lower CAC S compared with patients with an intermediate/high HEART score ($P < 0.001$). Also patients with a low HEART score were less likely to have nonobstructive CAD at CCTA ($P = 0.024$). However, the HEART score was not significantly correlated with the presence of obstructive CAD at CCTA ($P = 0.29$). The receiver operator curve showed poor diagnostic value of the HEART score for obstructive CAD with an area under the receiver–operator curve of 0.53. No difference was seen in medication changes after CCTA between low and intermediate/high HEART score patients (41.7%, n = 164 and 42.9%, n = 136, respectively; $p = 0.75$).

Discussion

Several scores have been developed to aid the ED physician in identifying chest pain patients with a high risk of MACE who warrant more aggressive diagnostic and treatment strategies and those with low risk, who can be safely discharged. For this purpose, the HEART score has been found to be a promising tool, outperforming more conventional risk scores, especially in low–intermediate risk population.(3,5,14)

Table 3. CCTA data

	Low HEART-score (n=393)	Intermediate/high HEART-score (n=317)	p-value
CACS			
0	213 (54.2%)	138 (43.5%)	0.005
0.1-100	138 (35.1%)	94 (29.7%)	0.12
100-400	27 (6.9%)	53 (16.7%)	<0.001
>400	15 (3.8%)	32 (10.1%)	0.001
CCTA results			
Normal coronary arteries	198 (50.4%)	124 (39.1%)	0.003
Non-obstructive CAD	154 (39.2%)	151 (47.6%)	0.024
Obstructive CAD (>50%)	42 (10.7%)	42 (13.2%)	0.29
1-vessel	29 (7.4%)	34 (10.7%)	-
2-vessel	7 (1.8%)	8 (2.5%)	-
3-vessel	5 (1.3%)	1 (0.3%)	-
Left main	1 (0.3%)	1 (0.3%)	-

CCTA = coronary computed tomography angiography; CAD = coronary artery disease

This study confirms the prognostic value of the HEART score in low to intermediate risk chest pain patients with a follow-up of over 2 years. Patients with a low HEART score had significantly better MACE -free survival than patients with intermediate/high HEART score. Multiple recent studies have been conducted on the prognostic value of the HEART score for the occurrence of MACE, reporting MACE in 0.99-2% of patients with a low HEART score.(5,15–18) All of these studies, however, have evaluated MACE within 60 days after ED discharge. This study reports occurrence of MACE in 4.7% of patients, with a median follow-up of more than 2 years. It is the first study to report on the medium-term prognosis of patients with a low HEART score.

The predictive value of the HEART score of obstructive CAD has not been determined before. Previous research suggests that due to the low event rate in patients with a low HEART score, the HEART score can identify the true low risk population unlikely to gain from additional testing.(6) Our CCTA analysis reveals that the prevalence of obstructive CAD did not differ between the low and intermediate risk population (10.4% and 13.5%, respectively) with an area under the curve of only 0.53 for prediction of obstructive CAD. Furthermore, the percentage of change in medication after CCTA did not differ between the HEART score groups. Our study thus shows

that the discriminatory power of the HEART score for presence of obstructive CAD between low and intermediate risk patients is not strong enough to aid in adequate patient treatment and referral for further testing.

Although the HEART score cannot predict the presence of obstructive CAD, our CCTA results do demonstrate that a low HEART score identifies patients with less cardiovascular disease burden. There is less nonobstructive CAD in patients with a low HEART score compared with the intermediate/high HEART score patient group ($p = 0.024$). Also there are significantly more patients with a CACS of 0 and a CACS of <100 in the low HEART –score group ($p = 0.005$ and $p < 0.001$, respectively). This is of prognostic importance as a CACS of 0 in chest pain patients has a high negative predictive value (99.4%) for MACE over an average of 21 months follow-up.(19) Just over half of the low HEART score patients had a CACS of 0. Extensive previous research also shows that for patients with a CACS <100, the chance of MACE is low, with 2.3% to 5.9% 10-year event rate.(20) Still, 10.6% of patients with a low HEART score has CACS >100.

Although not part of our hypothesis, this study confirms the value of CCTA in this ED patient population in identifying CAD and in optimizing medical therapy. Several recent studies have shown that in the low–intermediate risk ED patients, CCTA is a reliable diagnostic tool for further identification of obstructive CAD and has incremental prognostic value for predicting MACE.(7-10) Driven by CCTA, medication was changed in 41% of our patient population. Since patients with both obstructive and nonobstructive CAD have a significantly higher risk of 1 year myocardial infarction and all cause mortality, it is reasonable to speculate that identifying and treating both these groups improves patient outcome.(18,21) Our results are in accordance with the ROMICAT,(10) with MACE in only 1 patient among patients without CAD at CCTA (0.3%) during 2 years follow-up.

One of the main limitations of our study is a referral bias. Patients were referred for CCTA upon the physician's judgment of the pretest likelihood for CAD. CCTA is deemed to be inappropriate in patients with a low (<10%) and high (>90%) pretest likelihood, according to the CCTA appropriateness criteria.(22) As a result, patients with a very low HEART score (0-1, n = 37) and high HEART score (7-10; n = 2) were

underrepresented in this cohort. This may have led to underestimation of the ability of the HEART to identify those with obstructive CAD. However, in the validation studies by Backus et al,(5) distribution among the different categories of the HEART score was comparable with our study, with the vast majority (82.5%) of patient with low or intermediate HEART score.(23) Also of all events in our study population, 28 (77.8%) were revascularizations performed within 60 days after CCTA and can thus be considered CCTA-driven, possibly leading to overestimation of event rate. This can explain the relatively high percentage of MACE (4.7%) in the low HEART score group when compared with the HEART score validation study (MACE 1.7%), where CCTA was not part of the study protocol.(5) Furthermore, the retrospective nature of our study and the single centre design may somewhat limit its extrapolation to other populations.

Conclusion

This study is the first study to confirm the prognostic value of the HEART score with a medium-term follow-up of more than 2 years in ED patients with chest pain. However, the HEART score was unable to discern between the presence or absence of obstructive CAD. Excluding patients from additional testing based solely on a low HEART score may lead to suboptimal patient management. CCTA had important implications on patient management (41% of patients) and may be a more appropriate tool to further stratify risk in low to intermediate risk chest pain patients presenting to the ED.

References

1. Herlitz J, Bång A, Isaksson L, et al. Outcome for patients who call for an ambulance for chest pain in relation to the dispatcher's initial suspicion of acute myocardial infarction. Eur J Emerg Med. 1995;2:75–82.
2. Pope JH, Aufderheide TP, Ruthazer R, et al. Missed diagnoses of acute cardiac ischemia in the emergency department. N Engl J Med. 2000;342:1163–1170.
3. Backus BE, Six AJ, Kelder JH, et al. Risk scores for patients with chest pain: evaluation in the emergency department. Curr Cardiol Rev. 2011;7:2–8.
4. Ferencik M, Schlett CL, Bamberg F, et al. Comparison of traditional cardiovascular risk models and coronary atherosclerotic plaque as detected by computed tomography for prediction of acute coronary syndrome in patients with acute chest pain. Acad Emerg

Med. 2012;19:934–942.
5. Backus BE, Six AJ, Kelder JC, et al. A prospective validation of the HEART score for chest pain patients at the emergency department. Int J Cardiol. 2013;168:2153–2158.
6. Mahler SA, Hiestand BC, Goff DC Jr, et al. Can the HEART score safely reduce stress testing and cardiac imaging in patients at low risk for major adverse cardiac events? Crit Pathw Cardiol. 2011;10:128–133.
7. Hoffmann U, Truong QA, Schoenfeld DA, et al; ROMICAT -II Investigators. Coronary CT angiography versus standard evaluation in acute chest pain. N Engl J Med. 2012;367:299–308.
8. Manini AF, Dannemann N, Brown DF, et al; Rule-Out Myocardial Infarction using Coronary Artery Tomography (ROMICAT) Study Investigators. Limitations of risk score models in patients with acute chest pain. Am J Emerg Med. 2009;27:43–48.
9. Litt HI, Gatsonis C, Snyder B, et al. CT angiography for safe discharge of patients with possible acute coronary syndromes. N Engl J Med. 2012;366:1393–1403.
10. Schlett CL, Banerji D, Siegel E, et al. Prognostic value of CT angiography for major adverse cardiac events in patients with acute chest pain from the emergency department: 2-year outcomes of the ROMICAT trial. JACC Cardiovasc Imaging. 2011;4:481–491.
11. Hamm CW, Bassand JP, Agewall S, et al; ESC Committee for Practice Guidelines. ESC Guidelines for the management of acute coronary syndromes in patients presenting without persistent ST-segment elevation: the Task Force for the management of acute coronary syndromes (AC S) in patients presenting without persistent ST-segment elevation of the European Society of Cardiology (ESC). Eur Heart J. 2011;32:2999–3054.
12. Hou ZH, Lu B, Gao Y, et al. Prognostic value of coronary CT angiography and calcium score for major adverse cardiac events in outpatients. JACC Cardiovasc Imaging. 2012;5:990–999.
13. Bogaard K, van der Zant FM, Knol RJ, et al. High-pitch prospective ECGtriggered helical coronary computed tomography angiography in clinical practice: image quality and radiation dose. Int J Cardiovasc Imaging. 2015;31:125–133.
14. Six AJ, Backus BE, Kelder JC. Chest pain in the emergency room: value of the HEART score. Neth Heart J. 2008;16:191–196.
15. Leite L, Baptista R, Leitão J, et al. Chest pain in the emergency department: risk stratification with Manchester triage system and HEART score. BMC Cardiovasc Disord. 2015;15:48.
16. Visser A, Wolthuis A, Breedveld R, et al. HEART score and clinical gestalt have similar diagnostic accuracy for diagnosing AC S in an unselected population of patients with chest pain presenting in the ED. Emerg Med J. 2015;32:595–600.

17. Six AJ, Cullen L, Backus BE, et al. The HEART score for the assessment of patients with chest pain in the emergency department: a multinational validation study. Crit Pathw Cardiol. 2013;12:121–126.
18. Maddox TM, Stanislawski MA, Grunwald GK, et al. Nonobstructive coronary artery disease and risk of myocardial infarction. JAMA. 2014;312:1754–1763.
19. Tota-Maharaj R, McEvoy JW, Blaha MJ, et al. Utility of coronary artery calcium scoring in the evaluation of patients with chest pain. Crit Pathw Cardiol. 2012;11:99–106.
20. Hecht HS. Coronary artery calcium scanning: past, present, and future. JACC Cardiovasc Imaging. 2015;8:579–596.
21. Bittencourt MS, Hulten E, Ghoshhajra B, et al. Prognostic value of nonobstructive and obstructive coronary artery disease detected by coronary computed tomography angiography to identify cardiovascular events. Circ Cardiovasc Imaging. 2014;7:282–291.
22. Taylor AJ, Cerqueira M, Hodgson JMcB et al. 2010 Appropriate use criteria for cardiac computed tomography. Circulation. 2010;122:e525–e555.
23. Backus BE, Six AJ, Kelder JC, et al. Chest pain in the emergency room: a multicenter validation of the HEART Score. Crit Pathw Cardiol. 2010;9:164–169.

Chapter 5

Diagnostic value of comprehensive on-site and off-site coronary CT angiography for identifying hemodynamically obstructive coronary artery disease

Michiel J. Bom, Roel S. Driessen, A. Kurata, Henk Everaars, Stefan P. Schumacher, Pepijn A. van Diemen, Peter M. van de Ven, Albert C. van Rossum, Charles A. Taylor, J.K. Min, J.A. Leipsic, Ibrahim Danad, and Paul Knaapen

J Cardiovasc Comput Tomogr. 2021;15(1):37-45

Abstract

Background: This study aimed to investigate the diagnostic value of comprehensive on-site coronary computed tomography angiography (CCTA) using stenosis and plaque measures and subtended myocardial mass (V_{sub}) for fractional flow reserve (FFR) defined hemodynamically obstructive coronary artery disease (CAD). Additionally, the incremental diagnostic value of off-site CT-derived FFR (FFR_{CT}) was assessed.

Methods: Prospectively enrolled patients underwent CCTA followed by invasive FFR interrogation of all major coronary arteries. Vessels with ≥30% stenosis were included for analysis. On-site CCTA assessment included qualitative and quantitative stenosis (visual grading and minimal lumen area, MLA) and plaque measures (characteristics and volumes), and V_{sub}. Diagnostic value of comprehensive on-site CCTA assessment was tested by comparing area under the curves (AUC). In vessels with available FFR_{CT}, the incremental value of off-site FFR_{CT} was tested.

Results: In 236 vessels (132 patients), MLA, positive remodeling, non-calcified plaque volume, and V_{sub} were independent on-site CCTA predictors for hemodynamically obstructive CAD ($p<0.05$ for all). V_{sub}/MLA^2 outperformed all these on-site CCTA parameters (AUC=0.85) and V_{sub} was incremental to all other CCTA predictors (p=0.02). In subgroup analysis (n=194 vessels), diagnostic performance of FFR_{CT} and V_{sub}/MLA^2 was similar (AUC 0.89 and 0.85 respectively, p=0.25). Furthermore, diagnostic performance significantly albeit minimally increased when FFR_{CT} was added to on-site CCTA assessment (ΔAUC=0.03, p=0.02).

Conclusions: In comprehensive on-site CCTA assessment, V_{sub}/MLA2 demonstrated greatest diagnostic value for hemodynamically obstructive CAD and V_{sub} was incremental to all evaluated CCTA indices. Additionally, adding FFR_{CT} only minimally increased diagnostic performance, demonstrating that on-site CCTA assessment is a reasonable alternative to FFR_{CT}.

Introduction

Coronary computed tomography angiography (CCTA) is an established non-invasive imaging modality in the diagnostic work-up of patients with suspected coronary artery disease (CAD).(1) Visual assessment of stenosis severity using CCTA is characterized by a high sensitivity and negative predictive value rendering it ideal for to exclude the presence of hemodynamically obstructive CAD.(2) However, the diagnostic performance of CCTA is hampered by a relatively low specificity. Several novel CCTA indices, obtained on-site from standard CCTA data, have been linked with impaired fractional flow reserve (FFR) and subsequently have been proposed to increase specificity and diagnostic performance of CCTA. Among these parameters are quantitative measurements of stenosis severity such as minimal lumen area (MLA), qualitative and quantitative assessment of atherosclerotic plaques such as plaque characteristics and volume, and more recently subtended myocardial mass (V_{sub}).(3-8) Incorporation of subtending myocardial mass in CCTA assessment may improve detection of impaired FFR since the hyperemic pressure gradient across a lesion is directly depended on the hyperemic blood flow which in turn depends on the myocardial mass.(9) Additionally, V_{sub}/MLA^2, a mathematical CCTA index based on the Hagen-Poiseuille law, has been proposed to increase diagnostic performance of standard CCTA assessment.(7) Besides these on-site CCTA parameters, remotely performed CT-derived FFR (FFR_{CT}) has emerged as a promising tool for the functional assessment of stenoses.(10-13) To date, the diagnostic value of comprehensive on-site CCTA assessment including V_{sub}/MLA^2 has not been compared with off-site FFR_{CT}. The current study therefore aimed to investigate the diagnostic value of comprehensive on-site CCTA assessment including qualitative and quantitative plaque and stenosis measures and V_{sub}/MLA^2 for hemodynamically obstructive CAD as defined by invasive FFR. Additionally, the incremental diagnostic value of the off-site assessment of FFR_{CT} was tested.

Methods

Study population

The current report is a substudy of the PACIFIC trial and details regarding the study design are described previously.(14) In brief, 208 patients with suspected CAD

underwent non-invasive imaging including CCTA, followed by invasive coronary angiography with FFR measurement in all major coronary arteries. For the present study all vessels with ≥30% angiographic stenosis on invasive coronary angiography (ICA) were included. The following exclusion criteria were used: 1) insufficient image quality of CCTA; 2) vessels in which CCTA showed a total occlusion; 3) LAD and LCX were excluded in the presence of a left main stenosis ≥30%; 4) RCA vessels were excluded when analysis of V_{sub} showed no LV myocardial mass was supplied by the RCA. The study protocol was approved by the Medical Ethics Committee of the VU University Medical Center and written informed consent was obtained from all participants.

CCTA acquisition

Patients underwent CCTA on a 256-slice CT-scanner (Brilliance iCT, Philips Healthcare, Best, the Netherlands) with a collimation of 128 x 0.625 mm and a tube rotation time of 270 ms. Tube current was set between 200 and 360 mAs at 120 kV, adjusting primarily the mAs based on body habitus. Axial scanning was performed with prospective ECG-gating (Step & Shoot Cardiac, Philips Healthcare) at 75% of the R-R interval. A bolus of 100 mL iobitidol (Xenetix 350) was injected intravenously (5.7 mL/s) followed by a 50 mL saline flush. The scan was triggered using an automatic bolus tracking technique, with a region of interest placed in the descending thoracic aorta with a threshold of 150 Hounsfield Units (HU). In patients with a prescan heart rate of ≥65 beats per minute, metoprolol 50 to 150 mg was administered orally one hour before the start of the CT protocol. If necessary, 5 to 25 mg metoprolol was given intravenously just before the scan to achieve a heart rate <65 bpm. All patients received 800 mcg of sublingual nitroglycerine immediately before scanning.

CCTA analysis

A schematic overview of the combined on and off-site CCTA assessment is provided in Figure 1. Using dedicated semi-automated software (Comprehensive Cardiac Analysis, Philips Healthcare), all coronary segments with a diameter ≥2 mm were assessed by an experienced reader blinded to invasive data. The coronary tree was evaluated using axial, multiplanar reformation, maximum intensity projection, and cross-sectional images (slice thickness 0.9mm, increment 0.50mm). The centerline and vessel

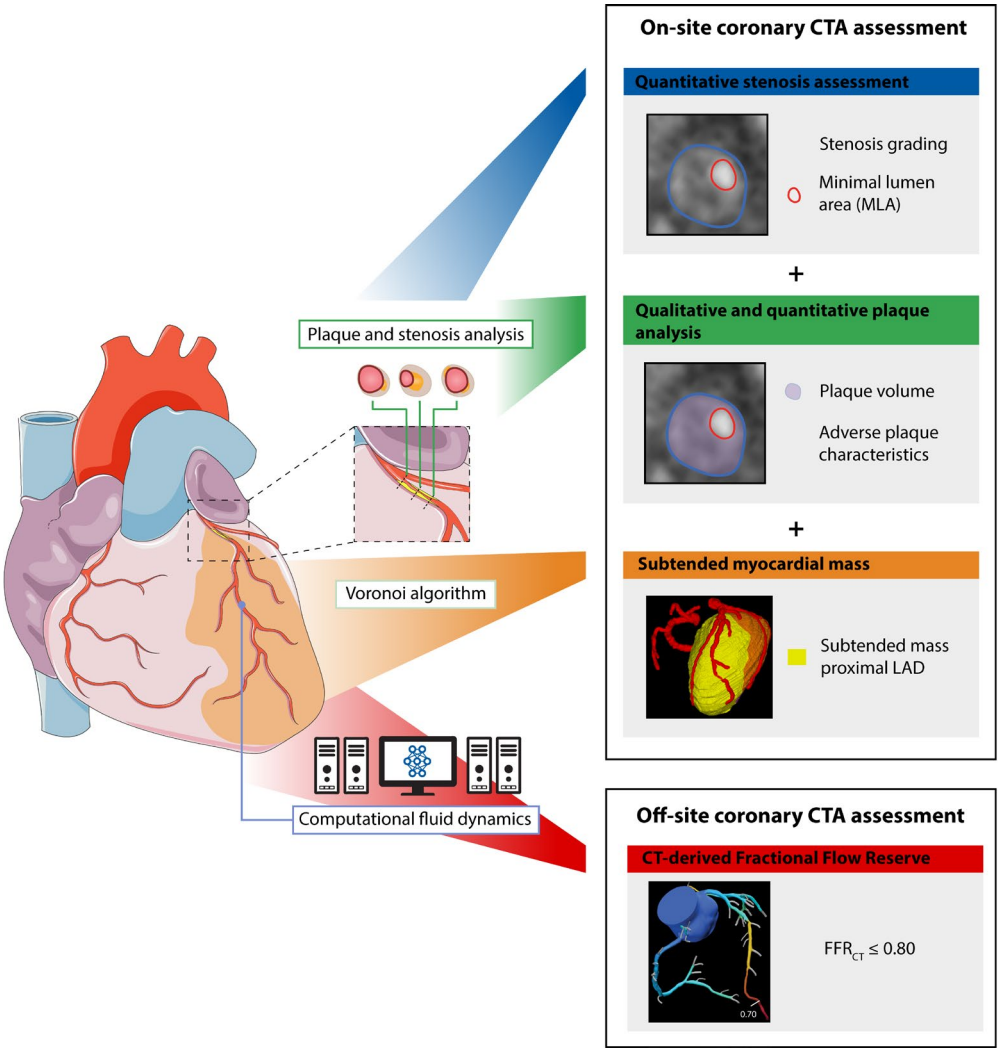

Figure 1. Combined on and off-site CCTA assessment
CCTA assessment comprised of both on-site and off-site assessment. In on-site assessment, qualitative and quantitative stenosis (visual grading and MLA) and plaque measures (characteristics and volumes) were obtained. Furthermore, subtended myocardial mass (Vsub) to a stenosis was calculated using the Voronoi algorithm. Off-site assessment comprised of FFRCT analysis which is based on computation fluid dynamics and performed off-site by HeartFlow. In this particular case, CCTA showed a >70% stenosis in the proximal LAD with a MLA of 0.30. Plaque analysis demonstrated a low-attenuation plaque with positive remodeling and a napkin ring sign, with a total plaque volume of 361 mm3, of which 242 mm3 was non-calcified. The myocardial mass subtended by this stenosis was 84.0 mL and off-site assessment demonstrated an FFRCT of 0.61. CCTA, coronary computed tomography angiography; FFR, fractional flow reserve; MLA, minimal lumen area; Vsub, subtended myocardial mass

contours were automatically reconstructed, with manual corrections if necessary. Stenosis severity was graded as 0, 1-24, 25-49, 50-69, and ≥70%. Qualitative coronary plaque analysis was performed to define the presence of the following adverse plaque characteristics: positive remodeling (PR), low attenuation plaque, spotty calcification, and napkin ring sign.(6) The remodeling index was computed as the ratio of vessel area at the site of the maximal lesion to that of a proximal reference point, with an index >1.1 representing PR. Low attenuation plaque was defined as a plaque containing any voxel <30 HU. Spotty calcification was characterized by a calcified plaque comprising <90° of the vessel circumference and <3 mm in length. Napkin ring sign was defined by a plaque core with low CT attenuation surrounded by a rim-like area of higher CT attenuation. Subsequently, quantitative plaque analysis was performed, automatically within manually designated regions. Total plaque lengths and volumes were calculated per vessel by summing the lengths and volumes of separate plaques along each coronary artery. A scanner-specific threshold of 150 HU was used for distinguishing non-calcified from calcified plaque components, which subsequently was used to determine non-calcified (NCPV) and calcified plaque volumes. MLA was assessed in short axis views at the site of maximal stenosis.

Analysis of subtended myocardial mass

Analysis of Vsub was performed by a core laboratory blinded to FFR and FFR_{CT} data (Ehime University Graduate School of Medicine, Ehime, Japan). All CCTA data together with still images of angiography were provided to the core laboratory to match the measurements of myocardial mass with stenoses sites. Analysis was performed using the Voronoi algorithm-based myocardial segmentation software (VirtualPlace Arata, AZE Ltd., Tokyo, Japan). The Voronoi diagram is a mathematical partitioning method that divides area based on predetermined points (15) and has been applied to divide organ sections (the left ventricular myocardium) by constructing surfaces representing the shortest bisectors for each vessel (coronary arteries) on CT, as previously validated.(16, 17) V_{sub} was defined as the myocardial mass subtended by a particular coronary stenosis.

FFR_{CT} analysis

FFR_{CT} analysis was performed by HeartFlow Inc. (Redwood City, CA, USA), blinded

to invasive data. FFR_{CT} is derived post hoc from standard CCTA data using previously described methodology.(13) In short, it involves extraction of a patient specific geometric model of the coronary arteries, population-derived physiological models, and computational fluid dynamics techniques to solve the governing equations of blood flow for velocity and pressure under simulated hyperemic conditions. In the current study HeartFlow FFR_{CT} v2.7 was used. All CCTA scans were quality checked by HeartFlow to assess eligibility for FFR_{CT} analysis. Cases with severe image artefacts (i.e. noise, blooming, motion and misalignment) were rejected for analysis. Extraction of FFR_{CT} values was performed by a researcher (R.D.) with knowledge of the FFR wire position but blinded to the invasive FFR values. FFR_{CT} was taken at the same position as the invasive FFR wire based on angiographic images of the wire position.

Invasive coronary angiography and FFR

ICA and FFR measurements were performed as described previously.(14) In brief, all major coronary arteries were routinely interrogated by FFR except for occluded or subtotal lesions with a diameter stenosis ≥90%. Maximal hyperemia was induced by intracoronary (150 μg) or intravenous (140 $\mu g \cdot kg^{-1} \cdot min^{-1}$) administration of adenosine. An FFR of ≤0.80 was considered hemodynamically significant. In case FFR measurement was not performed, a stenosis of ≥ 90% was deemed significant.(18) Invasive FFR measurements were performed in the distal part of the vessel and not at a specific post-stenosis location, as per PACIFIC study protocol.

Statistical analyses

All statistical analyses were performed using the SPSS software package (version 20.0.0, IBM SPSS Statistics, Armonk, New York), except for receiver operating characteristics (ROC) curve analyses which were performed with MedCalc for Windows (version 12.7.8.0, MedCalc Software, Oostende, Belgium). Categorical variables are presented as frequencies with percentages. Continuous variables were tested for normal distribution. Normal distributed continuous variables are presented as mean ± SD. Non-normal distributed variables are presented as median with interquartile range. Plaque length, plaque volumes (total, non-calcified, and calcified), and V_{sub}/MLA^2 were logarithmical transformed to allow for parametric testing. Categorical variables of stenosis grade and plaque characteristics and continuous variables of MLA, plaque length, plaque

volumes (total, non-calcified, and calcified), V_{sub}/MLA^2, and FFR_{CT} were compared between groups using Generalized Estimating Equations, with Bonferroni correction to account for multiple testing where applicable. An exchangeable correlation structure was used to account for within-subject correlation. Spearman's correlations were used to measure the association between FFR and V_{sub}, MLA, and V_{sub}/MLA^2.

The analyses on the diagnostic value of on-site and off-site CCTA parameters were performed in a step-wise manner. First, generalized estimating equations (GEE) analyses were performed to identify independent predictors for hemodynamically obstructive CAD as defined by FFR ≤0.80. Second, ROC curve analyses were performed and diagnostic accuracies were calculated for only the identified CCTA parameters independently predictive for FFR, in addition to stenosis grade which is the parameter used in clinical practice for CCTA assessment.

GEE analysis was comprised of univariable analyses with subsequent multivariable analysis in which variables with $p<0.05$ in univariable analyses were included using backward elimination. Predicted values for the outcomes based on the fixed parts of the obtained models were exported to MedCalc to perform ROC curve analyses. V_{sub}/MLA^2 was not included in the multivariable GEE model due to collinearity with MLA and V_{sub}. ROC curve analyses were performed to test the diagnostic value of the identified CCTA parameters for hemodynamically obstructive CAD and to determine their optimal cutoffs based on the maximal sum of specificity and sensitivity (Youden index). Additionally, the incremental diagnostic value of the V_{sub}/MLA^2 to the other identified coronary CT parameters was tested by comparing the respective areas under the ROC curves. The order for addition of CCTA parameters in this analysis was based on their novelty, i.e. (1) stenosis measures, (2) qualitative plaque measures, (3) quantitative plaque measures, (4) subtended myocardial mass. ROC curve analyses were also used in the subgroup with available FFR_{CT}, to establish diagnostic value. Area under the curves (AUCs) were compared using the method of DeLong. A p-value <0.05 was considered statistically significant.

Results

Study population

Of all 208 initial patients, 205 with analyzable CCTA images were evaluated for inclusion in the current study. In these patients, 286 (47%) vessels showed a ≥30% angiographic stenosis. Of these 286 vessels, 26 (9%) were excluded because of ≥30% LM stenosis, 18 (6%) because CCTA showed a total occlusion, and 1 (0.3%) because of insufficient scan quality. Additionally, 5 (2%) vessels were excluded because of a left-dominant coronary anatomy in which the right coronary artery did not subtend left ventricular myocardium. This resulted in a final study population of 236 vessels in 132 patients. The baseline characteristics of these patients are shown in Table 1.

Table 1. Baseline characteristics

Demographics	**N = 132**
Age, years	60 ± 8
Male	95 (72%)
Body mass index	27 ± 3
Cardiovascular risk factors – no (%)	
Diabetes Mellitus type II	23 (17%)
Hypertension	60 (46%)
Hyperlipidaemia	54 (41%)
Current tobacco use	23 (17%)
History of tobacco use	66 (50%)
Family history of CAD	70 (53%)
Type of chest-pain – no (%)	
Typical angina	52 (39%)
Atypical angina	54 (41%)
Non-specific chest discomfort	26 (20%)
CCTA myocardial segmentation	
Total LV myocardial mass, mL	187.4 ± 44.3
LAD territory, %	45 ± 7%
LCX territory, %	31 ± 11%
RCA territory, %	24 ± 11%

CAD = coronary artery disease; LV = left ventricular

On-site CCTA assessment and FFR-defined hemodynamically obstructive CAD

Analysis of total myocardial mass in all 132 patients showed that the LAD territory was the largest (45 ± 7% of total LV mass), followed by the LCX territory (31 ± 11%) and the RCA territory (24 ± 11%), Table 1). Visual assessment of CCTA demonstrated ≥50% stenosis in 119 (50%) vessels. Of all 236 included vessels, 207 (88%) vessels were interrogated with invasive FFR. All vessels in which FFR was not performed (n=29) had a subtotal (>90%) or total occlusion on ICA and were thus deemed hemodynamically obstructed. An overview of CCTA characteristics stratified by FFR-defined hemodynamically obstructive CAD is presented in table 2. In qualitative

Table 2. CCTA charateristics of all included vessels stratified by FFR

	Overall (n=236)	FFR ≤ 0.80 (n=117)	FFR > 0.80 (n=119)	p-value
Qualitative assessment				
Stenosis grade				<0.001 *
0-24%	47 (20%)	13 (11%)	34 (29%)	0.01 †
25-49%	70 (30%)	21 (18%)	49 (41%)	0.004 †
50-69%	39 (17%)	25 (21%)	14 (11%)	0.12 †
70-100%	80 (34%)	58 (50%)	22 (18%)	<0.001 †
Plaque characteristics				
Low-attenuation plaque	61 (26%)	46 (39%)	15 (13%)	<0.001
Positive remodelling	52 (22%)	39 (33%)	13 (11%)	<0.001
Napkin ring sign	19 (8%)	14 (12%)	5 (4%)	0.046
Spotty calcification	26 (11%)	19 (16%)	7 (6%)	0.01
Quantitative assessment				
MLA, mm^2	1.8 ± 1.2	1.2 ± 0.7	2.3 ± 1.3	<0.001
Total plaque volume, mm^3	227.4 [104.4 - 364.3]	304.2 [181.3 - 418.2]	152.5 [69.4 - 286.2]	<0.001
NCPV, mm^3	55.8 [20.2 - 103.3]	84.9 [46.7 – 146.6]	29.3 [10.6 - 67.6]	<0.001
Calcified plaque volume, mm^3	145.7 [66.2 – 261.3]	180.0 [100.6 - 304.3]	99.3 [36.8 - 220.8]	<0.001
Plaque length, mm	38.4 [21.8 – 59.8]	45.4 [33.2 - 65.0]	29.9 [15.6 - 46.8]	<0.001
V_{sub}, mL	51.7 ± 26.9	61.7 ± 28.9	41.9 ± 20.5	<0.001
V_{sub}/MLA^2, mL/mm^4	18.6 [7.3 - 65.8]	52.4 [19.6 - 184.2]	8.3 [4.0 - 17.7]	<0.001
FFR_{CT} (n=194)	0.74 ± 0.14	0.64 ± 0.12	0.83 ± 0.09	<0.001

* overall test for comparing distribution across four categories, † test for comparing proportion of vessels in total sample falling within this category. FFR = fractional flow reserve; MLA = minimal lumen area; NCPV = non-calcified plaque volume; V_{sub} = subtended myocardial mass.

CCTA assessment, visually assessed stenosis grade was higher and adverse plaque characteristics (low attenuation plaque, PR, napkin ring sign, and spotty calcification) were more frequently present in vessels with vs. vessels without FFR-defined hemodynamically obstructive CAD ($p<0.05$ for all). In quantitative assessment, MLA was lower and total plaque volume, NCPV, calcified plaque volume, plaque length, and V_{sub} were all greater in vessels with than vessels without FFR ≤0.80 ($p<0.001$ for all). Additionally, mean V_{sub}/MLA^2 was also higher in vessels with vs. vessels without FFR ≤0.80. Significant correlations were found between MLA and FFR ($r=0.55$, $p<0.001$) and between V_{sub} and FFR ($r= -0.42$, $p<0.001$). Furthermore, a significant inverse correlation was noted between V_{sub}/MLA^2 and FFR (Figure 2, $r= -0.66$, $p<0.001$).

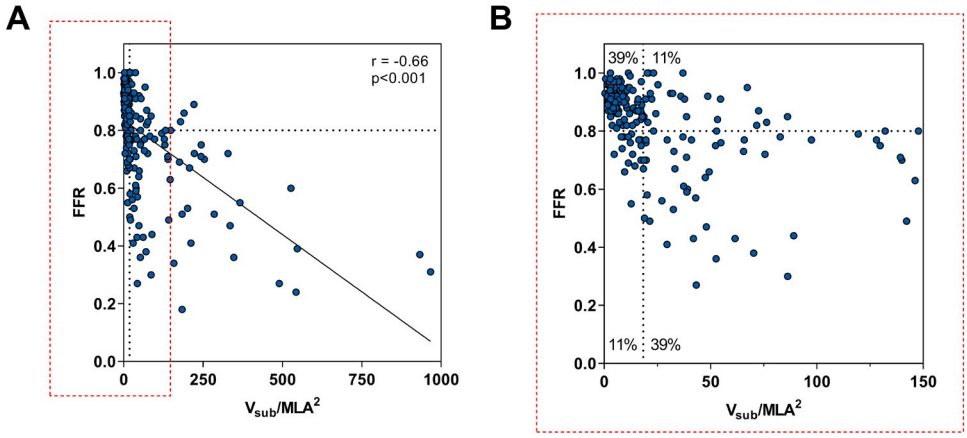

Figure 2. Relationship between Vsub/MLA2 and FFR
(A) Scatterplot demonstrating an inverse correlation between V_{sub}/MLA^2 and FFR ($r=-0.66$). (B) Zoomed in version of the scatterplot focusing on vessels with a Vsub/MLA2 of 0 – 150. Black dotted lines represent the cut-offs for FFR (0.80) and V_{sub}/MLA^2 (18.39). Concordance between V_{sub}/MLA^2 and FFR was 78%. Abbreviations as in Figure 1.

On-site CCTA derived predictors for FFR-defined hemodynamically obstructive CAD

Univariable and multivariable regression analyses identified MLA, PR, NCPV, and V_{sub} as independent predictors for FFR-defined hemodynamically obstructive CAD ($p<0.05$ for all, Table 3). The diagnostic value of these identified predictors was subsequently tested in ROC curve analysis (Figure 3). V_{sub}/MLA^2 significantly outperformed visual assessment of stenosis grading, NCPV, and MLA for the identification of

Table 3. Univariable and multivariable analysis on predictors of hemodynamically obstructive CAD as defined by FFR

	Univariable		Multivariable	
	OR (95% CI)	p-value	OR (95% CI)	p-value
Diameter stenosis	-	<0.001	-	-
0-24%	Reference	-	-	-
25-49%	1.33 (0.53 – 3.32)	0.54	-	-
50-69%	4.92 (1.85 – 13.09)	0.001	-	-
≥ 70%	6.94 (2.85 – 16.94)	<0.001	-	-
Plaque length, mm *	2.48 (1.73 – 3.55)	<0.001	-	-
Total PV, mm^3 *	2.16 (1.56 – 3.00)	<0.001	-	-
Non-calcified PV, mm^3 *	2.00 (1.49 – 2.69)	<0.001	1.74 (1.31 – 2.31)	<0.001
MLA, mm^2	0.27 (0.18 – 0.42)	<0.001	0.21 (0.13 – 0.34)	<0.001
Low-attenuation plaque	4.89 (2.47 – 9.68)	<0.001	-	-
Positive remodeling	4.31 (2.10 – 8.86)	<0.001	3.48 (1.40 – 8.63)	0.007
Spotty calcification	3.11 (1.40 – 6.91)	0.005	-	-
Napking ring sign	3.20 (1.02 – 10.07)	0.046	-	-
V_{sub} (per 10 mL)	1.36 (1.22 – 1.52)	<0.001	1.37 (1.18 – 1.59)	<0.001

* Plaque length, total PV, and non-calcified PV were logarithmical transformed. Abbreviations as in Table 2.

hemodynamically obstructive CAD (p-value for comparison with V_{sub}/MLA^2 <0.05 for all, Figure 3 left panel). Additionally, the incremental diagnostic value of V_{sub} to the other identified predictors is shown in Figure 3, right panel. Comprehensive on-site CCTA assessment including all identified predictors demonstrated excellent diagnostic performance with an AUC of 0.90 and V_{sub} was shown to possess incremental diagnostic value when added to MLA, PR, and NCPV (ΔAUC=0.02, p=0.03). ROC curve analysis identified 18.39 mL/mm^4 as optimal cut-off for V_{sub}/MLA^2, which was associated with a diagnostic accuracy of 78%. The diagnostic performance and identified cut-offs of all CCTA parameters for hemodynamically obstructive CAD are reported in Table 4.

Comparison of the diagnostic performance of on-site and off-site CCTA assessment

Off-site FFR_{CT} analysis was successfully performed in 194 (82%) vessels, due to failed analysis in 42 (18%) vessels. Reasons for failed analysis were related to increased heart rate during scanning, i.e. motion artefacts (38 vessels) and misalignment (4 vessels). Mean FFR_{CT} was lower in vessels with vs. without invasive FFR below the ischemic

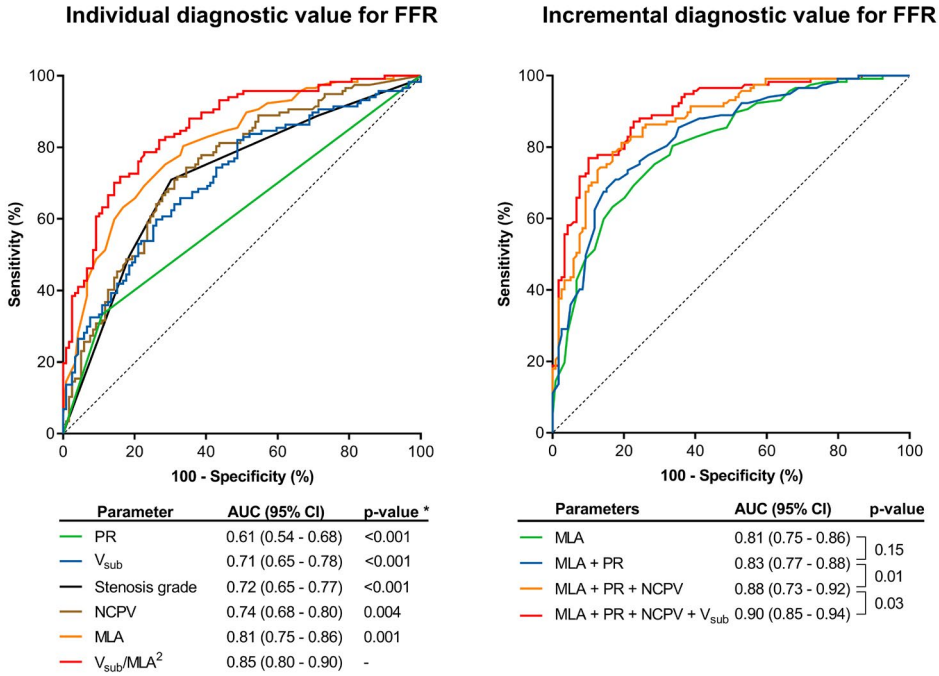

Figure 3. Diagnostic value of on-site CCTA parameters for hemodynamically obstructive CAD as defined by FFR

Receiver-operating characteristic (ROC) curve analysis with area under the curve (AUC) for the diagnostic value of different individual coronary computed tomography angiography (CTA) parameters for FFR-defined hemodynamically obstructive CAD is depicted on the left. The ROC curve analysis for the incremental diagnostic value of subsequently adding PR, NCPV and Vsub to MLA is depicted on the right. * p-value for comparison with V_{sub}/MLA^2. NCPV = non-calcified plaque volume; PR = positive remodeling; other abbreviations as in Figure 1.

cut-off (p<0.001, Table 2). Results of the ROC curve analysis on the diagnostic value of off-site CCTA assessment with FFR_{CT} as compared with on-site CCTA assessment are illustrated in Figure 4. Although numerically greater, no significant difference was found between the diagnostic values of FFR_{CT} and V_{sub}/MLA^2 for hemodynamically obstructive CAD (AUCs of 0.89 and 0.85 respectively, p=0.25, Figure 4 left panel). Furthermore, diagnostic performance did not significantly increase after addition of V_{sub} to CCTA assessment using MLA, PR, NCPV, and FFR_{CT} (ΔAUC=0.01, p=0.13). Contrary, addition of FFR_{CT} to comprehensive on-site CCTA assessment using MLA, PR, NCPV, and V_{sub} led to a significant albeit minimal increase in diagnostic performance (ΔAUC=0.03, p=0.02,Figure 4 right panel). Combined on and off-site CCTA assessment demonstrated excellent diagnostic value with an AUC of 0.94.

Table 4. Diagnostic performance of CCTA parameters for hemodynamically obstructive CAD as defined by FFR

	Sensitivity, %	Specificity, %	PPV, %	NPV, %	Accuracy, %
All vessels (n = 236)					
DS >50%	71 (62-79)	70 (61-78)	70 (63-76)	71 (64-77)	70 (64-76)
DS >70%	50 (40-59)	82 (73-88)	73 (63-80)	62 (57-67)	66 (59-72)
MLA (≤1.70 mm^2)	80 (72-87)	66 (57-75)	70 (64-75)	77 (70-84)	73 (67-79)
PR	33 (25-43)	89 (82-94)	75 (63-84)	58 (54-61)	61 (55-68)
NCPV (>49.8 mm^3)	74 (66-82)	65 (56-73)	67 (61-73)	72 (65-78)	69 (63-75)
V_{sub}	60 (50-69)	74 (65-82)	70 (62-76)	65 (59-71)	67 (61-73)
V_{sub}/MLA^2 (>18.39 mL/mm^4)	79 (70-86)	77 (69-84)	77 (71-83)	79 (72-84)	78 (72-83)
FFR_{CT} subgroup analysis (n = 194 vessels)					
MLA (≤1.20 mm^2)	63 (52-73)	83 (74-90)	78 (69-85)	70 (64-76)	73 (66-79)
V_{sub}/MLA^2 (>18.39 mL/mm^4)	78 (68-86)	78 (69-86)	77 (69-83)	79 (72-85)	78 (71-83)
FFR_{CT} (≤0.80)	90 (83-96)	68 (58-77)	73 (66-78)	88 (80-93)	79 (72-84)

DS = diameter stenosis; NPV = negative predictive value; PPV = positive predictive value; other abbreviations as in Table 2.

FFR_{CT} needed to be performed in 28 patients to correctly reclassify one patient using on-site CCTA assessment. Given the estimated costs of FFR_{CT} of $1.500, this resulted in an estimated cost per reclassification of $42.000.

Discussion

Our study evaluated the diagnostic value of comprehensive CCTA assessment for the identification of hemodynamically obstructive CAD as defined by FFR. On-site CCTA assessment revealed MLA, plaque measures (i.e. PR and NCPV), and V_{sub} to be independent predictors for hemodynamically obstructive CAD. Among the on-site parameters V_{sub}/MLA^2 demonstrated greatest diagnostic value and V_{sub} was shown to have incremental value to the other identified CCTA predictors. In the subgroup of vessels with available FFR_{CT}, the diagnostic value of off-site FFR_{CT} and V_{sub}/MLA^2 was found to be similar. Furthermore, diagnostic performance only minimally increased when FFR_{CT} was added to comprehensive on-site CCTA assessment. These results indicate that comprehensive on-site assessment is a reasonable alternative to off-site assessment using FFR_{CT}.

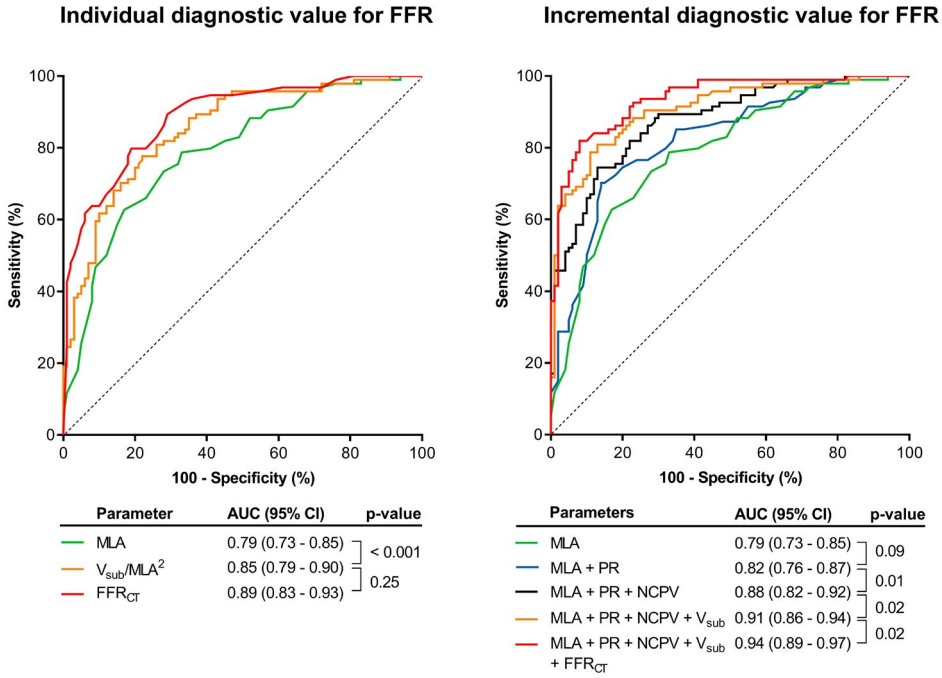

Figure 4. Diagnostic value of off-site FFR_{CT} for FFR-defined hemodynamically obstructive CAD
ROC curve analyses in the subgroup of vessels with available FFR_{CT} (n=194). ROC curves for the diagnostic value of the individual parameters MLA, V_{sub}/MLA^2 and FFR_{CT} for FFR-defined hemodynamically obstructive CAD are depicted on the left. ROC curves of the incremental diagnostic value of the different CCTA parameters is depicted on the right. FFR_{CT} had significant incremental diagnostic value for hemodynamically obstructive CAD (p=0.02). FFR_{CT} = computed tomography-derived FFR; other abbreviations as in Figure 3.

On-site plaque assessment using CCTA

Despite the excellent diagnostic potential of CCTA for the exclusion of CAD, its limited specificity has triggered the development of several functional CT parameters. In addition to quantitative measures of stenosis severity such as MLA, CCTA derived plaque measures have been extensively linked with FFR-defined hemodynamically obstructive CAD.(3-7) Two initial studies investigating plaque characterization using adverse plaque characteristics as well as total plaque volume have reported incremental value to MLA for prediction of hemodynamically obstructive CAD.(3, 4) More recently, Gaur et al. distinguished specific plaque composition volumes and showed that the non-calcified and in particular the low-attenuation plaque volume were predictive of FFR-defined hemodynamically obstructive CAD.(5) In line with this, a recent sub-study of the PACIFIC trial performed by our group, identified NCPV,

low attenuation plaque, spotty calcification, and PR to be associated with FFR.(6) The current PACIFIC trial sub-study corroborates these findings in the subgroup of vessels with ≥30% angiographic stenosis, showing independent predictive value of plaque measures, i.e. NCPV and PR. In addition, several studies have demonstrated a clear association between plaque characteristics and detrimental downstream myocardial perfusion.(6, 19) Despite this large body of evidence supporting the relationship between plaque characteristics and ischemia, the pathophysiological mechanisms underlying this relationship have yet to be clarified. It has been hypothesized that the presence of large necrotic cores within the neo-intima, visualized in CCTA as PR, low-attenuation plaque, and high NCPV, impairs the vasoregulatory ability of coronary arteries, predisposing to ischemia and abnormal FFR.(20) Future imaging studies however are warranted to test this hypothesis.

CCTA assessment of subtended myocardial mass

More recently, the CCTA based calculation of subtended myocardial mass has been proposed to improve CCTA prediction of FFR.(7, 8) The influence of the amount of subtended myocardial mass on the trans-stenotic pressure gradient and therefore on FFR, has been a longstanding physiological principle. However this hypothesized link has been primarily based on animal models showing that coronary flow is proportional to myocardial mass and on indirect data for clinical studies showing a relationship between ICA-derived estimates of mass and FFR.(9, 21) Recent advances in CCTA however have enabled calculation of myocardial mass subtended by a specific stenosis from standard CCTA data using the Voronoi algorithm.(16, 17). Two studies have recently used this analysis to confirm the dependence of FFR on subtended myocardial mass, showing an inverse correlation between V_{sub} and FFR.(7, 8) Additionally, Yang et al. demonstrated the independent diagnostic value of V_{sub} to comprehensive CCTA assessment including qualitative and quantitative stenosis and plaque measures, without specifying different plaque composition volumes (i.e. calcified and non-calcified). Contrary, total plaque volume and plaque characteristics had no incremental diagnostic value after correction for V_{sub} and MLA. Our study adds to these findings, by specifying different plaque composition volume and demonstrating independent diagnostic value of V_{sub} to comprehensive CCTA assessment including non-calcified plaque volume. Additionally, plaque quantification (i.e. NCPV and PR) remained

independently predictive for hemodynamically obstructive CAD after correction for MLA and V_{sub}. Hereby demonstrating the independent predictive value of both plaque characterization and V_{sub} in comprehensive on-site CCTA assessment.

Given the diagnostic potential of V_{sub}, Yang et al. proposed the mathematical index V_{sub}/MLA^2 as a potential functional CT index for the identification of hemodynamically obstructive CAD.(7) This novel index is based on the Hagen-Poiseuille law, which dictates that the trans-stenotic pressure drop is proportional to the flow rate divided by the square of the cross-sectional area. Since the flow rate is considered to be proportional to the myocardial mass and the MLA is a measure of the cross-sectional area for a given stenosis, V_{sub}/MLA^2 was proposed to resemble invasive FFR. Yang et al. showed that V_{sub}/MLA^2 indeed had good diagnostic performance for FFR (AUC=0.80), outperforming visual stenosis grading, MLA, and aggregated plaque volume. Furthermore, V_{sub} had incremental diagnostic value when added to comprehensive CCTA assessment including qualitative and quantitative stenosis and plaque measures. The current study confirms these findings, showing an inverse relationship between V_{sub}/MLA^2 and FFR (r = -0.66), superior diagnostic value of V_{sub}/MLA^2 to other on-site CCTA-derived predictors for FFR-defined hemodynamically obstructive CAD (i.e. MLA, PR, and NCPV) and incremental diagnostic value of V_{sub} to comprehensive on-site CCTA assessment. Comprehensive on-site CCTA assessment incorporating all predictive CCTA parameters demonstrated excellent diagnostic value with an AUC of 0.90. Of note, diagnostic performance of MLA, V_{sub}/MLA^2 and the combined on-site assessment were slightly better in the current study (AUCs of 0.80, 0.85, and 0.90 respectively) than in the study by Yang et al. (AUCs of 0.74, 0.80, and 0.84 respectively). This may be partly explained by the superior image quality of the 256-slice scanner used in the current report compared to the 64-slice scanner used partly in the study by Yang et al. Nonetheless, results from the current study clearly demonstrate the important diagnostic potential of a comprehensive on-site CCTA approach.

Off-site CCTA assessment using FFR_{CT}

In addition to the on-site assessment of CCTA, the remotely performed analysis of FFR_{CT}, in which computational fluid dynamics is employed on standard CCTA data,

has emerged as a promising tool for the functional assessment of coronary stenoses. The diagnostic value of remotely performed FFR_{CT} for FFR-defined hemodynamically obstructive CAD has been prospectively validated in several large multicenter studies (11, 12) and a recent head-to-head comparison demonstrated superiority on a per-vessel level to nuclear myocardial perfusion imaging.(10) The incremental value of FFR_{CT} to comprehensive on-site CCTA assessment was recently investigated by Gaur et al., showing improved prediction after addition of FFR_{CT} to stenosis severity and qualitative and quantitative plaque analyses.(5) In addition to the off-site assessment of FFR_{CT}, several studies have proposed diagnostic potential of a simplified on-site calculation of CT-derived FFR.(22, 23) Yang et al. tested the diagnostic performance of V_{sub}/MLA^2 against on-site CT-derived FFR and showed comparable performance between the two.(7) However, on-site CT-derived FFR tools have not been as extensively validated as remotely performed FFR_{CT} and further validation in large multicenter studies is warranted. The current report is the first to test the incremental diagnostic value of off-site FFR_{CT} to comprehensive on-site CCTA assessment using stenosis and plaque measures and V_{sub}. Results show that although diagnostic value of FFR_{CT} was numerically greater, no significant difference in diagnostic value was found between V_{sub}/MLA^2 and FFR_{CT} (AUCs of 0.85 and 0.89 respectively). Furthermore, the addition of FFR_{CT} to comprehensive on-site CCTA assessment led to a significant yet only minimal increase in diagnostic performance (AUC=0.94). These results indicate that the diagnostic potential of CCTA is optimized when on-site assessment of stenosis, plaque and V_{sub} is combined with off-site assessment of FFR_{CT}. Nonetheless, given the relatively small additional value of off-site FFR_{CT} and relatively high costs per reclassification, comprehensive on-site only CCTA assessment should be considered a reasonable alternative to off-site FFR_{CT}. Although V_{sub} is easy to perform and relatively independent of image quality and quick, clinical application of this comprehensive on-site approach is impeded by the laborious post-processing required for on-site plaque analysis. Advances in post-processing tools simplifying or automating comprehensive on-site CCTA assessment are warranted to allow widespread clinical application. Interestingly, diagnostic value of FFR_{CT} was remarkably lower in the current study than in the PACIFIC trial sub study by Driessen et al (AUC of 0.89 and 0.94 respectively).(10) This can be explained by the difference in cohort, since the current study only included vessels with ≥30% angiographic stenosis.

Limitations

First, the sample size of the current study was relatively small and the findings are not externally validated. Future prospective studies are warranted to validate the diagnostic value of comprehensive on and off-site assessment of CCTA in large clinical populations. Likewise, the identified optimal thresholds of the CCTA parameters are specific for the current population and were merely used to report on the diagnostic value of CCTA assessment. These threshold cannot be extrapolated to other populations and should be externally validated in larger prospective studies. Second, the analysis of V_{sub} was performed by a core laboratory for methodological purposes. Although not performed on-site in the current report, V_{sub}/MLA^2 was included in the comprehensive on-site CCTA assessment given the fact that V_{sub} analysis can be performed using commercially available software. Third, the current report included only stenosis with a ≥30% angiographic stenosis and excluded left main stenosis and chronic total occlusion, limiting the generalizability of our findings. Fourth, whereas V_{sub} analysis was possible in all vessels, FFR_{CT} analysis failed in a substantial amount of vessels (18%). Although in line with previous reports (11, 12), this relatively high rejection rate remains the most important limiting factor of the use of FFR_{CT} in clinical practice. Furthermore, the exclusion of cases in which FFR_{CT} analysis was not possible may have created an bias in favor of FFR_{CT}. Nonetheless, on-site assessment performed nearly as well as FFR_{CT}, demonstrating that comprehensive on-site CCTA assessment is a reasonable alternative to FFR_{CT}. Last, both invasive and CT angiography were used to match the V_{sub} measurements with the stenosis sites, while in clinical practice only CTA would be available. This may have created a bias in favor of V_{sub} and V_{sub}/MLA^2.

Conclusion

In comprehensive on-site CCTA assessment, MLA, plaque measures and V_{sub} were all independently predictive for the presence of FFR-defined hemodynamically obstructive CAD. V_{sub}/MLA^2 demonstrated greatest diagnostic value among the identified CCTA derived predictors and V_{sub} was shown to have incremental diagnostic value. The addition of off-site FFR_{CT} to on-site CCTA analysis only minimally increased diagnostic performance for the identification of hemodynamically obstructive CAD. These results demonstrate that comprehensive on-site CCTA assessment is a reasonable

alternative to off-site assessment using FFR_{CT}.

References

1. Knuuti J, Wijns W, Saraste A, et al. 2019 ESC Guidelines for the diagnosis and management of chronic coronary syndromes. Eur Heart J 2020;41:407-77.
2. Meijboom WB, Meijs MF, Schuijf JD, et al. Diagnostic accuracy of 64-slice computed tomography coronary angiography: a prospective, multicenter, multivendor study. J Am Coll Cardiol 2008;52:2135-44.
3. Nakazato R, Shalev A, Doh JH, et al. Aggregate plaque volume by coronary computed tomography angiography is superior and incremental to luminal narrowing for diagnosis of ischemic lesions of intermediate stenosis severity. J Am Coll Cardiol 2013;62:460-7.
4. Park HB, Heo R, Hartaigh B, et al. Atherosclerotic plaque characteristics by CT angiography identify coronary lesions that cause ischemia: a direct comparison to fractional flow reserve. JACC Cardiovasc Imaging 2015;8:1-10.
5. Gaur S, Ovrehus KA, Dey D, et al. Coronary plaque quantification and fractional flow reserve by coronary computed tomography angiography identify ischaemia-causing lesions. Eur Heart J 2016;37:1220-7.
6. Driessen RS, Stuijfzand WJ, Raijmakers PG, et al. Effect of Plaque Burden and Morphology on Myocardial Blood Flow and Fractional Flow Reserve. J Am Coll Cardiol 2018;71:499-509.
7. Yang DH, Kang SJ, Koo HJ, et al. Incremental Value of Subtended Myocardial Mass for Identifying FFR-Verified Ischemia Using Quantitative CT Angiography: Comparison With Quantitative Coronary Angiography and CT-FFR. JACC Cardiovasc Imaging 2019;12:707-17.
8. Kim HY, Lim HS, Doh JH, et al. Physiological Severity of Coronary Artery Stenosis Depends on the Amount of Myocardial Mass Subtended by the Coronary Artery. JACC Cardiovasc Interv 2016;9:1548-60.
9. Choy JS, Kassab GS. Scaling of myocardial mass to flow and morphometry of coronary arteries. J Appl Physiol (1985) 2008;104:1281-6.
10. Driessen RS, Danad I, Stuijfzand WJ, et al. Comparison of Coronary Computed Tomography Angiography, Fractional Flow Reserve, and Perfusion Imaging for Ischemia Diagnosis. J Am Coll Cardiol 2019;73:161-73.
11. Norgaard BL, Leipsic J, Gaur S, et al. Diagnostic performance of noninvasive fractional flow reserve derived from coronary computed tomography angiography in suspected coronary artery disease: the NXT trial (Analysis of Coronary Blood Flow Using CT Angiography: Next Steps). J Am Coll Cardiol 2014;63:1145-55.

12. Min JK, Leipsic J, Pencina MJ, et al. Diagnostic accuracy of fractional flow reserve from anatomic CT angiography. JAMA 2012;308:1237-45.
13. Taylor CA, Fonte TA, Min JK. Computational fluid dynamics applied to cardiac computed tomography for noninvasive quantification of fractional flow reserve: scientific basis. J Am Coll Cardiol 2013;61:2233-41.
14. Danad I, Raijmakers PG, Driessen RS, et al. Comparison of Coronary CT Angiography, SPECT, PET, and Hybrid Imaging for Diagnosis of Ischemic Heart Disease Determined by Fractional Flow Reserve. JAMA Cardiol 2017;2:1100-7.
15. Guibas LS, J. Primitives for the Manipulation of General Subdivisions and the Computations of Voronoi Diagrams. ACM Transactions on Graphics 1985;4:74-123.
16. Ide S, Sumitsuji S, Yamaguchi O, Sakata Y. Cardiac computed tomography-derived myocardial mass at risk using the Voronoi-based segmentation algorithm: A histological validation study. J Cardiovasc Comput Tomogr 2017;11:179-82.
17. Kurata A, Kono A, Sakamoto T, et al. Quantification of the myocardial area at risk using coronary CT angiography and Voronoi algorithm-based myocardial segmentation. Eur Radiol 2015;25:49-57.
18. Tonino PA, Fearon WF, De Bruyne B, et al. Angiographic versus functional severity of coronary artery stenoses in the FAME study fractional flow reserve versus angiography in multivessel evaluation. J Am Coll Cardiol 2010;55:2816-21.
19. Dey D, Diaz Zamudio M, Schuhbaeck A, et al. Relationship Between Quantitative Adverse Plaque Features From Coronary Computed Tomography Angiography and Downstream Impaired Myocardial Flow Reserve by 13N-Ammonia Positron Emission Tomography: A Pilot Study. Circ Cardiovasc Imaging 2015;8:e003255.
20. Ahmadi A, Stone GW, Leipsic J, et al. Association of Coronary Stenosis and Plaque Morphology With Fractional Flow Reserve and Outcomes. JAMA Cardiol 2016;1:350-7.
21. Leone AM, De Caterina AR, Basile E, et al. Influence of the amount of myocardium subtended by a stenosis on fractional flow reserve. Circ Cardiovasc Interv 2013;6:29-36.
22. Coenen A, Kim YH, Kruk M, et al. Approach to Coronary Computed Tomographic Angiography-Based Fractional Flow Reserve: Result From the MACHINE Consortium. Circ Cardiovasc Imaging 2018;11:e007217.
23. Fujimoto S, Kawasaki T, Kumamaru KK, et al. Diagnostic performance of on-site computed CT-fractional flow reserve based on fluid structure interactions: comparison with invasive fractional flow reserve and instantaneous wave-free ratio. Eur Heart J Cardiovasc Imaging 2019;20:343-52.

Chapter 6

Predictive value of targeted proteomics for coronary plaque morphology in patients with suspected coronary artery disease

Michiel J. Bom*, Evgeni Levin*, Roel S. Driessen, Ibrahim Danad, Cornelis C. Van Kuijk, Albert C. van Rossum, Jagat Narula, James K. Min, Jonathon A. Leipsic, João P. Belo Pereira, Charles A. Taylor, Max Nieuwdorp, Pieter G. Raijmakers, Wolfgang Koenig, Albert K. Groen, Erik S.G. Stroes, and Paul Knaapen

* Both authors contributed equally

EBioMedicine. 2019;39:109-117

Abstract

Background: Risk stratification is crucial to improve tailored therapy in patients with suspected coronary artery disease (CAD). This study investigated the ability of targeted proteomics to predict presence of high-risk plaque or absence of coronary atherosclerosis in patients with suspected CAD, defined by coronary computed tomography angiography (CCTA).

Methods: Patients with suspected CAD (n=203) underwent CCTA. Plasma levels of 358 proteins were used to generate machine learning models for the presence of CCTA-defined high-risk plaques or complete absence of coronary atherosclerosis. Performance was tested against a clinical model containing generally available clinical characteristics and conventional biomarkers.

Findings: A total of 196 patients with analyzable protein levels (n=332) was included for analysis. A subset of 35 proteins was identified predicting the presence of high-risk plaques. The developed machine learning model had fair diagnostic performance with an area under the curve (AUC) of 0.79±0.01, outperforming prediction with generally available clinical characteristics (AUC=0.65±0.04, $p<0.05$). Conversely, a different subset of 34 proteins was predictive for the absence of CAD (AUC=0.85±0.05), again outperforming prediction with generally available characteristics (AUC=0.70±0.04, $p<0.05$).

Interpretation: Using machine learning models, trained on targeted proteomics, we defined two complementary protein signatures: one for identification of patients with high-risk plaques and one for identification of patients with absence of CAD. Both biomarker subsets were superior to generally available clinical characteristics and conventional biomarkers in predicting presence of high-risk plaque or absence of coronary atherosclerosis. These promising findings warrant external validation of the value of targeted proteomics to identify cardiovascular risk in outcome studies.

Introduction

Coronary CT angiography (CCTA) is a commonly used non-invasive imaging modality for the diagnostic work-up of patients with suspected coronary artery disease (CAD). In addition to the evaluation of stenosis grade, CCTA allows in-vivo phenotyping of plaque morphology and identification of high-risk plaques, i.e. plaques with a high likelihood of causing an acute coronary event.(1-3) Although current guidelines emphasize the need for adequate risk-assessment in suspected CAD patients,(4) traditional risk stratification, using generally available clinical risk factors, plasma lipid levels and other conventional biomarkers (troponin T, NT-proBNP, and CRP) have only modest predictive value for the presence of coronary atherosclerosis and the occurrence of events.(5-9) This underscores the need for novel biomarkers predictive for coronary atherosclerosis. In the search for these biomarkers, several individual inflammatory plasma proteins have been linked to the pathophysiology of atherosclerosis.(10) Recently, the development of proximity extension assays (PEA) has enabled simultaneous measurement of large numbers of proteins using only one microliter of plasma, thereby enabling the use of proteomics in large clinical populations.(11) In parallel, the introduction of machine learning has emerged as a highly effective method for prediction.(12) This study therefore aimed to investigate the ability of a large set of 358 biomarkers to identify either CCTA-derived high-risk coronary lesions or absence of coronary atherosclerosis in patients with suspected CAD using machine learning. Additionally, the added value of these biomarker panels to generally available clinical characteristics and conventional biomarkers was tested.

Methods

Study population

The current report is a sub-study of the PACIFIC trial and details regarding the study design have been described previously.(13) The study population consisted of 208 consecutively selected out-patients with stable new-onset chest pain and suspected CAD. All patients were aged 40 years and above and had intermediate pre-test probability for CAD as defined by Diamond and Forrester criteria. Major exclusion criteria were renal failure (i.e. eGFR < 45 mL/min), history of COPD or chronic asthma, a prior history of CAD, atrial fibrillation, and second or third degree AV

block. All patients underwent a two day protocol, including CCTA on day 1 and blood sampling on day 2 (within 2 weeks). Both CCTA imaging and laboratory sampling were performed as dictated by the study protocol and independent of clinical status. For the current analysis all patients with CCTA images eligible for plaque analysis and with available laboratory samples were included (n=203). The study protocol was approved by the Medical Ethics Committee of the VU University Medical Center and written informed consent was obtained.

Proteomics analysis

Patients were fasting for at least 12 hours, resting for at least 10 minutes and sitting in a upright position before blood sampling was performed. After blood samples were collected, EDTA plasma samples were stored at -80 °C for a mean period of 4.1±0.8 years before analysis. None of the samples were thawed and refrozen before analysis. After completion of the study, available EDTA plasma samples of the complete cohort were shipped to Olink Proteomics AB (Uppsala, Sweden) for analysis. Using PEA technology, levels of 358 proteins were measured (Supplementary Table 1). The PEA technology has been described previously.(11) In brief, pairs of oligonucleotide-labeled antibody probes bind to their targeted protein, and if the two probes are brought in close proximity the oligonucleotides will hybridize in a pair-wise manner. The addition of a DNA polymerase leads to a proximity-dependent DNA polymerization event, generating a unique PCR target sequence. The resulting DNA sequence is subsequently detected and quantified using a microfluidic real-time PCR instrument (Biomark HD, Fluidigm Corporation, CA, USA). Data is quality controlled and normalized using an internal extension control and an inter-plate control, to adjust for intra- and inter-run variation. The extension control is composed of an antibody coupled to a unique pair of DNA-tags that serves as a synthetic control that is added to every sample well. It will adjust for technical variation introduced in the extension step and hence reduce intra-assay variability. The final assay read-out is presented in Normalized Protein eXpression (NPX) values, which is an arbitrary unit on a log2-scale where high values correspond to higher protein expressions. Patients with samples that failed quality control were excluded. Furthermore, proteins were excluded from analysis if >20% of individual measurements were below the lower limit of detection. When <20% was below lower limit of detection, missing values were replaced by the limit of detection

divided by two. All assay validation data for the proteins in the Cardiovascular II, Cardiovascular III, Cardiometabolic and Inflammation panels (detection limits, intra- and inter-assay precision data, accuracy, etc) are available on manufacturer's website (www.olink.com). Across all 92 assays in Cardiovascular II, the mean intra-assay (within-run) and inter-assay (between-run) variations expressed as coefficients of variation are reported to be 9.1% and 11.7%. For assays in the Cardiovascular III panel intra- and inter-assay variation are reported to be 8.1% and 11.4% respectively, for assays in the Inflammation panel 7% and 18% respectively, and for assays in the Cardiometabolic panel 12.9% and 9.5% respectively.

CCTA acquisition and plaque analysis

Patient preparation, acquisition of CCTA, methodology for plaque analysis, and coronary artery calcium scoring are described in detail in the Supplementary Methods. In short, patients underwent CCTA on a 256-slice CT-scanner (Brilliance iCT, Philips Healthcare, Best, the Netherlands) with prospective ECG-gating (Step & Shoot Cardiac, Philips Healthcare) at 75% of the R-R interval. Absence of CAD was defined as a coronary calcium score of zero and CT angiography showing no coronary plaques. Coronary lesions were analyzed for the following adverse plaque characteristics: positive remodeling, low attenuation plaque, spotty calcification, and napkin ring sign. A high-risk coronary lesion was defined as a lesion with ≥2 adverse plaque characteristics.(14)

Descriptive statistics

Descriptive statistical analyses were performed using the SPSS software package (version 20.0.0, IBM SPSS Statistics, Armonk, New York). Continuous variables were tested for normal distribution. Normal distributed continuous variables are presented as mean ± SD. Non-normal distributed variables are presented as median with interquartile range. Categorical variables are presented as frequencies with percentages and compared with the chi-square test or Fisher's exact test were applicable. Variables were compared with the chi-square test for categorical variables and by independent samples t-test for normal distributed continuous variables. Log transformation was applied to NT-proBNP and hs-Troponin T to enable parametric testing.

Statistical Machine Learning Analysis

We identified two panels of biomarkers that allowed accurate discrimination among 1) patients with high-risk vs. patients without high-risk plaques and 2) patients with presence vs. patients without coronary atherosclerosis, as defined by CCTA. Our multivariate analysis is described in detail in the Supplementary Methods. In brief, we used a combination of deep stacking generalization framework(15) with multiple levels of gradient boosting classifiers(16) to improve prediction accuracy. The strategy employed by our algorithm is to utilize sub-sampling and model stacking to control over-fitting and improve prediction. The method allows learning of non-linear multivariate relationships among the proteins and is applicable to structured and high-dimensional data.

We conducted a rigorous stability selection procedure(17) to ensure reliability of the biomarker signatures. A randomization test(18) was conducted to evaluate statistical validity of the results. We followed a standard procedure where the outcome variable (e.g. presence of high-risk plaque) was randomly reshuffled while the corresponding protein profiles were kept intact. This was repeated up to 100 times and Receiver-Operating-Characteristics Area-Under-Curve (ROC AUC) scores were computed each time. Predictive value of the biomarker model for the presence of high-risk plaques was tested against a clinical model that comprised generally available clinical characteristics and conventional biomarkers (referred to as clinical model), i.e. age, sex, total cholesterol, HDL cholesterol, diabetes, systolic blood pressure, current smoking, family history, BMI, statin use, eGFR, high-sensitive troponin T, NT-proBNP, and CRP levels. Additionally, a third model (referred to as combined model) was computed in which all variables from the clinical model and the predictive biomarkers from the biomarker model were included. This model was tested against the clinical model to establish the incremental predictive value of the identified biomarker panel for high-risk plaque. Subsequently, these three models (clinical, biomarker, and combined) were also computed for the identification of patients with absence of CAD.

Troponin and NT-proBNP values below limit of detection were replaced by the lower limit of detection divided by two. Since in 150 subjects (77%) CRP levels were below the limit of detection (2.5 mg/L), CRP was dichotomized for analysis, with the limit of

detection as threshold.

Data sharing

All individual participant data that underlie the results reported in this article will be made freely available, after de-identification, at Mendeley Data (http://dx.doi.org/10.17632/gdfvxvr7f2.1). There are no restrictions to obtaining the data.

Results

Study population

An initial 203 patients with interpretable CCTA images and available laboratory samples was evaluated for inclusion. After laboratory analysis was performed, 7 patients were excluded due to failure to pass the quality control of the proteomics measurements. This resulted in a final study population of 196 patients. The baseline characteristics of these patients are provided in table 1.

Coronary CT angiography

CCTA showed one or more coronary lesions with >50% stenosis in 143 (73.0%) patients. A high-risk coronary lesion was observed in 44 (22.4%) patients, whereas 26 (13.3%) patients had complete absence of CAD. An overview of CCTA results is given in table 2. Baseline characteristics stratified by patient groups, i.e. patients with and without high-risk plaque and patients with and without CAD, are presented in table 1.

There were some significant differences in baseline characteristics between patients with and without high-risk plaque and between patients with and without CAD (table 1). Typical chest pain, beta blocker use, and male gender were more frequent and creatinin and hs-Troponin T levels were significantly higher in the high-risk plaque vs non-high-risk plaque group ($p<0.05$ for all). Patients without CAD were younger, more frequently female, less likely to use aspirin and to suffer from hypertension as compared to patients with CAD ($p<0.05$ for all). Furthermore, patients without CAD had lower systolic blood pressure and Framingham Risk Score ($p<0.05$ for all).

Proteomics analysis

Of all 358 proteins initially included for analysis, 26 had more than 20% of cases

Table 1. Baseline characteristics

Demographics	Overall (n=196)	Non-HRP (n=152)	HRP (n=44)	p-value	No CAD (n=26)	CAD (n=170)	p-value
Age, years	58 ± 8	58 ± 9	59 ± 8	0.35	52 ± 6	59 ± 8	<0.001
Male	126 (64%)	90 (59%)	36 (82%)	0.006	12 (46%)	114 (67%)	0.04
Body mass index	27 ± 4	27 ± 4	27 ± 3	0.85	27 ± 4	27 ± 4	0.63
Risk factors – no (%)							
DM type II	30 (15%)	24 (16%)	6 (14%)	0.73	2 (8%)	28 (17%)	0.38
Hypertension	90 (46%)	74 (49%)	16 (36%)	0.15	7 (27%)	83 (49%)	0.04
Hyperlipidaemia	75 (38%)	56 (37%)	19 (43%)	0.45	8 (31%)	67 (39%)	0.40
Current smoker	40 (20%)	28 (18%)	12 (27%)	0.20	6 (23%)	34 (20%)	0.72
Family history	102 (52%)	80 (53%)	22 (50%)	0.76	14 (54%)	88 (52%)	0.84
Type of chest pain – no (%)							
Between groups				0.005			0.13
Typical angina	68 (35%)	44 (29%)	24 (55%)	0.002	8 (31%)	60 (35%)	NA
Atypical angina	76 (39%)	62 (41%)	14 (32%)	0.28	7 (27%)	69 (41%)	NA
Non-specific chest discomfort	52 (27%)	46 (30%)	6 (14%)	0,03	11 (42%)	41 (24%)	NA
Laboratory tests							
TC, mmol/L*	4.6 ± 1.1	4.5 ± 1.0	4.7 ± 1.3	0.33	4.5 ± 1.0	4.6 ± 1.1	0.57
LDL-C, mmol/L*	2.5 ± 0.9	2.5 ± 0.9	2.6 ± 1.0	0.39	2.4 ± 1.1	2.5 ± 0.9	0.41
HDL-C, mmol/L*	1.4 ± 0.5	1.4 ± 0.5	1.3 ± 0.4	0.14	1.4±0.3	1.4 ± 0.5	0.79
Triglycerides, mmol/L*	1.5 ± 0.9	1.5 ± 0.8	1.7 ± 1.2	0.33	1.4±0.6	1.5 ± 0.9	0.37
hs-Troponin T, ng/L*	5.0 [4.0-8.3]	5.0 [3.0-8.0]	7.0 [4.0-9.0]	0.044	4.0 [3.0-7.0]	6.0 [4.0-9.0]	0.05
NT-proBNP, ng/L*	67 [40-135]	65 [40-132]	69 [42-182]	0.35	59 [34-115]	69 [42-136]	0.42
Creatinin, µmol/L	72.8 ± 13.7	71.6 ± 13.4	76.8 ± 13.9	0.03	72.5±15.0	72.8 ± 13.5	0.93
eGFR < 60 mL/min, no (%)	5 (3%)	4 (3%)	1 (2%)	1.00	1 (4%)	4 (2%)	0.51
CRP ≥ 2.5 mg/L, no (%)	36 (18%)	28 (18%)	8 (18%)	0.97	5 (19%)	31 (18%)	1.00

Demographics	Overall (n=196)	Non-HRP (n=152)	HRP (n=44)	p-value	No CAD (n=26)	CAD (n=170)	p-value
Medication use – no (%)							
Statin	151 (77%)	112 (74%)	39 (89%)	0.04	18 (69%)	133 (78%)	0.31
Acetylsalicylic acid	175 (89%)	133 (88%)	42 (96%)	0.17	20 (77%)	155 (91%)	0.03
Betablocker	126 (64%)	90 (59%)	36 (82%)	0.006	16 (62%)	110 (65%)	0.75
ACE-inhibitor / ARB	73 (37%)	61 (40%)	12 (27%)	0.12	6 (23%)	67 (39%)	0.11
Other							
SBP, mm Hg	143 ± 20	143 ± 19	144 ± 21	0.62	135 ± 24	144 ± 19	0.04
DBP, mm Hg	82 ± 12	82 ± 12	84 ± 11	0.41	79 ± 15	83 ± 11	0.24
Framingham Risk Score *	6.3 ± 3.2	6.1 ± 3.4	6.7 ± 2.8	0.34	4.3 ± 4.0	6.6 ± 3.0	0.001

* Total cholesterol, LDL-C, HDL-C, triglycerides, NT-proBNP, and Framingham risk score were missing in 2 patients and hs-Troponin T is missing in 6 patients. HRP = high-risk plaque; CAD = coronary artery disease; NA = not applicable since no significant difference was found in type of chest pain in no CAD vs CAD (p=0.133), thus no post-hoc testing was performed; LDL-C = low density lipoprotein cholesterol = HDL-C = high density lipoprotein cholesterol; hs-Troponin = high-sensitive Troponin; NT-proBNP = N-terminal pro brain natriuretic peptide; eGFR = estimated glomerular filtration rate; CRP = C-reactive protein; ACE-inhibtor = angiotensin-converting-enzyme inhibitor; ARB = angiotensin receptor blocker; SBP = systolic blood pressure; DBP = diastolic blood pressure.

Table 2. CCTA results on a patient-basis

CAC score	
Median CAC score	170 [19 - 493]
Stenosis - no (%) *	
No stenosis	26 (13%)
0 – 50% stenosis	27 (14%)
50-70% stenosis	53 (27%)
>70% stenosis	90 (46%)
Plaque analysis - no (%)	
No atherosclerotic plaques	26 (13%)
Non-calcified plaque	78 (40%)
Partially calcified plaque	133 (68%)
Calcified plaque	133 (68%)
Low attenuation plaque	57 (29%)
Positive remodeling	49 (25%)
Spotty calcification	27 (14%)
Napkin ring sign	20 (10%)
High-risk plaque	44 (22%)

* stenosisgrade of most severe lesions was used for patient-based analysis. CCTA = coronary computed tomography angiography; CAC = coronary artery calcium score

below the lower limit of detection (Supplementary Table 1). These proteins were excluded from further analysis. The total number of proteins included for analysis on plaque morphology prediction was 332.

Protein signature associated with high-risk coronary lesions

A total number of 35 plasma proteins was predictive for the presence of CT-derived high-risk coronary lesions (Figure 1 and Supplementary Table 3). The 11 most predictive proteins and the association of protein levels with the presence of high-risk coronary lesions are illustrated in Figure 1. A complete list of proteins associated with high-risk plaques and the standardized mean protein levels in both groups is provided in the Supplementary Table 2. The machine learning model developed using biomarkers was found to have a high diagnostic value for the presence of high-risk coronary lesions with an AUC of 0.79±0.01 (Figure 2). Using the same methodology, the clinical model was computed. The relative importance of the variables in the clinical model is shown in Supplementary Table 3. The clinical model had only modest

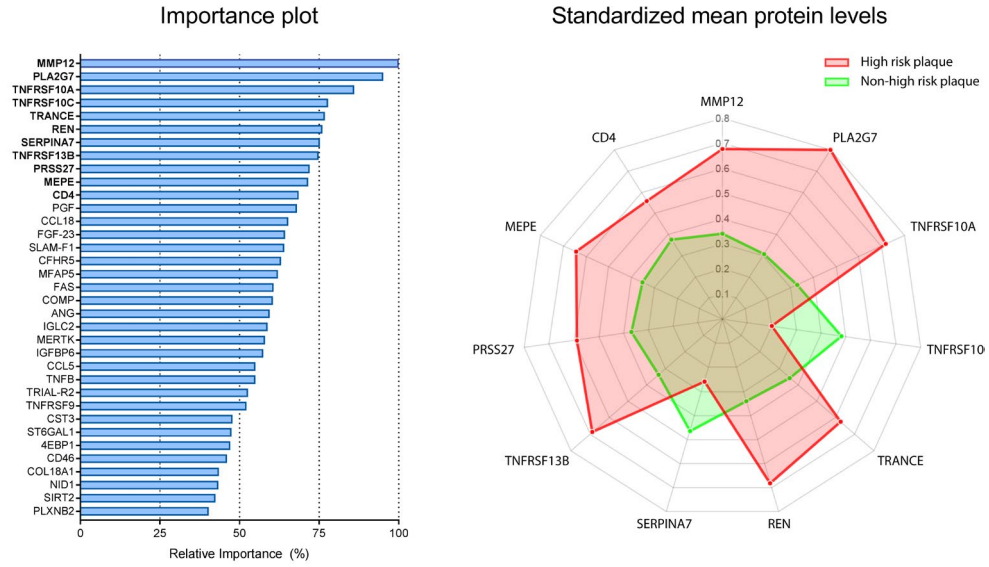

Figure 1. Protein subset predictive for the presence of a high-risk plaque
The importance plot (left panel) illustrates the relative importance of all 35 plasma proteins predictive for the presence of high-risk plaque. The spiderplot (right panel) depicts the 7 most important proteins in our machine learning model that differentiate between the presence (red) and absence of high-risk plaque (green). The axes of the spiderplot represent the standarized mean protein levels (scaled zero-mean unit-variance). Standaridized mean levels of MMP12, PLA2G7, TNFRSF10A, TRANCE, REN, TNFRSF13B, PRSS27, MEPE, and CD4 were higher in the high-risk plaque group compared to the non high-risk group. Conversely, TNFRSF10C and SERPINA7 levels were lower in the high-risk group. Abbrevations of protein names are defined in Supplementary Table 1.

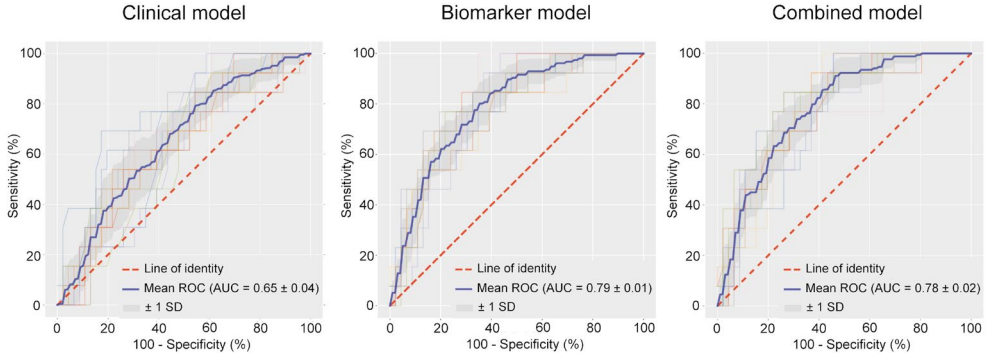

Figure 2. Diagnostic performance of the biomarker model versus the clinical model and the combined model for the presence of high-risk plaque
Receiver-operating characteristics curve with area under the curve (AUC) for the diagnostic performance of the clinical model (left), the biomarker model (middle) and the combined model (right) for the presence of high-risk coronary artery disease. The mean ROC curve for each model is depicted by the blue line. The grey shaded area represents the standard deviation of the curves. The clinical model was outperformed by both the biomarker model ($p<0.05$) and the combined model ($p<0.05$).

diagnostic accuracy and was inferior to our biomarker model, with AUC of 0.65±0.04 ($p<0.05$). The combined model, comprised of both clinical parameters and the identified predictive biomarkers (AUC of 0.78±0.02) also outperformed the clinical model ($p<0.05$). Relative importance of the variables included in the combined model is shown in Supplementary Table 4. All proteomic biomarkers were retained in the combined model, indicating the incremental value of the identified biomarker panel for the presence of high-risk plaque.

Protein signature associated with absence of coronary artery disease

A different subset of 34 proteins was predictive for the absence of CAD as visualized by CCTA (Figure 3 and Supplementary Table 5). The 11 most predictive proteins and the association of protein levels with the absence of CAD are illustrated in Figure 3. An overview of all proteins predictive for the absence of coronary atherosclerosis and the standardized mean protein levels in both groups is provided in Supplementary Table 5. The machine learning biomarker model had a high diagnostic accuracy for the identification of patients with absence of CAD with an AUC of 0.85±0.05 (Figure 4). The relative importance of the variables in the clinical and combined model are shown in the Supplementary Table 6 and 7. Again, the clinical model had only modest diagnostic value (AUC=0.70±0.04) and was outperformed by the proteomic model ($p<0.05$). The combined model also had greater diagnostic accuracy than the clinical model with an AUC of 0.83±0.04 ($p<0.05$). All proteomic biomarkers were retained in the combined model, indicating the incremental value of the identified biomarker panel for the absence of CAD.

Discussion

This study investigated the ability of a large set of biomarkers to identify patients with either high-risk coronary plaque morphology or absence of coronary atherosclerosis. Results show that a subset of 35 proteins was highly predictive for the presence of high-risk coronary lesions. The diagnostic value of this biomarker signature was significantly greater than prediction with generally available clinical characteristics and conventional biomarkers. Additionally, a distinct protein signature of 34 plasma proteins was found to identify patients with absence of coronary atherosclerosis.

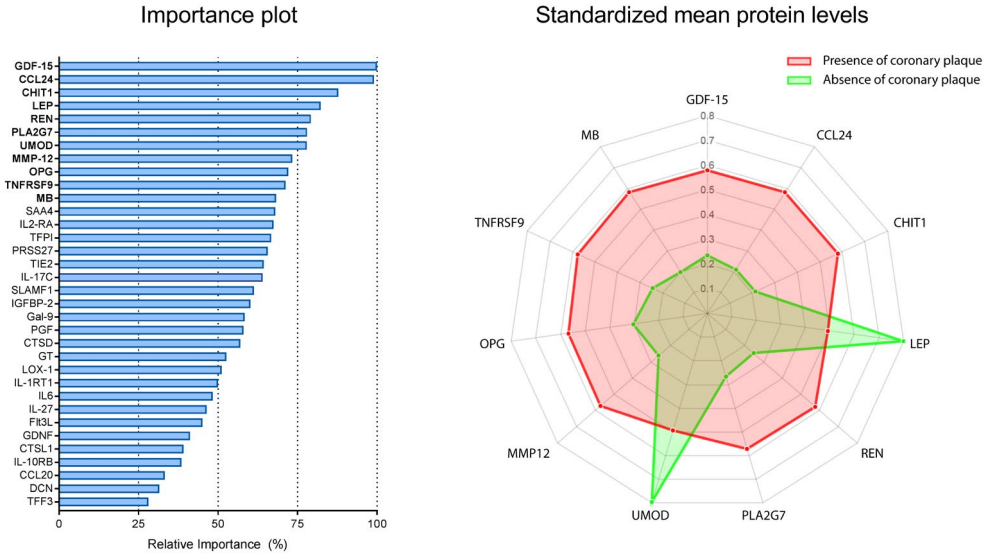

Figure 3. Protein subset predictive for CCTA-defined absence of coronary atherosclerosis
Importance plot (left panel) illustrates the relative importance of all 34 plasma proteins predictive for CCTA-defined absence of coronary atherosclerosis. The spiderplot (right panel) depicts the 11 most important proteins in our machine learning model that differentiate between the presence (red) and absence of coronary atherosclerosis (green). The axis of the spiderplot represents the standardized mean protein levels (scaled zero-mean unit-variance). Standaridized mean levels of LEP and UMOD were higher in the absence of CAD group compared to the presence of CAD group. Conversely GDF-15, CCL24, CHIT1, REN, PLA2G7, MMP12, OPG, TNFRSF9, and MB were lower in patients with absence of CAD. Abbrevations of protein names are defined in Supplementary Table 1.

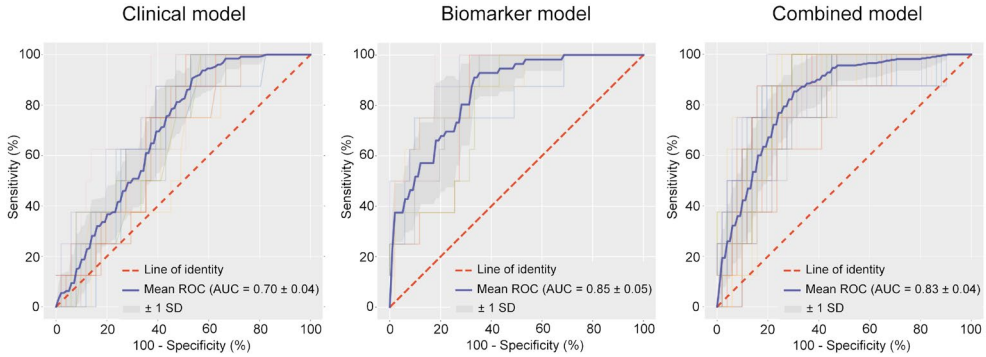

Figure 4. Diagnostic performance of the biomarker model versus the clinical model and the combined model for the absence of coronary atherosclerosis
Receiver-operating characteristics curve with area under the curve (AUC) for the diagnostic performance of the clinical model (left), biomarker model (middle) and combined model (right) for the absence of coronary artery disease. The mean ROC curve for each model is depicted by the blue line. The grey shaded area represents the standard deviation of the curves. The clinical model was outperformed by both the biomarker model ($p<0.05$) and the combined model ($p<0.05$).

Protein signature for the presence of high-risk plaques

Several studies have investigated the relationship between individual biomarkers and plaque morphology on invasive and non-invasive imaging modalities.(9,19,20) Recent technical advances have enabled the simultaneous measurement of large amounts of proteins and several studies have used these novel techniques to investigate the ability of large biomarker sets to identify patients with angiography-derived significant stenosis.(21,22) LaFramboise et al. studied the predictive ability of 56 proteins for the presence of a coronary stenosis requiring revascularization and found a model that included osteopontin, resistin, MMP7, and IFNγ to be highly predictive.(22) More recently, Ibrahim et al. evaluated the combined predictive value of clinical variables and 109 candidate proteins. The final model comprised several clinical variables and 4 biomarkers (midkine, adiponectin, apolipoprotein C-1, and kidney injury molecule-1) and showed high accuracy for the presence of angiography-derived stenosis. Although interesting from a diagnostic point of view, these studies do not provide any information on the predictive value for the presence of high-risk coronary lesions.

Our study is the first to assess the relationship between a large set of biomarkers and high-risk plaque morphology using high-throughput technology combined with state-of-the-art machine learning techniques. Results show that a protein signature of 35 proteins, many of which have not been linked with atherosclerosis previously, was highly predictive for the presence of high-risk plaques (AUC=0.79±0.01). A detailed description of the roles of the most important predictive proteins is provided in the supplementary material. Notably, although several predictive proteins identified by LaFramboise et al. and Ibrahim et al. were also tested in our study (osteopontin, kidney injury molecule-1, resistin, IFNy, and MMP7), none of these markers were included in our biomarker model. However, it is important to note that the predicted outcome in our study (high-risk plaque) was different from these previous studies (angiographic CAD) and therefore the current findings are not necessarily discordant with the aforementioned studies.

For decades, risk prediction in clinical practice has been based on generally available clinical characteristics. However, these clinical characteristics, often combined into risk scores, have only modest predictive value for coronary atherosclerosis and the

occurrence of events.(5) More recently, improved cardiovascular risk algorithms have been proposed using additional conventional biomarkers such as high-sensitive troponin, NT-proBNP and CRP.(6,8,23) To test the validity of our findings, our biomarker model was tested against a model which included generally available clinical characteristics and conventional biomarkers. Results show that the biomarker model outperformed this clinical model with AUCs of 0.79±0.01 and 0.65±0.04 respectively. Subsequently, to investigate the incremental value of the biomarker model to clinical risk prediction, the clinical model was tested against a combined model including both proteomic biomarkers and the generally available clinical variables. The combined model (AUC of 0.78±0.02) clearly outperformed the clinical model. Since all proteomic biomarkers were retained in the combined model, the identified biomarker panel had incremental value to generally available clinical characteristics and conventional biomarkers for the prediction of high-risk plaques.

Protein signature for the absence of coronary artery disease

In addition to the protein signature for high-risk plaques, a different subset of 34 proteins was found to be highly predictive of the CCTA-defined absence of CAD (AUC=0.85±0.05). The clinical model (AUC=0.70±0.04) was clearly outperformed by the proteomic biomarker model. Furthermore, the combined model for the absence of CAD (AUC=0.83±0.04) also more accurately predicted the absence of CAD than the clinical model. Again, all proteomic biomarkers were retained in the combined model, clearly demonstrating the incremental value of the identified biomarker panel to clinical variables for the prediction of the absence of CAD. A detailed description of the roles of the most important predictive proteins is provided in the supplementary material.

Common pathways in identified protein panels

Interestingly, in the top 11 biomarkers included in our biomarker model for the presence of high-risk plaques (Figure 1), we identified 7 proteins associated with pro-inflammatory, pro-apoptotic pathways in plaques. Number 1, metalloproteinase-12 (MMP12), a prominent member of the senescence associated secretory phenotype, has been extensively linked with inflammation, plaque stability and atherosclerotic plaque burden.(24,25) Number 2, PLA2G7, also referred to as Lp-PLA2, is an enzyme

produced by inflammatory cells, leading to enhanced atherosclerosis by increasing oxidation of LDL particles.(26) Numbers 3, 4, 5, and 8 TNFRSF10A, TNFRSF10C, TRANCE and TNFRS13B, are all involved in the tumor necrosis factor (TNF) signaling pathway and play a role in apoptosis, NFkB activation, and B-cell activation.(27) Number 10, surface CD4, is derived from the T-helper cells, which contribute to the pro-inflammatory cross-talk between T-cells and macrophages among other in the subendothelial compartment.(28)

In the top 11 biomarkers for absence of coronary atherosclerosis (Figure 3), nine are associated with inflammatory pathways. Number 1, GDF-15 (downregulated), a macrophage inhibitory cytokine, is higher in inflammatory states and elevated GDF-15 levels are associated with coronary plaque and occurrence of events.(29) Second, CCL24 (downregulated) contributes to recruitment of neutrophils and macrophages and inhibition of CCL24 is shown to attenuate inflammatory activity in pro-inflammatory disorders.(30,31) Third, chitotriosidase-1 (CHIT1), an enzyme secreted by activated macrophages, has been shown to be abundant in atherosclerotic plaques.(32) Interestingly, MMP12 and PLA2G7 were also present in the panel predictive for high-risk plaques. Closer exploration of the raw data revealed these proteins to be upregulated in the high-risk group but downregulated in the absence of CAD (Figure 1 and 3). In total, 6 proteins (i.e. MMP12, PLA2G7, renin, PRSS27, SLAMF1, and TNFRSF9) were present in both protein signatures. All six proteins show opposite regulation in the high-risk plaque versus the absence of CAD (Supplementary Table 2 and 5), confirming their potential biological involvement in plaque formation. Number 9 and 10, osteoprotegerin (OPG) and TNFRSF9, are both members of the TNF receptor family. OPG (downregulated) is reported to harbor protective effect by serving as decoy receptor for receptor-activator of nuclear factor kappa-B ligand and as inhibitor of vascular calcification.(27,33) However, several studies have associated elevated OPG levels with cardiovascular events.(34) TNFRSF9 (downregulated) plays a key role in activating pro-inflammatory T-helper cells and is implicated in the progression of atherosclerosis.(35)

Upon integration of the 'high-risk plaque' and 'absence of CAD' signatures, a concept emerges of a systemically quantifiable hyperactivity of pro-inflammatory signaling cascades involved in T-cell, macrophage, apoptotic activity, and cellular recruitment

in case of the presence of high-risk plaques. Conversely, there is hypo-activity of these signaling pathways in case of absence of coronary atherosclerosis.

Clinical implications and future perspectives

Despite recent advances in lipid-lowering therapies, patients with CAD remain at substantial risk for coronary events.(36) Elevated ***levels*** of biomarkers of vascular inflammation such as CRP have been proposed to indicate the extent of residual risk in these patients. The promise of this concept was recently confirmed by the CANTOS trial which showed that in patients with elevated CRP levels, anti-inflammatory therapy targeting interleukin-1β reduced the rate of cardiovascular events independent of lipid-level lowering.(37) These findings may be seen as a first step towards patient-tailored management in CAD patients, in which phenotyping of both residual lipid- and inflammatory-driven risk help guide therapeutic choices.(38) Given the non-specific nature of CRP, there is a need for more specific markers of the inflammatory processes in the arterial wall. Technical advances in proteomic analyses paralleled by advances in machine learning have paved the way for the introduction of proteomics. Given the relatively low costs compared to CCTA and routine laboratory testing of single biomarkers, and the rapid analysis of proteomic samples (within 24 hours), targeted proteomics offers the opportunity to be highly cost-effective. Ganz et al. recently demonstrated the ability of targeted proteomics, measured using modified aptamers, to identify patients at risk for cardiac events.(39) Given the limited patient population in our study cohort, validation with clinical events was not possible. Alternatively, we opted to investigate the predictive value of targeted proteomics for CCTA-defined high-risk coronary lesions and absence of coronary atherosclerosis. Since multiple studies have confirmed the link between CT-derived high-risk plaques and cardiovascular events(1,2) and conversely between the absence of CAD and event-free survival,(40,41) prognostic implication of both identified protein signatures seems plausible. Of course, our results must be seen as hypothesis-generating and validation in external cohorts with clinical events is necessary for clinical application. Hypothetically, identification of high-risk patients could help guide the use of expensive medication to the highest risk groups, with the promise of shedding light on the predominant risk factors in these patients (lipid, inflammation, thrombosis). Conversely, identification of patients without coronary atherosclerosis could help avoid overtreatment. Importantly, to

confirm the prognostic value of the two protein signatures, prospective validation in outcome studies is warranted. If confirmed, this may herald the introduction of targeted proteomics in the cardiovascular arena.

Limitations

Several aspects may need closer attention. First, the current report is a substudy of the PACIFIC trial and although blood samples were prospectively drawn and stored for analysis, the current report has a limited sample size and the analysis should be considered retrospective in nature. Second, external validation of our findings in a separate validation cohort was not possible due to the relatively small sample size. To minimize the risk of overfitting, state-of-the-art machine learning modelling was performed best suited to the nature of the data and the limited sample size. A rigorous stability selection procedure and specialized regularization strategy were used to ensure reliability of our findings. Subsequently, biomarker signatures were internally validated in the current cohort to avoid over-fitting, by using a 10-fold stratified cross-validation over the training partition of the data (80%) while the remaining 20% was used as the testing dataset. For increased confidence, this procedure was repeated multiple times on a reshuffled dataset. Although we believe these techniques corroborate the validity of our findings, external validation in larger cohorts is mandatory to confirm the predictive value of the identified biomarker subsets. Similarly, validation with coronary events was not possible in this cohort due to the relatively small sample size. Instead, the presence of high-risk plaque was used as a surrogate for coronary events. It must however be noted that although high-risk plaque has been extensively associated with adverse outcome, not all high-risk plaques cause events.(1,2,14) Validation with coronary events in an external cohort is therefore crucial to validate our findings. Third, our study population consisted of symptomatic patients with intermediate risk of CAD. Therefore, our prediction model may be less suitable for subjects in a low-risk, primary prevention cohort. Fourth, our predictive methodology focused on the performance of the developed machine learning model involving a joint panel of selected biomarkers which together, as a group, lead to reliable prediction. This is a crucial difference in comparison with univariate models that evaluate the up- or downregulation of single proteins. Contribution of all proteins included in the joint panel is needed to obtain a reliable prediction model. Our study therefore does not

provide definite information on the up- or downregulation of single proteins. Last, since some of the included proteins have not been implicated in the pathophysiology of atherosclerosis before, further studies are warranted to elucidate their role in atherogenesis.

Conclusions

Using statistical machine learning models, trained on targeted plasma proteomics, we defined two complementary protein signatures: one for the identification of patients with high-risk coronary lesions and one for the identification of patients with absence of coronary atherosclerosis. Both biomarker subsets were shown to be superior to generally available clinical characteristics and conventional biomarkers in predicting presence or absence of (high-risk) coronary atherosclerosis. These promising findings warrant external validation of the value of targeted proteomics to identify cardiovascular risk in cardiovascular outcome studies.

References

1. Motoyama S, Ito H, Sarai M et al. Plaque Characterization by Coronary Computed Tomography Angiography and the Likelihood of Acute Coronary Events in Mid-Term Follow-Up. J Am Coll Cardiol 2015;66:337-346.
2. Otsuka K, Fukuda S, Tanaka A et al. Napkin-ring sign on coronary CT angiography for the prediction of acute coronary syndrome. JACC Cardiovasc Imaging 2013;6:448-457.
3. Bom MJ, van der Heijden DJ, Kedhi E et al. Early Detection and Treatment of the Vulnerable Coronary Plaque: Can We Prevent Acute Coronary Syndromes? Circ Cardiovasc Imaging 2017;10.
4. Piepoli MF, Hoes AW, Agewall S et al. 2016 European Guidelines on cardiovascular disease prevention in clinical practice: The Sixth Joint Task Force of the European Society of Cardiology and Other Societies on Cardiovascular Disease Prevention in Clinical Practice (constituted by representatives of 10 societies and by invited experts) Developed with the special contribution of the European Association for Cardiovascular Prevention & Rehabilitation (EACPR). Eur Heart J 2016;37:2315-81.
5. Eichler K, Puhan MA, Steurer J, Bachmann LM. Prediction of first coronary events with the Framingham score: a systematic review. Am Heart J 2007;153:722-31, 731 e1-8.
6. Lindholm D, Lindback J, Armstrong PW et al. Biomarker-Based Risk Model to Predict Cardiovascular Mortality in Patients With Stable Coronary Disease. J Am Coll Cardiol

2017;70:813-826.
7. Oemrawsingh RM, Cheng JM, Garcia-Garcia HM et al. High-sensitivity Troponin T in relation to coronary plaque characteristics in patients with stable coronary artery disease; results of the ATHEROREMO-IVUS study. Atherosclerosis 2016;247:135-41.
8. Januzzi JL, Jr., Suchindran S, Coles A et al. High-Sensitivity Troponin I and Coronary Computed Tomography in Symptomatic Outpatients With Suspected Coronary Artery Disease: Insights From the PROMISE Trial. JACC Cardiovasc Imaging 2018.
9. Caselli C, De Graaf MA, Lorenzoni V et al. HDL cholesterol, leptin and interleukin-6 predict high risk coronary anatomy assessed by CT angiography in patients with stable chest pain. Atherosclerosis 2015;241:55-61.
10. Ruparelia N, Chai JT, Fisher EA, Choudhury RP. Inflammatory processes in cardiovascular disease: a route to targeted therapies. Nat Rev Cardiol 2017;14:133-144.
11. Assarsson E, Lundberg M, Holmquist G et al. Homogenous 96-plex PEA immunoassay exhibiting high sensitivity, specificity, and excellent scalability. PLoS One 2014;9:e95192.
12. Deo RC. Machine Learning in Medicine. Circulation 2015;132:1920-30.
13. Danad I, Raijmakers PG, Driessen RS et al. Comparison of Coronary CT Angiography, SPECT, PET, and Hybrid Imaging for Diagnosis of Ischemic Heart Disease Determined by Fractional Flow Reserve. JAMA Cardiol 2017;2:1100-1107.
14. Nerlekar N, Ha FJ, Cheshire C et al. Computed Tomographic Coronary Angiography-Derived Plaque Characteristics Predict Major Adverse Cardiovascular Events: A Systematic Review and Meta-Analysis. Circ Cardiovasc Imaging 2018;11:e006973.
15. Wolpert DH. Stacked generalization. Neural Networks 1992;5:241-259.
16. Tianqi C, Carlos G. XGBoost: A Scalable Tree Boosting System. Proceedings of the 22nd ACM SIGKDD International Conference on Knowledge Discovery and Data Mining . 978-1-4503-4232-2. San Francisco, California, USA: ACM, 2016:785-794.
17. Meinshausen N. Stability selection. J R Statist Soc B 2010;72:417-473.
18. Lovric M. International Encyclopedia of Statistical Science: Springer, Berlin, Heidelberg, 2011.
19. Koga S, Ikeda S, Yoshida T et al. Elevated levels of systemic pentraxin 3 are associated with thin-cap fibroatheroma in coronary culprit lesions: assessment by optical coherence tomography and intravascular ultrasound. JACC Cardiovasc Interv 2013;6:945-54.
20. Sawada T, Shite J, Shinke T et al. Low plasma adiponectin levels are associated with presence of thin-cap fibroatheroma in men with stable coronary artery disease. Int J Cardiol 2010;142:250-6.
21. Ibrahim NE, Januzzi JL, Jr., Magaret CA et al. A Clinical and Biomarker Scoring System to Predict the Presence of Obstructive Coronary Artery Disease. J Am Coll Cardiol

2017;69:1147-1156.
22. LaFramboise WA, Dhir R, Kelly LA et al. Serum protein profiles predict coronary artery disease in symptomatic patients referred for coronary angiography. BMC Med 2012;10:157.
23. Beatty AL, Ku IA, Bibbins-Domingo K et al. Traditional Risk Factors Versus Biomarkers for Prediction of Secondary Events in Patients With Stable Coronary Heart Disease: From the Heart and Soul Study. J Am Heart Assoc 2015;4.
24. Yamada S, Wang KY, Tanimoto A et al. Matrix metalloproteinase 12 accelerates the initiation of atherosclerosis and stimulates the progression of fatty streaks to fibrous plaques in transgenic rabbits. Am J Pathol 2008;172:1419-29.
25. Goncalves I, Bengtsson E, Colhoun HM et al. Elevated Plasma Levels of MMP-12 Are Associated With Atherosclerotic Burden and Symptomatic Cardiovascular Disease in Subjects With Type 2 Diabetes. Arterioscler Thromb Vasc Biol 2015;35:1723-31.
26. Rosenson RS, Hurt-Camejo E. Phospholipase A2 enzymes and the risk of atherosclerosis. Eur Heart J 2012;33:2899-2909.
27. Cheng W, Zhao Y, Wang S, Jiang F. Tumor necrosis factor-related apoptosis-inducing ligand in vascular inflammation and atherosclerosis: a protector or culprit? Vascul Pharmacol 2014;63:135-44.
28. Hansson GK. Inflammation, atherosclerosis, and coronary artery disease. N Engl J Med 2005;352:1685-95.
29. Rohatgi A, Patel P, Das SR et al. Association of growth differentiation factor-15 with coronary atherosclerosis and mortality in a young, multiethnic population: observations from the Dallas Heart Study. Clin Chem 2012;58:172-82.
30. Ablin JN, Entin-Meer M, Aloush V et al. Protective effect of eotaxin-2 inhibition in adjuvant-induced arthritis. Clin Exp Immunol 2010;161:276-83.
31. Menzies-Gow A, Ying S, Sabroe I et al. Eotaxin (CCL11) and eotaxin-2 (CCL24) induce recruitment of eosinophils, basophils, neutrophils, and macrophages as well as features of early- and late-phase allergic reactions following cutaneous injection in human atopic and nonatopic volunteers. J Immunol 2002;169:2712-8.
32. Boot RG, van Achterberg TA, van Aken BE et al. Strong induction of members of the chitinase family of proteins in atherosclerosis: chitotriosidase and human cartilage gp-39 expressed in lesion macrophages. Arterioscler Thromb Vasc Biol 1999;19:687-94.
33. Harper E, Forde H, Davenport C, Rochfort KD, Smith D, Cummins PM. Vascular calcification in type-2 diabetes and cardiovascular disease: Integrative roles for OPG, RANKL and TRAIL. Vascul Pharmacol 2016;82:30-40.
34. Venuraju SM, Yerramasu A, Corder R, Lahiri A. Osteoprotegerin as a predictor of

coronary artery disease and cardiovascular mortality and morbidity. J Am Coll Cardiol 2010;55:2049-61.

35. Soderstrom LA, Gertow K, Folkersen L et al. Human genetic evidence for involvement of CD137 in atherosclerosis. Mol Med 2014;20:456-65.
36. Sabatine MS, Giugliano RP, Keech AC et al. Evolocumab and Clinical Outcomes in Patients with Cardiovascular Disease. N Engl J Med 2017;376:1713-1722.
37. Ridker PM, Everett BM, Thuren T et al. Antiinflammatory Therapy with Canakinumab for Atherosclerotic Disease. N Engl J Med 2017;377:1119-1131.
38. Ridker PM. Residual inflammatory risk: addressing the obverse side of the atherosclerosis prevention coin. Eur Heart J 2016;37:1720-2.
39. Ganz P, Heidecker B, Hveem K et al. Development and Validation of a Protein-Based Risk Score for Cardiovascular Outcomes Among Patients With Stable Coronary Heart Disease. JAMA 2016;315:2532-41.
40. Cho I, Chang HJ, B OH et al. Incremental prognostic utility of coronary CT angiography for asymptomatic patients based upon extent and severity of coronary artery calcium: results from the COronary CT Angiography EvaluatioN For Clinical Outcomes InteRnational Multicenter (CONFIRM) study. Eur Heart J 2015;36:501-8.
41. Hulten EA, Carbonaro S, Petrillo SP, Mitchell JD, Villines TC. Prognostic value of cardiac computed tomography angiography: a systematic review and meta-analysis. J Am Coll Cardiol 2011;57:1237-47.

Supplementary data

Methods

Detailed in- and exclusion criteria

Inclusion criteria

1. First presentation to cardiologist with suspected CAD
2. No documented prior history of CAD
3. Intermediate pre-test likelihood for CAD as defined by Diamond and Forrester criteria
4. Presenting for a clinically referred ICA
5. Age above 40 years
6. Informed consent

Exclusion criteria

1. History of severe COPD or chronic asthma
2. Pregnancy
3. Renal failure (i.e. eGFR < 45 mL/min)
4. Use of sildenafil (Viagra) or dipyramidol (Persantin) that cannot be terminated
5. Contra-indications for β-blockers
6. Allergic reaction to iodized contrast
7. Concurrent or prior (within last 30 days) participation in other research studies using investigational drugs
8. Claustrophobia
9. Significant co-morbidities
10. Atrial fibrillation, second or third degree atrioventricular block
11. Tachycardia
12. (Acute) myocardial infarction
13. Percutaneous coronary intervention
14. Heart failure
15. LVEF estimated < 50%
16. Cardiomyopathies
17. Previous radiation exposure in the diagnostic work-up

18. Coronary artery bypass graft surgery (CABG)
19. Subjects intended for short-term medical treatment or an invasive coronary intervention

CCTA and coronary artery calcium scoring acquisition

Patient preparation and image acquisition were performed as described previously.(1) In short, patients underwent CCTA on a 256-slice CT-scanner (Brilliance iCT, Philips Healthcare, Best, the Netherlands) with a collimation of 128 x 0.625 mm and a tube rotation time of 270 ms. A tube current between 200 and 360 mAs at 120 kV, adjusting primarily the mAs based on body habitus. Axial scanning was performed with prospective ECG-gating (Step & Shoot Cardiac, Philips Healthcare) at 75% of the R-R interval. Coronary artery calcium (CAC) scoring was obtained during a single breath hold and coronary calcification was defined as a plaque with an area of 1.03 mm2 and a density ≥ 130 Hounsfield Units (HU). The CAC score was calculated according to the method described by Agatston.(2) For visualization of the coronary lumen a bolus of 100 mL iobitidol (Xenetix 350) was injected intravenously (5.7 $mL \cdot s^{-1}$) followed by a 50 mL saline flush. The scan was triggered using an automatic bolus tracking technique, with a region of interest placed in the descending thoracic aorta with a threshold of 150 HU.

CCTA plaque analysis

Using dedicated semi-automated software (Comprehensive Cardiac Analysis, Philips Healthcare), all coronary segments with a diameter ≥2 mm were assessed by an experienced reader blinded to laboratory results. The coronary tree was evaluated using axial, multiplanar reformation, maximum intensity projection, and cross-sectional images (slice thickness 0.9mm, increment 0.50mm). Manual corrections to centreline and vessel contours by the reader were allowed. Stenosis severity was graded as 0, 1-50, 50-70, and ≥ 70%. Patients with absence of CAD were defined with a coronary calcium score of zero and CT angiography showing no coronary plaques. Coronary lesions were subsequently analyzed for the following adverse plaque characteristics: positive remodelling, low attenuation plaque, spotty calcification, and napkin ring sign. A high-risk coronary lesion was defined as a lesion with ≥2 adverse plaque characteristics, since this definition has been shown to hold the highest predictive

value for cardiac events.(3) The remodelling index was computed as the ratio of vessel area at the site of the maximal lesion to that of a proximal reference point, with an index >1.1 representing positive remodelling.(4) Low attenuation plaque was defined as a plaque containing any voxel <30 HU.(4) Spotty calcification was characterized by a calcified plaque comprising <90° of the vessel circumference and <3 mm in length. (5) Napkin ring sign was defined by a plaque core with low CT attenuation surrounded by a rim-like area of higher CT attenuation.(4)

Statistical machine learning analysis

All 332 biomarkers were included in the machine learning modelling as individual proteins. While the biomarkers identified by our method frequently lead to statistically significant results, they can also be unstable. In our approach, we address this problem via the stability selection procedure coupled with the model selection.(6) Protein stability is reflected in the frequency that a particular protein was identified in multiple simulations on a re-randomized dataset. This measure is especially relevant for small to medium sized data collections, as in this study the number of patients was limited. Stability selection was performed by randomly subsampling 80% of the data 50 times.

As for the learning algorithm we used a combination stacking generalization framework(7,8) with multiple gradient boosting classifiers(9) to improve prediction accuracy. For each stability re-run we built separate level-0 models. These models were subsequently combined to form the final, level-1 predictor. To avoid over-fitting, we used a 10-fold stratified cross-validation over the training partition of the data (80%) while the remaining data (20%) was used as the test dataset. The stability selection procedure(6) to ensure the reliability and robustness of the biomarker signatures. This was repeated 50 times and Receiver-Operating-Characteristics Area-Under-Curve (ROC AUC) scores were computed each time and averaged for the final test ROC AUC. A permutation (randomization test)(10) was used to evaluate statistical validity of the results. In the permutation test, the outcome variable (i.e. presence/absence of high-risk plaque) was randomly reshuffled 1000 times while the corresponding proteomics profiles were kept intact. Relative importances are reported based on staked generalization (e.g. ensemble learning) with each level 0 model represented by gradient boosting classifier (GBC). These classifiers are in turn using multiple

classification trees to achieve best possible performance on the dataset. We use a standard approach utilized in multiple existing packages such as (extreme boosting machine or scikit-learn GBC) that sum up the feature importance's of the individual classification trees, divided by the total number of trees. We used Python v. 2.7.14 (www.python.org), with packages Numpy, Scipy and Scikits-learn for implementing stacking model and R version 3.4.4 for visualizations.

Detailed description of top 11 predictive proteins in both panels

Presence of high-risk plaque

Metalloproteinase-12 (MMP-12), the most important protein in our model is a prominent member of the senescence associated secretory phenotype and hence a prominent inductor of vascular inflammation.(11) Elevated plasma levels of MMP-12 have been linked to atherosclerotic plaque burden and inflammation in a clinical study.(12)

PLA2G7, also referred to as Lp-PLA2, is an enzyme produced by inflammatory cells and is reported to enhance atherosclerosis by increasing oxidation of LDL particles which results in enhanced internalization into the macrophage resulting in foam cell formation. Several clinical studies have reported adverse outcome in patients with elevated Lp-PLA2 levels.(13) Although direct inhibition of Lp-PLA2 with darapladib was shown to reduce necrotic core size, large randomized controlled trials on Lp-PLA2 inhibition have shown negative results.(14-16)

TNFRSF10A and TNFRSF10C are both receptors for TNF-related apoptosis-inducing ligand (TRAIL). TRAIL is mainly produced by activated leucocytes and plays an important role in cell apoptosis and NF-κB activation and subsequent inflammation.(17,18) Studies on the effects of TRAIL in atherosclerosis have reported discordant results. Whereas studies with TRAIL knockout mice have implied protective effects of TRAIL on atherogenesis,(19,20) several in vitro studies have suggested pro-atherogenic effects of TRAIL through endothelial cell apoptosis, VSMC proliferation and attenuated inflammatory response.(17) TNFRSF10A, also referred to as TRAIL-R1 is a functional transmembrane receptor that mediates TRAIL-induced cellular response, whereas TNFRSF10C, also referred to as TRAIL-R3, is a non-functional protein that antagonizes the function of TRAIL-R1. Lower plasma TRAIL levels have been associated with the presence of vulnerable plaque characteristics as defined by intravascular ultrasound.(21)

TRANCE, also referred to as receptor-activator of nuclear factor kappa-B ligand (RANKL), is produced by endothelial cells and has been shown to actively promote vascular calcification by inducing osteoblastic activity through activation of NF-κB

activation.(21) Although plasma levels of osteoprotegerin (OPG), the decoy receptor of RANKL, have been extensive implicated in clinical studies with coronary artery disease, data on the association of soluble RANKL levels with coronary plaque morphology are lacking.(22)

Renin is a central component of the renin-angiotensin-aldosterone system, cleaving angiotensinogen into angiotensin I, which is further converted to Angiotensin II by ACE. Angiotensin II is thought to induce atherosclerosis predominantly by promoting oxidative stress which in turn plays an important role in endothelial dysfunction and LDL oxidation.(23) Plasma renin levels have been associated with CV mortality and with carotid plaque prevalence.(24)

Thyroxine-binding globulin (SERPINA7 or TBG) is synthesized primarily in the liver and is the main transport protein that binds and transports thyroid hormone in the bloodstream. Although thyroid hormone has been implicated to harbor atheroprotective effects by influencing endothelial cells and vascular smooth muscle cells, data on the link between SERPINA7 and the pathophysiology of atherosclerosis is lacking.(25)

TNFRSF13B, also known as Transmembrane activator and CAML interactor (TACI), is a member of the TNF receptor superfamily and plays an important role in immunity by interacting with BAFF and APRIL. Reports on the effects of BAFF/TACI signaling pathways have shown discordant results.(26-29) While some studies have suggested pro-atherogenic properties of this pathway by inducing B-cell activation and proliferation,(28,29) recent studies have indicated atheroprotective effects by influencing macrophage polarization and B-cell activity.(26,27)

Serine protease 27 (PRSS27) is a member of the peptidase S1 family and exhibits endopeptidase activity. Data on the function of PRSS27 in general and its implications in atherosclerosis are lacking.

MEPE, also referred to as osteoblast/osteocyte factor 45 (OF45), is a protein that is involved in phosphate homeostasis and skeletal mineralization.(30) It is reported to be highly expressed in osteocytes. To date, no data is available on its role in the pathogenesis of atherosclerosis.

T-cell surface glycoprotein CD4 (CD4) is found on the surface of immune cells such as T helper cells and macrophages and is an accessory receptor in the binding of T-cell receptors with antigens. Mounting evidence has underlined the important role of the adaptive immune response in the pathogenesis of atherosclerosis.(31) Although higher levels of circulating CD4 T-cells have been associated with the presence of coronary atherosclerosis, studies on the use of plasma soluble CD4 to identify CAD are lacking.

Absence of coronary atherosclerosis

The eleven most predictive proteins for the absence of CAD were GDF-15, CCL24, CHIT1, leptin, renin, PLA2G7, MMP12, UMOD, OPG, TNFRSF9, and MB. GDF-15 is a stress-responsive member of the transforming growth factor β family and is reported to be upregulated in atherosclerotic plaques in both animal models and human studies.(32,33) Furthermore, a correlation between GDF-15 and the presence of coronary plaque and occurrence of cardiac events is reported in observational studies.(24,34)

CCL24 is a small cytokine that interacts with chemokine receptor CCR3 to induce chemotaxis in inflammatory cells and endothelial cells. Although CCL24 has not been linked to atherosclerosis in humans, a pre-clinical study has indicated increased atherosclerotic plaque development after CCL24 administation.(35)

CHIT1 is an enzyme secreted by activated macrophages and prior studies have shown abundance of CHIT1 in atherosclerotic plaques.(36) Furthermore, several observational studies have linked plasma CHIT1 levels to angiographic presence of CAD.(37) However, in a pre-clinical study suppression of CHIT1 activity was reported to polarize macrophage into the pro-atherogenic M1 phenotype, suggesting a possible atheroprotective effect of CHIT1.(38) Further studies need to elucidate the role of CHIT1 in atherosclerosis.

Leptin is a pro-inflammatory adipose cell-derived hormone, a so-called adipocytokine, that has been implicated to be induce atherosclerosis through a variety of mechanism, i.e. endothelial cell dysfunction, smooth muscle cell proliferation, and angiogenesis.(39) Although some studies have linked plasma leptin levels to coronary events, a recent meta-analysis showed no association after adjustment for cardiovascular risk factors.(40) Interestingly, Caselli et al. corroborate our findings, showing higher leptin

levels in patients without CAD defined by CCTA.(41)

Renin, PLA2G7, and MMP12 were described above as these proteins were also present in the panel predictive for high-risk plaque.

Uromodulin (UMOD), produced in the loop of Henle, plays a role in electrolyte homeostasis.(42) Additionally, prior studies have shown that UMOD may serve as a receptor for binding and endocytosis of inflammatory cytokines.(43) UMOD has subsequently been hypothesized to harbor anti-inflammatory properties. A recent study has corroborated this hypothesis by showing that high serum uromodulin levels are associated with event-free survival.(44)

OPG is expressed by endothelial cells and vascular smooth muscle cells and acts as a decoy receptor for the previously described RANKL.(21) It hereby limits vascular calcification. Additionally, OPG also serves as a decoy receptor to the previously discussed TRAIL and hereby has a protective function by blocking TRAIL-induced apoptosis. Plasma levels of OPG have been recently associated with carotid plaque presence in humans(24) and with adverse cardiovascular outcome.(45)

TNFRSF9, also called CD137, is a member of the TNF receptor superfamily and its main functions include T-cell activation, proliferation and survival.(46) TNFRSF9 has been implicated in plaque progression and destabilization through effects on T-effector cells, vascular smooth muscle cells and macrophages.(47-49) Furthermore, plasma levels of TNFRSF9 have been shown to correlate with the risk of cardiovascular events.(50)

Myoglobin (MB), is marker for muscle damage and has been widely used to detect myocardial damage to diagnose acute coronary syndrome, although it has been recently replaced by high-sensitivity Troponin.(51) Several studies have shown that myoglobin is an important predictor for cardiovascular outcome.(52)

Supplementary Table 1. List of all biomarker proteins measured (n=358)

Protein	Abbreviation	UniProt ID	Excluded from analysis
2,4-dienoyl-CoA reductase, mitochondrial	DECR1	Q16698	
A disintegrin and metalloproteinase with thrombospondin motifs 13	ADAM-TS13	Q76LX8	
Adenosine Deaminase	ADA	P00813	
ADM	ADM	P35318	
Agouti-related protein	AGRP	O00253	
Alpha-L-iduronidase	IDUA	P35475	
Aminopeptidase N	AP-N	P15144	
Angiogenin	ANG	P03950	
Angiopoietin-1	ANG-1	Q15389	
Angiopoietin-1 receptor	TIE2	Q02763	
Angiopoietin-related protein 3	ANGPTL3	Q9Y5C1	
Angiotensin-converting enzyme 2	ACE2	Q9BYF1	
Apolipoprotein M	APOM	O95445	
Artemin	ARTN	Q5T4W7	Yes
Axin-1	AXIN1	O15169	
Azurocidin	AZU1	P20160	
Beta-Ala-His dipeptidase	CNDP1	Q96KN2	
Beta-galactoside alpha-2,6-sialyltransferase 1	ST6GAL1	P15907	
Beta-nerve growth factor	Beta-NGF	P01138	
Bleomycin hydrolase	BLM hydrolase	Q13867	
Bone morphogenetic protein 6	BMP-6	P22004	
Brain-derived neurotrophic factor	BDNF	P23560	Yes
Brother of CDO	BOC	Q9BWV1	
Cadherin-1	CDH1	P12830	
Cadherin-5	CDH5	P33151	
Carbonic anhydrase 1	CA1	P00915	
Carbonic anhydrase 3	CA3	P07451	
Carbonic anhydrase 4	CA4	P22748	
Carbonic anhydrase 5A, mitochondrial	CA5A	P35218	
Carboxypeptidase A1	CPA1	P15085	
Carboxypeptidase B	CPB1	P15086	
Carcinoembryonic antigenrelated cell adhesion molecule 8	CEACAM8	P31997	
Cartilage acidic protein 1	CRTAC1	Q9NQ79	

Supplementary Table 1. ***Continued***

Protein	Abbreviation	UniProt ID	Excluded from analysis
Cartilage oligomeric matrix protein	COMP	P49747	
Caspase-3	CASP-3	P42574	
Caspase-8	CASP-8	Q14790	
Cathepsin D	CTSD	P07339	
Cathepsin L1	CTSL1	P07711	
Cathepsin Z	CTSZ	Q9UBR2	
C-C motif chemokine 14	CCL14	Q16627	
C-C motif chemokine 15	CCL15	Q16663	
C-C motif chemokine 16	CCL16	O15467	
C-C motif chemokine 17	CCL17	Q92583	
C-C motif chemokine 18	CCL18	P55774	
C-C motif chemokine 19	CCL19	Q99731	
C-C motif chemokine 20	CCL20	P78556	
C-C motif chemokine 22	CCL22	O00626	
C-C motif chemokine 23	CCL23	P55773	
C-C motif chemokine 24	CCL24	O00175	
C-C motif chemokine 25	CCL25	O15444	
C-C motif chemokine 28	CCL28	Q9NRJ3	
C-C motif chemokine 3	CCL3	P10147	
C-C motif chemokine 4	CCL4	P13236	
C-C motif chemokine 5	CCL5	P13501	
CD166 antigen	ALCAM	Q13740	
CD40 ligand	CD40-L	P29965	
CD40L receptor	CD40	P25942	
CD59 glycoprotein	CD59	P13987	
Chitinase-3-like protein 1	CHI3L1	P36222	
Chitotriosidase-1	CHIT1	Q13231	
Chymotrypsin C	CTRC	Q99895	
Coagulation factor VII	F7	P08709	
Coagulation factor XI	F11	P03951	
Collagen alpha-1(I) chain	COL1A1	P02452	
Collagen alpha-1(XVIII) chain	COL18A1	P39060	
Complement C1q tumor necrosis factor-related protein 1	C1QTNF1	Q9BXJ1	
Complement C2	C2	P06681	
Complement component C1q receptor	CD93	Q9NPY3	

Supplementary Table 1. ***Continued***

Protein	Abbreviation	UniProt ID	Excluded from analysis
Complement factor H-related protein 5	CFHR5	Q9BXR6	
Complement receptor type 2	CR2	P20023	
Contactin-1	CNTN1	Q12860	
CUB domain-containing protein 1	CDCP1	Q9H5V8	
C-X-C motif chemokine 1	CXCL1	P09341	
C-X-C motif chemokine 10	CXCL10	P02778	
C-X-C motif chemokine 11	CXCL11	O14625	
C-X-C motif chemokine 16	CXCL16	Q9H2A7	
C-X-C motif chemokine 5	CXCL5	P42830	
C-X-C motif chemokine 6	CXCL6	P80162	
C-X-C motif chemokine 9	CXCL9	Q07325	
Cystatin D	CST5	P28325	
Cystatin-B	CSTB	P04080	
Cystatin-C	CST3	P01034	
Decorin	DCN	P07585	
Delta and Notch-like epidermal growth factor-related receptor	DNER	Q8NFT8	
Dickkopf-related protein 1	Dkk-1	O94907	
Dipeptidyl peptidase 4	DPP4	P27487	
EGF-containing fibulin-like extracellular matrix protein 1	EFEMP1	Q12805	
Elafin	PI3	P19957	
Endoglin	ENG	P17813	
Eotaxin	CCL11	P51671	
Ephrin type-B receptor 4	EPHB4	P54760	
Epidermal growth factor receptor	EGFR	P00533	
Epithelial cell adhesion molecule	Ep-CAM	P16422	
E-selectin	SELE	P16581	
Eukaryotic translation initiation factor 4E-binding protein 1	4E-BP1	Q13541	
Fatty acid-binding protein, adipocyte	FABP4	P15090	
Fatty acid-binding protein, intestinal	FABP2	P12104	
Fetuin-B	FETUB	Q9UGM5	
Fibroblast growth factor 19	FGF-19	O95750	
Fibroblast growth factor 21	FGF-21	Q9NSA1	
Fibroblast growth factor 23	FGF-23	Q9GZV9	
Fibroblast growth factor 5	FGF-5	Q8NF90	

Supplementary Table 1. ***Continued***

Protein	Abbreviation	UniProt ID	Excluded from analysis
Ficolin-2	FCN2	Q15485	
Fms-related tyrosine kinase 3 ligand	Flt3L	P49771	
Follistatin	FS	P19883	
Fractalkine	CX3CL1	P78423	
Galectin-3	Gal-3	P17931	
Galectin-4	Gal-4	P56470	
Galectin-9	Gal-9	O00182	
Gastric intrinsic factor	GIF	P27352	
Gastrotropin	GT	P51161	
Glial cell line-derived neurotrophic factor	GDNF	P39905	
Glutaminyl-peptide cyclotransferase	QPCT	Q16769	
Granulins	GRN	P28799	
Granulysin	GNLY	P22749	
Growth arrest-specific protein 6	GAS6	Q14393	
Growth hormone	GH	P01241	
Growth/differentiation factor 15	GDF-15	Q99988	
Growth/differentiation factor 2	GDF-2	Q9UK05	
Heat shock 27 kDa protein	HSP 27	P04792	
Heme oxygenase 1	HO-1	P09601	
Hepatocyte growth factor	HGF	P14210	
Hepatocyte growth factor receptor	MET	P08581	
Hydroxyacid oxidase 1	HAOX1	Q9UJM8	
Ig lambda-2 chain C regions	IGLC2	P0CG05	
Insulin-like growth factor-binding protein 1	IGFBP-1	P08833	
Insulin-like growth factor-binding protein 2	IGFBP-2	P18065	
Insulin-like growth factor-binding protein 3	IGFBP3	P17936	
Insulin-like growth factor-binding protein 6	IGFBP6	P24592	
Insulin-like growth factor-binding protein 7	IGFBP-7	Q16270	
Integrin alpha-M	ITGAM	P11215	
Integrin beta-2	ITGB2	P05107	
Intercellular adhesion molecule 1	ICAM1	P05362	
Intercellular adhesion molecule 2	ICAM-2	P13598	
Intercellular adhesion molecule 3	ICAM3	P32942	
Interferon gamma	IFN-gamma	P01579	Yes
Interleukin-1 alpha	IL-1 alpha	P01583	Yes

Supplementary Table 1. ***Continued***

Protein	Abbreviation	UniProt ID	Excluded from analysis
Interleukin-1 receptor antagonist protein	IL-1ra	P18510	
Interleukin-1 receptor type 1	IL-1RT1	P14778	
Interleukin-1 receptor type 2	IL-1RT2	P27930	
Interleukin-1 receptor-like 2	IL1RL2	Q9HB29	
Interleukin-10	IL10	P22301	
Interleukin-10 receptor subunit alpha	IL-10RA	Q13651	Yes
Interleukin-10 receptor subunit beta	IL-10RB	Q08334	
Interleukin-12 subunit beta	IL-12B	P29460	
Interleukin-13	IL-13	P35225	Yes
Interleukin-15 receptor subunit alpha	IL-15RA	Q13261	
Interleukin-17 receptor A	IL-17RA	Q96F46	
Interleukin-17A	IL-17A	Q16552	Yes
Interleukin-17C	IL-17C	Q9P0M4	
Interleukin-17D	IL-17D	Q8TAD2	
Interleukin-18	IL-18	Q14116	
Interleukin-18 receptor 1	IL-18R1	Q13478	
Interleukin-18-binding protein	IL-18BP	O95998	
Interleukin-2	IL-2	P60568	Yes
Interleukin-2 receptor subunit alpha	IL2-RA	P01589	
Interleukin-2 receptor subunit beta	IL-2RB	P14784	Yes
Interleukin-20	IL-20	Q9NYY1	Yes
Interleukin-20 receptor subunit alpha	IL-20RA	Q9UHF4	Yes
Interleukin-22 receptor subunit alpha-1	IL-22 RA1	Q8N6P7	Yes
Interleukin-24	IL-24	Q13007	Yes
Interleukin-27	IL-27	Q8NEV9; Q14213	
Interleukin-33	IL-33	O95760	Yes
Interleukin-4	IL-4	P05112	Yes
Interleukin-4 receptor subunit alpha	IL-4RA	P24394	
Interleukin-5	IL-5	P05113	Yes
Interleukin-6	IL-6	P05231	
Interleukin-6 receptor subunit alpha	IL-6RA	P08887	
Interleukin-7	IL-7	P13232	
Interleukin-7 receptor subunit alpha	IL7R	P16871	
Interleukin-8	IL-8	P10145	
Junctional adhesion molecule A	JAM-A	Q9Y624	

Supplementary Table 1. ***Continued***

Protein	Abbreviation	UniProt ID	Excluded from analysis
Kallikrein-6	KLK6	Q92876	
Kidney Injury Molecule	KIM1	Q96D42	
Lactoylglutathione lyase	GLO1	Q04760	
Latency-associated peptide transforming growth factor beta-1	LAP TGF-beta-1	P01137	
Latent-transforming growth factor beta-binding protein 2	LTBP2	Q14767	Yes
Lectin-like oxidized LDL receptor 1	LOX-1	P78380	
Leptin	LEP	P41159	
Leukemia inhibitory factor	LIF	P15018	Yes
Leukemia inhibitory factor receptor	LIF-R	P42702	
Leukocyte immunoglobulin-like receptor subfamily B member 1	LILRB1	Q8NHL6	
Leukocyte immunoglobulin-like receptor subfamily B member 2	LILRB2	Q8N423	
Leukocyte immunoglobulin-like receptor subfamily B member 5	LILRB5	O75023	
Lipoprotein lipase	LPL	P06858	
Lithostathine-1-alpha	REG1A	P05451	
Liver carboxylesterase 1	CES1	P23141	
Low affinity immunoglobulin gamma Fc region receptor II-a	FCGR2A	P12318	
Low affinity immunoglobulin gamma Fc region receptor II-b	IgG Fc receptor II-b	P31994	
Low affinity immunoglobulin gamma Fc region receptor III-B	FCGR3B	O75015	
Low-density lipoprotein receptor	LDL receptor	P01130	
L-selectin	SELL	P14151	
Lymphatic vessel endothelial hyaluronic acid receptor 1	LYVE1	Q9Y5Y7	
Lymphotactin	XCL1	P47992	
Lymphotoxin-beta receptor	LTBR	P36941	
Lysosomal Pro-X carboxypeptidase	PRCP	P42785	Yes
Macrophage colony-stimulating factor 1	CSF-1	P09603	
Macrophage receptor MARCO	MARCO	Q9UEW3	
Mannose-binding protein C	MBL2	P11226	
Mast/stem cell growth factor receptor Kit	KIT	P10721	
Matrix extracellular phosphoglycoprotein	MEPE	Q9NQ76	

Supplementary Table 1. ***Continued***

Protein	Abbreviation	UniProt ID	Excluded from analysis
Matrix metalloproteinase-1	MMP-1	P03956	
Matrix metalloproteinase-10	MMP-10	P09238	
Matrix metalloproteinase-12	MMP-12	P39900	
Matrix metalloproteinase-2	MMP-2	P08253	
Matrix metalloproteinase-3	MMP-3	P08254	
Matrix metalloproteinase-7	MMP-7	P09237	
Matrix metalloproteinase-9	MMP-9	P14780	
Melusin	ITGB1BP2	Q9UKP3	
Membrane cofactor protein	CD46	P15529	
Membrane primary amine oxidase	AOC3	Q16853	
Metalloproteinase inhibitor 1	TIMP1	P01033	
Metalloproteinase inhibitor 4	TIMP4	Q99727	
Microfibrillar-associated protein 5	MFAP5	Q13361	
Monocyte chemotactic protein 1	MCP-1	P13500	
Monocyte chemotactic protein 2	MCP-2	P80075	
Monocyte chemotactic protein 3	MCP-3	P80098	
Monocyte chemotactic protein 4	MCP-4	Q99616	
Multiple epidermal growth factor-like domains protein 9	MEGF9	Q9H1U4	
Myeloblastin	PRTN3	P24158	
Myeloperoxidase	MPO	P05164	
Myoglobin	MB	P02144	
Natriuretic peptides B	BNP	P16860	
Natural killer cell receptor 2B4	CD244	Q9BZW8	
Neural cell adhesion molecule 1	NCAM1	P13591	
Neural cell adhesion molecule L1-like protein	CHL1	O00533	
Neurogenic locus notch homolog protein 1	NOTCH1	P46531	
Neurogenic locus notch homolog protein 3	Notch 3	Q9UM47	
Neuropilin-1	NRP1	O14786	
Neurotrophin-3	NT-3	P20783	
Neurturin	NRTN	Q99748	Yes
Neutrophil defensin 1	DEFA1	P59665	
Neutrophil gelatinase-associated lipocalin	LCN2	P80188	Yes
NF-kappa-B essential modulator	NEMO	Q9Y6K9	
Nidogen-1	NID1	P14543	
N-terminal prohormone brain natriuretic peptide	NT-proBNP	N/A	
Oncostatin-M	OSM	P13725	

Supplementary Table 1. ***Continued***

Protein	Abbreviation	UniProt ID	Excluded from analysis
Oncostatin-M-specific receptor subunit beta	OSMR	Q99650	
Osteoclast-associated immunoglobulin-like receptor	hOSCAR	Q8IYS5	
Osteopontin	OPN	P10451	
Osteoprotegerin	OPG	O00300	
Pappalysin-1	PAPPA	Q13219	
Paraoxonase	PON3	Q15166	
Pentraxin-related protein PTX3	PTX3	P26022	
Peptidoglycan recognition protein 1	PGLYRP1	O75594	
Peptidyl-glycine alpha-amidating monooxygenase	PAM	P19021	
Perlecan	PLC	P98160	
Phospholipid transfer protein	PLTP	P55058	
Placenta growth factor	PlGF	P49763	
Plasma serine protease inhibitor	SERPINA5	P05154	
Plasminogen activator inhibitor 1	PAI	P05121	
Platelet endothelial cell adhesion molecule	PECAM-1	P16284	
Platelet glycoprotein Ib alpha chain	GP1BA	P07359	
Platelet-activating factor acetylhydrolase	PLA2G7	Q13093	
Platelet-derived growth factor subunit A	PDGF subunit A	P04085	
Platelet-derived growth factor subunit B	PDGF subunit B	P01127	
Plexin-B2	PLXNB2	O15031	
Poly [ADP-ribose] polymerase 1	PARP-1	P09874	
Polymeric immunoglobulin receptor	PIgR	P01833	
Procollagen C-endopeptidase enhancer 1	PCOLCE	Q15113	
Programmed cell death 1 ligand 1	PD-L1	Q9NZQ7	
Programmed cell death 1 ligand 2	PD-L2	Q9BQ51	
Proheparin-binding EGF-like growth factor	HB-EGF	Q99075	
Pro-interleukin-16	IL16	Q14005	
Prolargin	PRELP	P51888	
Prolyl endopeptidase FAP	FAP	Q12884	
Proprotein convertase subtilisin/kexin type 9	PCSK9	Q8NBP7	
Prostasin	PRSS8	Q16651	
Protein AMBP	AMBP	P02760	
Protein delta homolog 1	DLK-1	P80370	
Protein S100-A12	EN-RAGE	P80511	
Proteinase-activated receptor 1	PAR-1	P25116	

Supplementary Table 1. ***Continued***

Protein	Abbreviation	UniProt ID	Excluded from analysis
Protein-glutamine gamma-glutamyltransferase 2	TGM2	P21980	
Proto-oncogene tyrosine-protein kinase Src	SRC	P12931	
P-selectin	SELP	P16109	
P-selectin glycoprotein ligand 1	PSGL-1	Q14242	
Pulmonary surfactant-associated protein D	PSP-D	P35247	
Receptor for advanced glycosylation end products	RAGE	Q15109	
Receptor-type tyrosine-protein phosphatase S	PTPRS	Q13332	
Regenerating islet-derived protein 3-alpha	REG3A	Q06141	Yes
Renin	REN	P00797	
Resistin	RETN	Q9HD89	
Retinoic acid receptor responder protein 2	RARRES2	Q99969	
Scavenger receptor cysteine-rich type 1 protein M130	CD163	Q86VB7	
Secretoglobin family 3A member 2	SCGB3A2	Q96PL1	
Serine protease 27	PRSS27	Q9BQR3	
Serine/threonine-protein kinase 4	STK4	Q13043	
Serpin A12	SERPINA12	Q8IW75	
Serum amyloid A-4 protein	SAA4	P35542	
Signaling lymphocytic activation molecule	SLAMF1	Q13291	
SIR2-like protein 2	SIRT2	Q8IXJ6	
SLAM family member 5	CD84	Q9UIB8	
SLAM family member 7	SLAMF7	Q9NQ25	Yes
Sortilin	SORT1	Q99523	
SPARC-like protein 1	SPARCL1	Q14515	
Spondin-1	SPON1	Q9HCB6	
Spondin-2	SPON2	Q9BUD6	
ST2 protein	ST2	Q01638	
STAM-binding protein	STAMBP	O95630	
Stem cell factor	SCF	P21583	
Sulfotransferase 1A1	ST1A1	P50225	
Superoxide dismutase [Cu-Zn]	SOD1	P00441	Yes
Superoxide dismutase [Mn], mitochondrial	SOD2	P04179	
T cell surface glycoprotein CD6 isoform	CD6	Q8WWJ7	
Tartrate-resistant acid phosphatase type 5	TR-AP	P13686	
T-cell immunoglobulin and mucin domain-containing protein 4	TIMD4	Q96H15	
T-cell surface glycoprotein CD4	CD4	P01730	

Supplementary Table 1. ***Continued***

Protein	Abbreviation	UniProt ID	Excluded from analysis
T-cell surface glycoprotein CD5	CD5	P06127	
Tenascin	TNC	P24821	
Tenascin-X	TNXB	P22105	
Thrombomodulin	TM	P07204	
Thrombopoietin	THPO	P40225	
Thrombospondin-2	THBS2	P35442	
Thrombospondin-4	THBS4	P35443	
Thymic stromal lymphopoietin	TSLP	Q969D9	Yes
Thyroxine-binding globulin	SERPINA7	P05543	
Tissue factor	TF	P13726	
Tissue factor pathway inhibitor	TFPI	P10646	
Tissue-type plasminogen activator	t-PA	P00750	
TNF ligand superfamily member 13B	TNFSF13B	Q9Y275	
TNF receptor superfamily member 10A	TNFRSF10A	O00220	
TNF receptor superfamily member 10C	TNFRSF10C	O14798	
TNF receptor superfamily member 11A	TNFRSF11A	Q9Y6Q6	
TNF receptor superfamily member 13B	TNFRSF13B	O14836	
TNF receptor superfamily member 14	TNFRSF14	Q92956	
TNF receptor superfamily member 6	FAS	P25445	
TNF-beta	TNFB	P01374	
TNF-related activation-induced cytokine	TRANCE	O14788	
TNF-related apoptosis-inducing ligand	TRAIL	P50591	
TNF-related apoptosis-inducing ligand receptor 2	TRAIL-R2	O14763	
Transcobalamin-2	TCN2	P20062	
Transferrin receptor protein 1	TR	P02786	
Transforming growth factor alpha	TGF-alpha	P01135	
Transforming growth factor beta receptor type 3	TGFBR3	Q03167	
Transforming growth factor-beta-induced protein ig-h3	TGFBI	Q15582	
Trefoil factor 3	TFF3	Q07654	
Trem-like transcript 2 protein	TLT-2	Q5T2D2	
Trypsin-2	PRSS2	P07478	
Tumor necrosis factor	TNF	P01375	Yes
Tumor necrosis factor (Ligand) superfamily, member 12	TWEAK	Q4ACW9	
Tumor necrosis factor ligand superfamily member 14	TNFSF14	O43557	
Tumor necrosis factor receptor 1	TNF-R1	P19438	

Supplementary Table 1. ***Continued***

Protein	Abbreviation	UniProt ID	Excluded from analysis
Tumor necrosis factor receptor 2	TNF-R2	P20333	
Tumor necrosis factor receptor superfamily member 9	TNFRSF9	Q07011	
Tyrosine-protein kinase Mer	MERTK	Q12866	
Tyrosine-protein kinase receptor Tie-1	TIE1	P35590	
Tyrosine-protein kinase receptor UFO	AXL	P30530	
Tyrosine-protein phosphatase non-receptor type substrate 1	SHPS-1	P78324	
Urokinase plasminogen activator surface receptor	U-PAR	Q03405	
Urokinase-type plasminogen activator	uPA	P00749	
Uromodulin	UMOD	P07911	
Vascular cell adhesion protein 1	VCAM1	P19320	
Vascular endothelial growth factor A	VEGF-A	P15692	
Vascular endothelial growth factor D	VEGFD	O43915	
Vasorin	VASN	Q6EMK4	
Vitamin K-dependent protein C	PROC	P04070	
von Willebrand factor	vWF	P04275	
V-set and immunoglobulin domain-containing protein 2	VSIG2	Q96IQ7	

Supplementary Table 2. Biomarkers predictive for high-risk plaques

Protein	Abbreviation	UniProt ID	Relative importance (%)	Standardized mean protein levels *	
				Absence of high-risk plaque	Presence of high-risk plaque
Matrix metalloproteinase-12	MMP-12	P39900	100	0.360	0.682
Platelet-activating factor acetylhydrolase	PLA2G7	Q13093	95.1	0.326	0.800
TNF factor receptor superfamily member 10A	TNFRSF10A	O00220	86.1	0.349	0.721
TNF receptor superfamily member 10C	TNFRSF10C	O14798	77.8	0.493	0.224
TNF-related activation-induced cytokine	TRANCE	O14788	76.8	0.375	0.633
Renin	REN	P00797	76.1	0.360	0.685
Thyroxine-binding globulin	SERPINA7	P05543	75.2	0.477	0.280
TNF receptor superfamily member 13B	TNFRSF13B	O14836	74.9	0.357	0.692
Serine protease 27	PRSS27	Q9BQR3	72.1	0.385	0.596
Matrix extracellular phosphoglycoprotein	MEPE	Q9NQ76	71.6	0.369	0.651
T-cell surface glycoprotein CD4	CD4	P01730	68.6	0.393	0.568
Placenta growth factor	PGF	P49763	68.1	0.371	0.645
C-C motif chemokine 18	CCL18	P55774	65.3	0.387	0.590
Fibroblast growth factor 23	FGF-23	Q9GZV9	64.3	0.375	0.632
Signaling lymphocytic activation molecule	SLAMF1	Q13291	64.0	0.377	0.624
Complement factor H-related protein 5	CFHR5	Q9BXR6	63.1	0.364	0.670
Microfibrillar-associated protein 5	MFAP5	Q13361	62.1	0.378	0.622
TNF receptor superfamily member 6	FAS	P25445	60.7	0.410	0.510
Cartilage oligomeric matrix protein	COMP	P49747	60.5	0.386	0.592
Angiogenin	ANG	P03950	59.5	0.385	0.596
Ig lambda-2 chain C regions	IGLC2	P0CG05	58.9	0.377	0.625
Tyrosine-protein kinase Mer	MERTK	Q12866	58.0	0.393	0.568
C-C motif chemokine 5	CCL5	P13501	55.0	0.387	0.589
TNF-beta	TNFB	P01374	55.0	0.474	0.288

Supplementary Table 2. ***Continued***

Protein	Abbreviation	UniProt ID	Relative importance (%)	Standardized mean protein levels *	
				Absence of high-risk plaque	Presence of high-risk plaque
TNF-related apoptosis-inducing ligand receptor 2	TRAIL-R2	O14763	52.7	0.408	0.518
TNF receptor superfamily member 9	TNFRSF9	Q07011	52.2	0.379	0.618
Cystatin-C	CST3	P01034	47.8	0.375	0.630
Beta-galactoside alpha-2,6-sialyl-transferase 1	ST6GAL1	P15907	47.5	0.394	0.567
Eukaryotic translation initiation factor 4E-binding protein 1	4E-BP1	Q13541	47.1	0.500	0.200
Membrane cofactor protein	CD46	P15529	46.1	0.402	0.539
Collagen alpha-1(XVIII) chain	COL18A1	P39060	43.5	0.398	0.552
Nidogen-1	NID1	P14543	43.4	0.404	0.530
SIR2-like protein 2	SIRT2	Q8IXJ6	42.5	0.472	0.297
Plexin-B2	PLXNB2	O15031	40.3	0.393	0.569

* standardized mean protein levels for both groups are given in scaled zero-mean unit-variance.

Supplementary Table 3. Relative importance of variables included in the clinical model for the presence of high-risk coronary lesions

Variable	Relative importance (%)
Troponin-T	100
Total cholesterol	99.4
Systolic bloodpressure	96.6
eGFR	94.2
HDL-cholesterol	93.8
BMI	93.1
NT-proBNP	86.6
LDL-cholesterol	82.1
Age	82.1
Family history of CAD	61.2
Current smoker	59.8
Statin use	52.2
CRP <2.5 mg/L	40.2
Diabetes Mellitus	31.2

eGFR: estimated glomerular filtration rate; HDL, high-density lipoprotein; NT-proBNP: N-terminal pro brain natriuretic peptide; BMI, body mass index; CAD: coronary artery disease; CRP: C-reactive protein.

Supplementary Table 4. Relative importance of variables included in the combined model for the presence of high-risk coronary lesions

Variable	Relative importance (%)
PLA2G7	100.0
MMP12	92.9
REN	91.1
SERPINA7	90.0
TNFRSF10A	89.1
TRANCE	87.0
CD4	86.7
Statin use	78.6
Troponin-T	78.0
PRSS27	74.3
SLAMF1	73.1
MEPE	73.0
TNFRSF13B	70.0
eGFR	67.1
FGF-23	66.9
Smoker	66.8

Supplementary Table 4. ***Continued***

Variable	Relative importance (%)
CCL5	66.7
TRAIL-R2	65.1
TNFB	64.8
CFHR5	63.9
TNFRSF10C	63.5
ANG	62.2
Total-cholesterol	61.8
Family history of CAD	61.6
FAS	61.2
IGFBP6	60.4
CCL18	60.0
HDL-cholesterol	59.4
COMP	58.8
TNFRSF9	58.6
MERTK	58.4
PGF	58.0
Systolic bloodpressure	57.0
MFAP5	56.6
ST6GAL1	56.3
Age	55.1
LDL-cholesterol	54.3
IGLC2	52.1
CD46	51.5
BMI	51.4
NT-proBNP	50.5
COL18A1	49.9
NID1	48.1
PLXNB2	47.8
SIRT2	47.2
4E-BP1	47.1
CST3	44.6
CRP<2.5 mg/L	39.0
Diabetes	37.3

Abbreviations as in Supplementary Table 2 and 3.

Supplementary Table 5. Biomarkers predictive for absence of coronary atherosclerosis

Protein	Abbreviation	UniProt ID	Relative importance (%)	Standardized mean protein levels *	
				Presence of CAD	Absence of CAD
Growth/differentiation factor 15	GDF-15	Q99988	100	0.583	0.249
C-C motif chemokine 24	CCL24	O00175	99.1	0.586	0.226
Chitotriosidase-1	CHIT1	Q13231	87.9	0.586	0.229
Leptin	LEP	P41159	82.3	0.499	0.800
Renin	REN	P00797	79.2	0.581	0.260
Platelet-activating factor acetylhydrolase	PLA2G7	Q13093	78.0	0.578	0.280
Uromodulin	UMOD	P07911	78.0	0.500	0.794
Matrix metalloproteinase-12	MMP-12	P39900	73.4	0.579	0.274
Osteoprotegerin	OPG	O00300	72.1	0.573	0.314
TNF receptor superfamily member 9	TNFRSF9	Q07011	71.3	0.582	0.258
Myoglobin	MB	P02144	68.3	0.588	0.215
Serum amyloid A-4 protein	SAA4	P35542	68.0	0.518	0.674
Interleukin-2 receptor subunit alpha	IL2-RA	P01589	67.5	0.573	0.316
Tissue factor pathway inhibitor	TFPI	P10646	66.7	0.561	0.392
Serine protease 27	PRSS27	Q9BQR3	65.6	0.568	0.345
Angiopoietin-1 receptor	TIE2	Q02763	64.4	0.565	0.365
Interleukin-17C	IL-17C	Q9P0M4	64.0	0.500	0.793
Signaling lymphocytic activation molecule	SLAMF1	Q13291	61.4	0.577	0.288
Insulin-like growth factor-binding protein 2	IGFBP-2	P18065	60.2	0.590	0.200
Galectin-9	Gal-9	O00182	58.4	0.568	0.349
Placenta growth factor	PGF	P49763	58.0	0.571	0.327
Cathepsin D	CTSD	P07339	57.0	0.573	0.313
Gastrotropin	GT	P51161	52.7	0.555	0.429
Lectin-like oxidized LDL receptor 1	LOX-1	P78380	51.2	0.568	0.344
Interleukin-1 receptor type 1	IL-1RT1	P14778	50.1	0.565	0.368
Interleukin-6	IL6	P05231	48.4	0.557	0.421
Interleukin-27	IL-27	Q14213; Q8NEV9	46.4	0.559	0.403
Fms-related tyrosine kinase 3 ligand	Flt3L	P49771	45.1	0.570	0.335
Glial cell line-derived neurotrophic factor	GDNF	P39905	41.2	0.566	0.359
Interleukin-10 receptor subunit beta	IL-10RB	Q08334	38.5	0.519	0.668

Supplementary Table 5. ***Continued***

Protein	Abbreviation	UniProt ID	Relative importance (%)	Standardized mean protein levels *	
				Presence of CAD	Absence of CAD
C-C motif chemokine 20	CCL20	P78556	33.3	0.521	0.656
Decorin	DCN	P07585	31.6	0.562	0.385
Trefoil factor 3	TFF3	Q07654	28.1	0.521	0.653

* standardized mean protein levels for both groups are given in scaled zero-mean unit-variance.

Supplementary Table 6. Relative importance of variables included in the clinical model for the absence of coronary atherosclerosis

Variable	Relative importance (%)
Age	100
Systolic bloodpressure	63.3
LDL-cholesterol	45.0
Family history of CAD	39.9
BMI	38.0
Troponin-T	37.0
HDL-cholesterol	31.5
eGFR	27.7
Total cholesterol	26.8
Smoker	26.4
Statin use	26.2
CRP <2.5 mg/L	23.7
NT-proBNP	22.8
Diabetes Mellitus	13.5

Abbreviations as in Supplementary Table 3

Supplementary Table 7. Relative importance of variables included in the combined model for the absence of coronary atherosclerosis

Variable	Relative importance (%)
Age	100.0
Family history of CAD	58.6
REN	56.1
CCL24	55.0
GDF-15	54.8
CHIT1	53.2
MB	53.2
LEP	51.6
Systolic bloodpressure	51.3
CRP <2.5 mg/L	50.0
PLA2G7	47.5
OPG	47.4
Statin use	45.9
IGFBP-2	40.8
MMP12	40.3
PRSS27	40.3

Supplementary Table 7. ***Continued***

Variable	Relative importance (%)
TNFRSF9	38.9
TFPI	37.9
IL-17C	37.0
UMOD	36.2
TIE2	36.2
PGF	36.1
LDL-cholesterol	35.6
SLAMF1	35.2
Gal-9	34.6
IL2-RA	34.2
Smoker	34.0
SAA4	34.0
IL-1RT1	33.5
GT	33.0
IL-10RB	31.0
GDNF	30.2
CTSD	29.3
BMI	28.6
IL-27	28.5
Flt3L	28.4
Troponin-T	27.4
CTSL1	25.3
IL6	24.4
HDL-cholesterol	23.8
TFF3	23.7
CCL20	23.1
DCN	22.0
LOX-1	20.9
Total cholesterol	18.5
Diabetes	18.2
eGFR	17.9
NT-proBNP	17.8

Abbreviations as in Supplementary Table 3 and 5

References

1. Danad I, Raijmakers PG, Driessen RS et al. Comparison of Coronary CT Angiography, SPECT, PET, and Hybrid Imaging for Diagnosis of Ischemic Heart Disease Determined by Fractional Flow Reserve. JAMA Cardiol 2017;2:1100-1107.
2. Agatston AS, Janowitz WR, Hildner FJ, Zusmer NR, Viamonte M, Jr., Detrano R. Quantification of coronary artery calcium using ultrafast computed tomography. J Am Coll Cardiol 1990;15:827-832.
3. Nerlekar N, Ha FJ, Cheshire C et al. Computed Tomographic Coronary Angiography-Derived Plaque Characteristics Predict Major Adverse Cardiovascular Events: A Systematic Review and Meta-Analysis. Circ Cardiovasc Imaging 2018;11:e006973.
4. Otsuka K, Fukuda S, Tanaka A et al. Napkin-ring sign on coronary CT angiography for the prediction of acute coronary syndrome. JACC Cardiovasc Imaging 2013;6:448-457.
5. Park HB, Heo R, Hartaigh B et al. Atherosclerotic plaque characteristics by CT angiography identify coronary lesions that cause ischemia: a direct comparison to fractional flow reserve. JACC Cardiovasc Imaging 2015;8:1-10.
6. Meinshausen N. Stability selection. J R Statist Soc B 2010;72:417-473.
7. Wolpert DH. Stacked generalization. Neural Networks 1992;5:241-259.
8. Caruana R, Niculescu-Mizil A, Crew G, Ksikes A. Ensemble Selection from Libraries of Models. Twenty-first international conference on Machine learning - ICML '04 ACM 2014;18.
9. Chen T, Guestrin C. XGBoost: A Scalable Tree Boosting System. Proceedings of the 22nd ACM SIGKDD International Conference on Knowledge Discovery and Data Mining ACM 2016:785–794.
10. Lovric M. International Encyclopedia of Statistical Science: Springer, Berlin, Heidelberg, 2011.
11. Yamada S, Wang KY, Tanimoto A et al. Matrix metalloproteinase 12 accelerates the initiation of atherosclerosis and stimulates the progression of fatty streaks to fibrous plaques in transgenic rabbits. Am J Pathol 2008;172:1419-29.
12. Goncalves I, Bengtsson E, Colhoun HM et al. Elevated Plasma Levels of MMP-12 Are Associated With Atherosclerotic Burden and Symptomatic Cardiovascular Disease in Subjects With Type 2 Diabetes. Arterioscler Thromb Vasc Biol 2015;35:1723-31.
13. Lp PLASC, Thompson A, Gao P et al. Lipoprotein-associated phospholipase A(2) and risk of coronary disease, stroke, and mortality: collaborative analysis of 32 prospective studies. Lancet 2010;375:1536-44.
14. Serruys PW, Garcia-Garcia HM, Buszman P et al. Effects of the direct lipoprotein-

associated phospholipase A(2) inhibitor darapladib on human coronary atherosclerotic plaque. Circulation 2008;118:1172-1182.
15. White HD, Held C, Stewart R et al. Darapladib for preventing ischemic events in stable coronary heart disease. N Engl J Med 2014;370:1702-1711.
16. O'Donoghue ML, Braunwald E, White HD et al. Effect of darapladib on major coronary events after an acute coronary syndrome: the SOLID-TIMI 52 randomized clinical trial. JAMA 2014;312:1006-1015.
17. Cheng W, Zhao Y, Wang S, Jiang F. Tumor necrosis factor-related apoptosis-inducing ligand in vascular inflammation and atherosclerosis: a protector or culprit? Vascul Pharmacol 2014;63:135-44.
18. Harper E, Forde H, Davenport C, Rochfort KD, Smith D, Cummins PM. Vascular calcification in type-2 diabetes and cardiovascular disease: Integrative roles for OPG, RANKL and TRAIL. Vascul Pharmacol 2016;82:30-40.
19. Secchiero P, Candido R, Corallini F et al. Systemic tumor necrosis factor-related apoptosis-inducing ligand delivery shows antiatherosclerotic activity in apolipoprotein E-null diabetic mice. Circulation 2006;114:1522-30.
20. Watt V, Chamberlain J, Steiner T, Francis S, Crossman D. TRAIL attenuates the development of atherosclerosis in apolipoprotein E deficient mice. Atherosclerosis 2011;215:348-54.
21. Deftereos S, Giannopoulos G, Kossyvakis C et al. Association of soluble tumour necrosis factor-related apoptosis-inducing ligand levels with coronary plaque burden and composition. Heart 2012;98:214-8.
22. Van Campenhout A, Golledge J. Osteoprotegerin, vascular calcification and atherosclerosis. Atherosclerosis 2009;204:321-9.
23. van Thiel BS, van der Pluijm I, te Riet L, Essers J, Danser AH. The renin-angiotensin system and its involvement in vascular disease. Eur J Pharmacol 2015;763:3-14.
24. Lind L, Arnlov J, Lindahl B, Siegbahn A, Sundstrom J, Ingelsson E. Use of a proximity extension assay proteomics chip to discover new biomarkers for human atherosclerosis. Atherosclerosis 2015;242:205-10.
25. Ichiki T. Thyroid hormone and atherosclerosis. Vascul Pharmacol 2010;52:151-6.
26. Tsiantoulas D, Sage AP, Goderle L et al. BAFF Neutralization Aggravates Atherosclerosis. Circulation 2018.
27. Jackson SW, Scharping NE, Jacobs HM, Wang S, Chait A, Rawlings DJ. Cutting Edge: BAFF Overexpression Reduces Atherosclerosis via TACI-Dependent B Cell Activation. J Immunol 2016;197:4529-4534.
28. Kyaw T, Tay C, Hosseini H et al. Depletion of B2 but not B1a B cells in BAFF receptor-

deficient ApoE mice attenuates atherosclerosis by potently ameliorating arterial inflammation. PLoS One 2012;7:e29371.
29. Sage AP, Tsiantoulas D, Baker L et al. BAFF receptor deficiency reduces the development of atherosclerosis in mice--brief report. Arterioscler Thromb Vasc Biol 2012;32:1573-6.
30. Quarles LD. FGF23, PHEX, and MEPE regulation of phosphate homeostasis and skeletal mineralization. Am J Physiol Endocrinol Metab 2003;285:E1-9.
31. Miteva K, Madonna R, De Caterina R, Van Linthout S. Innate and adaptive immunity in atherosclerosis. Vascul Pharmacol 2018.
32. Schlittenhardt D, Schober A, Strelau J et al. Involvement of growth differentiation factor-15/macrophage inhibitory cytokine-1 (GDF-15/MIC-1) in oxLDL-induced apoptosis of human macrophages in vitro and in arteriosclerotic lesions. Cell Tissue Res 2004;318:325-33.
33. Bonaterra GA, Zugel S, Thogersen J et al. Growth differentiation factor-15 deficiency inhibits atherosclerosis progression by regulating interleukin-6-dependent inflammatory response to vascular injury. J Am Heart Assoc 2012;1:e002550.
34. Rohatgi A, Patel P, Das SR et al. Association of growth differentiation factor-15 with coronary atherosclerosis and mortality in a young, multiethnic population: observations from the Dallas Heart Study. Clin Chem 2012;58:172-82.
35. Tsai CS, Huang CY, Chen CH et al. Eotaxin-2 increased toll-like receptor 4 expression in endothelial cells in vitro and exacerbates high-cholesterol diet-induced atherogenesis in vivo. Am J Transl Res 2016;8:5338-5353.
36. Boot RG, van Achterberg TA, van Aken BE et al. Strong induction of members of the chitinase family of proteins in atherosclerosis: chitotriosidase and human cartilage gp-39 expressed in lesion macrophages. Arterioscler Thromb Vasc Biol 1999;19:687-94.
37. Artieda M, Cenarro A, Ganan A et al. Serum chitotriosidase activity is increased in subjects with atherosclerosis disease. Arterioscler Thromb Vasc Biol 2003;23:1645-52.
38. Kitamoto S, Egashira K, Ichiki T et al. Chitinase inhibition promotes atherosclerosis in hyperlipidemic mice. Am J Pathol 2013;183:313-25.
39. Payne GA, Tune JD, Knudson JD. Leptin-induced endothelial dysfunction: a target for therapeutic interventions. Curr Pharm Des 2014;20:603-8.
40. Yang H, Guo W, Li J et al. Leptin concentration and risk of coronary heart disease and stroke: A systematic review and meta-analysis. PLoS One 2017;12:e0166360.
41. Caselli C, De Graaf MA, Lorenzoni V et al. HDL cholesterol, leptin and interleukin-6 predict high risk coronary anatomy assessed by CT angiography in patients with stable chest pain. Atherosclerosis 2015;241:55-61.
42. Torffvit O, Melander O, Hulten UL. Urinary excretion rate of Tamm-Horsfall protein is

related to salt intake in humans. Nephron Physiol 2004;97:p31-6.
43. Hession C, Decker JM, Sherblom AP et al. Uromodulin (Tamm-Horsfall glycoprotein): a renal ligand for lymphokines. Science 1987;237:1479-84.
44. Leiherer A, Muendlein A, Saely CH et al. Serum uromodulin is a predictive biomarker for cardiovascular events and overall mortality in coronary patients. Int J Cardiol 2017;231:6-12.
45. Venuraju SM, Yerramasu A, Corder R, Lahiri A. Osteoprotegerin as a predictor of coronary artery disease and cardiovascular mortality and morbidity. J Am Coll Cardiol 2010;55:2049-61.
46. Jung IH, Oh GT. The Roles of CD137 Signaling in Atherosclerosis. Korean Circ J 2016;46:753-761.
47. Jung IH, Choi JH, Jin J et al. CD137-inducing factors from T cells and macrophages accelerate the destabilization of atherosclerotic plaques in hyperlipidemic mice. FASEB J 2014;28:4779-91.
48. Olofsson PS, Soderstrom LA, Wagsater D et al. CD137 is expressed in human atherosclerosis and promotes development of plaque inflammation in hypercholesterolemic mice. Circulation 2008;117:1292-301.
49. Soderstrom LA, Gertow K, Folkersen L et al. Human genetic evidence for involvement of CD137 in atherosclerosis. Mol Med 2014;20:456-65.
50. Yan J, Wang C, Chen R, Yang H. Clinical implications of elevated serum soluble CD137 levels in patients with acute coronary syndrome. Clinics (Sao Paulo) 2013;68:193-8.
51. Thygesen K, Mair J, Giannitsis E et al. How to use high-sensitivity cardiac troponins in acute cardiac care. Eur Heart J 2012;33:2252-7.
52. Jaffery Z, Nowak R, Khoury N et al. Myoglobin and troponin I elevation predict 5-year mortality in patients with undifferentiated chest pain in the emergency department. Am Heart J 2008;156:939-45.

Chapter 7

Independent prognostic value of coronary artery calcium score and coronary computed tomography angiography in an outpatient cohort of low to intermediate risk chest pain patients

Michiel J. Bom, Petrus M. van der Zee, Friso M. van der Zant,
Remco J.J. Knol, and Jan H. Cornel

Neth Heart J. 2016;24(5):332-42

Abstract

Background. Limited studies report on the additional prognostic value of coronary computed tomography angiography (CCTA) and the coronary artery calcium score (CACS).

Methods. For a median of 637 days, 1551 chestpain out-patients without known coronary artery disease (CAD) and low or intermediate PTP of CAD were followed for major adverse cardiac events (MACE), defined as death, myocardial infarction or late revascularization. Cox proportional hazard regression was used to evaluate the independent prognostic value of CCTA and CACS.

Results. MACE occurred in 23 patients (1.5%): 3 (0.2%) death, 4 (0.3%) myocardial infarctions and 16 (1.3%) late revascularizations. Multivariate analysis showed independent prognostic value of CCTA ($p<0.001$), CACS of 100-400 ($p=0.035$) and CACS of >400 ($p=0.021$). CCTA showed obstructive CAD in 3.1% of patients with CACS=0. No events occurred in patients with CACS=0 without obstructive CAD at CCTA, whereas 2/23 patients (9%) with CACS=0 with obstructive CAD had a MACE.

Conclusions. Our study shows that both CCTA and higher CACS categories have independent prognostic value in chestpain patients with low to intermediate PTP of obstructive CAD, in which CCTA is appropriate. Furthermore a non-negligible amount of patients with CACS of zero have obstructive CAD at CCTA. CCTA can be used in these patients to identify those at risk for MACE.

Introduction

Quantification of coronary artery calcium by computed tomography represents a reliable estimate of atherosclerotic plaque burden and the prognostic value of the coronary artery calcium score (CACS) is well-established.(1,2) Recently, coronary computed tomographic angiography (CCTA) has emerged as an important imaging tool to detect the presence and extent of CAD.(3,4) Several large prospective trials have demonstrated the prognostic value of CCTA, with a high negative predictive value for the occurrence of major adverse cardiac events (MACE).(5-11) Overestimation of severity of CAD in patient with a high pre-test probability (PTP), however, is a known limitation of CCTA.(12,13) Thus the appropriate use criteria advise to use CCTA only in patients with low or intermediate PTP.(14) The aim of this study was therefore to evaluate the independent prognostic value of CCTA and CACS in a routine clinical cohort of symptomatic patients with low or intermediate PTP, in which CCTA is appropriate.

Methods

Population

From December 13, 2011 to August 26, 2014 all patients with chest pain with low or intermediate PTP of CAD, referred for CCTA from the outpatient clinic after a diagnostic work up, were prospectively included. None of the patients had a prior history of CAD. The PTP was calculated using the Duke Clinical Score.(15) PTP <15% was defined low and PTP 15-85% was defined intermediate, according to the ESC guidelines.(3) Baseline characteristics including age, gender, and cardiovascular risk factors, were prospectively entered in the database. All patients gave written informed consent for usage of their data.

Follow-up

Patients were followed for MACE, defined as all-cause mortality, myocardial infarction or revascularization (either CABG or PCI). A 60-day landmark was used to differentiate between CCTA-driven ICA and late revascularization, which is considered to be indicative for the prognostic value of CCTA. Patients with referral for ICA in the out-patient setting within 60 days after CCTA and subsequent revascularization were

considered as CCTA-driven and not as MACE. All other revascularizations within follow-up were considered as MACE. Information on myocardial infarction and revascularization was obtained from the electronic medical records. Information on mortality was obtained from the municipal personal records database.

CCTA preparation, acquisition and analysis

Patient preparation, image acquisition, and image analysis were performed as previously described(16) and as briefly described below. All scans were performed with a 2x64–slice flying focal spot, effectively 2x128–slice (Somatom Definition Flash; Siemens Medical Systems, Erlangen, Germany) and were evaluated by a CBCCT accredited nuclear medicine physician and a cardiologist experienced in the interpretation of CCTA in consensus. In case of disagreement a third opinion was decisive.

Radiation dose

The delivered radiation dose was generated automatically by the scanner software and represented as dose length product (DLP). The effective dose was calculated by multiplying the DLP with the k-factor of 0.014 mSv x $(mGy \times cm)^{-1}$, which is generally used in cardiac CT studies.

Definition of CAD

Obstructive CAD was defined as a lumen stenosis in any of the large vessels of >50%, either left main artery, left anterior descending artery, circumflex artery or right coronary artery. Normal coronary arteries were defined as CACS=0 and no coronary plaques. Non-obstructive CAD was defined as CACS>0 and/or any plaque that did not meet the criteria for obstructive CAD.

Statistical analysis

Statistical analysis was performed using SPSS software, version 22.0.0 (SPSS Inc, Chicago, Illinois). Continuous variables are presented as mean±SD and categorical variables as frequencies with percentages. Continuous variables were tested for normal distribution.

Kaplan-Meier analysis was used to assess MACE-free survival stratified by CACS and CCTA results. Univariate and subsequent multivariate cox proportional hazard

regression were used to evaluate the independent prognostic value of CACS and CCTA beyond clinical risk factors. The multivariate Cox regression was done stepwise according to the backwards approach, with $p<0.10$ as threshold for removal of variables. Clinical risk factors included for univariate analysis were male gender, age, diabetes, smoking, hyperlipidaemia, hypertension, and family history of CAD. Selection of variables for entry in the multivariable Cox proportional hazard regression was based on univariate analysis with a threshold of $p < 0.10$.

Results

Population

1560 patients were initially included in the database for follow-up. Follow-up could be obtained in 99.4% of patients. Nine patients emigrated to a foreign country and were lost to follow-up. The total number of studied patients was 1551. An overview of the baseline characteristics is shown in table 1.

CCTA data

CACS, CCTA results and radiation dose are summarized in table 2. Two patients with left main CAD on CCTA also had three-vessel disease.

Follow-up

The cohort was followed for a median of 637 days. MACE occurred in 23 patients during follow-up. Three (0.2%) patients died, 4 (0.3%) patients had a myocardial infarction, and 20 (1.3%) patients had non-CCTA-driven revascularizations. Four (0.3%) were acute revascularization in myocardial infarction patients and 16 (1.0%) were late revascularizations, referred beyond 60 days after CCTA because of ongoing symptoms. The mean revascularization time was 205.3 (±220.5) days.

Figure 1 shows the MACE-free survival estimates stratified by CACS and CCTA results. Both increase in CACS and presence of obstructive CAD at CCTA were associated with decreased MACE-free survival (log-rank p-value <0.01).

MACE occurred in 0 patients with normal coronary arteries at CCTA, in 1.0% of patients with non-obstructive CAD at CCTA and in 7.5% of patients with obstructive

Table 1 Baseline characteristics

Demographics	Total (n=1551)
Age	58.0 ± 10.2
Women	968 (62.4%)
Body Mass Index	26.6 ± 4.5
Diabetes	121 (7.8%)
Hba1c (n=53) *	6.8 ± 1.6
Hypertension	464 (29.9%)
Hyperlipidemia	393 (25.3%)
Family history of CAD †	731 (47.2%)
Smoking	277 (17.9%)
eGFR<60	44 (2.8%)
Duke Clinical Score	
Low (<15%)	527 (34.0%)
Low-intermediate (15-50%)	760 (49.0%)
High-intermediate (50-85%)	264 (17.0%)
Baseline medication use	
Aspirin	499 (32.2%)
Statin	531 (34.2%)
Beta-blocker	604 (38.9%)
ACE-i / ARB	390 (25.1%)
Calcium channel blocker	96 (6.2%)
Nitrate	49 (3.2%)
Acenocoumarol	38 (2.5%)

* = Hba1C was documented in only 53 patients; † = in 2 patients family history was missing. ACE-I / ARB = ACE-inhibitor / Angiotensin receptor blocker; eGFR = estimated glomerular filtration rate

CAD at CCTA. MACE occurred during follow-up in patients with CACS of zero in 0.3% of cases, in patients with CACS 1-100 in 1.0% of cases, in patients with CACS 101-400 in 4.2% cases and in patients with CACS>400 in 7.1% of cases.

Of all 739 patients with CACS of zero 23 (3.1%) had obstructive CAD at CCTA and 62 (8.4%) had non-obstructive CAD at CCTA. No events occurred in patients with CACS of zero and no obstructive CAD at CCTA, whereas 2/23 patients (9%) with CACS of zero and obstructive CAD at CCTA had a MACE during follow-up: late revascularization in both cases. MACE-free survival was significantly worse in CACS

Table 2 CCTA data

	Total (n=1551)
Coronary artery calcium score	
0	739 (47.6%)
0.1-100	498 (32.1%)
100-400	215 (13.9%)
>400	99 (6.5%)
CCTA results	
Normal coronary arteries	654 (42.2%)
Non-obstructive CAD	683 (44.0%)
Obstructive CAD (>50%)	214 (13.8%)
1-vessel	164 (10.6%)
2-vessel	34 (2.2%)
3-vessel	13 (0.8%)
Left main	4 (0.3%)
High risk lesions*	48 (3.1%)
Radiation dose	
All patients (n=1551)	2.4±2.0 mSv
High-pitch FLASH scans (n=1130)	1.6±0.7 mSv
Prospectively triggered scans (n=386)	4.5±2.5 mSv
Retrospectively triggered scans (n=35)	6.5±2.7 mSv

* high risk lesions were defined as left main, 3-vessel and/or proximal LAD disease; CAD = coronary artery disease; CCTA = coronary computed tomography angiography; PTP = pre-test probability

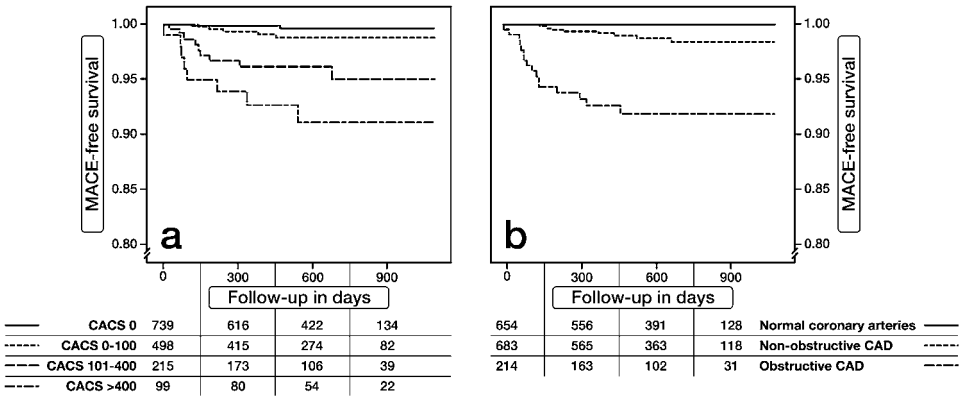

Figure 1. Kaplan-Meier curves of MACE-free survival stratified by CACS (a) and CCTA results (b)

zero patients with obstructive CAD, log-rank p-value<0.001.

Independent prognostic value of CACS and CCTA

The evaluation of the predictive value of CACS and CCTA by univariate and multivariate cox proportional hazard regression is shown in table 3. By univariate analysis, increased risk of MACE was observed with increasing CACS (p-value <0.001). Furthermore, obstructive CAD at CCTA was associated with a 13-fold increase in unadjusted risk of MACE. Of all clinical risk factors male gender and hypertension had a p-value of <0.10 and were subsequently included in the multivariate analysis.

Table 3 Univariate and multivariate Cox regression of risk factors, CACS and CCTA

	Hazard ratio	95% CI	P-value
Univariate analysis			
Male gender	2.18	0.96 – 4.97	0.064*
Age	1.02	0.98 – 1.07	0.26
DM	1.15	0.55 – 2.43	0.71
Hypertension	2.31	1.02 – 5.24	0.045*
Family history	1.76	0.76 – 4.07	0.19
Smoking	0.71	0.21 – 2.40	0.58
Hyperlipidemia	1.97	0.85 – 4.55	0.11
CACS			
CACS=0	Reference	Reference	-
CACS 0-100	3.71	0.72 – 19.12	0.12
CACS 100-400	15.82	3.42 – 72.23	<0.001*
CACS >400	26.81	5.57 – 129.09	<0.001*
Obstructive CAD at CCTA	15.28	6.28 – 37.14	<0.001*
Multivariate analysis			
Obstructive CAD at CCTA	7.03	2.57 – 19.22	<0.001
CACS			
CACS=0	Reference	Reference	-
CACS 0-100	2.46	0.46 – 13.14	0.29
CACS 100-400	5.97	1.14 – 31.31	0.035
CACS >400	7.72	1.37 – 43.55	0.021

*: variables with p<0.10 on univariate analysis.

In the multivariate model obstructive disease on CCTA was independently associated with increased risk of MACE (p<0.001). Furthermore, CACS of 100-400 (p=0.035) and CACS of >400 (0.021) were independent predictors for the occurrence of MACE, whereas CACS of 0-100 (p=0.29) had no independent predictive value for the occurrence of MACE.

Discussion

Our study shows that in a routine clinical cohort of patients referred from the outpatient clinic with chest pain with low to intermediate PTP of obstructive CAD, the prognosis of a CACS of zero is excellent, with MACE during follow-up in only 0.3% of patients. However a non-negligible amount of patients with CACS of zero had obstructive CAD (3%). Presence of CAD in patients with CACS of zero was associated with worse prognosis.

Furthermore our study shows that although overall prognosis in this clinical cohort was excellent, presence of obstructive CAD on CCTA had independent prognostic value. CACS of 0-100 did not show independent prognostic value of CCTA, however CACS 100-400 and >400 did show independent prognostic value.

Prognostic value of CACS and CCTA

The prognostic value of CACS has been previously demonstrated in large meta-analyses.(1,2) A recently published large multicentre international cohort by Al-Mallah et al. reported gradual increase in event-rate in patients with CACS of zero, CACS 1-100, 100-399 and >400, with comparable event-rates to our study.(10)

Multiple studies have previously reported on the prognostic value of CCTA for the occurrence of adverse events.(6-11) Our study results are in line with a recently published meta-analysis of 41,960 patients which reported that normal coronary arteries at CCTA are associated with a very low annual event rate of <0.5% and that obstructive CAD at CCTA is associated with higher event rates of 12.5%.(17) The slightly lower event rate in our study in patients with obstructive CAD at CCTA might be explained by the fact that no patients with high PTP were included in our study.

CACS of zero

Our study, in accordance with prior studies, showed an excellent prognosis of symptomatic patients with CACS of zero, with an event rate <1% within 2 years of follow-up.(10,18-20) Because of higher costs, the need to administer intravenous contrast and higher radiation burden of CCTA, it remains subject of discussion whether one should proceed with CCTA after CACS of zero in all patients, given the excellent prognosis of these patients. The ESC guidelines on stable CAD do not recommend the use of CACS to identify individuals at risk.(3) However a recent update of the American College of Cardiology and the American Heart Association stated that the exclusion of coronary calcium by CACS may be reasonable before considering further testing in symptomatic patients with low to intermediate PTP.(21) Our study confirms findings of recent studies that in symptomatic patients with CACS of zero a non-negligible rate of 1.4-4.5% have evidence of obstructive CAD at CCTA.(10,18,19) No events occurred during follow-up in patients with CACS of zero and no obstructive CAD at CCTA in our study and obstructive CAD at CCTA was significantly associated with worse prognosis. CCTA thus was able to accurately identify those with CACS of zero at risk for future events. Performing CCTA after CACS of zero may still be advisable in symptomatic patients with low to intermediate PTP to identify those at risk for future events.

Independent prognostic value of CCTA

Several studies have been published on the independent prognostic value of CCTA to CACS. Cho et al. reported that in 7590 studied asymptomatic patients, CCTA did not have prognostic value independent of CACS.(22) Other studies have shown that in predominantly symptomatic patients, CCTA has added prognostic value to CACS and clinical risk factors.(6,10,23) These studies, however, differ in study populations from our study. Hadamitzky et al. reported on the added prognostic value of CCTA to CACS in a population of both symptomatic and asymptomatic patients.(23) The single centre study by Hou et al. included a substantial amount of asymptomatic patients and patients with high PTP.(6) Both Al-Mallah et al. and Van Werkhoven et al. studied solely symptomatic patients, 10% of their population, however, had a high PTP.(8,10) The appropriate use criteria advise to only use CCTA in low or intermediate PTP.(14) While our findings are mainly of confirmatory nature, our study does provides some

additional information about the independent prognostic value of CCTA to CACS in a Dutch routine clinical cohort of symptomatic patients, in which CCTA is appropriate. (14)

Independent prognostic value of CACS

Data on the independent prognostic value of CACS in the CCTA era is limited.(24-26) Chaikriangkrai et al recently reported independent prognostic value of both CCTA and CACS, with prognostic value across all categories of CACS.(24) In our study CACS had independent prognostic value, however only in the categories CACS 100-400 and >400, whereas CACS 0-100 did not have prognostic value. This may be partly explained by the relatively low event rate and the lower risk population compared to the study population of Chaikriangkrai et al. The independent prognostic power of higher categories of CACS together with the fact that severe coronary calcification is associated with decreased diagnostic accuracy of CCTA,(27) support the use of CACS with CCTA as compared to CCTA only.

Clinical implications

The recently published PROMISE trial investigated symptomatic patients with suspected CAD who require non-invasive testing and reported no difference in outcome between an initial strategy of CCTA and functional testing. (28) However, questions were raised about the safety of the CCTA strategy because of a relatively high radiation dose. Reported radiation dose in previous reports on the prognostic value of CCTA, ranged from 3-18mSv.(5,23,28). With the use of a high resolution (2x128) scanner and predominantly flash or prospective scanning protocol, we were able to perform a complete CCTA (calcium score and angiography) with an excellent prognostic value and a substantially lower radiation burden of 2.4±2.0 mSv. Although the event-rate was relatively low in our study, this further supports the use of an initial CCTA strategy in patients with low to intermediate PTP of obstructive CAD.

Study limitations

The single centre design of our study allows for the evaluation of prognosis in a "real world" clinical setting. However, our results may not be applied to any out-patient chest pain population, i.e. asymptomatic or high risk patients. As in previous studies,

a 60-day landmark was used to differentiate between CCTA-driven ICA and long term revascularization, which is considered to be indicative for the prognostic value of CCTA.(6) Recently several studies have reported that CCTA has significant effect on downstream patient management.(29,30) In our study 93 (6.0%) patients underwent CCTA-guided revascularization (referral for PCI/CABG within 60 days of CCTA). Since the aim of our study was to evaluate the prognostic value of CCTA in a routine clinical cohort, these patients were not excluded for analysis. However, outcome of patient might have been confounded by CCTA-guided management changes.

Conclusion

This study shows that both CCTA and CACS of 100-400 and >400 have independent prognostic value for the occurrence of MACE in a routine clinical cohort of patients presenting to the outpatient clinic with atypical chest pain with low to intermediate PTP of obstructive CAD, in which CCTA is appropriate. Furthermore our study shows that a non-negligible amount of patients with CACS of zero have obstructive CAD at CCTA. CCTA can be used in patients with CACS of zero to identify those at risk for MACE.

References

1. Bellasi A, Lacey C, Taylor AJ, et al. Comparison of prognostic usefulness of coronary artery calcium in men versus women (results from a meta- and pooled analysis estimating all-cause mortality and coronary heart disease death or myocardial infarction). Am J Cardiol 2007;100:409-414.
2. Budoff MJ, Shaw LJ, Liu ST, et al. Long-term prognosis associated with coronary calcification: observations from a registry of 25,253 patients. J Am Coll Cardiol 2007;49:1860-1870.
3. Task Force Members, Montalescot G, Sechtem U, et al. 2013 ESC guidelines on the management of stable coronary artery disease: the Task Force on the management of stable coronary artery disease of the European Society of Cardiology. Eur Heart J 2013;34:2949-3003.
4. van der Wall EE. Crown years for non-invasive cardiovascular imaging (Part IV): 30 years of cardiac computed tomography. Neth Heart J 2013;21:315-318.
5. Min JK, Dunning A, Lin FY, et al. Age- and sex-related differences in all-cause mortality risk based on coronary computed tomography angiography findings results from the

International Multicenter CONFIRM (Coronary CT Angiography Evaluation for Clinical Outcomes: An International Multicenter Registry) of 23,854 patients without known coronary artery disease. J Am Coll Cardiol 2011;58:849-860.

6. Hou ZH, Lu B, Gao Y, et al. Prognostic value of coronary CT angiography and calcium score for major adverse cardiac events in outpatients. JACC Cardiovasc Imaging 2012;5:990-999.
7. Hadamitzky M, Taubert S, Deseive S, et al. Prognostic value of coronary computed tomography angiography during 5 years of follow-up in patients with suspected coronary artery disease. Eur Heart J 2013;34:3277-3285.
8. van Werkhoven JM, Schuijf JD, Gaemperli O, et al. Incremental prognostic value of multi-slice computed tomography coronary angiography over coronary artery calcium scoring in patients with suspected coronary artery disease. Eur Heart J 2009;30:2622-2629.
9. de Graaf FR, van Velzen JE, de Boer SM, et al. Non-invasive computed tomography coronary angiography as a gatekeeper for invasive coronary angiography. Int J Cardiovasc Imaging 2013;29:221-228.
10. Al-Mallah MH, Qureshi W, Lin FY, et al. Does coronary CT angiography improve risk stratification over coronary calcium scoring in symptomatic patients with suspected coronary artery disease? Results from the prospective multicenter international CONFIRM registry. Eur Heart J Cardiovasc Imaging 2014;15:267-274.
11. van Werkhoven JM, Gaemperli O, Schuijf JD, et al. Multislice computed tomography coronary angiography for risk stratification in patients with an intermediate pretest likelihood. Heart 2009;95:1607-1611.
12. Budoff MJ, Dowe D, Jollis JG, et al. Diagnostic performance of 64-multidetector row coronary computed tomographic angiography for evaluation of coronary artery stenosis in individuals without known coronary artery disease: results from the prospective multicenter ACCURACY (Assessment by Coronary Computed Tomographic Angiography of Individuals Undergoing Invasive Coronary Angiography) trial. J Am Coll Cardiol 2008;52:1724-1732.
13. Meijboom WB, van Mieghem CA, Mollet NR, et al. 64-Slice Computed Tomography Coronary Angiography in Patients with High, Intermediate, Or Low Pretest Probability of Significant Coronary Artery Disease. J Am Coll Cardiol 2007;50:1469-1475.
14. Taylor AJ, Cerqueira M, Hodgson JM, et al. ACCF/SCCT/ACR/AHA/ASE/ASNC/NASCI/SCAI/SCMR 2010 appropriate use criteria for cardiac computed tomography. A report of the American College of Cardiology Foundation Appropriate Use Criteria Task Force, the Society of Cardiovascular Computed Tomography, the American

College of Radiology, the American Heart Association, the American Society of Echocardiography, the American Society of Nuclear Cardiology, the North American Society for Cardiovascular Imaging, the Society for Cardiovascular Angiography and Interventions, and the Society for Cardiovascular Magnetic Resonance. J Am Coll Cardiol 2010;56:1864-1894.

15. Bayliss J. Duke Clinical Score: Prediction of Coronary Heart Disease in a Patient with Chest Pain. April 2, 2009; Available at: http://www.zunis.org/DukeChestPain-CADPredictor.htm.
16. Krul MM, Bogaard K, Knol RJ, et al. Coronary artery disease in patients with atypical chest pain with and without diabetes mellitus assessed with coronary CT angiography. BMJ Open Diabetes Res Care 2014;2:e000004.
17. Habib PJ, Green J, Butterfield RC, et al. Association of cardiac events with coronary artery disease detected by 64-slice or greater coronary CT angiography: a systematic review and meta-analysis. Int J Cardiol 2013;169:112-120.
18. Villines TC, Hulten EA, Shaw LJ, et al. Prevalence and severity of coronary artery disease and adverse events among symptomatic patients with coronary artery calcification scores of zero undergoing coronary computed tomography angiography: results from the CONFIRM (Coronary CT Angiography Evaluation for Clinical Outcomes: An International Multicenter) registry. J Am Coll Cardiol 2011;58:2533-2540.
19. Kim YJ, Hur J, Lee HJ, et al. Meaning of zero coronary calcium score in symptomatic patients referred for coronary computed tomographic angiography. Eur Heart J Cardiovasc Imaging 2012;13:776-785.
20. Rijlaarsdam-Hermsen D, Kuijpers D, van Dijkman PR. Diagnostic and prognostic value of absence of coronary artery calcification in patients with stable chest symptoms. Neth Heart J 2011;19:223-228.
21. Greenland P, Bonow RO, Brundage BH, et al. ACCF/AHA 2007 clinical expert consensus document on coronary artery calcium scoring by computed tomography in global cardiovascular risk assessment and in evaluation of patients with chest pain: a report of the American College of Cardiology Foundation Clinical Expert Consensus Task Force (ACCF/AHA Writing Committee to Update the 2000 Expert Consensus Document on Electron Beam Computed Tomography) developed in collaboration with the Society of Atherosclerosis Imaging and Prevention and the Society of Cardiovascular Computed Tomography. J Am Coll Cardiol 2007;49:378-402.
22. Cho I, Chang HJ, Sung JM, et al. Coronary computed tomographic angiography and risk of all-cause mortality and nonfatal myocardial infarction in subjects without chest pain syndrome from the CONFIRM Registry (coronary CT angiography evaluation for

clinical outcomes: an international multicenter registry). Circulation 2012;126:304-313.
23. Hadamitzky M, Distler R, Meyer T, et al. Prognostic value of coronary computed tomographic angiography in comparison with calcium scoring and clinical risk scores. Circ Cardiovasc Imaging 2011;4:16-23.
24. Chaikriangkrai K, Velankar P, Schutt R, et al. Additive prognostic value of coronary artery calcium score over coronary computed tomographic angiography stenosis assessment in symptomatic patients without known coronary artery disease. Am J Cardiol 2015;115:738-744.
25. Kwon SW, Kim YJ, Shim J, et al. Coronary artery calcium scoring does not add prognostic value to standard 64-section CT angiography protocol in low-risk patients suspected of having coronary artery disease. Radiology 2011;259:92-99.
26. Hulten E, Bittencourt MS, Ghoshhajra B, et al. Incremental prognostic value of coronary artery calcium score versus CT angiography among symptomatic patients without known coronary artery disease. Atherosclerosis 2014;233:190-195.
27. Abdulla J, Pedersen KS, Budoff M, Kofoed KF. Influence of coronary calcification on the diagnostic accuracy of 64-slice computed tomography coronary angiography: a systematic review and meta-analysis. Int J Cardiovasc Imaging 2012;28:943-953.
28. Douglas PS, Hoffmann U, Patel MR, et al. Outcomes of anatomical versus functional testing for coronary artery disease. N Engl J Med 2015;372:1291-1300.
29. Cheezum MK, Hulten EA, Smith RM, et al. Changes in preventive medical therapies and CV risk factors after CT angiography. JACC Cardiovasc Imaging 2013;6:574-581.
30. Hulten E, Bittencourt MS, Singh A, et al. Coronary artery disease detected by coronary computed tomographic angiography is associated with intensification of preventive medical therapy and lower low-density lipoprotein cholesterol. Circ Cardiovasc Imaging 2014;7:629-38.

Chapter 8

Prognostic Value of RCA Pericoronary Adipose Tissue CT-Attenuation Beyond High-Risk Plaques, Plaque Volume, and Ischemia

Michiel J. Bom*, Pepijn A. van Diemen*, Roel S. Driessen, Stefan P. Schumacher, Henk Everaars, Ruben W. de Winter, Peter M. van de Ven, Moti Freiman, Liran Goshen, Dennis Heijtel, Eran Langzam, James K. Min, Jonathon A. Leipsic, Pieter G. Raijmakers, Albert C. van Rossum, Ibrahim Danad, and Paul Knaapen

* Both authors contributed equally

JACC Cardiovasc Imaging. 2021;14(8):1598-1610

Abstract

Objectives: To assess the prognostic value of pericoronary adipose tissue CT-attenuation (PCATa) beyond quantitative coronary computed tomography angiography (CCTA)-derived plaque volume and positron emission tomography (PET) determined ischemia.

Background: Inflammation plays a crucial role in atherosclerosis. PCATa has been demonstrated to assess coronary specific inflammation and is of prognostic value in patients with suspected coronary artery disease (CAD).

Methods: 539 patients who underwent CCTA and $[^{15}O]H_2O$ PET perfusion imaging because of suspected CAD were included. Imaging assessment included coronary artery calcium score (CACS), presence of obstructive CAD (≥50% stenosis) and high-risk plaques (HRP), total plaque volume (TPV), calcified/noncalcified plaque volume (CPV/NCPV), PCATa, and myocardial ischemia. The endpoint was a composite of death and non-fatal myocardial infarction (MI). Prognostic thresholds were determined for quantitative CCTA variables.

Results: During a median follow-up of 5.0 [interquartile range: 4.7-5.0] years, 33 events occured. CACS >59 Agatston, obstructive CAD, HRPs, TPV >220mm^3, CPV>110mm^3, NCPV >85mm^3, and myocardial ischemia were associated with shorter time to the endpoint with unadujsted hazard ratio's (HR) of 4.17 (95% confidence interval (CI): 1.80-9.64), 4.88 (95% CI: 1.88-12.65), 3.41 (95% CI: 1.72-6.75), 7.91 (95% CI: 3.05-20.49), 5.82 (95% CI: 2.40-14.10), 8.07 (95% CI: 3.33-19.55), and 4.25 (95% CI: 1.84-9.78), respectively ($p<0.05$ for all). RCA PCATa above scanner specific thresholds was associated with worse prognosis (unadjusted HR: 2.84 (95% CI: 1.44-5.63), p=0.003), whereas LAD and Cx PCATa were not related to outcome. RCA PCATa above scanner specific thresholds retained is prognostic value adjusted for imaging variables and clincal chacteristics associated with the endpoint (adjusted HR: 2.45 (95% CI: 1.23-4.93), p=0.011).

Conclusions: Parameters associated with atherosclerotic burden and ischemia were more strongly associated with outcome than RCA PCATa. Nonetheless, RCA PCATa was of prognostic value beyond clinical characteristics, CACS, obstructive CAD, HRPs, TPV, CPV, NCPV, and ischemia.

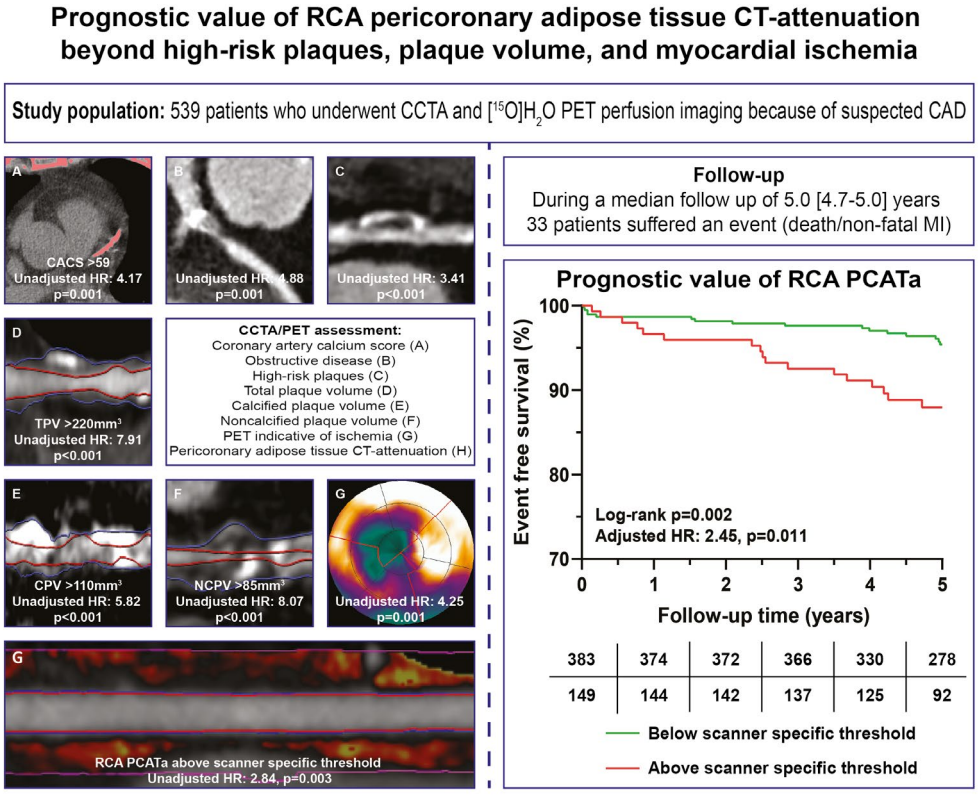

Central illustration.
The present study assessed the prognostic value of PCATa among 539 patients with suspected CAD that underwent CCTA and [15O]H2O PET perfusion imaging. Imaging assessment consisted of CACS, presence of obstructive CAD and HRPs, TPV, CPV, NCPV, PCATa, and myocardial ischemia. Prognostic thresholds were determined for quantitative CCTA variables. All imaging variables were associated with events. With regard to PCATa, only RCA PCATa above scanner specific thresholds was associated with detrimental outcome in terms of death and non-fatal MI and remained a significant predictor of events adjusted for clinical characteristics and imaging parameters. Abbreviations; CACS: coronary artery calcium score, CAD: coronary artery disease, CCTA: coronary computed tomography angiography, CPV: calcified plaque volume, HR: hazard-ratio, HRP: high-risk plaque, HU: Hounsfield units, MI: myocardial infarction, NCPV: non-calcified plaque volume, PCATa: pericoronary adipose tissue CT-attenuation, PET: positron emission tomography, RCA: right coronary artery, TPV: total plaque volume.

Introduction

Traditionally assessment of coronary artery disease (CAD) involves determining the anatomical severity and it's functional significance (1). Non-invasively this can be achieved by combined positron emission tomography (PET) and coronary computed tomography angiography (CCTA) imaging (2). In the present cohort we have previously demonstrated that obstructive CAD, high-risk plaques (HRP), and ischemia are associated with outcome, of which obstructive CAD and HRPs were of independent prognostic value (2). However, these markers of CAD do not harbor information regarding the inflammatory burden of a patient. Inflammation plays a crucial role in atherosclerosis, as such accurate assessment of inflammatory risk might improve risk stratification and allow patient tailored anti-inflammatory treatment (3). Currently, detection of coronary inflammation is hampered by a lack of specificity (e.g. serum biomarkers) or by limited availability and relatively high costs (^{18}F-FDG or ^{18}F-NaF PET) (3). Interestingly, CCTA as a widely available and utilized diagnostic tool might mediate these limitations by being able to detect changes in pericoronary adipose tissue as a response to inflammation (4). Inflamed coronaries release mediators that can lead to morphological changes of the adipocytes residing in pericoronary adipose tissue (4, 5). These alterations can be evaluated by quantifying pericoronary adipose tissue CT-attenuation (PCATa) (4). The CRISP-CT study, demonstrated that the perivascular fat attenuation index (FAI) of the right coronary artery (RCA) was of prognostic importance over clinical characteristics, qualitatively assessed extent of CAD, and HRP features (6). However, recent studies suggest superior prognostic value of quantitative plaque analysis over qualitative assessment (7, 8). Studies investigating the prognostic value of PCATa beyond quantitative plaque volume are lacking. Therefore, the present study investigated whether PCATa retained its prognostic value beyond quantitative plaque measurements and ischemia.

Methods

Study population

650 patients who underwent CCTA and [^{15}O]H_2O PET perfusion imaging at the Amsterdam UMC: Vrije Universiteit Amsterdam between 2008 and 2014 because of suspected obstructive CAD were evaluated for inclusion. Of these, 32 (5%) were

excluded because of a documented history of CAD (prior myocardial infarction (MI), percutaneous coronary intervention, or coronary artery bypass grafting), whereas 25 (4%) were excluded due to uninterpretable image results. Of the remainder of patients, 54 (10%) were lost to follow-up, resulting in a study population of 539 patients (2) (Figure 1). The study complied with the Declaration of Helsinki. The local ethics committee approved the study protocol and waived the need for written informed consent.

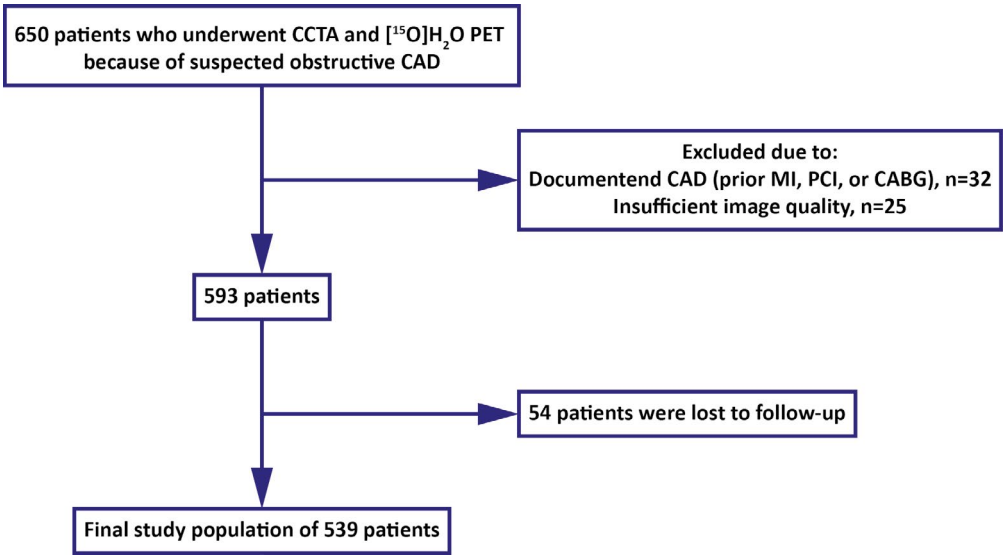

Figure 1. Flowchart of the included study population.
CABG: coronary artery bypass grafting, PCI: percutaneous coronary intervention, other abbreviations as in Central illustration.

CCTA acquisition

Images were acquired on a Gemini TF 64 PET/CT-scanner (352 patients) and on a 256-slice Brilliance iCT-scanner (187 patients) (both: Philips Healthcare, Best, The Netherlands). Prior to scanning, sublingual nitroglycerine spray was administered to all patients and metoprolol if necessary, aiming for a heart rate of <65 beats per minute. Coronary artery calcium scoring (CACS) in Agatston units was obtained during a single breath-hold on a non-contrast CT. Respective CCTA parameters for the 64-slice and 256-slice scanner entailed, a section collimation of 64*0.625mm and 128*0.625mm, a gantry rotation time of 420ms and 270ms, a tube current of 800-

1000mA and 200-360mA (adjusting mA based on patient's body size), and a tube voltage of 120kVp for both. Prospective ECG-gated CCTA acquisition was applied when allowed by heartrate, triggered at 75% of the R-R interval. For visualization of the coronary lumen, a bolus of 100 mL iobitidol (Xenetix 350) was injected intravenously (5.7 mL/s) followed immediately by a 50 mL saline chaser. Scans were triggered using an automatic bolus tracking technique, with a region of interest in the descending thoracic aorta.

CCTA assessment

Coronary segments with a diameter ≥2mm were assessed by a single reader (R.S.D. or M.J.B.) blinded to clinical outcome using semi-automated software (Comprehensive Cardiac Analysis, Philips Healthcare, Best, The Netherlands). The coronaries were evaluated using axial, multiplanar reformation, maximum intensity projection, and cross-sectional images (slice thickness 0.9mm, increment 0.50mm). The centerline and vessel contours were automatically detected and manually corrected if needed. A stenosis ≥50% was considered obstructive. The following HRP features were assessed: positive remodeling (PR), low-attenuation plaque (LAP), spotty calcification, and napkin-ring sign. The remodeling index was computed as the ratio of vessel area at the site of the maximal lesion to that of a proximal reference point, with an index >1.1 representing PR (9). LAP was defined as a plaque containing any voxel <30 Hounsfield units (HU). Spotty calcification was characterized by a calcified plaque comprising <90° of the vessel circumference and <3 mm in length (9). Napkin ring sign was defined by a plaque core with low attenuation surrounded by a rim-like area of higher attenuation (9). The presence of ≥2 HRP features defined a HRP. Quantitative plaque analyses were performed within manually designated regions. Total plaque volume (TPV) was calculated by summing volumes of separate plaques along each coronary artery. A threshold of 150 HU was used to distinguish non-calcified from calcified plaque and calculation of calcified/noncalcified plaque volume (CPV/NCPV) Supplemental Figure 1 presents a case example of quantitative plaque analysis.

PCATa

Coronaries with centerlines were segmented by a single reader blinded (M.J.B.) to clinical outcome via semi-automated software and manually corrected if needed

(Comprehensive Cardiac Analysis, Philips Healthcare, Best, The Netherlands). We were, due to technical difficulties, unable to extract the segmentations of 7 RCAs, 6 left anterior descending arteries (LAD), and 7 circumflex arteries (Cx). The extracted segmentations were utilized by our PCAT research prototype (Philips Healthcare, Best, the Netherlands) to detect the coronary lumen and walls using an automated algorithm (10). The automated algorithm defined the diameter of the vessel for each point along the centerline. Using the location specific diameter, PCAT was defined as tissue with HU ranging from -190 to -30 within a single concentric layer with a radial distance from the outer vessel wall equal to the diameter of the vessel (4, 6). The first mm of tissue following the vessel wall was excluded to prevent partial volume effects and artefacts due to contrast media in the lumen. PCATa analysis of the RCA involved the proximal 10mm to 50mm of the vessel, excluding the first 10mm to prevent noise from the aortic wall (6). Regarding the left coronary system, the proximal 40mm of the LAD and Cx were assessed, excluding the left main given its variable length and possible absence (6). Lastly, PCATa was calculated by averaging the attenuation of PCAT within region of interest of the corresponding coronary and presented as mean PCATa (HU). PCATa was obtained in <15 seconds. Figure 2 presents case examples of PCATa analyses.

$[^{15}O]H_2O$ PET

Images were acquired on a Gemini TF 64 PET/CT-scanner (Philips Healthcare, Best, The Netherlands). A dynamic perfusion scan was performed during resting as well as adenosine (140μg/kg/min) induced hyperemia using 370 MBq of $[^{15}O]H_2O$ as radioactive tracer. Low-dose CT-scans allowed for attenuation correction. Parametric images of myocardial blood flow (MBF) were generated using in-house developed software (*CardiacVUer,* Amsterdam UMC: Vrije Universiteit Amsterdam, Amsterdam, the Netherlands) (11). Vascular territories were defined according to the standardized 17-segment model of the American Heart Association. A hyperemic MBF ≤2.3 ml/min/g in two adjacent segments within a vascular territory was considered indicative of myocardial ischemia (12).

Follow-up

Follow-up data was obtained using a national registry database, medical records,

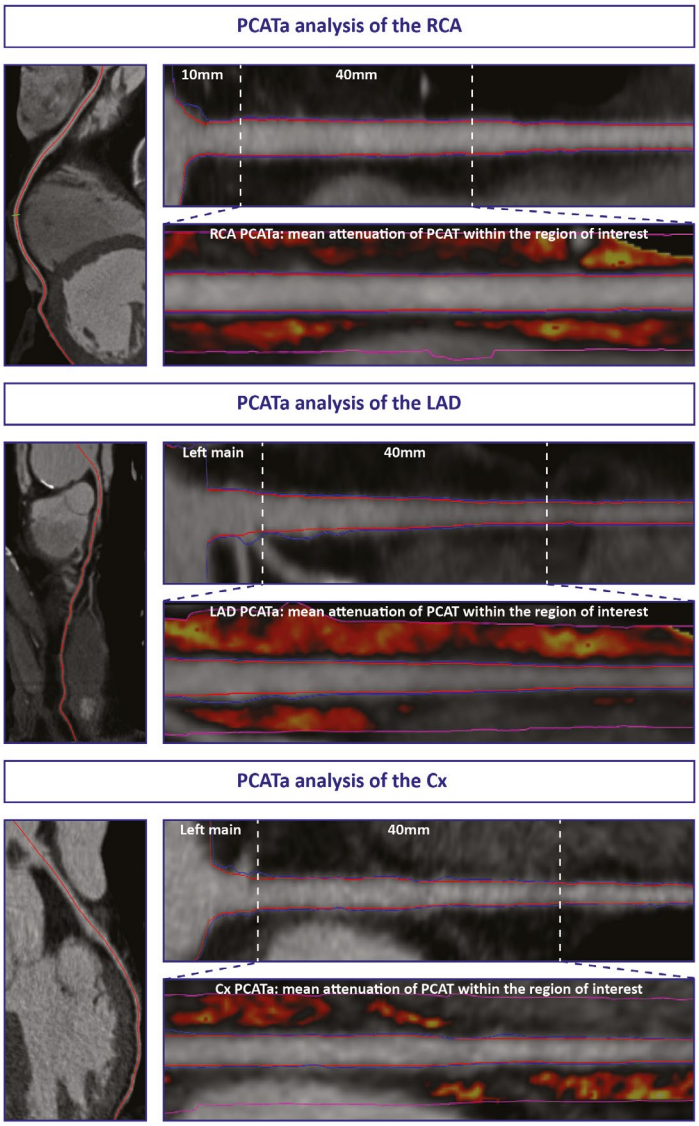

Figure 2. Case examples of RCA, LAD, and Cx PCATa analyses.
Coronary lumen and wall were automatically detected based on semi-automated coronary segmentation and centerlines. An automated algorithm defined the diameter of the vessel for each point along the centerline. PCAT was defined as tissue with HU ranging from -190 to -30 within a single concentric layer with a radial distance from the outer vessel wall equal to the diameter of the vessel of which the first mm following the coronary wall was excluded. PCATa analysis of the right coronary artery (RCA) involved the proximal 10mm to 50mm of the vessel, excluding the first 10mm to prevent noise from the aortic wall. Regarding the left coronary system, the proximal 40mm of the left anterior descending artery (LAD) and circumflex artery (Cx) were assessed, excluding the left main given its variable length and possible absence. PCATa was calculated by averaging the attenuation of PCAT within the region of interest of the corresponding coronary and presented as mean PCATa (HU). Cx = circumflex artery; LAD = left anterior descending artery, other abbreviations as in Central Illustration.

and telephonic contact. The endpoint was a composite of death and non-fatal MI. Events were adjudicated in accordance with current guidelines (13). Early and late revascularization were defined as revascularization based on the initial diagnostic work-up or revascularization after an initially conservative treatment, respectively.

Statistical analysis

Statistical analyses were performed using SPSS version 26.0 (IBM SPSS Statistics, Armonk, New-York), except for the construction of time-dependent receiver operating characteristics (ROC) curves which were performed using the survivalROC package of R (R Foundation for Statistical Computing, Vienna, Austria). Normally distributed variables are presented as mean ± standard deviation and compared between groups using independent sample t-tests. Non-normally distributed variables are presented as median with interquartile range and compared with a Mann-Whitney U test. Categorical variables are presented as frequencies with percentages and compared with the Fisher's Exact test, except for type of chest pain which was compared using the Pearson Chi-Square test. Correlations were assessed using Pearson's and Spearman's correlations when appropriate. Time-dependent ROC curves of quantitative CCTA variables for prediction of events within the first 5 years of follow-up were constructed. Optimal cut-offs were determined by maximizing the Youden-index. The first 5 years of follow-up were utilized as the majority of patients without an event (74%) had 5 year follow-up available, allowing assessment of prognostic thresholds in an adequate sample of the population. Follow-up was censored after 5 years to match the time span on which the time dependent ROC curve derived prognostic thresholds were based. Kaplan-Meier curves were plotted to visualize event-free survival and compared with Log-rank tests. Univariable Cox proportional hazard regression analyses were used to identify variables associated with outcome ($p<0.10$). Multivariable Cox proportional hazard regression analyses using backward selection and enter mode were used to assess the independent prognostic value of clinical and imaging variables. A two-sided p-value <0.05 was considered statistically significant.

Results

Patient characteristics and follow-up results

Patient characteristics and imaging results are displayed in Table 1. During a median follow-up of 5.0 [4.7-5.0] years, 17 (3%) patients suffered an MI and 16 (3%) died. Of the 17 patients that had an MI, 11 (65%) had a non-ST segment elevation myocardial infarction (NSTEMI), 5 (29%) had an ST segment elevation myocardial infarction, and 1 (6%) MI was not further specified. The RCA and LAD were the culprit in 4 (24%) patients each, whereas the Cx was the culprit in 3 (18%) patients. Four (24%) patients had an NSTEMI witout clear culprit and in 2 (11%) patients culprit vessel was not documented. In total, 109 (20%) patients underwent early revascularization and 31 (6%) underwent late revascularization.

PCATa values

RCA, LAD, and Cx PCATa values were normally distributed and differed between the 64-slice and 256-slice CT-scanner (Figure 3). RCA PCATa correlated with LAD and Cx PCATa on the 64-slice *(*R=0.480, p<0.001 and R=0.472, p<0.001) and 256-slice (R=0.354, p<0.001 and R=0.425, p<0.001) CT-scanner, LAD and Cx PCATa correlated on both scanners as well (R=0.808, p<0.001 and R=0.776, p<0.001) (Supplemental Figure 2).

Association of PCATa with plaque volume and perfusion

RCA, LAD, and Cx PCATa did not correlate with TPV, CPV, and NCPV of the respective coronary (Supplemental Figure 3, 4, and 5). Futhermore, hyperemic MBF of the RCA, LAD, and Cx did not correlate with PCATa of the RCA, LAD, and Cx, respectively (Supplemental Figure 6).

Association of imaging parameters with outcome

Obstructive CAD, HRPs, and ischemia were more prevalent among patient with an endpoint (Table 1). Furthermore, CACS, TPV, CPV, and NCPV were higher in patients who experienced an event as compared to those who did not, whereas PCATa did not differ between patients with and without an event. Prognostic thresholds for quantitative CCTA variables and scanner specific PCATa thresholds are presented in

Table 1. Patient and imaging characteristics.

	Overall (N=539)	No event (N=506)	Event (N=33)	p-value
Demographics				
Age, years	58.6 ± 9.2	58.3 ± 9.2	62.5 ± 7.4	0.011
Male	297 (55%)	275 (54%)	22 (67%)	0.207
BMI, kg/m^2	27.0 ± 4.1	27.0 ± 4.2	26.3 ± 3.1	0.287
Cardiovascular risk factors				
Diabetes Mellitus	94 (17%)	84 (17%)	10 (30%)	0.059
Hypertension	251 (47%)	232 (46%)	19 (58%)	0.280
Hyperlipidemia	196 (36%)	179 (35%)	17 (52%)	0.092
Current smoker	184 (34%)	173 (34%)	11 (33%)	>0.999
Family history of CAD	286 (53%)	270 (53%)	16 (49%)	0.591
Type of chestpain				0.325
Typical angina	165 (31%)	154 (30%)	11 (33%)	-
Atypical angina	188 (35%)	174 (34%)	14 (42%)	-
Non-specific chestpain	180 (33%)	173 (34%)	7 (21%)	-
Medication				
Statin	356 (66%)	329 (65%)	27 (82%)	0.059
Acetylsalicylic acid	404 (75%)	374 (74%)	30 (91%)	0.036
Beta-blocker	325 (60%)	299 (59%)	26 (79%)	0.041
ACE-inhibitor/ARB	190 (35%)	173 (34%)	17 (52%)	0.060
Calcium-channel blocker	141 (26%)	126 (25%)	15 (46%)	0.014
PET perfusion imaging	N=539	N=506	N=33	
Indicative of ischemia	259 (48%)	233 (46%)	26 (79%)	<0.001
CCTA	N=535	N=503	N=32	
CACS, Agatston	53 [0-312]	44 [0-287]	330 [89-1418]	<0.001
Qualitative results	N=539	N=506	N=33	
Obstructive CAD	302 (56%)	274 (54%)	28 (85%)	<0.001
High-risk plaque	127 (24%)	111 (22%)	16 (49%)	0.001
Quantitative results	N=539	N=506	N=33	
TPV, mm^3	166 [14-489]	148 [9-430]	506 [302-878]	<0.001
CPV, mm^3	95 [6-316]	79 [3-299]	300 [152-628]	<0.001
NCPV, mm^3	48 [2-148]	40 [1-135]	201 [106-284]	<0.001
64-slice CT-scanner				
RCA PCATa, HU	-72.7 ± 8.4 (N=347)	-72.9 ± 8.4 (N=322)	-70.0 ± 8.1 (N=25)	0.097
RCA PCATa >-67.4 HU	100 (28%)	88 (27%)	12 (48%)	0.038
LAD PCATa, HU	-76.4 ± 8.0 (N=351)	-76.5 ± 8.0 (N=326)	-74.7 ± 7.9 (N=25)	0.286
Cx PCATa, HU	-74.6 ± 8.2 (N=348)	-74.7 ± 8.3 (N=323)	-74.2 ± 7.0 (N=25)	0.778

	Overall (N=539)	No event (N=506)	Event (N=33)	p-value
256-slice CT scanner				
RCA PCATa, HU	-80.2 ± 7.7 (N=185)	-80.3 ± 7.6 (N=177)	-78.7 ± 11.2 (N=8)	0.697
RCA PCATa >-76.3 HU	49 (26%)	44 (25%)	5 (63%)	0.032
LAD PCATa, HU	-84.5 ± 7.2 (N=182)	-84.4 ± 7.2 (N=174)	-87.2 ± 5.9 (N=8)	0.274
Cx PCATa, HU	-83.9 ± 7.3 (N=184)	-83.8 ± 7.2 (N=176)	-87.1 ± 8.6 (N=8)	0.216

Values are expressed as mean ± SD, median [IQR], or numbers (%). ACE = angiotensine converting enzyme; ARB = angiotensine receptor blocker; BMI = body mass index; CACS = coronary artery calcium score; CAD = coronary artery disease; CPV = calcified plaque volume; Cx = cicumflex artery; HU = Houndsfield units'; IQR = interquartile range; LAD = left anterior descending artery; MI = myocardial infarction; MBF = myocardial blood flow; NCPV = non-calcified plaque volume; PCATa = pericoronary addipose tissue CT-attenuation; RCA = right coronary artery; SD = standard deviation; TPV = total plaque volume.

Supplemental Figure 7 and 8, respectively. Obstructive CAD, HRPs, CACS >59, TPV >220mm^3, CPV >110mm^3, NCPV >85mm^3, and ischemia were associated with worse outcome (Table 2 and Figure 4). Regarding PCATa, scanner specific RCA thresholds of >-67.4 HU (64-slice CT-scanner) and >-76.3 HU (256-slice CT-scanner) were associated with outcome, whereas LAD and Cx PCATa were not associated with events (Table 2, Figure 4, and Supplemental Figure 9).

RCA PCATa as predictor of outcome

Age, diabetes mellitus, hyperlipidemia, early revascularization, and all imaging parameters were identified as variables associated with outcome (Table 2). RCT PCATa above scanner specific thresholds and NCPV >85mm^3 were of independent predictive value beyond the aforementioned variables. In a similar analyses that excluded patients that underwent early revascularization, RCA PCATa above scanner specific thresholds (HR: 2.65, 95% CI: 1.12-6.26, p=0.026), NCPV >83mm^3 (HR: 6.42, 95% CI: 2.25-18.33, p=0.001), and ischemia (HR: 2.95, 95% CI: 1.03-8.41, p=0.044) were independent predictors of events (Supplemental Table 1). RCA PCATa remained of prognostic value when separately adjusted for variables associated with outcome, clinical characteristics, and imaging parameters (Table 3). Lastly, RCA PCATa was higher among 55 patients that underwent early and/or late revascularization scanned on the 64-slice CT-scanner (-69.4±7.8 HU vs. -73.3±8.3 HU, p=0.001), but did not differ among 76 patients that underwent early and/or late revascularization scanned on the 256-slice CT-scanner (-80.3±8.1 HU vs. -80.1±7.2 HU, p=0.859).

Table 2. Univariable and multivariable cox proportional hazard regression analyses for determing predictors of events.

	Univariable analyses		Multivariable analysis (backward selection)	
	HR (95% CI)	p-value	HR (95% CI)	p-value
Patient characteristics				
Age, years	1.05 (1.01-1.09)	0.012	-	-
Male gender	1.73 (0.84-3.56)	0.139		
Body mass index, kg/m^2	0.95 (0.87-1.04)	0.291		
Smoking	0.89 (0.43-1.83)	0.748		
Hypertension	1.54 (0.77-3.06)	0.223		
Diabetes Mellitus	2.06 (0.98-4.32)	0.057	-	-
Hyperlipidemia	1.85 (0.93-3.66)	0.078	-	-
Family history of CAD	0.81 (0.41-1.60)	0.544		
Treatment				
Early revascularization	2.22 (1.07-4.58)	0.031	-	-
PET perfusion imaging				
Indicative of ischemia	4.25 (1.84-9.78)	0.001	-	-
CCTA results				
CACS >59 Agatston	4.17 (1.80-9.64)	0.001	-	-
Qualitative results				
Obstructive CAD	4.88 (1.88-12.65)	0.001	-	-
High-risk plaque	3.41 (1.72-6.75)	<0.001	-	-
Quantitative results				
TPV >220 mm^3	7.91 (3.05-20.49)	<0.001	-	-
CPV >110 mm^3	5.82 (2.40-14.10)	<0.001	-	-
NCPV >85 mm^3	8.07 (3.33-19.55)	<0.001	9.13 (3.51-23.73)	<0.001
PCATa				
RCA PCATa above scanner specific threshold	2.84 (1.44-5.63)	0.003	2.45 (1.23-4.93)	0.011

Abbreviations; HR: hazard ratio, CI: confidence interval, other abbriations as in table 1.

Discussion

The present study assessed the prognostic value of PCATa beyond quantitative plaque volume and ischemia among patients with suspected CAD. RCA PCATa above scanner specific thresholds was associated with outcome. Furthermore, PET/CCTA-derived CACS, obstructive CAD, HRPs, TPV, CPV, NCPV, and myocardial ischemia were related to occurrence of death and non-fatal MI as well and were so to a greater

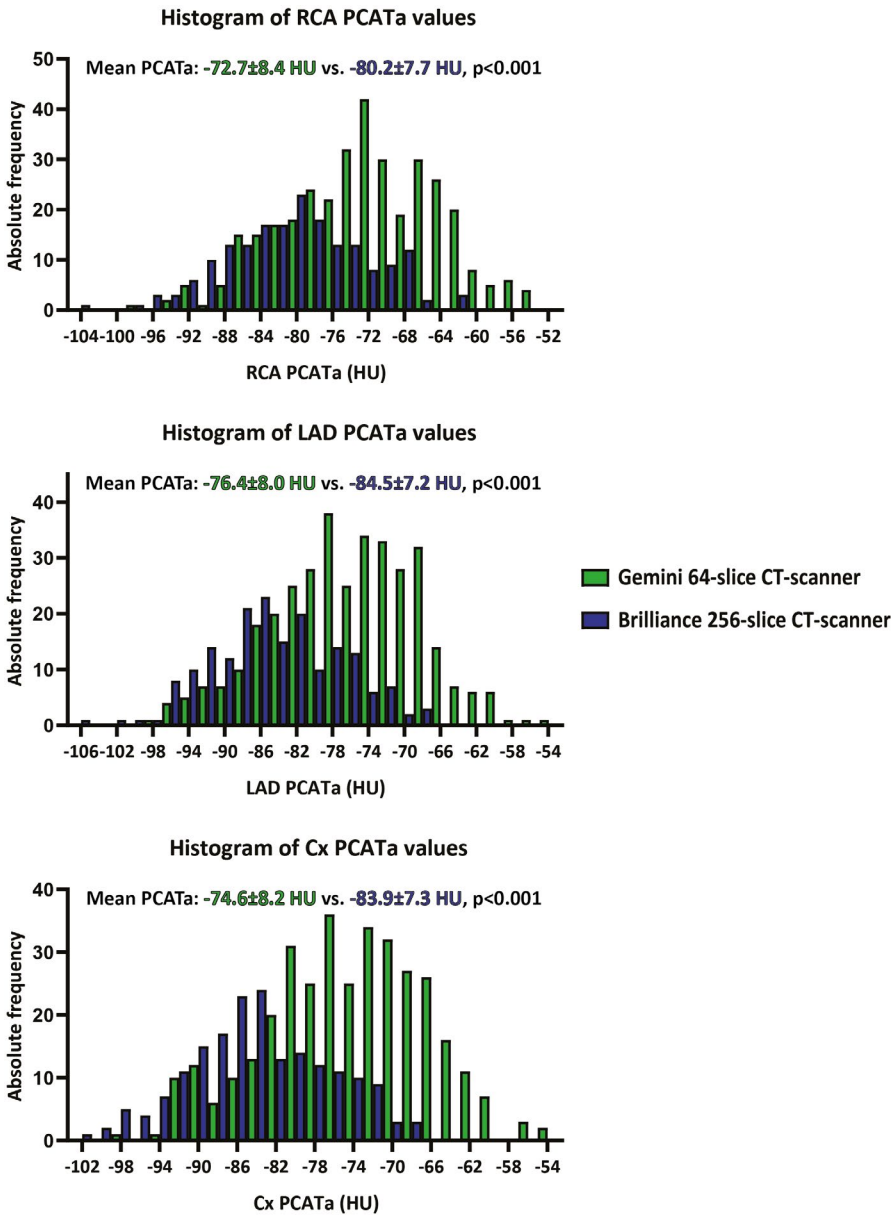

Figure 3. Histograms of absolute frequencies of PCATa values stratified for CT-scanner.
Figure demonstrating the distribution of RCA, LAD, and Cx PCATa values stratified for scanner type. Mean PCATa values differed significantly between scanners. Abbreviations as in Central illustration.

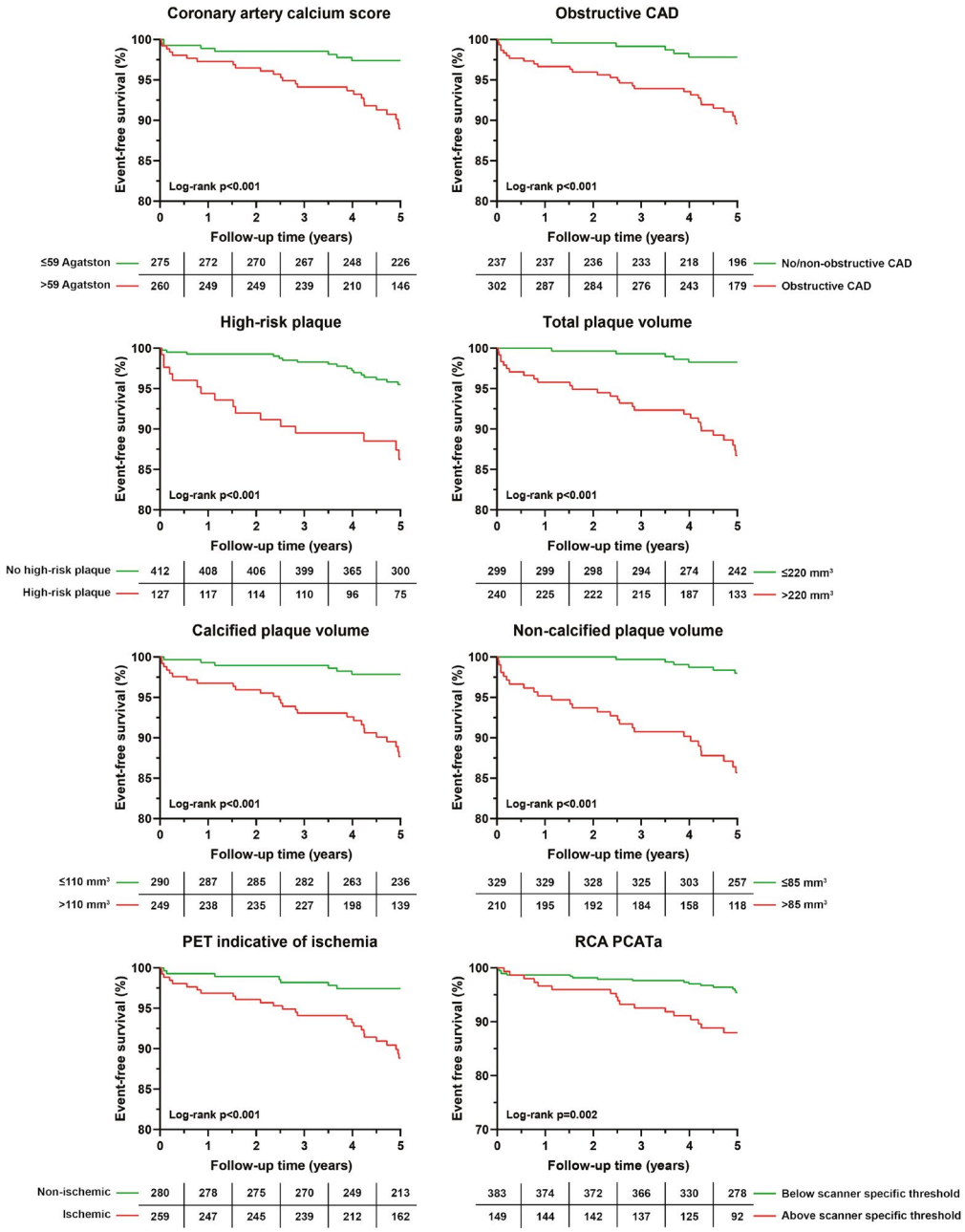

Figure 4. Prognostic value of imaging variables.
Figure 4 demonstrates the association of imaging variables with event-free survival presented by Kaplan-Meier curves with corresponding Log-rank p-values. Abbreviations as in Central Illustration.

extent as compared to RCA PCATa. Nevertheless, RCA PCATa was of prognostic value beyond clinical characteristics and imaging variables linked to extent and severity of atherosclerosis (Central illustration).

Prognostic value of plaque burden and vulnerability

In the present study markers of plaque burden and vulnerability were all associated with outcome of which NCPV was the strongest independent prognostic predictor adjusted for clinical characteristics and imaging parameters. The superior prognostic value of anatomical assessment over that of functional assessment is substantiated by substudies of the PROMISE-trial and ISCHEMIA-trial (14, 15). Regarding anatomical assessment, several studies have demonstrated that presence of obstructive CAD and HRPs are associated with detrimental outcome (2, 8, 16). However, substudies of the SCOT-HEART trial revealed that this relation might be driven by overall plaque burden as the prognostic value of obstructive disease and HRPs was dependent on CACS and as quantitative LAP burden proved to be a stronger predictor of outcome compared to obstructive CAD and CACS. (8, 17). In line with these findings, Andreini et al. show quantitative TPV, CPV, and NCPV to be of incremental prognostic value over cardiovascular risk factors and visually assessed CCTA-derived multivessel disease and similarly as the present study demonstrate NCPV to be the strongest predictor of events (7). Interestingly, RCA PCATa as a possible marker of global coronary inflammation proved to be of prognostic value over CCTA-derived parameters linked to plaque burden, vulnerability, and myocardial ischemia.

Pathophysiological mechanism of PCATa

Coronary atherosclerosis is marked by a lipid-driven inflammation, which precedes the formation of plaques (18). The inflammatory process within the coronary wall can, by excretion of pro-inflammatory cytokines, impede the maturation and thereby influence the size of the adipocytes in the surrounding PCAT (4). The balance between the lipid and aqueous phases of PCAT is largely dependent on adipocyte size, wherein larger adipocytes have an increased lipid content (4, 19). CT-derived attenuation values of adipose tissue can therefore be used to assess the phenotype of PCAT (4). PCATa is inversely associated with adipose differentiation and size, i.e. the lower the attenuation (HU closer to -190) the larger the adipocytes (4). Pro-inflammatory signals excreted

by inflamed coronaries inhibit maturation of adipocytes and lead to smaller more aqueous adipocytes and a higher PCATa (HU closer to -30) (4).

Association of PCATa with CAD and perfusion

Antonopoulos et al. demonstrate RCA PCATa to correlate with atherosclerotic plaque burden but not with calcification volume of the underlying coronary segment (4). Furthermore, RCA PCATa predicted presence of obstructive CAD in any of the coronaries, independent of CACS (4). High PCATa has also been associated with impaired coronary flow reserve on PET perfusion imaging, a relationship that was independent of cardiovascular risk factors, CACS, and presence of obstructive CAD (20). Interestingly, this association persevered among patients with low CACS or non-obstructive CAD, indicating that PCATa may identify 'low-risk' patients prone to ischemia (20). In contrast, the present study does not observe an association between PCATa and plaque volume nor hyperemic MBF. Our study included patients with CAD ranging from non-existent to extensive multivessel CAD. Although speculative, patients with no or a low plaque burden might have high PCATa as expression of beginning atherosclerosis, whereas patients with extensive CAD can have high PCATa delineating ongoing inflammation or low PCATa as a result of an extinguished inflammatory response due to e.g. medical therapy. Notably, in the present study 66% and 75% of patients were prescribed statins and acetylsalicylic acid at baseline, respectively. This might explain the absence of association between PCATa, plaque volume, and perfusion. As PCATa highlights ongoing inflammation it might be more suitable to describe progression of CAD (21). In line with this statement, Goeller et al. show baseline RCA PCATa to be independently associated with an increase in NCP burden and demonstrate changes in RCA PCATa to correlate with changes in NCP burden and low-density NCP burden assessed on serial CCTA (21). Noteworthy, a decrease in PCATa among patients in which statin therapy was initiated was observed (21).

Prognostic value of PCATa

In the CRISP-CT study PCATa was incorporated in calculating the FAI using a proprietary algorithm (*CaRiHEART*, Caristo Diagnostics, Oxford, United Kingdom) (3, 6). FAI of the RCA and LAD were associated with all-cause and cardiac mortality,

whereas FAI Cx was associated with all-cause but not cardiac mortality (6). High FAI RCA (≥-70.1 HU), as a suggested marker of global coronary inflammation, was predictive of all-cause and cardiac mortality beyond clinical characteristics, epicardial adipose tissue volume, number of HRP features, and Duke index for extent of CAD (6). The increased risk of all-cause mortality in patients with high FAI was driven by a higher rate of cardiac deaths and not in non-cardiac deaths (6). We corroborate these findings by demonstrating that RCA PCATa above scanner specific thresholds was independently associated with occurrence of death and non-fatal MI. The scanner specific RCA PCATa thresholds of the present study identify relatively outlying PCATa values. These 'abnormal' values are associated with events to a greater extent as compared to PCATa values below the cut-off. However, it should be noted that given the similar RCA PCATa of patients with and without an event and the discriminating ability of the ROC curves, RCA PCATa as a sole prognostic determinant might not be useful for risk stratification but should possibly be utilized in conjunction with other CAD markers. This is illustrated by a substudy of the CRISP-CT study in which patients with high FAI and HRP features were at an increased risk of suffering events, whereas patients with low FAI and HRP features were not (22). The association of RCA PCATa with all-cause mortality is possibly, similar to the CRISP-CT study, driven by a higher rate of cardiac deaths (6). The association of PCATa with MI has previously been substantiated by Goeller et al. who observed higher PCATa values surrounding culprit lesions of MI patients as compared to non-culprit lesions, healthy controls, and patients with stable CAD (4, 23). We extent the findings of the CRISP-CT study by demonstrating that RCA PCATa retains its prognostic value beyond quantitative plaque volume, high-risk plaques, and myocardial ischemia. Contrary to the CRISP-CT study, LAD and Cx PCATa were not associated with event-free survival. This is in line with the study of Bengs et al. in which RCA PCATa was associated with occurrence of events, whereas LAD and left main PCATa were not (24). A possible explanation for this discordancy is the fact that PCAT is more prevalent around the RCA as compared to the left coronary system and has less hindering non-fatty structures (e.g. side branches and myocardium) in its proximity (4, 21, 25). Therefore RCA PCATa might be a more robust and easily accessible measurement of global inflammatory status and it might explain the superior prognostic value as compared to PCATa of the LAD and Cx.

Future prospects

Recent randomized trials highlight inflammation as an important risk-factor in patients with CAD by demonstrating that anti-inflammatory treatment reduces events rates as compared to placebo (26-28). Identifying patients at a "high" inflammatory risk might further improve outcome (3). Interestingly, in the CRISP-CT study, the increased risk of cardiac mortality in patients with high FAI was nullified among those that received the recommendation to initiate treatment with statins and aspirin, whereas the risk was 18-fold higher in patients with high FAI that did not change medical regime (6). Furthermore, inflammation is a dynamic process and PCATa/FAI might be utilized to monitor the effect of treatment. PCATa around culprit lesions of MI patients is elevated and diminishes overtime, possibly indicating an effect of commenced medical treatment (4). Furthermore, Elnabawi et al. demonstrate that in patients with psoriasis, FAI diminishes among those on anti-inflammatory medication while no change is observed in those that are not (29).

Limitations

The power of the study is hampered by the low number of events. In this regard, the multivariable analyses should be interpreted with causing as they are prone to overfitting given the relatively large number of predictors that were included. Results should be seen as hypothesis generating and need further validation. To that extent, the provided prognostic cut-offs for CCTA variables should not be extrapolated to other datasets but serve to show the incremental prognostic value of PCATa on top of other CCTA variables for which optimal cut-offs were calculated as well. Prognostic thresholds for PCATa should be assessed in larger CCTA cohorts and validated in independent cohorts taking into account scanner differences. Obstructive CAD is defined as ≥50% stenosis, which can be considered low on CCTA. Next, PCATa is defined as the average attenuation of PCAT, which might result in an underestimation of coronary inflammation in obese individuals as attenuation will be lower given the larger adipocytes, vice versa this can lead to an overestimation in lean patients (3). Furthermore, PCATa is assumed to be a marker of coronary inflammation however the present study lacks data to confirm the presence of coronary inflammation by means of e.g. PET imaging. Next, despite the fact that an early invasive strategy does not seem to alter outcome regardless of the anatomical severity of CAD or degree

of ischemia, inclusion of patients that underwent early revascularization might have introduced unmeasured confounding (15). Lastly, the present study uses a composite endpoint of death and non-fatal MI but does not provide information on cause of death as this was unavailable.

Conclusion

Parameters associated with atherosclerotic burden and ischemia were more strongly associated with outcome than RCA PCATa. Nonetheless, RCA PCATa above scanner specific thresholds, as a marker of global coronary inflammation, provides incremental prognostic value beyond clinical characteristics, CACS, obstructive CAD, HRPs, quantitative plaque volume, and myocardial ischemia.

References

1. Knuuti J, Wijns W, Saraste A, et al. 2019 ESC Guidelines for the diagnosis and management of chronic coronary syndromes. Eur Heart J. 2020;41(3):407-77.
2. Driessen RS, Bom MJ, van Diemen PA, et al. Incremental prognostic value of hybrid [15O]H2O positron emission tomography-computed tomography: combining myocardial blood flow, coronary stenosis severity, and high-risk plaque morphology. Eur Heart J Cardiovasc Imaging. 2020;21(10):1105-13.
3. Antoniades C, Antonopoulos AS, Deanfield J. Imaging residual inflammatory cardiovascular risk. Eur Heart J. 2020;41(6):748-758.
4. Antonopoulos AS, Sanna F, Sabharwal N, et al. Detecting human coronary inflammation by imaging perivascular fat. Sci Transl Med. 2017;9(398).
5. Mazurek T, Zhang LF, Zalewski A, et al. Human epicardial adipose tissue is a source of inflammatory mediators. Circulation. 2003;108(20):2460-6.
6. Oikonomou EK, Marwan M, Desai MY, et al. Non-invasive detection of coronary inflammation using computed tomography and prediction of residual cardiovascular risk (the CRISP CT study): a post-hoc analysis of prospective outcome data. The Lancet. 2018;392(10151):929-39.
7. Andreini D, Magnoni M, Conte E, et al. Coronary Plaque Features on CTA Can Identify Patients at Increased Risk of Cardiovascular Events. JACC Cardiovasc Imaging. 2020;13(8):1704-17.
8. Williams MC, Kwiecinski J, Doris M, et al. Low-Attenuation Noncalcified Plaque on Coronary Computed Tomography Angiography Predicts Myocardial Infarction:

Results From the Multicenter SCOT-HEART Trial (Scottish Computed Tomography of the HEART). Circulation. 2020;141(18):1452-62.

9. Bom MJ, van der Heijden DJ, Kedhi E, et al. Early Detection and Treatment of the Vulnerable Coronary Plaque: Can We Prevent Acute Coronary Syndromes? Circ Cardiovasc Imaging. 2017;10(5): e005973.
10. Freiman M, Nickisch H, Prevrhal S, et al. Improving CCTA-based lesions' hemodynamic significance assessment by accounting for partial volume modeling in automatic coronary lumen segmentation. Med Phys. 2017;44(3):1040-9.
11. Harms HJ, Knaapen P, de Haan S, et al. Automatic generation of absolute myocardial blood flow images using [15O]H2O and a clinical PET/CT scanner. Eur J Nucl Med Mol Imaging. 2011;38(5):930-9.
12. Danad I, Raijmakers PG, Driessen RS, et al. Comparison of Coronary CT Angiography, SPECT, PET, and Hybrid Imaging for Diagnosis of Ischemic Heart Disease Determined by Fractional Flow Reserve. Jama Cardiology. 2017;2(10):1100-7.
13. Knuuti J, Wijns W, Saraste A, et al. 2019 ESC Guidelines for the diagnosis and management of chronic coronary syndromes. European Heart Journal. 2019;00:1-71.
14. Hoffmann U, Ferencik M, Udelson JE, et al. Prognostic Value of Noninvasive Cardiovascular Testing in Patients With Stable Chest Pain: Insights From the PROMISE Trial (Prospective Multicenter Imaging Study for Evaluation of Chest Pain). Circulation. 2017;135(24):2320-32.
15. Maron D. Relationships of ischemia severity and coronary artery disease extent with clinical outcomes in the ISCHEMIA trial. Paper presented at: The American College of Cardiology Sientific Sessions. March 2020.
16. Chang HJ, Lin FY, Lee SE, et al. Coronary Atherosclerotic Precursors of Acute Coronary Syndromes. J Am Coll Cardiol. 2018;71(22):2511-22.
17. Williams MC, Moss AJ, Dweck M, et al. Coronary Artery Plaque Characteristics Associated With Adverse Outcomes in the SCOT-HEART Study. J Am Coll Cardiol. 2019;73(3):291-301.
18. Ross R. Atherosclerosis--an inflammatory disease. N Engl J Med. 1999;340(2):115-26.
19. DiGirolamo M, Owens JL. Water content of rat adipose tissue and isolated adipocytes in relation to cell size. Am J Physiol. 1976;231(5 Pt. 1):1568-72.
20. Nomura CH, Assuncao-Jr AN, Guimarães PO, et al. Association between perivascular inflammation and downstream myocardial perfusion in patients with suspected coronary artery disease. Eur Heart J Cardiovasc Imaging. 2020;21(6):599-605.
21. Goeller M, Tamarappoo BK, Kwan AC, et al. Relationship between changes in pericoronary adipose tissue attenuation and coronary plaque burden quantified

from coronary computed tomography angiography. Eur Heart J Cardiovasc Imaging. 2019;20(6):636-43.

22. Oikonomou EK, Desai MY, Marwan M, et al. Perivascular Fat Attenuation Index Stratifies Cardiac Risk Associated With High-Risk Plaques in the CRISP-CT Study. J Am Coll Cardiol. 2020;76(6):755-7.
23. Goeller M, Achenbach S, Cadet S, et al. Pericoronary Adipose Tissue Computed Tomography Attenuation and High-Risk Plaque Characteristics in Acute Coronary Syndrome Compared With Stable Coronary Artery Disease. JAMA Cardiol. 2018;3(9):858-63.
24. Bengs S, Haider A, Warnock GI, et al. Quantification of perivascular inflammation does not provide incremental prognostic value over myocardial perfusion imaging and calcium scoring. Eur J Nucl Med Mol Imaging. 2020.
25. Balcer B, Dykun I, Schlosser T, et al. Pericoronary fat volume but not attenuation differentiates culprit lesions in patients with myocardial infarction. Atherosclerosis. 2018;276:182-8.
26. Ridker PM, Everett BM, Thuren T, et al. Antiinflammatory Therapy with Canakinumab for Atherosclerotic Disease. N Engl J Med. 2017;377(12):1119-31.
27. Tardif JC, Kouz S, Waters DD, et al. Efficacy and Safety of Low-Dose Colchicine after Myocardial Infarction. N Engl J Med. 2019;381(26):2497-505.
28. Nidorf SM, Fiolet ATL, Mosterd A, et al. Colchicine in Patients with Chronic Coronary Disease. N Engl J Med. 2020; doi: 10.1007/s00259-020-05106-0.
29. Elnabawi YA, Oikonomou EK, Dey AK, et al. Association of Biologic Therapy With Coronary Inflammation in Patients With Psoriasis as Assessed by Perivascular Fat Attenuation Index. JAMA Cardiol. 2019;4(9):885-891.

Supplementary data

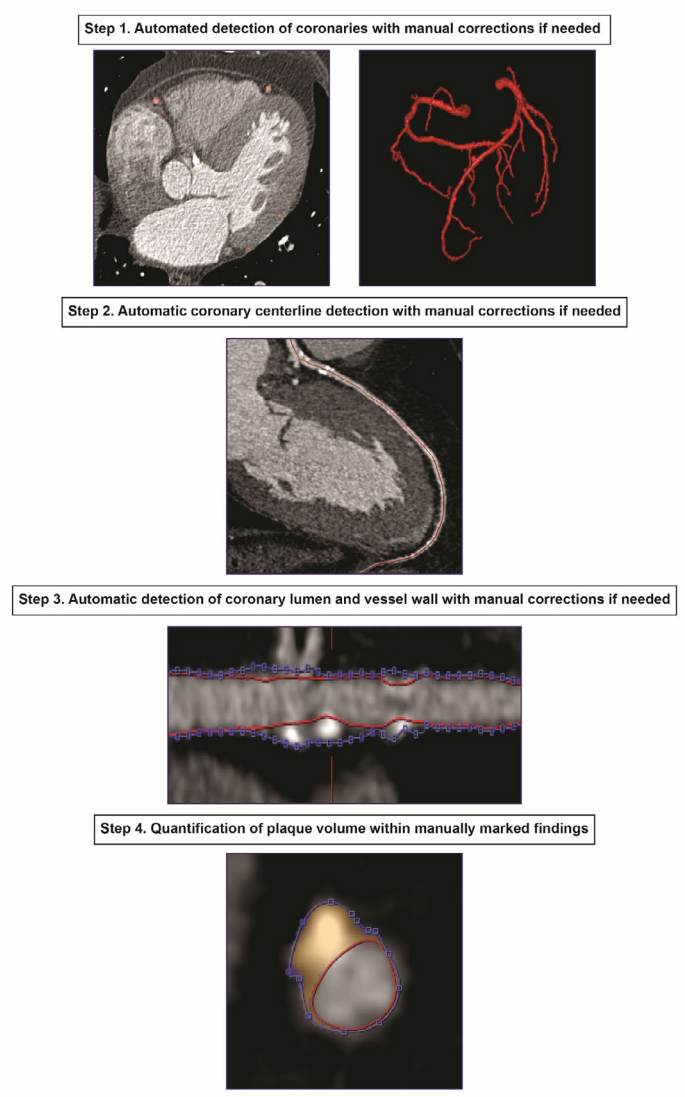

Supplemental Figure 1. Case example of plaque volume quantifiication using semi-automated software.
Plaque volumes were quantified using Comprehensive Cardiac Analysis (Philips Healthcare, Best, The Netherlands). As first step the software automatically detects the coronaries, if needed undected tissue that was deemed a coronary was manually added or manually deleted if detected tissue was not deemed a coronary. Second, the software automatically generates a centerline through the detected coronaries if needed the centerlines were manually adjusted. Third, coronary lumen and vessel wall were automatically detected, again if needed maually corrections were applied. Lasly, the software quantifies plaque volume among manually marked findings. A threshold of 150 HU was used to distinguish non-calcified from calcfied plaque. Plaque volume was calculated by summing volumes of separte plaques along each coronary artery. HU = Hounsfield units.

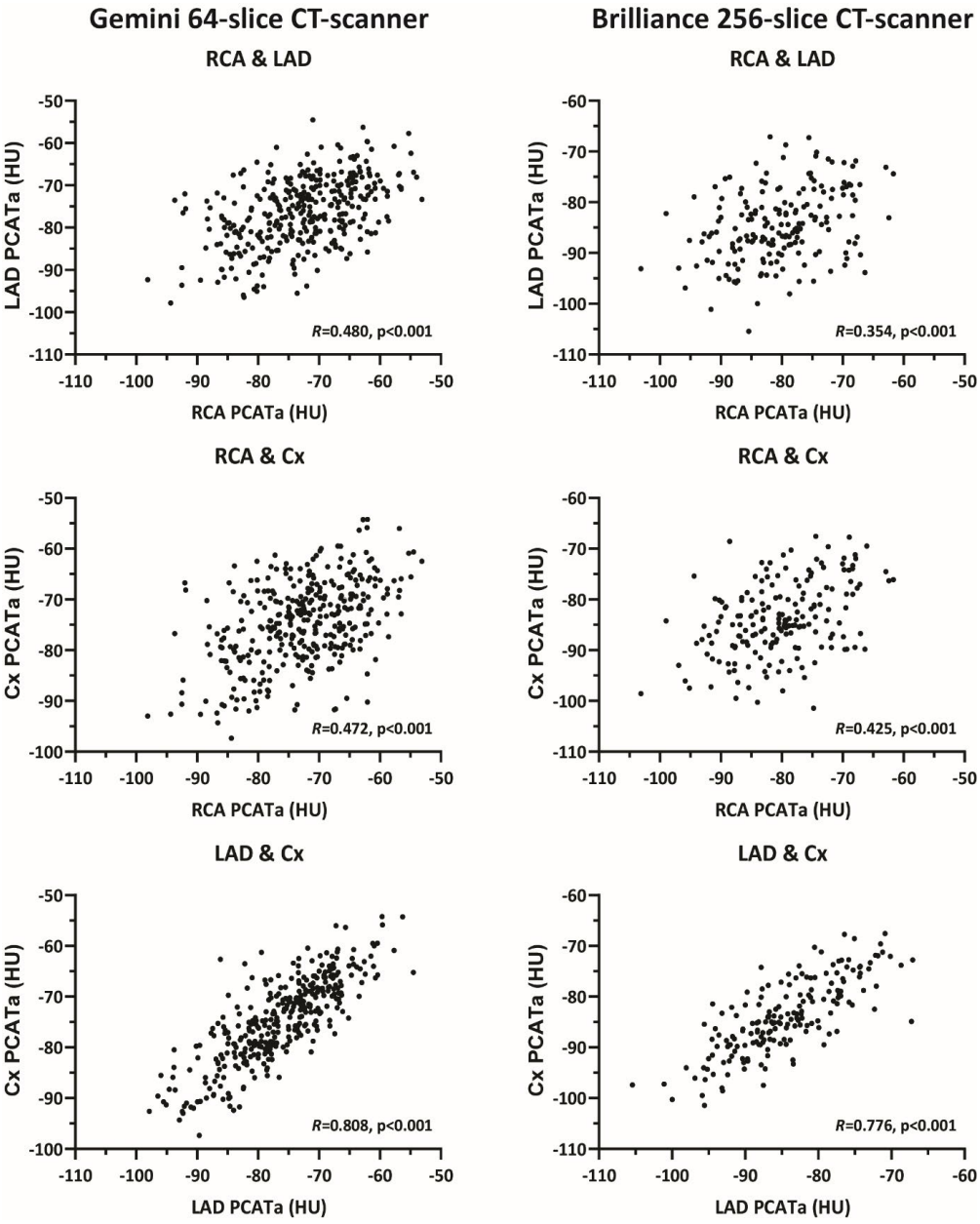

Supplemental Figure 2. Correlation between RCA, LAD, and Cx PCATa stratified for CT-scanner. Figure presenting the correlation between RCA PCATa and PCATa of the LAD and Cx, and the correlcation between PCATa of the LAD and Cx stratified for CT-scanner. CT = computed tomography; Cx = Circumflex artery; LAD = left anterior descending artery; PCATa = pericoronary adipose tissue CT-attenuation; RCA = right coronary artery; other abbreviations as in Supplemental Figure 1.

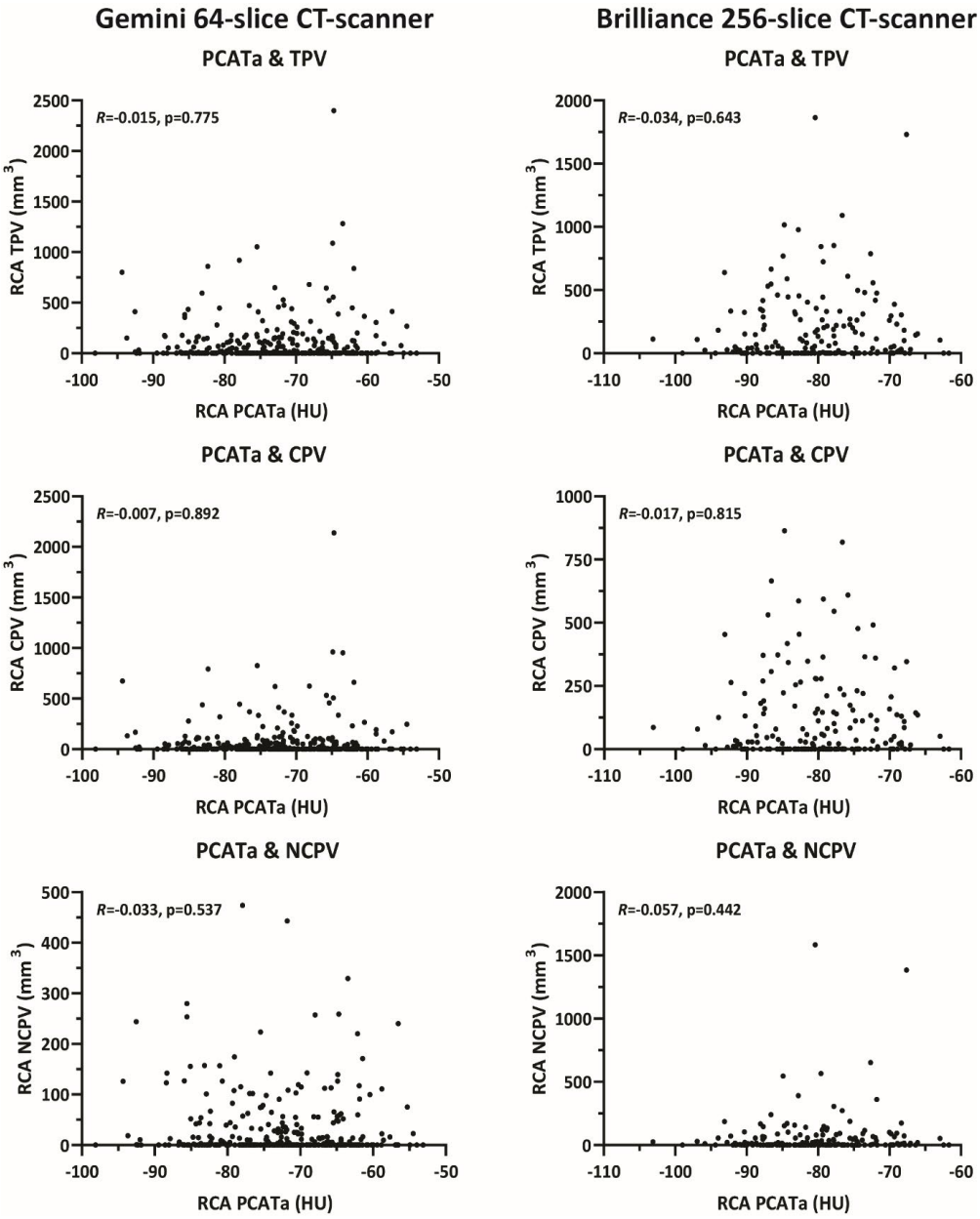

Supplemental Figure 3. Correlation between RCA PCATa and CCTA variables stratified for CT-scanner.
Figure demonstrating that RCA PCATa was not found to correlate with TPV, CPV, and NCPV of the RCA. Abbreviations: CCTA = coronary computed tomography angiography; CPV = calcified plaque volume, NCPV = non-calcified plaque volume; TPV = total plaque volume; other abbreviations as in Supplemental Figure 1 and 2.

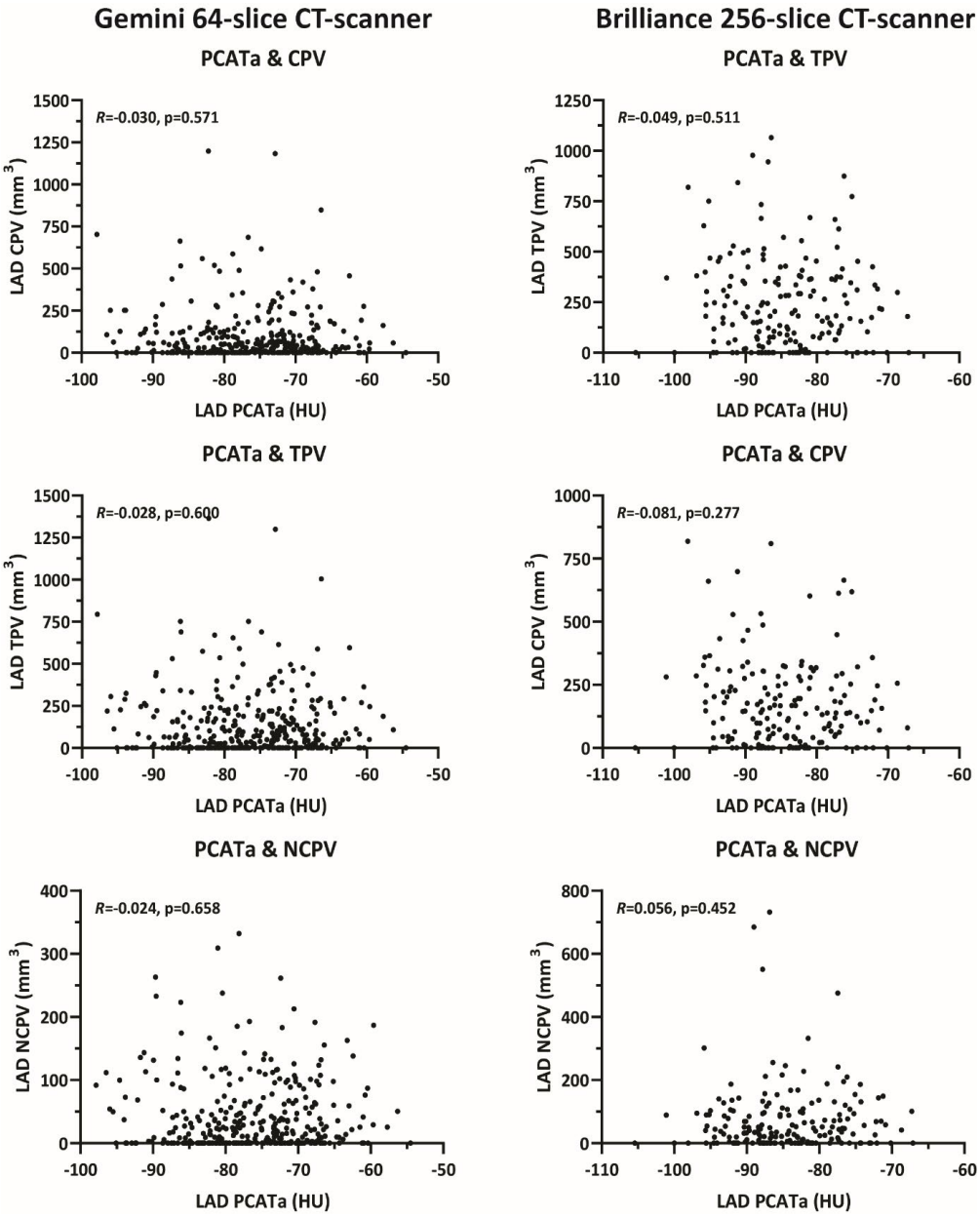

Supplemental Figure 4. Correlation between LAD PCATa and CCTA variables stratified for CT-scanner.
Supplemental Figure 4 demonstrates that LAD PCATa was not found to correlate with TPV, CPV, and NCPV of the LAD. Abbreviations as in Supplemental Figure 1, 2, and 3.

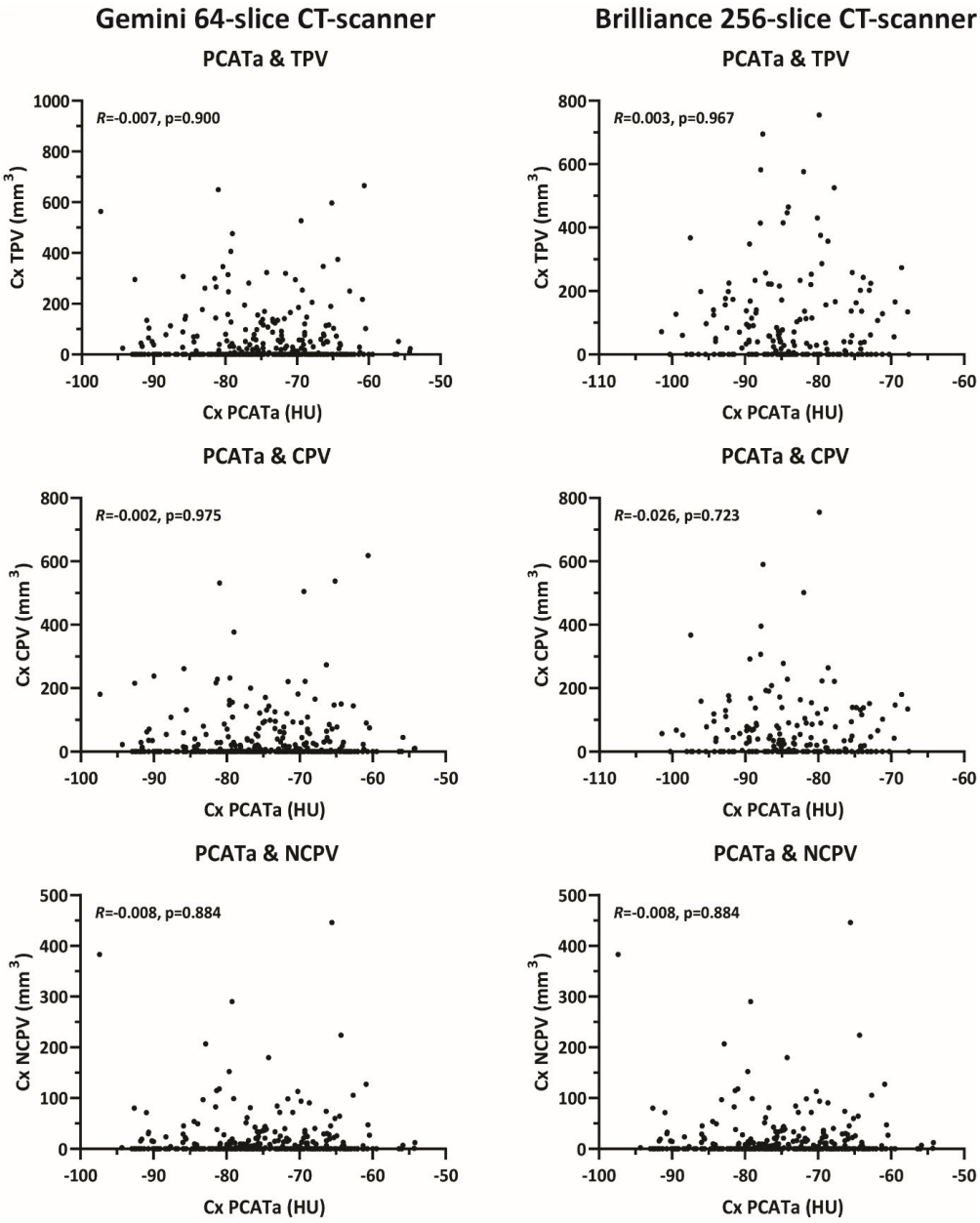

Supplemental Figure 4. Correlation between Cx PCATa and CCTA variables stratified for CT-scanner. Figure demonstrating that Cx PCATa was not found to correlate with TPV, CPV, and NCPV of the Cx. Abbreviations as in Supplemental Figure 1, 2, and 3.

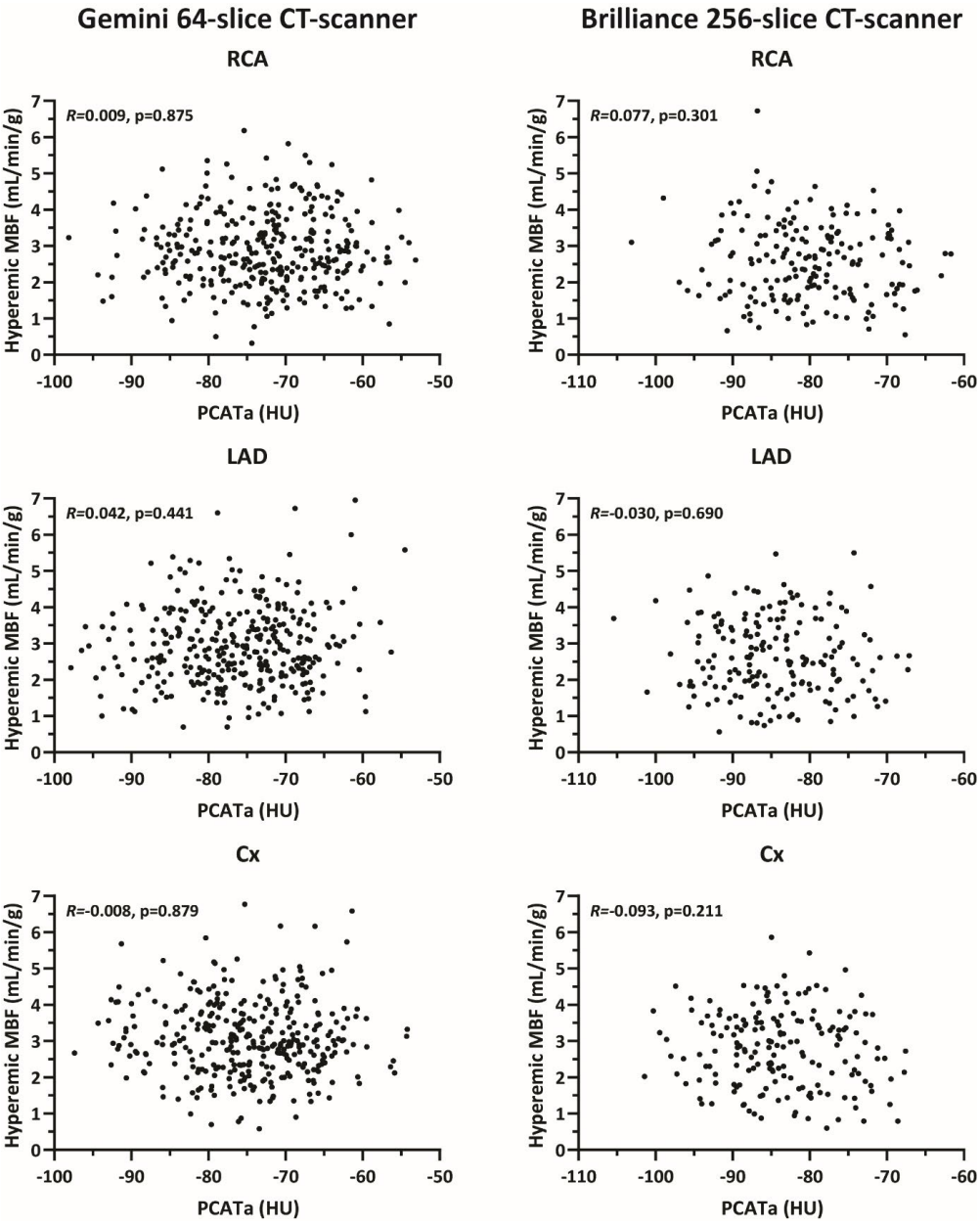

Supplemental Figure 6. Correlation between PCATa of the RCA, LAD, and Cx and hyperemic MBF of the respective coronary.
Supplemental Figure 6 demonstrates that PCATa of the RCA, LAD, and Cx did not correlate with hyperemic MBF of the RCA, LAD, and Cx, respectively. Abbreviations: MBF: myocardial blood flow, other abbrevations as in Supplemental Figure 2.

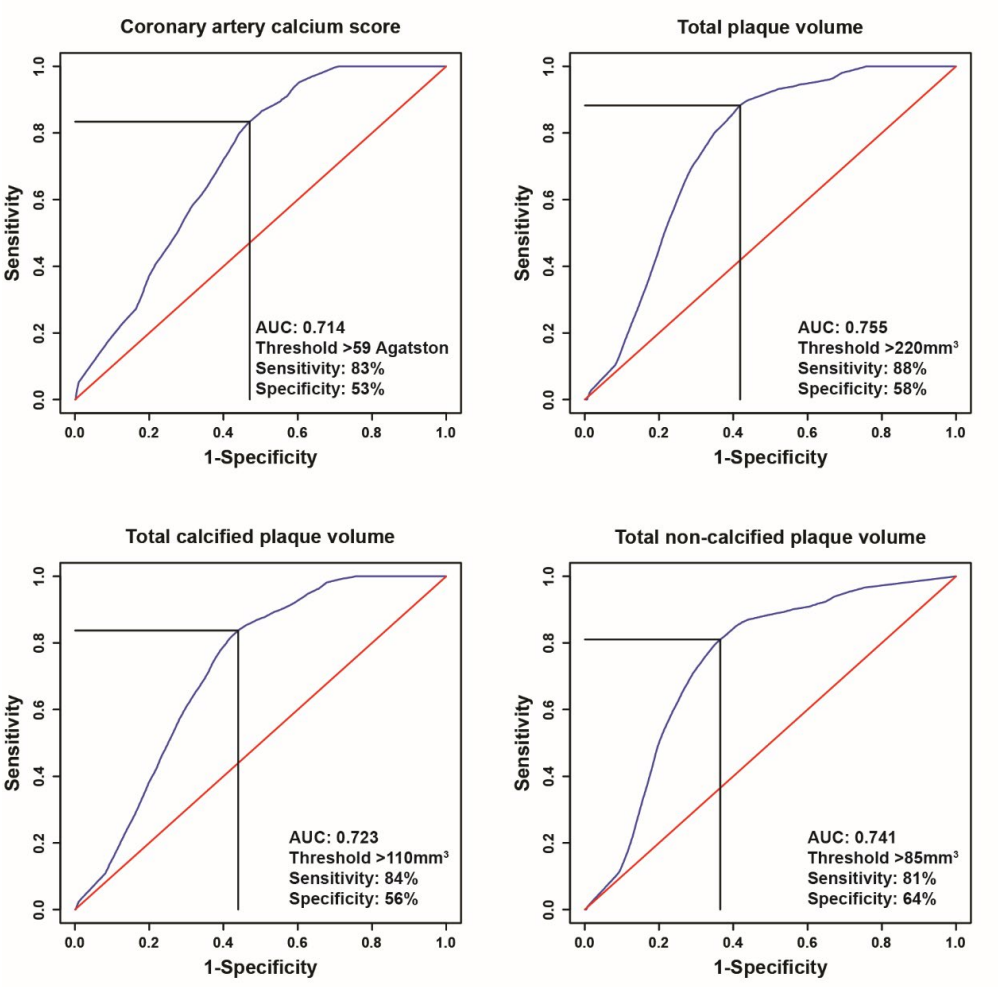

Supplemental Figure 7. Time-dependent receiver operating characteristic curves of quantitative CCTA parameters for prediction of events.
Figure displaying time-dependent receiver operating characteristic curves and area under the curves of CACS, TPV, CPV, NCPV for prediction of events with prognostic thresholds and corresponding sensitivity and specificty. Abbreviations: CACS: coronary artery calcium score, other abbreviations as in Supplemental Figure 3.

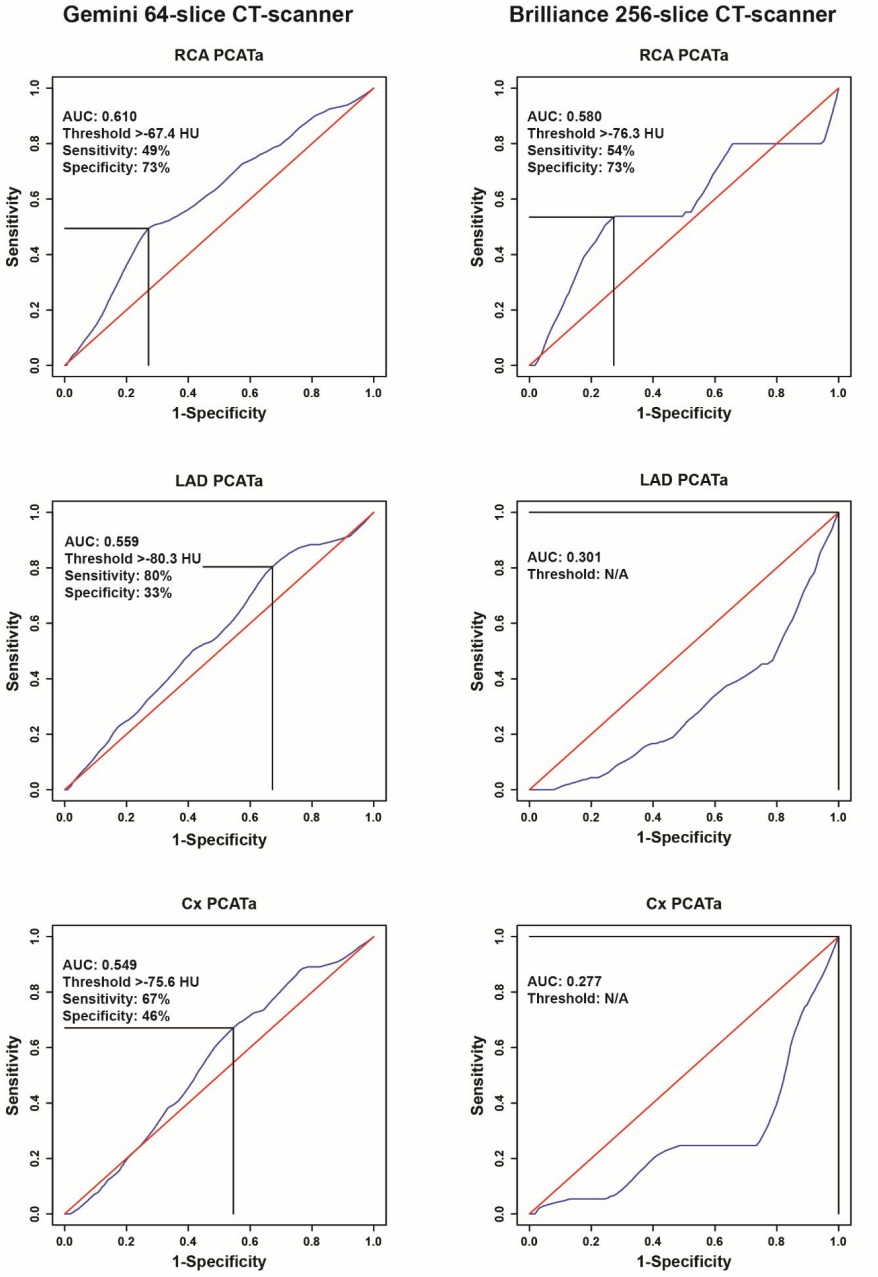

Supplemental Figure 8. Time-dependent receiver operating characteristic curves of RCA, LAD, and Cx PCATa stratfied for CT-scanner.
Figure displaying time-dependent receiver operating characteristic curves and area under the curves of PCATa of the RCA, LAD, and Cx for prediction of events with prognostic thresholds and corresponding sensitivity and specificty, stratified for CT-scanner. Abbreviations as in Supplemental Figure 1 and 2.

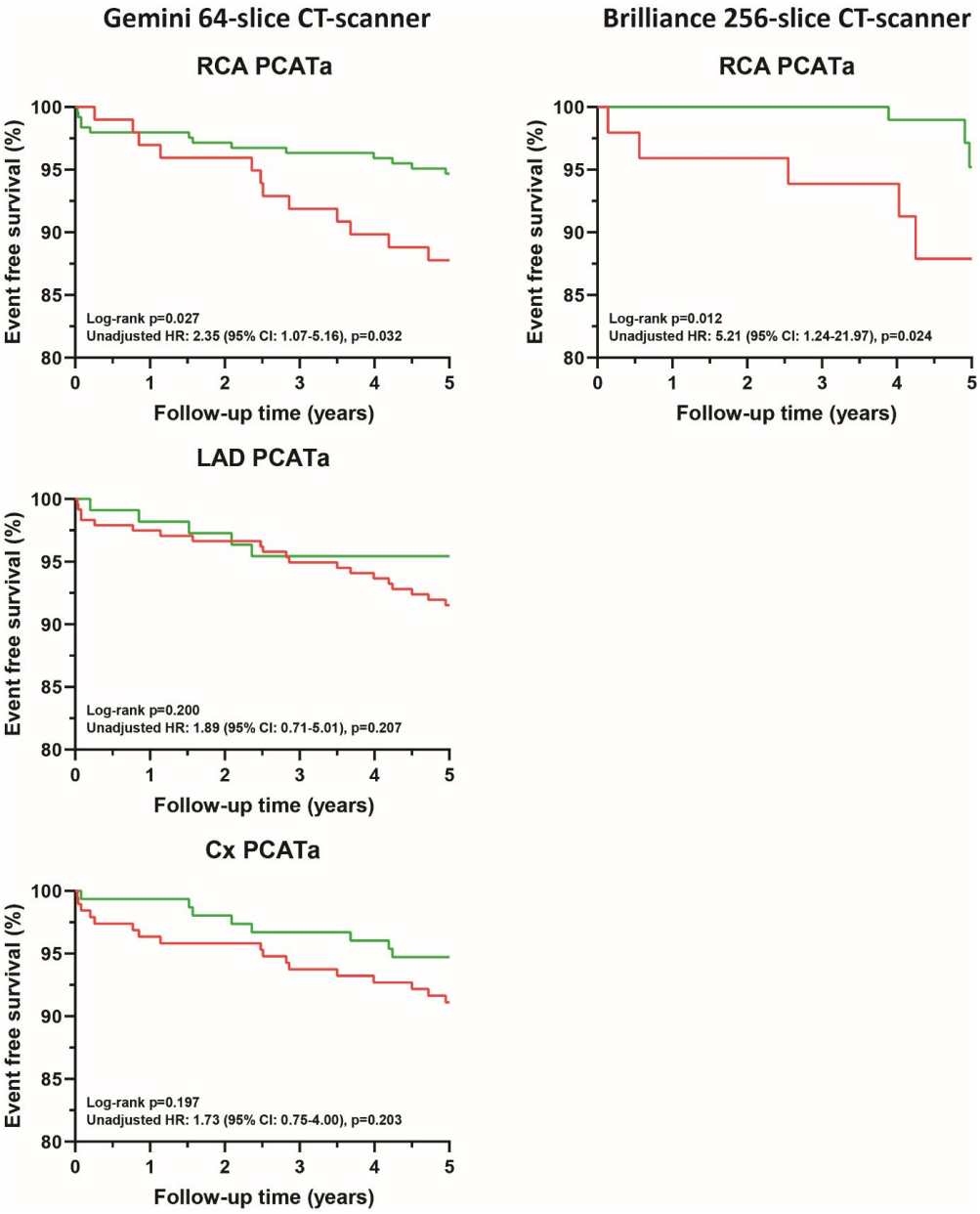

Supplemental Figure 9. Association of scanner specific PCATa prognostic thresholds with event-free survival.
Supplemental Figure 9 shows that scanner specific prognostic thresholds of RCA PCATa were associated with event-free survival, whereas scanner specific prognostic threshold of LAD and Cx PCATa were not associated with event-free survial, as demonstrated by Kaplan-Meier curves with corresponding Log-rank p-values and unadjusted HRs obtained via univariable Cox proportional hazard regression analyses. CI = confidence interval; HR = Hazard-ratio; other abbreviations as in Supplemental Figure 2.

Supplemental table 1. Univariable and multivariable cox proportional hazard regression analyses for determing predictors of events among patients that did not undergo early revascularization.

	Univariable analyses		Multivariable analysis (backward selection)	
	HR (95% CI)	p-value	HR (95% CI)	p-value
Patient characteristics				
Age, years	1.05 (1.01-1.10)	0.024	-	-
Gender, male	1.60 (0.69-3.75)	0.277		
Body mass index, kg/m^2	0.92 (0.82-1.03)	0.165		
Smoking	0.97 (0.41-2.32)	0.951		
Hypertension	1.68 (0.72-3.92)	0.234		
Diabetes Mellitus	2.83 (1.19-6.75)	0.019	-	-
Hyperlipidemia	2.28 (0.99-5.28)	0.054	-	-
Family history of CAD	0.55 (0.23-1.28)	0.163		
PET perfusion imaging				
Indicative of ischemia	4.72 (1.85-12.07)	0.001	2.95 (1.03-8.41)	0.044
CCTA results				
CACS >58 Agatston	4.10 (1.59-10.58)	0.003	-	-
Qualitative results				
Obstructive CAD	4.49 (1.66-12.17)	0.003	-	-
High-risk plaque	5.18 (2.24-12.00)	<0.001	-	-
Quantitative results				
TPV >269 mm^3	7.38 (2.72-20.01)	<0.001	-	-
CPV >145 mm^3	4.94 (1.93-12.63)	0.001	-	-
NCPV >83 mm^3	7.96 (3.11-20.35)	<0.001	6.42 (2.25-18.33)	0.001
PCATa				
RCA PCATa above scanner specific threshold	3.37 (1.45-7.79)	0.005	2.65 (1.12-6.26)	0.026

BMI = body mass index; CACS = coronary artery calcium score; CAD = coronary artery disease; CI = confidencte interval; CPV = calcified plaque volume; HR = hazard-ratio; NCPV = non-calcified plaque volume; PCATa = pericoronary addipose tissue CT-attenuation; RCA = right coronary artery; TPV = total plaque volume.

Chapter 9

Non-invasive procedural planning using computed tomography-derived fractional flow reserve

Michiel J. Bom, Stefan P. Schumacher, Roel S. Driessen, Pepijn A. van Diemen, Henk Everaars, Ruben W. de Winter, Peter M. van de Ven, Albert C. van Rossum, Ralf W. Sprengers, Niels J.W. Verouden, Alexander Nap, Maksymilian P. Opolski, Jonathon A. Leipsic, Ibrahim Danad, Charles A. Taylor, and Paul Knaapen

Catheter Cardiovasc Interv. 2021;97(4):614-622

Abstract

Objectives: This study aimed to investigate the performance of computed tomography derived fractional flow reserve based interactive planner (FFR_{CT} planner) to predict the physiological benefits of percutaneous coronary intervention (PCI) as defined by invasive post-PCI FFR.

Background: Advances in FFR_{CT} technology have enabled the simulation of hyperemic pressure changes after virtual removal of stenoses.

Methods: In 56 patients (63 vessels) invasive FFR measurements before and after PCI were obtained and FFR_{CT} was calculated using pre-PCI coronary CT angiography. Subsequently, FFR_{CT} and invasive coronary angiography models were aligned allowing virtual removal of coronary stenoses on pre-PCI FFR_{CT} models in the same locations as PCI was performed. Relationships between invasive FFR and FFR_{CT}, between post-PCI FFR and FFR_{CT} planner, and between delta FFR and delta FFR_{CT} were evaluated.

Results: Pre PCI, invasive FFR was 0.65±0.12 and FFR_{CT} was 0.64±0.13 (p=0.34) with a mean difference of 0.015 (95% CI: -0.23–0.26). Post-PCI invasive FFR was 0.89±0.07 and FFR_{CT} planner was 0.85±0.07 (p<0.001) with a mean difference of 0.040 (95% CI: -0.10–0.18). Delta invasive FFR and delta FFR_{CT} were 0.23±0.12 and 0.21±0.12 (p=0.09) with a mean difference of 0.025 (95% CI: -0.20–0.25). Significant correlations were found between pre-PCI FFR and FFR_{CT} (r=0.53, p<0.001), between post-PCI FFR and FFR_{CT} planner (r=0.41, p=0.001), and between delta FFR and delta FFR_{CT} (r=0.57, p<0.001).

Conclusions: The non-invasive FFR_{CT} planner tool demonstrated significant albeit modest agreement with post-PCI FFR and change in FFR values after PCI. The FFR_{CT} planner tool may hold promise for PCI procedural planning, however improvement in technology is warranted before clinical application.

Introduction

Coronary revascularization with percutaneous coronary intervention (PCI) aims to relieve myocardial ischemia caused by a coronary stenosis through augmenting coronary flow and myocardial perfusion. Fractional flow reserve (FFR), calculated as the pressure ratio across a coronary stenosis during maximal hyperemia, is regarded the gold standard for the detection of lesion-specific ischemia and is used to guide revascularization.(1) Furthermore, post-PCI FFR provides important insight into the restoration of perfusion following revascularization, given the close correlation between post-PCI FFR and absolute myocardial blood flow measured with positron emission tomography.(2) FFR values and changes in FFR following PCI have also been linked with adverse events, demonstrating the importance of FFR to predict outcome after stenting.(3-8) Over the last few years, FFR derived from computed tomography (FFR_{CT}) has emerged as a non-invasive alternative to invasive FFR. In FFR_{CT} computational fluid dynamics are used to assess coronary flow impairment across a coronary stenosis from standard coronary CT angiography (CTA) data.(9) Several studies have demonstrated excellent diagnostic accuracy of FFR_{CT} when referenced by invasive FFR.(10-12) Recent advances in FFR_{CT} technology have led to the development of an FFR_{CT}-based interactive planner tool (FFR_{CT} planner) which enables the simulation of blood flow after virtual removal of a stenosis, hereby predicting the hemodynamic effects of stenting.(13,14) The non-invasive prediction of the potential physiological benefit of stenting might be useful for PCI planning and lesion selection. This study therefore aimed to investigate the accuracy of FFR_{CT} planner to predict invasive post-PCI FFR and change in invasive FFR following PCI.

Materials and methods

Study population

This study is a combined substudy of the PACIFIC trial and the AR-PCI trial. The PACIFIC trial included consecutive patients with suspected coronary artery disease (CAD) who underwent coronary CTA, single photon emission computed tomography and positron emission tomography, followed by invasive coronary angiography (ICA) with FFR measurement in all major coronary arteries regardless of non-invasive imaging findings.(15) In patients in whom PCI was performed, invasive FFR

measurements were obtained after stenting. The AR-PCI trial was a randomized study on the effect of coronary CTA guided stenting versus angiography guided stenting in patients with a clinical indication for PCI (NCT03531424). Both studies included patients with stable CAD, without prior PCI in the target vessel. Both studies were approved by the Medical Ethics Committee of the VU University Medical Center and written informed consent was obtained from all participants.

Coronary CTA acquisition

Patients underwent coronary CTA on a 256-slice CT-scanner (Brilliance iCT, Philips Healthcare, Best, the Netherlands) with a collimation of 128 x 0.625 mm and a tube rotation time of 270 ms. Tube current was set between 200 and 360 mAs at 120 kV, adjusting primarily mAs based on body habitus. Axial scanning was performed with prospective ECG-gating (Step & Shoot Cardiac, Philips Healthcare) at 75% of the R-R interval. A bolus of 100 mL iobitidol (Xenetix 350) was injected intravenously (5.7 mL/s) followed by a 50 mL saline flush. The scan was triggered using an automatic bolus tracking technique, with a region of interest placed in the descending thoracic aorta with a threshold of 150 Hounsfield Units (HU). In patients with a prescan heart rate of ≥65 beats per minute, metoprolol 50 to 150 mg was administered orally one hour before the start of the CT acquisition. If necessary, 5 to 25 mg metoprolol was given intravenously directly before the scan to achieve a heart rate <65 bpm. All patients received 800 mcg of sublingual nitroglycerine immediately before scanning.

FFR_{CT} analysis

FFR_{CT} was performed by HeartFlow Inc. (Redwood City, CA, USA), blinded to angiographic and physiological data. FFR_{CT} is derived post hoc from standard coronary CTA data using previously described methodology.(9) In short, it involves extraction of a patient specific geometric model of the coronary arteries, population-derived physiological models, and computational fluid dynamics techniques to solve the governing equations of blood flow for velocity and pressure under simulated hyperemic conditions. In the current study HeartFlow FFR_{CT} v2.7 was used, which comprises deep-learning artificial intelligence methods to aid in identifying the lumen boundary, physiological models incorporating vessel lumen volume as well as myocardial mass data and hybrid 3-dimensional–1-dimensional computational fluid

dynamics methods to improve computational efficiency while maintaining accuracy. (16) All coronary CTA scans were quality checked by HeartFlow to assess eligibility for FFR_{CT} analysis. Cases with severe image artefacts (i.e. noise, blooming, motion and misalignment) hampering analysis and cases in which the myocardium or coronary arteries were partly outside the field of view were rejected for analysis. Current FFR_{CT} technology is not validated for the calculation of values below 0.50, given the limited number of patients with invasive FFR below 0.50 in the validation phase of FFR_{CT}. Therefore, occluded vessels and vessels with an FFR_{CT} <0.50 were assigned a value of 0.50.

FFR_{CT} planner analysis

A researcher blinded to invasive FFR measurement aligned the location of FFR_{CT} measurement and the modification of coronary stenosis on FFR_{CT} planner with the location of invasive FFR measurement and actual stent implantation performed by the interventionalist during PCI in a computational model to determine the corresponding FFR_{CT} value and the FFR_{CT} planner value (Figure 1). This process was performed to ensure that the modification of stenosis on the FFR_{CT} planner tool matched the stent length and location actually performed by the interventional cardiologist in that particular case. For FFR_{CT} planner computation, an accelerated method for updating FFR_{CT} is used which is based on a reduced order model derived from computational fluid dynamics. The idealized vessel lumen dimensions are calculated by evaluating the stenosis and subsequently calculating the dimensions in which there would be no lumen narrowing using the idealized vessel algorithm. This algorithm uses a monotonic radius optimization to compute a radius value along the entire length of the vessel, from the ostium to the most distal vessel outlet. This model fits closely to the original lumen, but requires that the radius can only decrease in value going from proximal to distal. Finally, to enable real time computation, a computational fluid dynamics reduced order model is used to calculate the FFR_{CT} planner values.(17) In addition to FFR_{CT} and FFR_{CT} planner, delta FFR_{CT} (FFR_{CT} planner - FFR_{CT}) was calculated. Based on previous prognostic invasive FFR data, cut-offs of <0.90 for FFR_{CT} planner (3-5) and <0.24 for delta FFR_{CT} were used to define failed PCI (7)

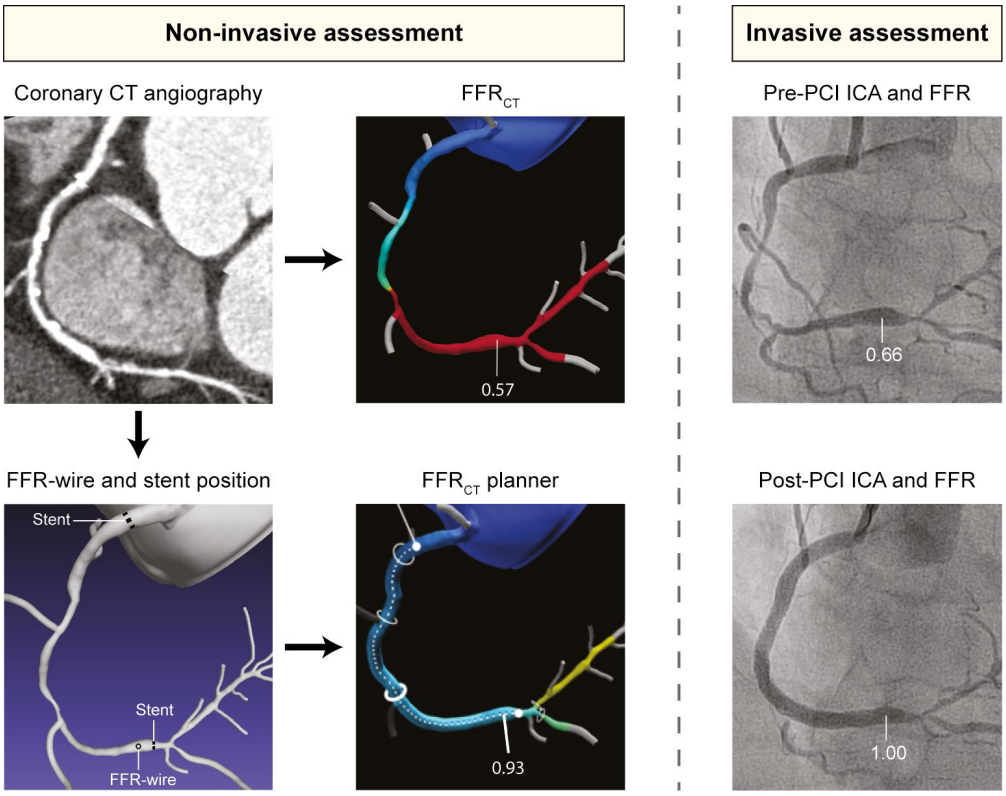

Figure 1. Case example of non-invasive assessment with FFRCT and FFRCT planner and invasive assessment with ICA and FFR in a patient undergoing revascularization.
Non-invasive coronary computed tomography (CT) angiography showed diffuse disease in the RCA, with multiple severe stenoses along the course of the vessel. FFRCT derived from standard coronary CT angiography images was calculated to be 0.57 in the distal RCA. Invasive assessment pre-PCI confirmed diffuse disease in the mid and distal RCA with a corresponding FFR in the distal RCA of 0.66. Subsequently, PCI was performed with implantation of 3 stents with a total stent length of 81 mm, resulting in a post-PCI FFR of 1.00. For computation of FFRCT planner, the location of invasive FFR measurement and actual stent location were annotated in a computational model by a researcher blinded to invasive data. After simulation of stenosis removal, FFRCT planner value was shown to 0.93. Abbreviations: FFR = fractional flow reserve; FFRCT = computed tomography derived FFR; ICA = invasive coronary angiography; PCI = percutaneous coronary intervention

Invasive coronary angiography and FFR

ICA and FFR measurements were performed as described previously.(15) ICA was performed using a standard protocol in at least 2 orthogonal directions per evaluated coronary artery segment. For the induction of epicardial coronary vasodilation, 0.2 ml of intracoronary nitroglycerin was administered prior to contrast injection. Lesion length, reference vessel diameter, minimal luminal diameter and percentage diameter stenosis were analyzed using quantitative coronary angiography analysis (CAAS II,

Pie Medical, Maastricht, the Netherlands). FFR was measured using a pressure sensor-tipped guidewire (Volcano Corporation, Rancho Cordova, CA, USA). Maximal hyperemia was induced by intracoronary (150 μg) or intravenous (140 $\mu g \cdot kg^{-1} \cdot min^{-1}$) administration of adenosine. FFR was calculated as the ratio of mean distal coronary pressure to mean aortic pressure and an FFR of ≤0.80 was considered hemodynamically significant. The choice of revascularization was left to the discretion of the operator and the heart team. In the event of PCI, post-procedural FFR measurements were performed to assess the direct effect of coronary stenting. Care was taken to position the pressure wire tip at the same location as during pre-PCI FFR measurements. All FFR tracings were evaluated by experienced interventional cardiologists blinded to FFR_{CT} findings. In case of significant drift (Pd/Pa at the level of the guiding of >1.02 or <0.98), FFR measurements were recalculated after correcting Pd.(18) Vessels with a subtotal occlusion in which the operator refrained from obtaining FFR measurement (2 vessels) were assigned an FFR value of 0.50. Additionally, in concordance with FFR_{CT}, vessels with FFR <0.50 were also assigned a value of 0.50. Delta FFR was calculated as the difference between pre and post PCI FFR (post-PCI FFR – pre-PCI FFR). As in FFR_{CT}, cut-offs of <0.90 post-PCI FFR(3-5) and <0.24 for delta invasive FFR were used to distinguish between an appropriate and inappropriate hemodynamic result after stenting.(7)

Statistical analyses

All statistical analyses were performed using the SPSS software package (version 20.0.0, IBM SPSS Statistics, Armonk, New York), except for receiver operating characteristics (ROC) curve analyses which were performed with MedCalc for Windows (version 12.7.8.0, MedCalc Software, Oostende, Belgium). Continuous variables were tested for normal distribution. Normal distributed continuous variables are presented as mean ± SD. Non-normal distributed variables are presented as median with interquartile range. The associations between FFR_{CT} (FFR_{CT}, FFR_{CT} planner and delta FFR_{CT}) and invasive FFR (pre-PCI FFR, post-PCI FFR and delta FFR) were quantified using Spearman's correlation coefficients and agreement was assessed with Bland-Altman analysis and using intraclass correlation coefficients (ICCs) based on a two-way mixed model. To account for clustering of multiple vessel measurements per patient, means of FFR_{CT} (FFR_{CT}, FFR_{CT} planner and delta FFR_{CT}) and invasive FFR (pre-PCI FFR,

post-PCI FFR and delta FFR) were compared using a mixed linear model with a fixed effect for the technique and random effects for patient and vessel nested within patient. Receiver-operating characteristic (ROC) curve analysis with calculation of area under the curve (AUC) was performed to investigate the diagnostic value of FFR_{CT} planner for post-PCI FFR <0.90 and the diagnostic value of delta FFR_{CT} for delta FFR <0.24. Subsequently, sensitivity, specificity, positive predictive value, and negative predictive value were calculated. A p-value <0.05 was considered statistically significant.

Results

Study population

An initial number of 82 patients (95 vessels) were evaluated for inclusion in the current study. Two vessels were excluded from analysis prior to FFR_{CT} analysis; because FFR wire position was not recorded during angiography in one case and because of prior stenting in the target vessel in the other case. Of the 93 vessels submitted for FFR_{CT} analysis, 5 vessels (5%) were rejected after initial image quality check because of motion artefacts in 1 case and misalignment artefacts in 4 cases. Additionally, 8 (9%) vessels were not processed due to technical errors with the FFR_{CT} planner software, i.e. merging of two adjacent vessels during computation of idealized lumen dimensions leading to unsuitable models for FFR_{CT} planner computation. The technical rejection rate for FFR_{CT} analysis was therefore 14%. In 17 (18%) vessels, FFR_{CT} analysis was technically possible and completed, however FFR_{CT} values could not be calculated at the same location as invasive FFR measurements due to a vessel diameter <1.80 mm at the site of measurement (14 vessels) or the presence of a total occlusion on coronary CTA (3 vessels). This resulted in a total study population of 56 patients and 63 vessels. Baseline clinical, angiographic, and procedural characteristics of the 56 included patients are presented in table 1. The target lesion was most frequently located in the LAD (39 vessels, 62%) and diameter stenosis before and after PCI were 69 ± 13% and 12 ± 9%, respectively.

Relationship between FFR_{CT} and invasive FFR

The relationships between FFR_{CT} / FFR_{CT} planner and invasively measured FFR values before and after PCI are illustrated in figure 2. Pre-PCI, invasive FFR was 0.65±0.12 and FFR_{CT} was 0.64±0.13 (p=0.34). A significant correlation (r=0.53, p<0.001, Figure

Table 1. Clinical, angiographic and procedural characteristics

Clinical characteristics (n = 56 patients)	
Age, years	62 ± 10
Male	47 (84%)
Body mass index	27 ± 3
Diabetes Mellitus type II	4 (7%)
Hypertension	25 (45%)
Hyperlipidaemia	28 (50%)
Current tobacco use	5 (9%)
Family history of CAD	28 (50%)
Prior myocardial infarction	7 (13%)
Prior PCI	7 (13%)
Invasive coronary angiography (n = 63 vessels)	
Treated vessel	
LAD	39 (62%)
LCX	8 (13%)
RCA	16 (25%)
Before PCI *	
Reference diameter, mm	2.77 ± 0.46
MLD, mm	0.86 ± 0.39
Diameter stenosis, %	69 ± 13
Lesion length	17.1 [11.9 – 31.0]
After PCI *	
Reference diameter, mm	2.83 ± 0.42
MLD, mm	2.49 ± 0.46
Diameter stenosis, %	12 ± 9
Procedural characteristics (n = 63 vessels)	
Stent length, mm	28 [18 - 38]
Nominal stent diameter, mm	3.32 ± 0.35
Final stent diameter after implantation, mm	3.74 ± 0.44

*: Quantitative coronary analysis. Abbreviations: CAD = coronary artery disease; PCI = percutaneous coronary intervention; MLD = minimal luminal diameter.

2A) and agreement (ICC=0.50, p<0.001) were found between pre-PCI FFR and FFR_{CT}. Bland-Altman analysis (Figure 2B) showed a mean difference of 0.015 (95% CI: -0.23 to 0.26) between pre-PCI FFR and FFR_{CT}. Post-PCI invasive FFR values were significantly higher than FFR_{CT} planner values (0.89±0.07 vs. 0.85±0.07, p<0.001).

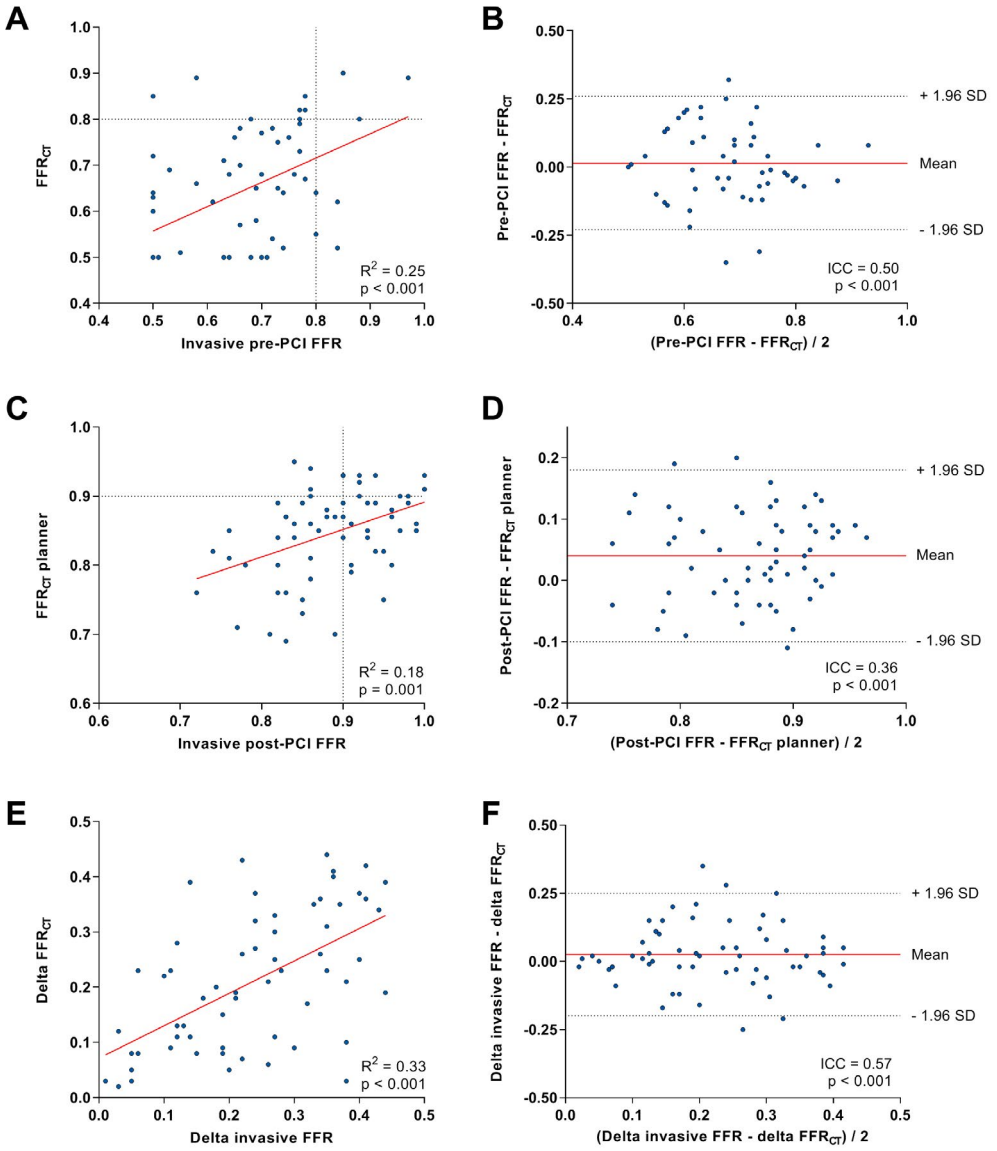

Figure 2. Relationship between pre-PCI, post-PCI and delta invasive FFR and FFR$_{CT}$, FFRCT planner and delta FFR$_{CT}$.
Scatter (A, C, and E) and Bland-Altman plots (B, D, and F) depicting the relationship between pre-PCI invasive FFR and FFR$_{CT}$ (A and B), between invasive post-PCI FFR and FFR$_{CT}$ planner (C and D) and between delta invasive FFR and delta FFR$_{CT}$ (E and F). Abbrevations as in figure 1.

A significant correlation (r=0.41, p=0.001, Figure 2C) and agreement (ICC=0.36, p<0.001) were observed between post-PCI FFR and FFR_{CT} planner. The Bland-Altman plot (Figure 2D) showed a mean difference of 0.040 (95% CI: -0.10 to 0.18) between post-PCI FFR and FFR_{CT} planner. Delta invasive FFR and delta FFR_{CT} were 0.23±0.12 and 0.21±0.12, respectively (p=0.09). A significant correlation (r=0.57, p<0.001, Figure 2E) was observed between delta invasive FFR and delta FFR_{CT}. Bland-Altman analysis (Figure 2F) showed a mean difference of 0.025 (95% CI: -0.20 to 0.25) and a significant agreement was noted between delta invasive FFR and delta FFR_{CT} (ICC=0.57, p<0.001).

Diagnostic accuracy of FFR_{CT} planner for prediction of FFR and change in FFR after stenting

The diagnostic performance of FFR_{CT} planner for predicting FFR and change in FFR after stenting is listed in the supplementary data (Table S1). Accuracy of FFR_{CT} planner <0.90 for post-PCI FFR <0.90 was 62% and accuracy of FFR_{CT} planner for change in FFR, defined by delta invasive FFR of <0.24, was 76%. ROC curve analysis showed moderate diagnostic value of FFR_{CT} planner for post-PCI FFR <0.90 (Supporting information, Figure S1, AUC = 0.70, 95% CI 0.57 - 0.81). Furthermore, ROC curve analysis showed good diagnostic value of delta FFR_{CT} for delta invasive FFR <0.24 with an AUC of 0.80 (95% CI 0.68 - 0.89, supplementary data Figure S1).

Discussion

The current study evaluated the performance of the novel non-invasive FFR_{CT} planner tool to predict the hemodynamic gain of PCI. Results show significant albeit modest agreement between FFR_{CT} planner and invasive post-PCI FFR. Additionally, the changes in FFR_{CT} after simulated removal of stenosis demonstrated significant agreement with changes in invasive FFR after PCI. These hypothesis generating results indicate that the FFR_{CT} planner tool may hold promise for the non-invasive prediction of the hemodynamic gain of PCI and for PCI procedural planning. However, given the modest performance of the FFR_{CT} planner tool improvement in technology is warranted before clinical application.

Using FFR_{CT} planner to predict post-PCI FFR and changes in FFR after stenting

FFR_{CT} has emerged as a promising non-invasive imaging tool among a myriad of imaging modalities. Recent head-to-head comparisons have shown either comparable or superior diagnostic performance of FFR_{CT} as compared to SPECT, the workhorse in functional imaging of patients with suspected CAD.(12,19) In addition to the functional assessment of coronary stenoses, recent advances in FFR_{CT} technology have enabled the simulated removal of stenoses hereby predicting the hemodynamic gain of PCI.(13,20) Kim et al. were the first to report on this concept in a small cohort of 44 patients (48 lesions).(13) Invasive post-PCI FFR and the FFR_{CT} derived values displayed moderate correlation, demonstrating the feasibility of coronary CTA based simulation of stenosis removal. Although these initial findings demonstrated the feasibility of using FFR_{CT} technology to predict post-PCI FFR, these analyses were time consuming and not commercially available. Recent advances however have led to the development of the interactive FFR_{CT} planner tool, which enables physicians to interactively examine the effects of different treatment strategies on FFR_{CT} in real time. The performance of this novel tool was investigated in the present study. Results show significantly lower values for FFR_{CT} planner as compared to invasive post-PCI FFR ($p<0.001$), with a mean difference of 0.04. Furthermore, a modest albeit slightly weaker correlation between FFR_{CT} planner and post-PCI FFR was noted in the current report than in the study by Kim et al. Kim et al. subsequently reported a diagnostic accuracy of FFR_{CT} of 96% to predict a post-PCI FFR ≤0.80. Although an FFR value of ≤0.80 is established to determine the hemodynamic relevance of stenosis pre-PCI, this cut-off might not be suited for the evaluation of coronary flow after PCI. Since prospective studies on the optimal cut-off for post-PCI FFR are lacking, the optimal threshold to define a satisfactory hemodynamic result of PCI remains unclear. Retrospective studies have identified different cut-off values ranging from 0.89 to 0.96, with two recent meta-analyses indicated 0.90 as optimal prognostic cut-off for invasive post-PCI FFR.(3-5) Additionally, a recent study has suggested that different cut-off values may apply for non-LAD vessels and LAD vessels.(21) Despite the limited data on the optimal cut-off for post-PCI FFR, we opted to test the diagnostic accuracy of FFR_{CT} planner for identifying post-PCI FFR of <0.90. FFR_{CT} planner demonstrated modest diagnostic performance with an AUC of 0.70 and a diagnostic accuracy of 62%.

In addition to post-PCI FFR values, absolute and relative changes in FFR following stenting have also been associated with cardiovascular events, indicating that prognosis is not solely driven by the final result after PCI but also by the increase in coronary flow following PCI.(6,7) In the current study, moderate correlation (r=0.57) and agreement (ICC=0.57) were found between delta FFR_{CT} and delta FFR. Furthermore, using a previously described cut-off of 0.24 for invasive delta FFR,(7) diagnostic performance of delta FFR_{CT} for delta FFR was good with an AUC of 0.80 and an accuracy of 76%. This indicates that the current technology of FFR_{CT} planner may be more useful in predicting the increase in hyperemic pressure changes after PCI then in predicting the absolute post-PCI FFR value. Given the significant albeit modest relationship between FFR_{CT} planner and invasive measurements, the findings from the current proof of principle study may be interpreted as hypothesis-generating, indicating the potential that FFR_{CT} planner holds for non-invasive treatment planning. However, advances in technology are mandatory before clinical application. Furthermore, future large prospective studies are warranted to validate our findings and eventually to test whether FFR_{CT} planner guided PCI may improve clinical outcome as compared to standard-of-care invasive angiography-guided PCI.

Non-invasive versus invasive treatment planning

In addition to non-invasive prediction of invasive FFR with FFR_{CT}, recent studies have investigated the use of computational fluid dynamics to compute FFR from ICA to predict the hemodynamic effects of a stenosis.(22,23) More recently, two studies have investigated novel applications of this technology in which FFR is calculated from ICA after simulation of stenosis removal.(24,25) Both studies, one using virtual FFR and the other using QFR, have reported good agreement of the computed FFR after simulation of stenosis removal with invasive FFR post-PCI. Notwithstanding these promising results, it is important to note that these technologies are based on ICA and therefore do not allow for patient selection and treatment planning before the invasive procedure. Contrary, non-invasive treatment planning based on coronary CTA is limited by the availability of a sufficient quality coronary CTA scan before PCI and by an inferior resolution as compared with invasive coronary angiography. Further prospective studies are warranted to compare the ability of these promising techniques head-to-head against invasive measurements of FFR to predict the hemodynamic gain

after PCI.

Potential clinical application of the FFR_{CT} planner tool

Although non-invasive treatment planning using FFR_{CT} planner may help select the most optimal stent size for maximal reduction of lesion-specific ischemia in all cases, treatment planning may be redundant for experienced PCI operators in non-complex focal lesions with documented ischemia. However, in patients with serial lesions or diffuse disease the FFR_{CT} planner tool may be a useful aid in guiding these more complex PCI procedures. In serial lesions, predicting the hemodynamic effects of stenting individual lesions using invasive FFR is very complex and impractical, requiring balloon dilation of one of the lesion and subsequent wedge pressure measurements.(26) Therefore, in clinical practice, interventionalists tend to treat the most severe lesion, either based on angiographic stenosis severity or on the magnitude of the pressure gradient, which may lead to suboptimal stenting. The FFR_{CT} planner tool may assist the operator in these cases to decide between treatment strategies, as illustrated in the case example presented in Figure 3. Modi et al. have recently highlighted the promise of the FFR_{CT} planner tool to predict the hemodynamic effects of individual stenoses in serial lesions. In a small cohort of 19 vessels, FFR_{CT} planner resulted in improved prediction of residual FFR following stenting of an accompanying serial stenosis as compared to invasive FFR pullback.(20) In diffuse disease the hemodynamic gain after PCI is also difficult to predict, with operators often encountering minimal increase in FFR after stenting a focal part of the diffusely diseased vessel. Contrary, as illustrated in the case example presented in Figure 1, stenting from proximal to distal with the use of multiple stents is often needed to achieve a satisfactory hemodynamic result after PCI. The FFR_{CT} planner tool could be useful in these patients to predict the hemodynamic effects of all available stent strategies. However, it is important to note that one should incorporate clinical judgment to avoid excessive stent dimensions, hereby balancing optimal reduction in lesion-specific ischemia limiting and minimization of mechanical complications such as edge dissection. Furthermore, clinical applicability is currently hampered by both the modest performance of the current FFR_{CT} planner tool and the relatively high rejection rate. Improvement in technology is warranted before clinical application.

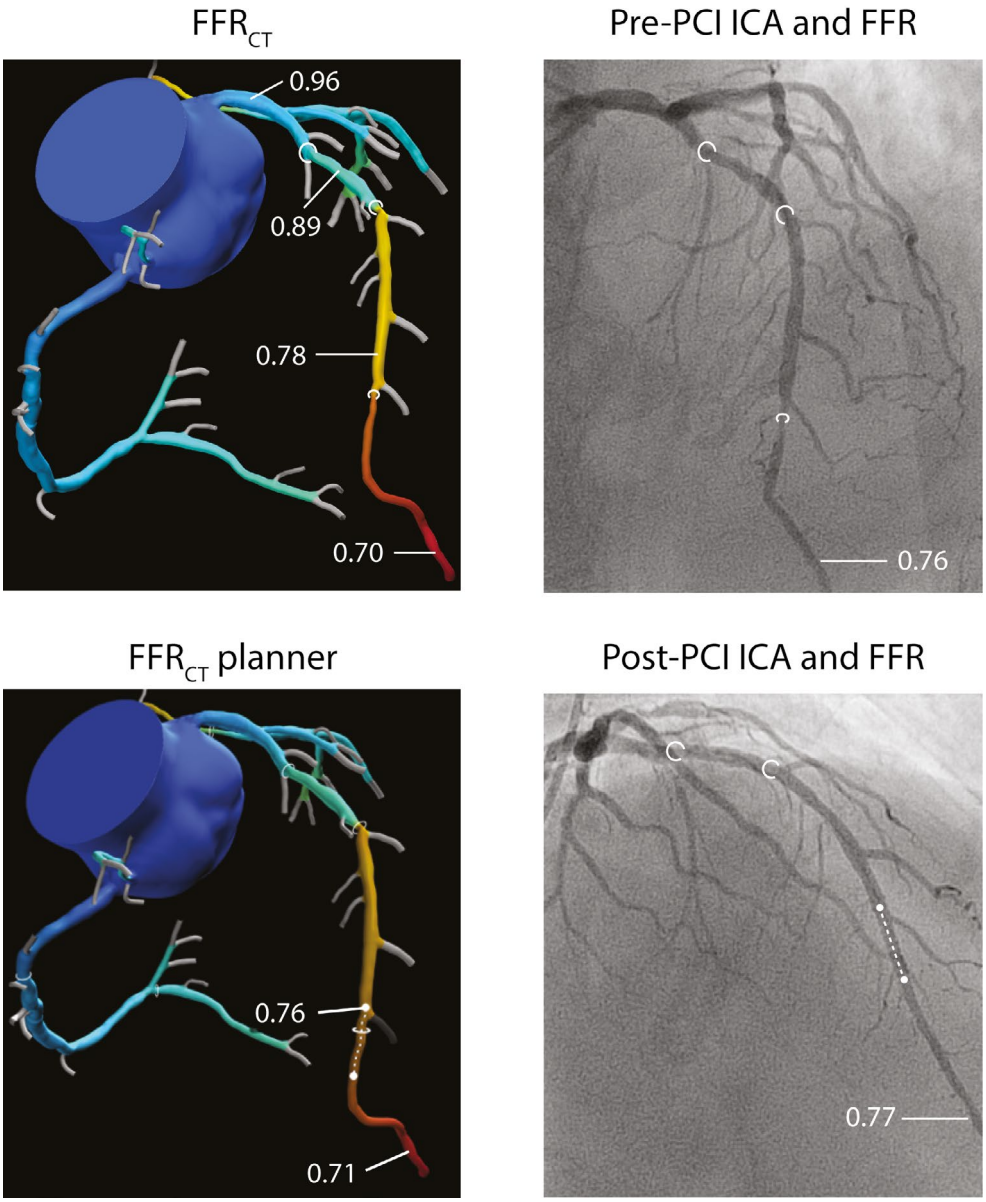

Figure 3. Case example illustrating the use of the FFRCT planner tool in a patient with serial stenoses.
FFRCT models of coronary CTA and ICA showed serial lesions in the proximal, mid, and distal LAD (stenosis labeled by white circles). FFRCT analysis showed comparable delta FFRCT for the proximal (0.07), mid (0.11), and distal (0.08) lesions, with an FFRCT in the distal LAD of 0.70. Invasive FFR pre-PCI was shown to be 0.76 and since the distal lesions was angiographically most severe, the operator chose to treat the distal LAD. After PCI (stent labeled by white doted line), there was little increase in FFR (delta FFR of 0.01), with a post-PCI FFR of 0.77. FFRCT planner analysis (stenosis modification labeled by white doted line) showed comparable results with a delta FFRCT of 0.01 and a FFRCT planner value of 0.71, demonstrating the usefullness of FFRCT planner in treatment planning of serial lesions. Abbrevations as in figure 1.

Limitations

This study has several limitations. First, our study is a single-center experience with a relatively small number of patients. Results must therefore be interpreted as hypothesis generating. The international prospective multicenter Precise Percutaneous Coronary Intervention Plan P3 Study is currently ongoing and will test the diagnostic accuracy of FFR_{CT} planner in a large clinical population (NCT03782688). Second, of all initially evaluated cases 14% were rejected for FFR_{CT} planner analysis because of motion artefacts, misalignment, or technical software issues. This is an important limiting factor for the clinical application of FFR_{CT} planner at the current stage of technology. Improvement in technology is warranted to enable clinical applicability. Third, although care was taken to match FFR_{CT} stenosis modification sites to the location of the actual stent implantation, inaccuracies may have occurred. This could have importantly influenced our results. Last, unlike the threshold of 0.80 for pre-PCI which has been extensively validated for clinical events,(1,27) the thresholds for post-PCI FFR and delta FFR used in the current study are based on retrospective data.(3-5,7) Further studies are needed to establish the prognostic value of post-PCI and delta FFR. The analyses on the diagnostic accuracy for post-PCI FFR and delta FFR must therefore be interpreted with caution.

Conclusion

The novel non-invasive FFR_{CT} planner tool demonstrated significant yet limited agreement with invasive post-PCI FFR values and with changes in FFR values after PCI. These hypothesis generating results indicate that the FFR_{CT} planner tool may hold promise for the non-invasive prediction of the hemodynamic gain of PCI and for PCI procedural planning. However, given the modest accuracy improvement of the technology is warranted to enable clinical introduction of non-invasive treatment planning.

References

1. De Bruyne B, Fearon WF, Pijls NH, et al. Fractional flow reserve-guided PCI for stable coronary artery disease. N Engl J Med. 2014;371:1208-17.
2. Driessen RS, Danad I, Stuijfzand WJ, et al. Impact of Revascularization on Absolute Myocardial Blood Flow as Assessed by Serial [(15)O]H2O Positron Emission Tomography Imaging: A Comparison With Fractional Flow Reserve. Circ Cardiovasc Imaging. 2018;11:e007417.
3. Johnson NP, Toth GG, Lai D, et al. Prognostic value of fractional flow reserve: linking physiologic severity to clinical outcomes. J Am Coll Cardiol. 2014;64:1641-54.
4. Pijls NH, Klauss V, Siebert U, et al. Coronary pressure measurement after stenting predicts adverse events at follow-up: a multicenter registry. Circulation. 2002;105:2950-4.
5. Rimac G, Fearon WF, De Bruyne B, et al. Clinical value of post-percutaneous coronary intervention fractional flow reserve value: A systematic review and meta-analysis. Am Heart J. 2017;183:1-9.
6. Lee JM, Hwang D, Choi KH, et al. Prognostic Implications of Relative Increase and Final Fractional Flow Reserve in Patients With Stent Implantation. JACC Cardiovasc Interv. 2018;11:2099-109.
7. Fournier S, Ciccarelli G, Toth GG, et al. Association of Improvement in Fractional Flow Reserve With Outcomes, Including Symptomatic Relief, After Percutaneous Coronary Intervention. JAMA Cardiol. 2019;4:370-4.
8. Piroth Z, Toth GG, Tonino PAL, et al. Prognostic Value of Fractional Flow Reserve Measured Immediately After Drug-Eluting Stent Implantation. Circ Cardiovasc Interv. 2017;10:e005233.
9. Taylor CA, Fonte TA, Min JK. Computational fluid dynamics applied to cardiac computed tomography for noninvasive quantification of fractional flow reserve: scientific basis. J Am Coll Cardiol. 2013;61:2233-41.
10. Min JK, Leipsic J, Pencina MJ, et al. Diagnostic accuracy of fractional flow reserve from anatomic CT angiography. JAMA. 2012;308:1237-45.
11. Norgaard BL, Leipsic J, Gaur S, et al. Diagnostic performance of noninvasive fractional flow reserve derived from coronary computed tomography angiography in suspected coronary artery disease: the NXT trial (Analysis of Coronary Blood Flow Using CT Angiography: Next Steps). J Am Coll Cardiol. 2014;63:1145-55.
12. Driessen RS, Danad I, Stuijfzand WJ, et al. Comparison of Coronary Computed Tomography Angiography, Fractional Flow Reserve, and Perfusion Imaging for

Ischemia Diagnosis. J Am Coll Cardiol. 2019;73:161-73.
13. Kim KH, Doh JH, Koo BK, et al. A novel noninvasive technology for treatment planning using virtual coronary stenting and computed tomography-derived computed fractional flow reserve. JACC Cardiovasc Interv. 2014;7:72-8.
14. Ihdayhid AR, White A, Ko B. Assessment of Serial Coronary Stenoses With Noninvasive Computed Tomography-Derived Fractional Flow Reserve and Treatment Planning Using a Novel Virtual Stenting Application. JACC Cardiovasc Interv. 2017;10:e223-e5.
15. Danad I, Raijmakers PG, Driessen RS, et al. Comparison of Coronary CT Angiography, SPECT, PET, and Hybrid Imaging for Diagnosis of Ischemic Heart Disease Determined by Fractional Flow Reserve. JAMA Cardiol. 2017;2:1100-7.
16. LeCun Y, Bengio Y, Hinton G. Deep learning. Nature. 2015;521:436-44.
17. Sankaran SL, D.; Tombropoulos, R.; Xiao, N.; Kim, H. J.; Spain, D.; Schaap, M.; Taylor, C. A. Physics driven real-time flow simulations. Computer Methods in Applied Mechanics and Engineering. 2020;364:112963.
18. Pijls NH, Bruyne BD. Fractional Flow Reserve, Coronary Pressure Wires, and Drift. Circ J. 2016;80:1704-6.
19. Sand NPR, Veien KT, Nielsen SS, et al. Prospective Comparison of FFR Derived From Coronary CT Angiography With SPECT Perfusion Imaging in Stable Coronary Artery Disease: The ReASSESS Study. JACC Cardiovasc Imaging. 2018;11:1640-50.
20. Modi BN, Sankaran S, Kim HJ, et al. Predicting the Physiological Effect of Revascularization in Serially Diseased Coronary Arteries. Circ Cardiovasc Interv. 2019;12:e007577.
21. Hwang D, Lee JM, Lee HJ, et al. Influence of Target Vessel on Prognostic Relevance of Fractional Flow Reserve After Coronary Stenting. EuroIntervention. 2019;15:457-64.
22. Morris PD, Ryan D, Morton AC, et al. Virtual fractional flow reserve from coronary angiography: modeling the significance of coronary lesions: results from the VIRTU-1 (VIRTUal Fractional Flow Reserve From Coronary Angiography) study. JACC Cardiovasc Interv. 2013;6:149-57.
23. Xu B, Tu S, Qiao S, et al. Diagnostic Accuracy of Angiography-Based Quantitative Flow Ratio Measurements for Online Assessment of Coronary Stenosis. J Am Coll Cardiol. 2017;70:3077-87.
24. Gosling RC, Morris PD, Silva Soto DA, Lawford PV, Hose DR, Gunn JP. Virtual Coronary Intervention: A Treatment Planning Tool Based Upon the Angiogram. JACC Cardiovasc Imaging. 2019;12:865-72.
25. Rubimbura V, Guillon B, Fournier S, et al. Quantitative flow ratio virtual stenting and post stenting correlations to post stenting fractional flow reserve measurements from

the DOCTORS (Does Optical Coherence Tomography Optimize Results of Stenting) study population. Catheter Cardiovasc Interv. 2019.

26. Pijls NH, De Bruyne B, Bech GJ, et al. Coronary pressure measurement to assess the hemodynamic significance of serial stenoses within one coronary artery: validation in humans. Circulation. 2000;102:2371-7.

27. Pijls NH, van SP, Manoharan G, et al. Percutaneous coronary intervention of functionally nonsignificant stenosis: 5-year follow-up of the DEFER Study. J Am Coll Cardiol. 2007;49:2105-11.

Supplementary Data

Table S1. Diagnostic performance of FFR_{CT} on the hemodynamic outcome after stenting as defined by invasive FFR

	Sensitivity, %	Specificity, %	PPV, %	NPV, %	Accuracy, %
Post-PCI FFR <0.90					
FFR_{CT} planner	88 (71-96)	36 (19-55)	58 (51-65)	73 (49-89)	62 (49-74)
Delta FFR <0.24					
Delta FFR_{CT}	88 (71-97)	65 (45-81)	72 (61-81)	83 (66-93)	76 (64-86)

Abbreviations: FFR = fractional flow reserve; FFR_{CT} = computed tomography derived FFR; NPV = negative predictive value; PCI = percutaneous coronary intervention; PPV = positive predictive value

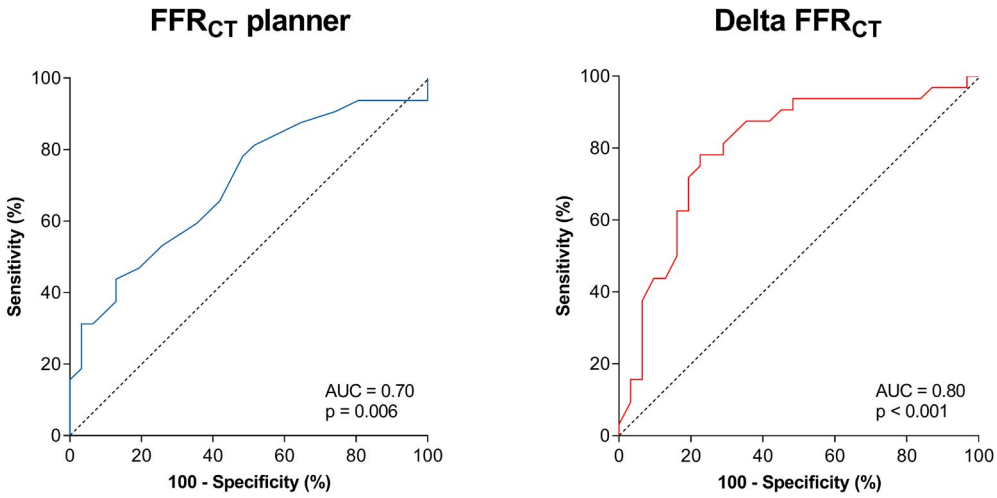

Figure S1.
Receiver-operating characteristic curve analysis with corresponding area under the curve (AUC) for the diagnostic value of FFRCT planner for post-PCI FFR <0.90 (left) and for the diagnostic value of delta FFRCT for delta FFR <0.24 (right). Abbrevations as in figure 1.

PART II

$[^{15}O]H_2O$ positron emission tomography

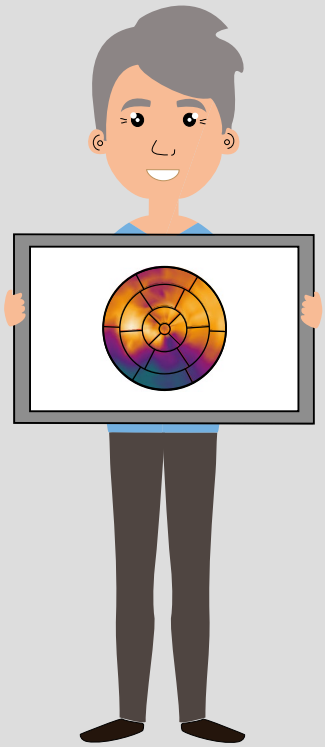

Chapter 10

Diagnostic value of longitudinal flow gradient for the presence of haemodynamically significant coronary artery disease

Michiel J. Bom, Roel S. Driessen, Pieter G. Raijmakers, Henk Everaars, Adriaan A. Lammertsma, Albert C. van Rossum, Niels van Royen, Juhani Knuuti, Maija Mäki, Ibrahim Danad, and Paul Knaapen

Eur Heart J Cardiovasc Imaging. 2019;20(1):21-30

Abstract

Aims: The longitudinal myocardial blood flow (MBF) gradient derived from position emission tomography (PET) has been proposed as an emerging non-invasive index of hemodynamically significant coronary artery disease (CAD). This study aimed to investigate the diagnostic value of longitudinal MBF gradient for the presence of hemodynamically significant CAD.

Methods and results: A total of 204 patients (603 vessels) with suspected CAD underwent [^{15}O]H_2O PET followed by invasive coronary angiography with fractional flow reserve (FFR) of all major coronary arteries. Longitudinal base-to-apex MBF gradients were assessed by two methods, using MBF in apical and mid (method 1) or in apical and basal (method 2) myocardial segments to calculate the gradient. The hyperemic longitudinal MBF gradient was only weakly correlated with FFR (method 1: $r=0.12$, $p=0.02$; method 2: $r=0.22$, $p<0.001$). The hyperemic longitudinal MBF gradient (by both methods), had lower diagnostic value as compared to hyperemic MBF for the presence of hemodynamically significant CAD, defined as a FFR≤0.80. No significant correlations between longitudinal MBF gradients and FFR were noted in proximal lesions, whereas longitudinal MBF gradients and FFR were significantly correlated in non-proximal lesions ($r=0.57$, $p<0.001$).

Conclusions: PET measured longitudinal flow parameters had lower diagnostic value as compared to hyperemic MBF for the presence of hemodynamically significant CAD. Since lesion location was found to affect the correlation of PET measured longitudinal flow parameters and FFR, presence of a longitudinal flow gradient may be partly caused by normalization to a relatively normal perfused areas.

Introduction

Ischemia detection is of importance in the management of patients with suspected coronary artery disease (CAD) (1) and quantitative assessment of myocardial blood flow (MBF) with positron emission tomography (PET) is considered the current non-invasive gold standard for this purpose.(2) Despite the excellent diagnostic value of PET-defined hyperemic MBF and myocardial flow reserve,(2) reductions in these regional flow parameters are considered relatively non-specific as they can be a consequence of both the flow-limiting effects of an epicardial stenosis and microvascular dysfunction.(3) Several studies have reported on the relationship between CAD and the longitudinal flow gradient, an abnormal decrease in hyperemic MBF from the base to the apex of the left ventricle (LV).(4-8) While initial reports have shown that this abnormal decrease in MBF occurs only in vessels with diffuse CAD, recent studies have reported on this phenomenon in vascular territories with a focal epicardial stenosis.(5-7) A proof-of-principle study has even shown a close correlation between the hyperemic longitudinal MBF gradient and the invasively measured fractional flow reserve (FFR), a specific index for the hemodynamic consequences of an epicardial coronary stenosis.(6) The hyperemic longitudinal MBF gradient has since been postulated as an emerging non-invasive index of hemodynamically significant CAD.(9) This study therefore aimed to investigate the diagnostic value of the hyperemic longitudinal MBF gradient for the presence of hemodynamically significant CAD as defined by FFR. Additionally, the influence of lesion location on the relationship between longitudinal flow parameters and FFR was explored.

Methods

Study population

The current report is a substudy of the PACIFIC trial and details regarding the study design and population are described previously.(2) In brief, 208 patients with suspected CAD underwent coronary computed tomography angiography, single photon emission computed tomography, and $[^{15}O]H_2O$ PET imaging, followed by invasive coronary angiography with FFR measurement in all major coronary vessels. For the current analysis all patients with PET imaging were included (n=204). In patients with a left dominant coronary anatomy in which the RCA did not subtend LV myocardium, the

RCA was excluded from analysis. The study protocol was approved by the Medical Ethics Committee of the VU University Medical Center and written informed consent was obtained.

Invasive coronary angiography and FFR

Invasive coronary angiography and FFR measurements were performed as described previously.(2) In brief, all major coronary arteries were routinely interrogated by FFR except for occluded or subtotal lesions ≥90%. Maximal hyperemia was induced by infusion of intracoronary (150 μg) or intravenous (140 $\mu g \cdot kg^{-1} \cdot min^{-1}$) adenosine. An FFR of ≤0.80 was considered hemodynamically significant. In case of a missing FFR, subtotal stenoses of ≥ 90% were deemed significant, whereas lesions with stenosis of ≤30% (obtained with QCA) were deemed non-significant. For a subgroup analysis on the influence of lesion location, vessels were divided into 3 groups: vessels with a proximal stenosis of ≥40%, vessels with a non-proximal stenosis of ≥40% and vessels without a stenosis of ≥40%.(10,11) Coronary lesions were deemed proximal if localized in one the following coronary segments (according to the ACC/AHA guidelines): segment 12 for the LAD, segment 18 for the LCX and segment 1, 2 and 3 for the RCA. (12) Lesions in other segments were deemed non-proximal.

$[^{15}O]H_2O$ positron emission tomography

Patients were scanned using a hybrid PET-CT device (Philips Gemini TF 64, Philips Healthcare, Best, The Netherlands). The scanning protocol has been described in detail previously.(13) In summary, a dynamic PET perfusion scan was performed during resting conditions using 370 MBq of $[^{15}O]H_2O$. A 6 min emission scan was started simultaneously with the administration of $[^{15}O]H_2O$. This dynamic scan sequence was followed immediately by a low dose CT scan for attenuation correction. After a 10 min interval to allow for decay of radioactivity, an identical PET sequence was performed during hyperemic conditions induced by an intravenous adenosine infusion (140 $\mu g \cdot kg^{-1} \cdot min^{-1}$), initiated 2 min before the hyperemic scan for maximal vasodilation. Images were reconstructed using the 3D row action maximum likelihood algorithm and applying all appropriate corrections. Parametric MBF images were generated and quantitatively analyzed using in-house developed software (Cardiac VUer).(14) Myocardial blood flow was expressed in $mL \cdot min^{-1} \cdot g^{-1}$. In addition to the calculation

of both resting and hyperemic MBF for the left ventricle as a whole, MBF was also calculated for each of the three vascular territories derived from the 17-segment standard American Heart Association model: LAD, LCX, and RCA. Myocardial flow reserve was defined as the ratio between hyperemic and resting MBF. Two separate methods were used to calculate the longitudinal MBF gradient (Fig. 1). In method 1, in accordance with previous ^{13}N-ammonia PET studies, MBF in the apical and mid myocardial segments were used to calculate the base-to-apex MBF gradient (longitudinal MBF gradient 1 = hyperemic MBF apical segment - hyperemic MBF mid segment).(5,8) In method 2 the longitudinal MBF gradient was defined as the difference of the MBF in the apical and the basal segments (longitudinal MBF gradient

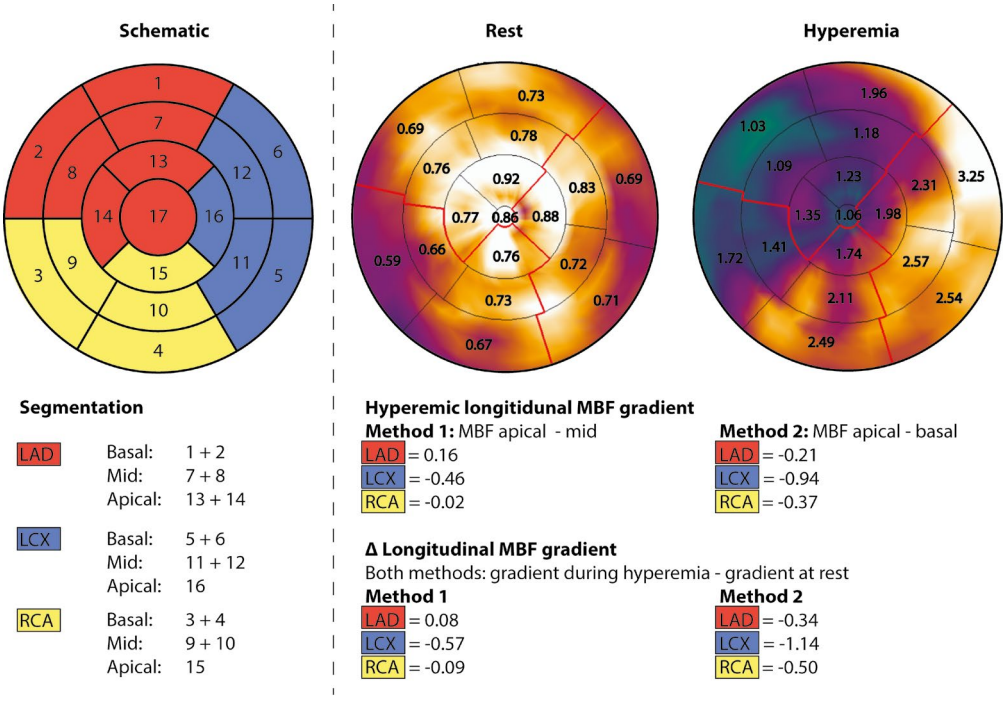

Figure 1. Case example of longitudinal MBF gradient analysis
A schematic representation of the left ventricle segmentation into 17 segments according to the standard American Heart Association (AHA) model is depicted in the left panel. The right panel shows [15O]H2O PET images of a 58 year-old male with chest pain. Polarmaps and quantitative MBF values per segment during rest and hyperemia show a clear reversible perfusion defect in the anterior and septal wall with hyperemic MBF values well below the commonly used cut-off of 2.3 ml/min/g. Calculation of the longitudinal MBF gradient for the different vascular territories is shown in the lower panel. First, the basal, mid and apical segments for each vascular territory are identified according to the AHA model. Subsequently the longitudinal MBF gradients are calculated by both method 1 (MBF apical segment – MBF mid segment) and method 2 (MBF apical segment – MBF basal segment). Lastly, Δ Longitudinal MBF gradients are calculated by subtracting the gradient at rest from the gradient during hyperemia.

2 = hyperemic MBF apical segment - hyperemic MBF basal segment). The longitudinal MBF gradients were calculated for the myocardial segments of the LV corresponding to the vascular territories of the LAD (basal: segment 1 and 2; mid: segments 7 and 8; apical: segments 13 and 14), LCX (basal: segments 5 and 6; mid: segments 11 and 12; apical: segment 16) and RCA (basal: segments 3 and 4; mid: segments 9 and 10; apical: segment 15). The Δlongitudinal MBF gradient was defined as the difference in longitudinal MBF gradient between hyperemia and rest (Δlongitudinal MBF gradient = longitudinal MBF gradient during hyperemia - longitudinal MBF gradient at rest). (5,8)

Statistical analyses

All statistical analyses were performed using the SPSS software package (version 20.0.0, IBM SPSS Statistics), except for ROC curve analyses which were performed with MedCalc for Windows (version 12.7.8.0, MedCalc Software, Oostende, Belgium). Continuous variables were tested for normal distribution. Normal distributed continuous variables are presented as mean ± SD. Non-normal distributed variables are presented as median with interquartile range. Categorical variables are presented as frequencies with percentages. Continuous variables of the various PET-derived flow parameters using both method 1 and 2 were compared between groups using Generalized Estimating Equations in order to account for multiple observations within patients. Models included a main effect for the grouping variables and an exchangeable correlation structure was used. Spearman's correlation was used to measure association between the various PET-derived flow parameters and FFR and between PET-derived flow parameters and QCA stenosis grade. Receiver-operating characteristic (ROC) curve analysis was performed to determine optimal cut-off values for the hyperemic MBF, hyperemic longitudinal MBF gradient and Δ longitudinal MBF gradient (by both method 1 and 2) for the presence of hemodynamically significant CAD as defined by FFR. The diagnostic value of the hyperemic longitudinal MBF gradient and Δ longitudinal MBF gradient (by both method 1 and 2) for the presence of hemodynamically significant CAD was tested against the diagnostic value of hyperemic MBF by comparing the ROC curve using the method of DeLong. Subgroup analyses were performed for vessels with a proximal lesion and vessels with a non-proximal lesions. Again, spearman's correlation was used in these subgroups to measure the

association between the PET-derived flow parameters and FFR. A p-value <0.05 was considered statistically significant.

Results

Study population

The baseline characteristics of all 204 included patients are shown in table 1. Nine patients had a left-dominant coronary anatomy in which the RCA did not subtend left ventricular myocardium. Therefore, in these 9 cases the RCA was excluded from analysis. Finally, the total number of vessels included for analysis was 603 (98.5%).

Table 1. Baseline characteristics

Demographics	**N = 204**
Age, yrs	58 ± 9
Male	129 (63%)
Body mass index	27 ± 4
Cardiovascular risk factors – no (%)	
Diabetes Mellitus type II	32 (16%)
Hypertension	96 (47%)
Hyperlipidaemia	81 (40%)
Current tobacco use	40 (20%)
History of tobacco use	99 (49%)
Family history of CAD	104 (51%)
Type of chest-pain – no (%)	
Typical angina	71 (35%)
Atypical angina	77 (38%)
Non-specific chest discomfort	56 (28%)

CAD = coronary artery disease

Invasive coronary angiography and fractional flow reserve

FFR measurements were performed in 542 (89.9%) vessels. In 58 (9.6%) vessels FFR was not performed because of the presence of a total/sub-total lesion. These vessels all showed >90% diameter stenosis and were thus deemed hemodynamically significant. Additionally, FFR measurement was not possible in 3 (0.5%) vessels because of severe tortuosity. None of these vessels showed a coronary lesion of ≥30% diameter stenosis and they were thus deemed non-obstructed. The total number of vessels with

hemodynamically obstructive CAD as defined by FFR was 160 (26.5%).

$[^{15}O]H_2O$ PET imaging

Regional and longitudinal flow parameters stratified by FFR results are depicted in table 2. Mean rest MBF did not differ between vessels with and without hemodynamically significant CAD (p=0.62). Mean hyperemic MBF and MFR values however were significantly lower in vessels with than vessels without hemodynamically significant CAD (p<0.001 for both). There was no significant difference between mean rest longitudinal MBF gradient by either of the two methods between vessels with and vessels without hemodynamically significant CAD (p=0.76 for method 1 and p=0=38 for method 2). Although numerically slightly lower there was also no significant difference in mean hyperemic longitudinal MBF gradient and mean Δ longitudinal MBF gradient calculated by method 1 between vessels with and without FFR-defined hemodynamically significant CAD (p=0.31 and p=0.20 respectively). However, when using method 2 both the mean hyperemic longitudinal MBF gradient and the mean Δ longitudinal MBF gradient were significantly lower in vessels with than vessels without hemodynamically significant CAD (p<0.001 for both). Fig. 2 shows the relationship of the various longitudinal flow parameters with fractional flow reserve. A significant

Table 2. PET-derived flow parameters per vascular territory stratified by FFR

Regional flow	Overall N=603	FFR ≤0.80 N=160	FFR >0.80 N=443	p-value
Rest MBF	0.90 ± 0.23	0.83 ± 0.20	0.93 ± 0.24	0.62
Hyperemic MBF	2.78 ± 1.15	1.79 ± 0.74	3.14 ± 1.06	<0.001
MFR	3.12 ± 1.20	2.15 ± 0.80	3.47 ± 1.13	<0.001
Longitudinal flow - Method 1: Apical - Mid				
Rest MBF gradient	0.03 ± 0.15	0.03 ± 0.12	0.03 ± 0.15	0.76
Hyperemic MBF gradient	0.02 ± 0.52	-0.03 ± 0.42	0.04 ± 0.55	0.31
Δ Gradient	-0.004 ± 0.50	-0.06 ± 0.41	0.01 ± 0.53	0.20
Longitudinal flow - Method 2: Apical - Basal				
Rest MBF gradient	0.08 ± 0.17	0.07 ± 0.15	0.09 ± 0.18	0.38
Hyperemic MBF gradient	0.16 ± 0.66	-0.07 ± 0.56	0.24 ± 0.67	<0.001
ΔGradient	0.08 ± 0.64	-0.14 ± 0.53	0.16 ± 0.66	<0.001

FFR = fractional flow reserve; MBF = myocardial bloodflow; MFR = myocardial flow reserve; PET = positron emission tomography

but weak correlation was found between hyperemic longitudinal MBF gradient and FFR calculated by method 1 (r=0.10, p=0.02). Δ Longitudinal MBF gradient and FFR however were not significantly correlated (r=0.08, p=0.052). For method 2, a significant but fairly weak correlation was found between hyperemic longitudinal MBF gradient

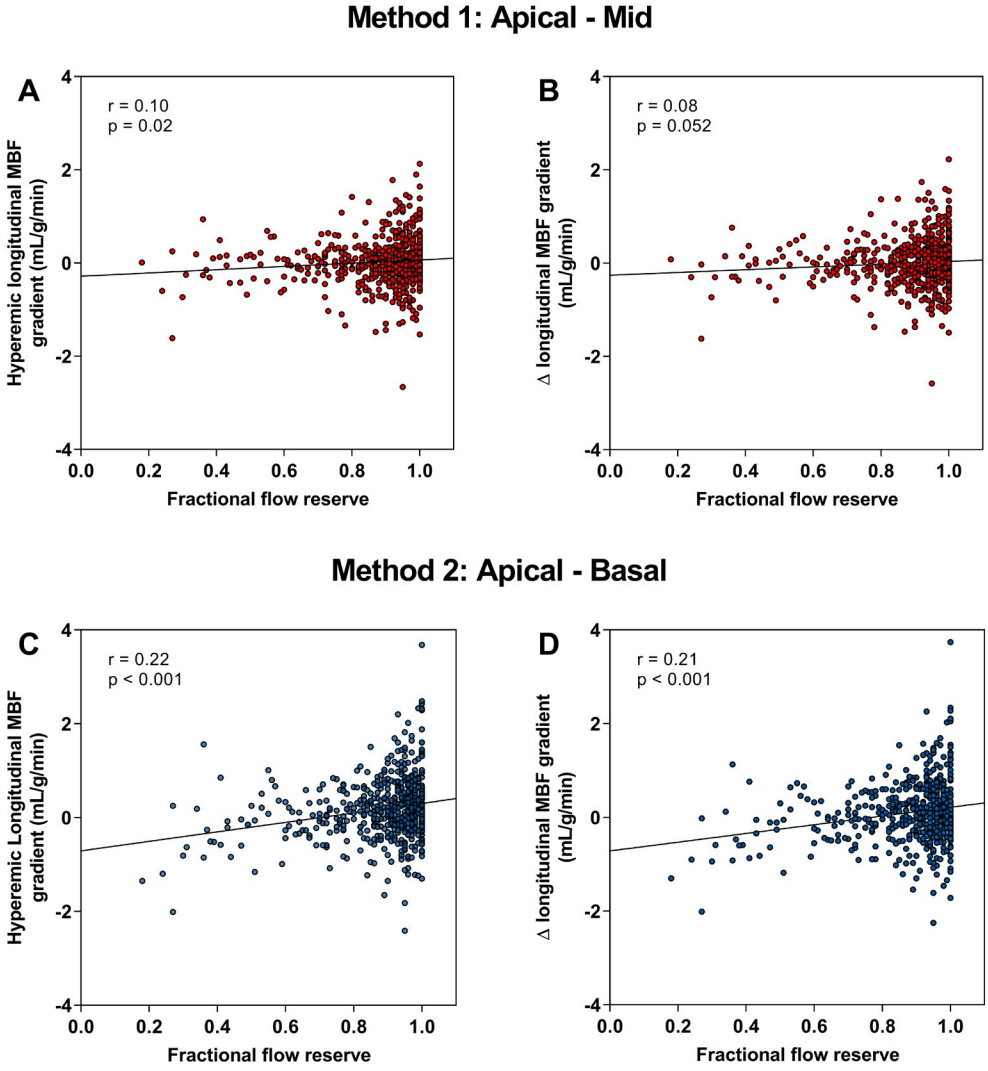

Figure 2. Relationship among hyperemic longitudinal flow parameters and fractional flow reserve
Correlation of hyperemic longitudinal MBF gradient (A) and Δ longitudinal MBF gradient (B) as defined by method 1 are depicted in the top panel. A weak correlation is found for the hyperemic longitudinal MBF gradient, whereas no significant correlation is found for the Δ longitudinal MBF gradient. The hyperemic longitudinal MBF gradient (C) and Δ longitudinal MBF gradient (D) as defined by method 2 are shown in the lower panel. A sligthly stronger but still relatively weak correlation is found for both the hyperemic longitudinal MBF gradient and Δ longitudinal MBF gradient.

and FFR (r=0.22, p<0.001) and between Δ longitudinal MBF gradient and FFR (r=0.21, p<0.001). Fig. 3 shows the relationship between the various longitudinal MBF gradient parameters and QCA stenosis grade. For method 1, no significant correlation was noted between hyperemic longitudinal MBF gradient (r=-0.07, p=0.11) and QCA stenosis grade and between Δ longitudinal MBF gradient and QCA stenosis grade

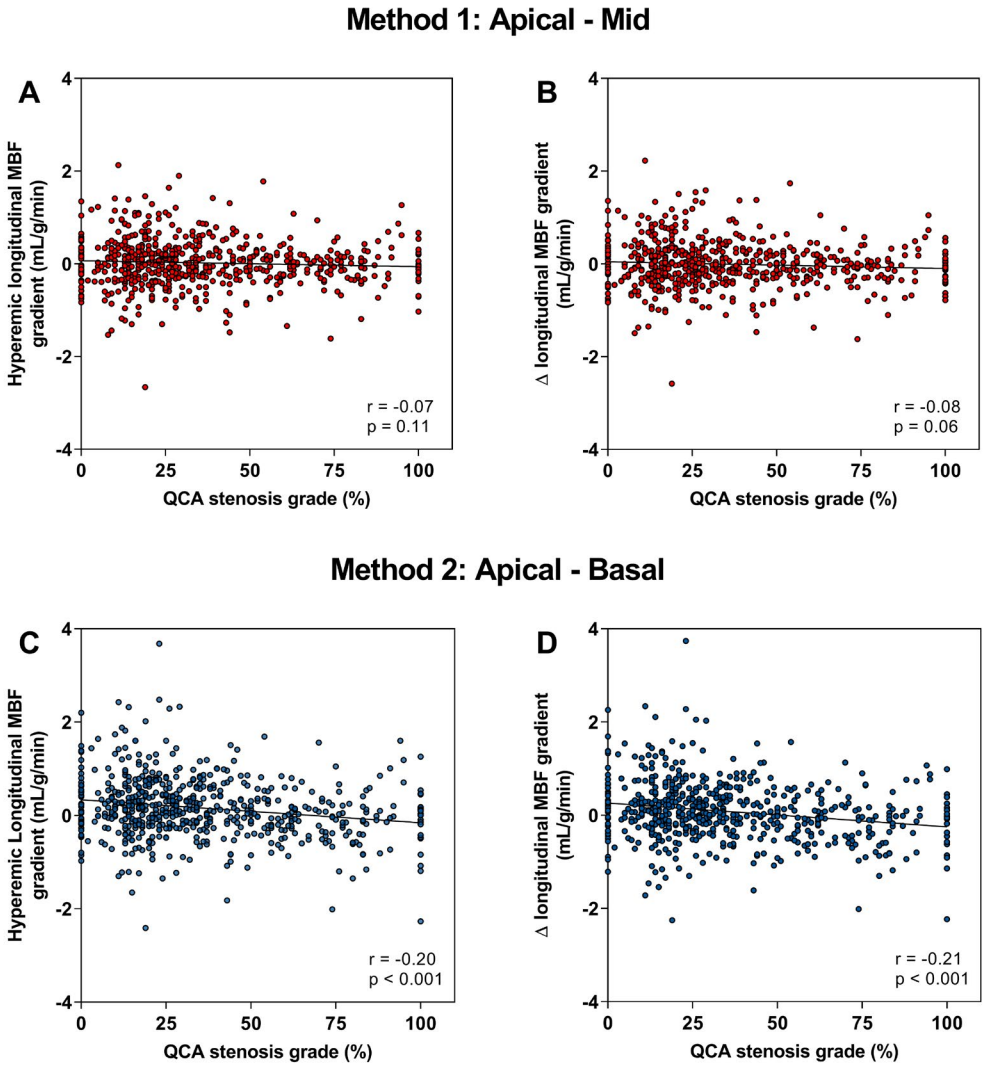

Figure 3 Relationship among hyperemic longitudinal flow parameters and QCA stenosis grade There was no significant correlation between QCA stenosis grade and hyperemic longitudinal MBF gradient (A) and Δ longitudinal MBF gradient (B) as defined by method 1. A significant but still weak correlation was found between QCA stenosis grade and method 2 defined hyperemic longitudinal MBF gradient (C) and Δ longitudinal MBF gradient (D).

(r=-0.09, p=0.06). For method 2, a significant but weak correlation was noted between hyperemic longitudinal MBF gradient and QCA stenosis grade (r=-0.20, p<0.001) and between Δ hyperemic longitudinal MBF gradient and QCA stenosis grade (r=-0.21, p<0.001).

Diagnostic value of longitudinal flow parameters

The results of the ROC analysis on the diagnostic value of the different PET perfusion parameters is illustrated in Fig. 4. Sensitivity, specificity, negative predictive value, positive predictive value, and diagnostic accuracy of hyperemic MBF, hyperemic longitudinal MBF gradient and Δ longitudinal MBF gradient (by both methods) and the addition of hyperemic longitudinal MBF gradient to hyperemic MBF for the presence of hemodynamically significant CAD are shown in Table 3. The diagnostic

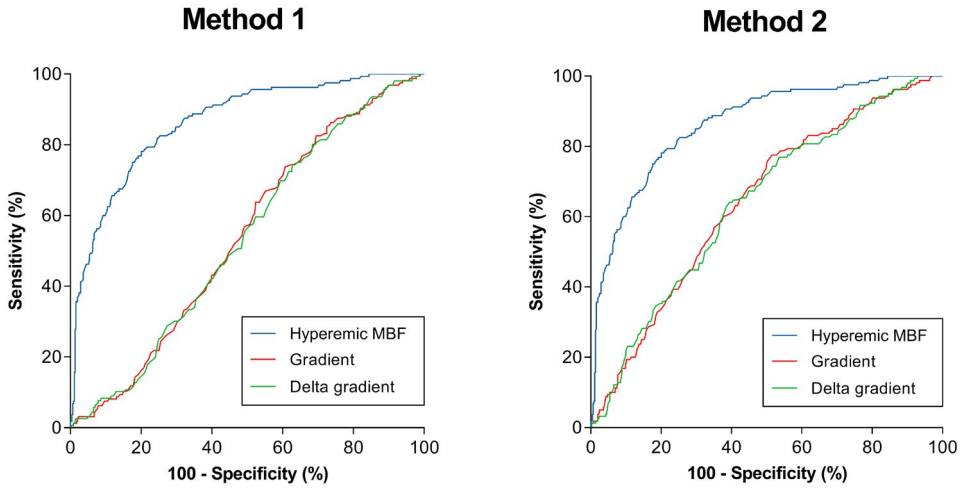

Test	AUC	(95% CI)	p-value *
Hyperemic MBF	0.87	(0.84 - 0.90)	-
Gradient	0.54	(0.50 - 0.58)	<0.001
Δ Gradient	0.54	(0.49 - 0.58)	<0.001

** p-value for comparison with hyperemic MBF*

Test	AUC	(95% CI)	p-value *
Hyperemic MBF	0.87	(0.84 - 0.90)	-
Gradient	0.65	(0.61 - 0.68)	<0.001
Δ Gradient	0.64	(0.60 - 0.68)	<0.001

** p-value for comparison with hyperemic MBF*

Figure 4. Diagnostic value of longitudinal flow parameters for the presence of obstructive CAD as defined by FFR
Receiver-operating characteristic curve analysis with area under the curve (AUC) for the diagnostic value of hyperemic MBF for the presence of hemodynamically significant CAD (FFR≤0.80) versus hyperemic longitudinal MBF gradient (gradient) and Δ longitudinal MBF gradient (Δ Gradient). Results of the two different methods of longitudinal flow gradient calculation are shown separately. For both methods, hyperemic longitudinal MBF gradient and Δ longitudinal MBF gradient had significantly lower diagnostic value than hyperemic MBF.

value of hyperemic longitudinal MBF gradient and Δ longitudinal MBF gradient (by both methods) for the presence of hemodynamically significant CAD were tested against the diagnostic value of hyperemic MBF. For both methods, diagnostic value of hyperemic longitudinal MBF gradient and Δ longitudinal MBF gradient were significantly smaller than that of hyperemic MBF ($p<0.001$ for all). Interestingly, longitudinal flow parameters calculated by method 2 had significantly greater diagnostic value than those calculated by method 1 ($p<0.001$ for all).

Table 3. Diagnostic accuracy of longitudinal flow parameters (by method 1 and 2), hyperemic MBF and the addition of longitudinal flow parameters to hyperemic MBF for the presence of hemodynamically significant CAD on a per-vessel basis

Flow parameters (optimal cut-off)	Sensitivity, %	Specificity, %	PPV, %	NPV, %	Accuracy, %
Regional flow					
hMBF (≤2.28 mL/min/g)	78 (71-84)	79 (75-83)	58 (52-65)	91 (88-94)	79 (75-84)
Longitudinal flow - Method 1					
hMBF gradient (≤0,15)	74 (66-80)	39 (35-44)	31 (26-35)	81 (75-86)	48 (43-54)
Δ Gradient (≤0,21)	80 (73-86)	32 (27-36)	29 (25-34)	82 (75-87)	44 (39-49)
hMBF gradient + hMBF (N/A)	79 (72-85)	79 (74-82)	57 (50-64)	91 (88-94)	79 (74-83)
Longitudinal flow - Method 2					
hMBF gradient (≤0,22)	78 (70-84)	49 (44-53)	35 (30-41)	86 (81-90)	56 (51-61)
Δ Gradient (≤-0,01)	64 (56-72)	61 (56-65)	37 (31-43)	83 (78-87)	61 (56-67)
hMBF gradient + hMBF (N/A)	80 (73-86)	79 (75-83)	58 (51-64)	92 (88-94)	79 (74-83)

hMBF = hyperemic MBF; M1 = method 1; M2 = method 2; N/A = not applicable; NPV = negative predictive value; PPV = positive predictive value

Subgroup analysis on the influence of lesion location on longitudinal flow parameters

To test the influence of coronary lesion location on the relationship between longitudinal flow parameters and FFR, subgroup analyses was performed in patients with proximal (n=176) and non-proximal (n=77) lesions. This analysis was possible in 126 proximal lesions and 69 non-proximal lesions in which FFR was available. Correlation between longitudinal flow parameters defined by method 2 and FFR in these subgroups are illustrated in Fig. 5. No significant correlation between longitudinal flow parameters and FFR was found in vascular territories with proximal lesions. However, significant

and relatively strong correlations were found between hyperemic longitudinal MBF gradient and FFR (r=0.57, p<0.001) and between Δ longitudinal MBF gradient and FFR (r=0.55, p<0.001) in non-proximal lesion.

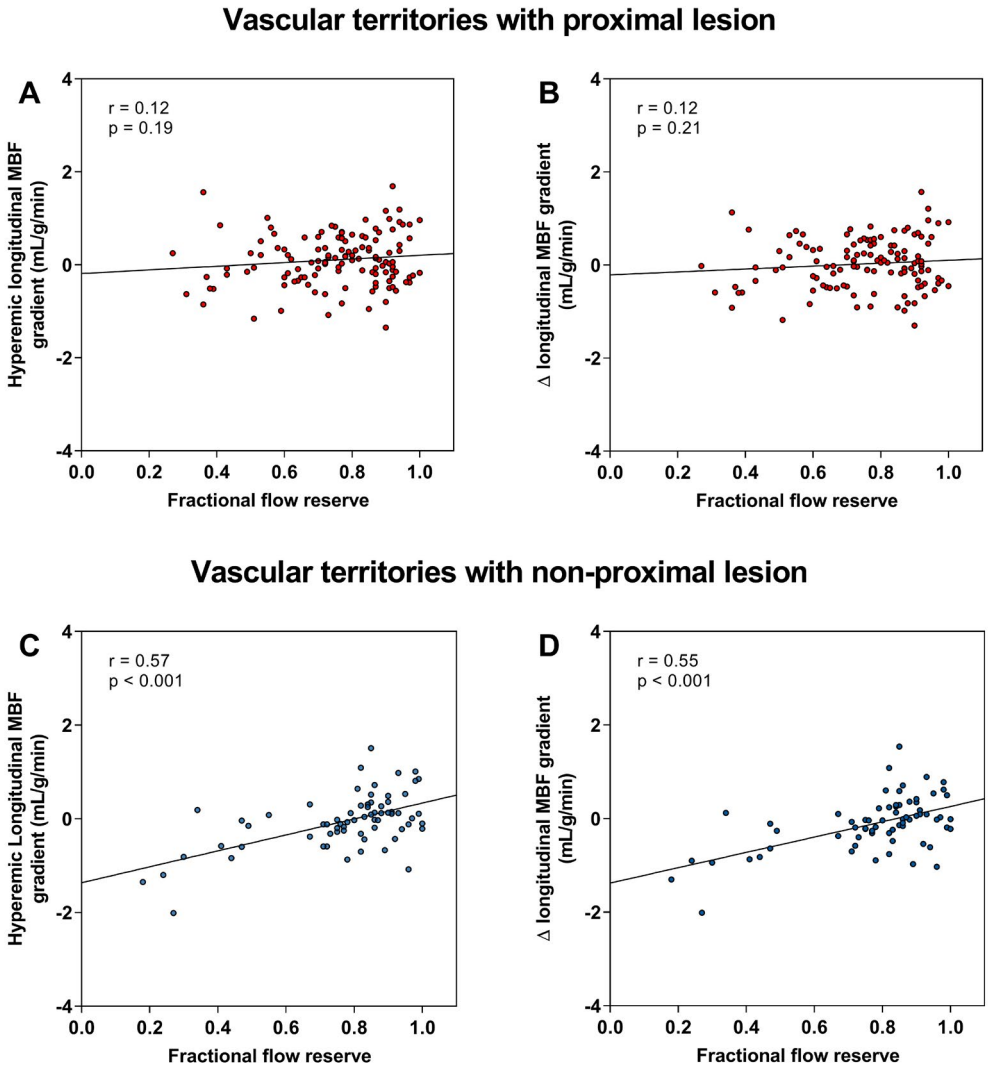

Figure 5. Influence of lesion location on the correlation between longitudinal flow parameters and fractional flow reserve.
The relationship between longitudinal MBF parameters and fractional flow reserve, stratified by lesion location: vascular territories with a proximal lesion (top panel) and with a non-proximal lesion (lower panel). There was no significant correlation between (A) hyperemic longitudinal MBF gradient and FFR and between (B) Δ longitudinal MBF gradient and FFR in vascular territories with proximal lesions. However, in vascular territories with non-proximal lesions a significant correlation was found between both (C) hyperemic longitudinal MBF gradient and FFR and between (D) Δ longitudinal MBF gradient and FFR.

When using method 1 for longitudinal flow gradient calculation, similar results are found. Again, no correlation was found in proximal lesions between hyperemic longitudinal MBF gradient and FFR (r=-0.037, p=0.68) and Δ longitudinal MBF gradient and FFR (r=-0.043, p=0.640). In non-proximal lesions however, both hyperemic longitudinal MBF gradient (r=0.36, p=0.003) and Δ longitudinal MBF gradient (r=0.32, p=0.008) were significantly correlated with FFR.

Discussion

Our study evaluated the diagnostic value of longitudinal flow parameters by two different methods for the presence of hemodynamically significant CAD. Results show that hyperemic longitudinal MBF gradient and Δ longitudinal MBF gradient, by both methods, had lower diagnostic value as compared to hyperemic MBF for the presence of hemodynamically significant CAD. Furthermore, subgroup analysis showed an important influence of lesion location on the relationship between longitudinal flow parameters and FFR.

The concept of the longitudinal MBF gradient is assumed to be induced by an increase in epicardial resistance during hyperemia in vessels with CAD.(5-7,9) In normal coronary circulation, an increase in coronary flow due to metabolic-mediated vasodilation in the microcirculation induces a flow-mediated vasodilatation of the epicardial coronary artery. This mechanism reduces the velocity-induced resistance and thereby ascertains the maintenance of low coronary resistance in the epicardial conductance vessels.(15) The presence of diffuse CAD or advanced focal CAD lesions is suggested to impair this flow-induced and endothelium dependent vasodilation of the epicardial vessel.(5-7,9) This will lead to an increase in epicardial resistance, accompanied by continuous decrease in intracoronary pressure from proximal to distal.(4) The decrease in pressure in the course of the epicardial artery is considered to account for the longitudinal MBF gradient.

Gould et al. were the first to report on the relationship between the longitudinal flow gradient and CAD.(7) In a large cohort of 1001 patients, the authors showed that in patients with diffuse CAD there was a graded decrease in longitudinal base-to-apex perfusion. More recently, Valenta et al. reported that this decrease in longitudinal

hyperemic myocardial perfusion is also present in advanced focal lesions.(5,6) The authors conducted two separate studies with ^{13}N-ammonia PET imaging in which they defined the longitudinal MBF gradient as the difference between the MBFs of the mid and apical LV segments. The basal segments and the apex were excluded from analysis to avoid inaccurate MBF measurements due to count variability and partial volume effects. In these studies, the longitudinal MBF gradient and the Δ longitudinal MBF gradient were highly related to both stenosis severity (5) and to FFR (6). The authors subsequently proposed the hyperemic longitudinal MBF gradient as a novel index to identify the flow-limiting effects of coronary lesions.(9) Our results however are in contrast with these findings. When using the same methodology to calculate the longitudinal MBF gradient (method 1), there was only a very weak correlation between the hyperemic longitudinal MBF gradient and FFR and no correlation between the hyperemic longitudinal MBF gradient and QCA stenosis grade. Furthermore, diagnostic value for the presence of hemodynamically obstructive CAD was lower for the longitudinal MBF gradient as compared to diagnostic value of hyperemic MBF alone. To improve accuracy of the longitudinal flow gradient in our study, the gradient was measured over a longer longitudinal distance: from basal to apical segments (method 2). Using this methodology, correlation with FFR and QCA was slightly better, however still relatively poor. Although diagnostic value of the longitudinal MBF gradient calculated with method 2 for the presence of hemodynamically significant lesions was significantly greater than that of the gradient calculated with method 1, it was still inferior to the diagnostic value of hyperemic MBF.

Several factors may have contributed to these apparently conflicting findings. First, in the current study [^{15}O]H_2O was used as PET-tracer, whereas prior studies have all used ^{13}N-ammonia.(5-7) [^{15}O]H_2O is metabolically inert and freely diffusible across myocyte membrane and therefore uptake in/and clearance from the myocardium are linear to perfusion.(16) It is thus considered the optimal tracer for quantification of MBF. ^{13}N-ammonia PET on the other hand is actively transported across the cell membrane and becomes metabolically trapped while cleared from the arterial blood pool. MBF values detected with ^{13}N-ammonia PET are therefore underestimated, especially in higher flow conditions. To date, only one other study has investigated the relationship between CAD and the longitudinal flow gradient in [^{15}O]H_2O PET imaging. Danad

et al. found no correlation between longitudinal MBF gradient and coronary calcium score.(17) Second, the pathophysiological mechanism underlying the presence of a longitudinal MBF gradient in vessels with high-grade focal lesions is not fully understood. Several studies have suggested that impairment of the flow-induced and endothelium dependent vasodilation of the epicardial vessel causes a graded pressure fall along the artery which in turn causes the gradual base-to-apex MBF gradient.(5-7,9) Whereas this theory has been tested in vessels with diffuse CAD(4,7) it remains unclear why flow-induced vasodilation of the epicardial vessel would be specifically impaired in vessels with FFR-positive lesions, compared to vessels with FFR-negative high-grade lesions. Further studies are warranted to clarify the potential physiological concept underlying the longitudinal MBF gradient in high grade lesions. Third, there are important differences in study population and design between studies. Our study population comprised a large clinical cohort of consecutive patients with suspected CAD referred for angiography in whom all major coronary arteries were routinely interrogated by FFR. Patient populations in the previous studies however were much smaller and inclusion criteria were more selective. In both studies by Valenta et al. only vessels with lesions in the proximal or mid segment of the coronary artery were included.(5,6)

To explore the effect of these differences in study population, the influence of coronary lesion location on the diagnostic value of the longitudinal flow parameters was tested in the current report. In vessels with an angiography-defined proximal lesion, there was no significant correlation between hyperemic longitudinal MBF gradient and FFR. However, in the subgroup of vessels with a non-proximal lesion, a significant and relatively strong correlation between hyperemic longitudinal MBF gradient and FFR was found ($r=0.36$ for method 1 and $r=0.57$ for method 2). The presence of a correlation between hyperemic longitudinal MBF gradient and FFR in vessels with non-proximal lesions but not in vessels with proximal lesions, might be an important factor in the discordance between the current and previous findings. When calculating the longitudinal MBF gradient in vessels with a non-proximal lesion, the apical segment which is distal to the stenosis is normalized to the normal perfused basal/mid segment which is proximal to the stenosis. This will logically lead to a lower longitudinal MBF gradient compared to vessels without a stenosis and compared to

vessels with a proximal stenosis in which no normal perfused basal/mid segment exist for normalization. It is therefore not unanticipated that longitudinal MBF gradients in vessels with non-proximal lesions will be correlated with FFR. This concept of normalizing to a relatively normal perfused area is similar to the concept used for the relative flow reserve. In relative flow reserve measurement, the hyperemic MBF in a stenotic area is normalized to hyperemic MBF in a normal perfused area.(18) This commonly used perfusion index has been shown to be highly correlated with FFR, although it may be not superior to hyperemic MBF in $[^{15}O]H_2O$ PET imaging.(19-21) The relationship of the longitudinal MBF gradient with FFR might be partly caused by the comparison with a normal perfused area, rather than by a distinct physiological phenomenon.

Limitations

This study has several limitations. First, although an effort was made to improve accuracy of the longitudinal MBF gradient by incorporating the basal MBF values in the calculation of method 2, the perfusion of the apex was not used for calculation. In theory, this may have led to underestimation of the longitudinal MBF gradient. Furthermore, the more elaborate approach by Gould et al in which the relative tracer activity was measured in 34 tomographic slices generated by a 3D restructuring algorithm would also potentially have yielded different results.(7) Third, count variability in the basal segments may have influenced the calculation of the longitudinal MBF gradient by method 2. These may have hampered the diagnostic value for the presence of hemodynamically obstructive CAD. Fourth, since standard segmentation according to the American Heart Association was used to assign coronary arteries to PET perfusion territories, some mismatch may have occurred. Prior studies however have reported that mismatch is uncommon and that standard segmentation yields similar results compared with the individualized approach in which angiography is used to assign arteries to perfusion territories.(22) Nonetheless, since calculation of the longitudinal MBF gradient is based on MBF values in a smaller number of segments, mismatch may have affected our results. Fifth, the subgroup analysis on the influence of lesion location was hampered by the relatively small sample size of 126 proximal lesions and 69 non-proximal lesions in which FFR measurements were available. Furthermore, although care was taken to establish lesion location based on

invasive angiography, lesion location was simplified for analysis into proximal or non-proximal. The influence of exact lesion location on longitudinal flow measurements was not determined in this study. Differences in lesion location, patient population, and tracer kinetics may hamper comparison with prior studies and therefore care must be taken when interpreting our results.

Conclusion

In this study, the current methodology of PET-measured longitudinal flow parameters had lower diagnostic value as compared to hyperemic MBF for the presence of hemodynamically significant CAD. Since a possible influence of lesion location on the correlation of PET measured longitudinal flow parameters with FFR was identified, presence of a longitudinal flow gradient might be partly caused by normalization to a relatively normal perfused area.

References

1. Montalescot G, Sechtem U, Achenbach S et al. 2013 ESC guidelines on the management of stable coronary artery disease: the Task Force on the management of stable coronary artery disease of the European Society of Cardiology. Eur Heart J 2013;34:2949-3003.
2. Danad I, Raijmakers PG, Driessen RS et al. Comparison of Coronary CT Angiography, SPECT, PET, and Hybrid Imaging for Diagnosis of Ischemic Heart Disease Determined by Fractional Flow Reserve. JAMA Cardiol 2017;2:1100-1107.
3. van de Hoef TP, Siebes M, Spaan JA, Piek JJ. Fundamentals in clinical coronary physiology: why coronary flow is more important than coronary pressure. Eur Heart J 2015;36:3312-9a.
4. De Bruyne B, Hersbach F, Pijls NH et al. Abnormal epicardial coronary resistance in patients with diffuse atherosclerosis but "Normal" coronary angiography. Circulation 2001;104:2401-6.
5. Valenta I, Quercioli A, Schindler TH. Diagnostic value of PET-measured longitudinal flow gradient for the identification of coronary artery disease. JACC Cardiovasc Imaging 2014;7:387-96.
6. Valenta I, Antoniou A, Marashdeh W et al. PET-measured longitudinal flow gradient correlates with invasive fractional flow reserve in CAD patients. Eur Heart J Cardiovasc Imaging 2017;18:538-548.
7. Gould KL, Nakagawa Y, Nakagawa K et al. Frequency and clinical implications of fluid

dynamically significant diffuse coronary artery disease manifest as graded, longitudinal, base-to-apex myocardial perfusion abnormalities by noninvasive positron emission tomography. Circulation 2000;101:1931-9.

8. Hernandez-Pampaloni M, Keng FY, Kudo T, Sayre JS, Schelbert HR. Abnormal longitudinal, base-to-apex myocardial perfusion gradient by quantitative blood flow measurements in patients with coronary risk factors. Circulation 2001;104:527-32.
9. Leucker TM, Valenta I, Schindler TH. Positron Emission Tomography-Determined Hyperemic Flow, Myocardial Flow Reserve, and Flow Gradient-Quo Vadis? Front Cardiovasc Med 2017;4:46.
10. Tobis J, Azarbal B, Slavin L. Assessment of intermediate severity coronary lesions in the catheterization laboratory. J Am Coll Cardiol 2007;49:839-48.
11. Fischer JJ, Samady H, McPherson JA et al. Comparison between visual assessment and quantitative angiography versus fractional flow reserve for native coronary narrowings of moderate severity. Am J Cardiol 2002;90:210-5.
12. Scanlon PJ, Faxon DP, Audet AM et al. ACC/AHA guidelines for coronary angiography. A report of the American College of Cardiology/American Heart Association Task Force on practice guidelines (Committee on Coronary Angiography). Developed in collaboration with the Society for Cardiac Angiography and Interventions. J Am Coll Cardiol 1999;33:1756-1824.
13. Danad I, Raijmakers PG, Harms HJ et al. Impact of anatomical and functional severity of coronary atherosclerotic plaques on the transmural perfusion gradient: a [15O]H2O PET study. Eur Heart J 2014;35:2094-105.
14. Harms HJ, Knaapen P, de Haan S, Halbmeijer R, Lammertsma AA, Lubberink M. Automatic generation of absolute myocardial blood flow images using [15O]H2O and a clinical PET/CT scanner. Eur J Nucl Med Mol Imaging 2011;38:930-9.
15. de Waard GA, Cook CM, van Royen N, Davies JE. Coronary autoregulation and assessment of stenosis severity without pharmacological vasodilation. Eur Heart J 2017.
16. Driessen RS, Raijmakers PG, Stuijfzand WJ, Knaapen P. Myocardial perfusion imaging with PET. Int J Cardiovasc Imaging 2017;33:1021-1031.
17. Danad I, Raijmakers PG, Appelman YE et al. Quantitative relationship between coronary artery calcium score and hyperemic myocardial blood flow as assessed by hybrid 15O-water PET/CT imaging in patients evaluated for coronary artery disease. J Nucl Cardiol 2012;19:256-64.
18. De Bruyne B, Baudhuin T, Melin JA et al. Coronary flow reserve calculated from pressure measurements in humans. Validation with positron emission tomography. Circulation 1994;89:1013-22.

19. Stuijfzand WJ, Uusitalo V, Kero T et al. Relative flow reserve derived from quantitative perfusion imaging may not outperform stress myocardial blood flow for identification of hemodynamically significant coronary artery disease. Circ Cardiovasc Imaging 2015;8.
20. Lee JM, Kim CH, Koo BK et al. Integrated Myocardial Perfusion Imaging Diagnostics Improve Detection of Functionally Significant Coronary Artery Stenosis by 13N-ammonia Positron Emission Tomography. Circ Cardiovasc Imaging 2016;9.
21. Marques KM, Knaapen P, Boellaard R, Lammertsma AA, Westerhof N, Visser FC. Microvascular function in viable myocardium after chronic infarction does not influence fractional flow reserve measurements. J Nucl Med 2007;48:1987-92.
22. Thomassen A, Petersen H, Johansen A et al. Quantitative myocardial perfusion by O-15-water PET: individualized vs. standardized vascular territories. Eur Heart J Cardiovasc Imaging 2015;16:970-6.

Chapter 11

Prognostic value of [^{15}O]H_2O positron emission tomography derived global and regional myocardial perfusion

Michiel J. Bom, Pepijn A. van Diemen, Roel S. Driessen, Henk Everaars, Stefan P. Schumacher, Jan-Thijs Wijmenga, Pieter G. Raijmakers, Peter M. van de Ven, Adriaan A. Lammertsma, Albert C. van Rossum, Juhani Knuuti, Ibrahim Danad, and Paul Knaapen

Eur Heart J Cardiovasc Imaging. 2020;21(7);777-786

Abstract

Aims: To evaluate the prognostic value of global and regional quantitative [^{15}O]H_2O positron emission tomography (PET) perfusion.

Methods and results: In this retrospective study, 648 patients with suspected or known coronary artery disease (CAD) who underwent [^{15}O]H_2O PET were followed for the occurrence of death and myocardial infarction (MI). Global and regional hyperemic myocardial blood flow (hMBF) and coronary flow reserve (CFR) were obtained from [^{15}O]H_2O PET. During median follow-up of 6.9 [5.0–7.9] years, 64 (9.9%) patients experienced the composite of death (36, 5.6%) and MI (28, 4.3%). Impaired global hMBF (<2.65 ml/min/g) and CFR (<2.88) were both significant prognostic factors for death/MI after adjusting for clinical characteristics (both p<0.001). However, after adjusting for clinical parameters and the combined use of hMBF and CFR, only hMBF remained an independent prognostic factor (p=0.04). For regional perfusion, both impaired hMBF (<2.10 ml/min/g) and CFR (<2.07) demonstrated prognostic value for events (both p<0.001). Similarly, after adjusting for clinical characteristics and combined use of hMBF and CFR, only hMBF had independent prognostic value (p=0.04). The combination of global and regional perfusion did not improve prognostic performance over either global (p=0.55) or regional perfusion (p=0.37) alone.

Conclusions: Global and regional hMBF and CFR were all prognostic factors for death and MI. However, for both global and regional perfusion, hMBF remained the only independent prognostic factor after adjusting for the combined use of hMBF and CFR. Additionally, integrating global and regional perfusion did not increase prognostic performance compared to either regional or global perfusion alone.

Introduction

Myocardial perfusion imaging yields important prognostic value for the prediction of cardiovascular events in patients with suspected coronary artery disease (CAD).(1) Unlike single photon emission tomography which visualizes relative differences in tracer uptake within the myocardium, positron emission tomography (PET) enables the quantification of absolute myocardial blood flow (MBF) in mL/min/g.(2) Several studies have investigated the prognostic value of hyperemic MBF (hMBF) and coronary flow reserve (CFR), when calculated for the left ventricle as a whole. These studies however reported conflicting findings.(3-9) Although, regional instead of global MBF values are used in clinical practice to diagnose ischemia and to guide decision making and revascularization, data on the prognostic value of these regional quantitative PET perfusion parameters are scarce. Furthermore, recent reports have suggested incremental value of the coronary flow capacity, an approach which incorporates both CFR and hMBF, for the prediction of cardiovascular events.(10-12) Additionally, although ample data exists on the prognostic thresholds for hMBF and CFR in $^{13}NH_3$ and ^{82}Rb PET imaging, the optimal prognostic thresholds for $[^{15}O]H_2O$ PET have yet to be established. The aim of the current study was therefore to determine optimal prognostic thresholds for global and regional hMBF and CFR obtained using $[^{15}O]H_2O$ PET and to evaluate the independent prognostic value of these global and regional PET perfusion parameters.

Methods

Study population

A total of 736 consecutive patients who underwent $[^{15}O]H_2O$ PET imaging because of suspected or known CAD at the Amsterdam University Medical Centers, location VU University Medical Center between 2008 and 2014, were evaluated for inclusion. Post-imaging treatment strategy was left to the discretion of the referring physician. Of the 736 patients initially evaluated, 3 patients were excluded due to stress-only PET imaging and 11 patients were excluded due to technical issues which precluded analysis of regional perfusion. Of the remaining 722 patients, 74 (10%) were lost to follow up, resulting in a final study population of 648 patients. The need for written informed consent was waived by the institutional review board (Medical Ethics Committee of

the VU University Medical Center) due to the nature of the study.

$[^{15}O]H_2O$ PET acquisition

Patients were scanned using a hybrid PET-CT device (Philips Gemini TF 64, Philips Healthcare, Best, The Netherlands). The scanning protocol has been described previously.(13) In summary, a dynamic PET perfusion scan was performed during resting conditions using 370 MBq of $[^{15}O]H_2O$. A 6 min emission scan was started simultaneously with the administration of the tracer. This dynamic scan sequence was followed immediately by a low dose CT scan for attenuation correction. After a 10 minute interval to allow for decay of radioactivity, an identical PET sequence was performed during hyperemic conditions induced by intravenous adenosine infusion (140 μg/kg/min), initiated 2 minute before the hyperemic scan to ensure maximal vasodilation. Images were reconstructed using the 3D row action maximum likelihood algorithm and applying all appropriate corrections. Parametric MBF images were generated and quantitatively analyzed using in-house developed software (Cardiac VUer). Myocardial blood flow was expressed in mL/min/g. Global resting and hMBF were calculated for the left ventricle as a whole. CFR was defined as the ratio between hMBF and resting MBF. Additionally, resting MBF and hMBF were calculated for each of the 17 left ventricle segments according to the standard American Heart Association model with standardized allocation of segments to the three vascular territories.(14) Regional hMBF and CFR values were calculated per vascular territory by averaging the perfusion values of the two adjacent segments with the lowest values, to avoid impact of overlapping adjacent vascular regions.(15) To account for the differences in hemodynamic conditions, the resting MBF was corrected for the rate pressure product, using the following equation: corrected resting MBF = (resting MBF / rate pressure product) x 10^4. The corrected CFR was subsequently calculated as the ratio of the hMBF divided by the corrected resting MBF.

Follow-up

Patients were followed by observers blinded to PET imaging results using national registry databases, electronic medical records, and standardized telephonic follow-up. The primary endpoint of the study was a composite of all-cause death and non-fatal myocardial infarction (MI). Identified events were scored in accordance with current

guidelines.(16) Peri-procedural MIs and deaths as a result of revascularizations guided by the initial diagnostic imaging work-up were not included as endpoints. Adjudication of events as guided by diagnostic work-up was performed by an independent researcher. The first and most serious event was considered as the event of the patient, with death being considered more serious than non-fatal MI.

Statistical analysis

Statistical analyses were performed using the SPSS software version 22.0.0 (IBM SPSS Statistics, Armonk, New York), except for the construction of time-dependent receiver operating characteristic (ROC) curves which was performed using R (R Foundation for Statistical Computing, Vienna, Austria). Continuous variables were tested for normal distribution. Normal distributed continuous variables are presented as mean ± SD. Non-normal distributed variables are presented as median with interquartile ranges. Categorical variables are presented as frequencies with percentages. Variables were compared with chi-square test for categorical variables and by using Mann-Whitney U or independent samples t-test for continuous variables where appropriate. The SurvivalROC package (version 3.4.4) in R was used to construct time-dependent ROC curves using the nearest neighbor estimation method.(17) Separate ROC curves were made for global and regional hMBF, CFR, and corrected CFR for the prognostic value of the composite of death/MI within the first 5 years of follow-up. Based on these ROC curves, thresholds were selected for which specificity was maximized and sensitivity was at least 75%. Kaplan-Meier curves were plotted to analyze event-free survival and log-rank was used to assess the prognostic value of the separate PET perfusion parameters. Annualized response rates were calculated as marginal estimated means from a generalized linear model with a Poisson-distributed outcome and log-link and with MBF/CFR-group as an independent variable. The logarithm of follow-up time was used as the offset variable. To calculate adjusted annualized event rates confounders were added as covariates to the model. Adjusted annualized response rates were calculated as marginal estimated means from the extended model while fixing all confounders at their mean value in the sample. Adjustment was performed for the following confounders: age, gender, BMI, diabetes, hypertension, smoking status, family history, and hyperlipidemia. Univariate and multivariate Cox proportional hazard regression were used to analyze the independent prognostic value

for the occurrence of the composite of death/MI of PET perfusion parameters. An additional Cox-regression analysis was performed to test the incremental prognostic value of PET perfusion over clinical baseline characteristics alone. Incremental value was tested separately for each sequentially added imaging result using the likelihood ratio test. Additionally, internal validation of the prognostic quality of the dichotomized PET parameters was performed using 100 different random splits of the data in equally sized training and validation set (i.e. the dataset was randomly split in half - 50% derivation cohort, 50% validation cohort - a hundred times). The cut-off values were determined in the training set and hazard ratios were subsequently estimated in the validation set. A p-value <0.05 was considered statistically significant.

Results

Study population

Baseline characteristics of all 648 patients are shown in table 1. Revascularization based on the initial diagnostic work-up occurred in 117 (18.1%) patients, i.e. 73 (11.3%) PCIs and 44 (6.8%) CABGs. During a median follow-up time of 6.9 [5.0 – 7.9] years, 64 (9.9%) patients experienced the composite endpoint of death and MI, comprised of all-cause mortality in 36 (5.6%) patients and MI in 28 (4.3%). Three additional MIs occurred in patients with subsequent death. The annualized event rate for the composite of death/MI was 1.44%. Annualized event rates for the individual endpoints of death and MI were 0.81% and 0.69% respectively.

Global and regional [^{15}O]H_2O PET perfusion imaging and optimal threshold for prognosis

Results of global and regional PET perfusion stratified by the occurrence of the composite of death/MI are presented in table 1. Mean global hMBF (p=0.002) and CFR (p<0.001) and mean regional hMBF (p<0.001) and CFR (p<0.001) were all significantly lower in patients with than patients without death/MI during follow-up. Calculated optimal prognostic thresholds for events were <2.65 mL/min/g for global hMBF and <2.88 for CFR. Optimal thresholds for regional hMBF and CFR were numerically lower, <2.10 mL/min/g and 2.07 respectively. Based on these thresholds, global hMBF was impaired in 292 (45%) patients, whereas global CFR was impaired in

Table 1. Baseline characteristics

Demographics	Overall (n = 648)	No Death/MI (n = 584)	Death/MI (n = 64)	p-value
Age, years	59 ± 10	58 ± 9	64 ± 10	<0.001
Male	353 (55%)	313 (54%)	40 (63%)	0.17
Body mass index (n = 639)	27 ± 4	27 ± 4	27 ± 3	0.85
Cardiovascular risk factors (n = 626)				
Diabetes Mellitus type II	124 (20%)	102 (18%)	22 (37%)	0.001
Hypertension	302 (48%)	265 (47%)	37 (62%)	0.03
Hyperlipidaemia	242 (39%)	212 (38%)	30 (50%)	0.06
Current tobacco use	209 (34%)	186 (33%)	23 (39%)	0.35
Family history of CAD	328 (53%)	303 (54%)	25 (42%)	0.09
Type of chest-pain (n = 632)				
Between groups				0.31
Typical angina	195 (31%)	172 (30%)	23 (38%)	-
Atypical angina	220 (35%)	198 (35%)	22 (36%)	-
Non-specific chest discomfort	217 (34%)	201 (35%)	16 (26%)	-
Medication use (n = 633)				
Statin	427 (68%)	379 (66%)	48 (77%)	0.08
Acetylsalicylic acid	474 (75%)	420 (73%)	54 (87%)	0.02
Betablocker	391 (62%)	345 (60%)	46 (74%)	0.03
ACE-inhibtor	133 (21%)	115 (20%)	18 (29%)	0.10
Calcium-channel blocker	176 (28%)	152 (27%)	24 (39%)	0.04
PET perfusion imaging				
Global hMBF	2.90 ± 1.19	2.95 ± 1.15	2.45 ± 1.49	0.002
Global CFR	2.99 ± 1.18	3.05 ± 1.13	2.43 ± 1.50	<0.001
Regional hMBF	2.21 ± 0.98	2.26 ± 0.97	1.77 ± 0.97	<0.001
Regional CFR	2.19 ± 0.93	2.25 ± 0.93	1.68 ± 0.82	<0.001

ACE-inhibtor = angiotensin-converting-enzyme inhibitor; CAD = coronary artery disease; CFR = coronary flow reserve; hMBF = hyperemic myocardial blood flow; MI = myocardial infarction

344 (53%) patients. For regional perfusion, hMBF was impaired in 302 (47%) patients and CFR was impaired in 308 (48%) patients. The relationship between hMBF and CFR for both global and regional perfusion is depicted in Fig. 1. Discordance between hMBF and CFR occurred in 164 (25%) patients in global perfusion and in 134 (21%) patients in regional perfusion.

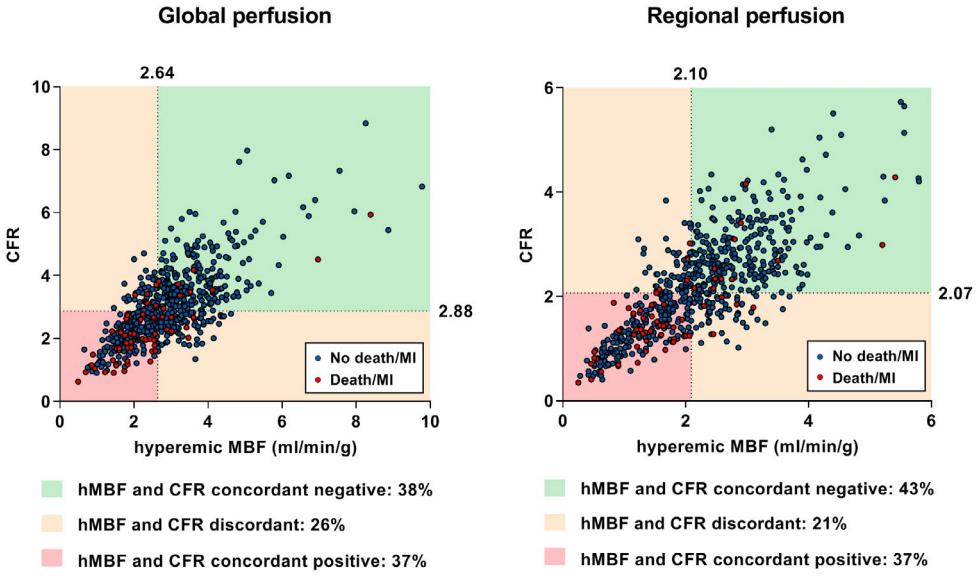

Figure 1. Relationship between hyperemic myocardial blood flow (hMBF) and coronary flow reserve (CFR) in patients with and without death/MI during follow-up
Scatterplot displaying concordant and discordant impairment of hMBF and CFR in patients with (red dots) and without death/MI (blue dots) during follow-up, for both global (left) and regional PET perfusion (right). The calculated optimal thresholds for hMBF and CFR are respectively 2.64 ml/min/g and 2.88 for global perfusion and 2.10 ml/min/g and 2.07 for regional perfusion. MI = myocardial infarction; PET = positron emission tomography.

Kaplan-Meier estimates of event-free survival were computed stratified by impairment of global and regional PET perfusion (Fig. 2). For both global and regional perfusion, worse outcome was noted in patients with impaired hMBF vs patients with preserved hMBF ($p<0.001$) and patients with impaired CFR vs patients with preserved CFR ($p<0.001$).

Results of the internal validation analyses using 100 random splits of the dataset into equally sized training and validation sets are provided in Supplementary Table 1. Median optimal cut-off values in the training sets were similar to the thresholds determined in the entire cohort, i.e. 2.74 mLmin/g and 2.81 for global hMBF and CFR, and 2.14 mL/min/g and 2.11 for regional hMBF and CFR respectively. Using these cut-off values in the validation sets, global and regional hMBF and CFR all had prognostic value for the occurrence of death/MI (median $p<0.05$ for all).

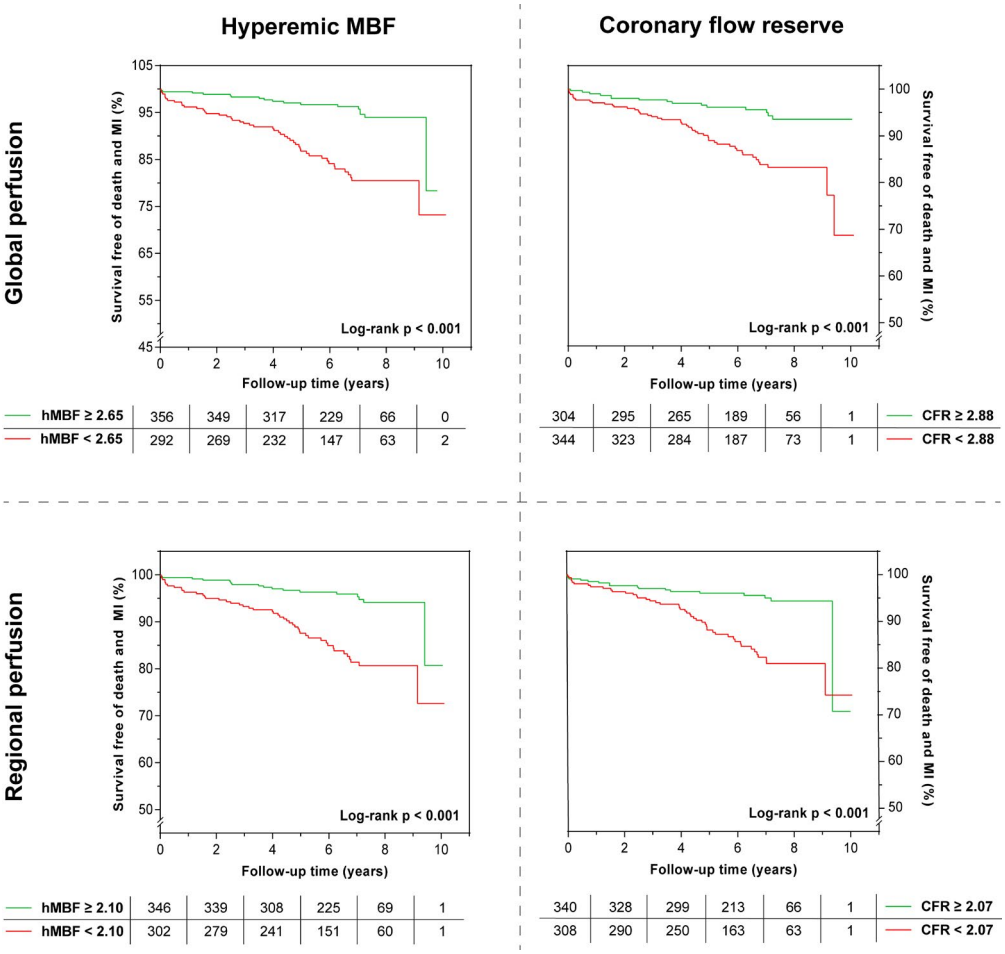

Figure 2. Kaplan-Meier curves of event-free survival stratified by global and regional PET perfusion
Kaplan-Meier curves of event-free survival stratified by global (top) and regional (bottom) PET perfusion, with hMBF on the left and CFR on the right. Abbreviations as in figure 1.

Prognostic value of combined global and regional [^{15}O]H_2O PET perfusion

Kaplan-Meier estimates of survival free of death/MI for the combined use of hMBF and CFR for global and regional perfusion are depicted in Fig. 3. For both global and regional perfusion the combination of hMBF and CFR led to significant identification of patients that experienced death/MI (log-rank p-value <0.001). Annualized event-rates for the combined use of hMBF and CFR, both unadjusted and adjusted for clinical characteristics, are depicted in Fig. 4. For both global and regional perfusion,

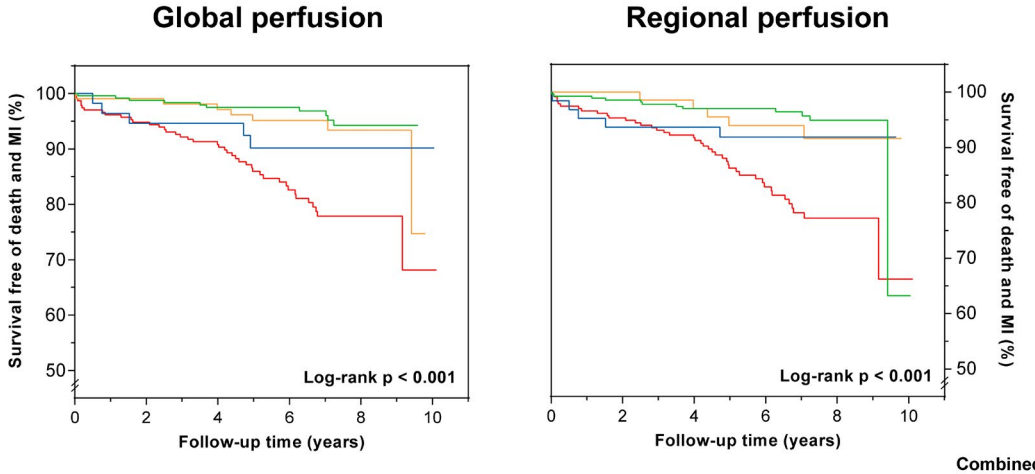

Combined hMBF and CFR							Combined hMBF and CFR
hMBF ≥ 2.65 & CFR ≥ 2.88	248	242	218	154	41	0	276	269	244	174	48	1	hMBF ≥ 2.10 & CFR ≥ 2.07
hMBF < 2.65 & CFR ≥ 2.88	56	53	47	35	15	1	64	59	55	39	18	0	hMBF < 2.10 & CFR ≥ 2.07
hMBF ≥ 2.65 & CFR < 2.88	108	107	99	75	25	0	70	70	64	51	21	0	hMBF ≥ 2.10 & CFR < 2.07
hMBF < 2.65 & CFR < 2.88	236	216	185	112	48	1	238	220	168	112	42	1	hMBF < 2.10 & CFR < 2.07

Figure 3. Survival free of death and MI according to combined use of CFR and hMBF
Kaplan-Meier curves of event-free survival stratified by combined use of hMBF and CFR for global (left) and regional PET perfusion (right) stratified by the concordance of impairment in hMBF and CFR. Abbreviations as in figure 1.

adjusted annualized event rates increased numerically based on the concordance of impairment in hMBF and CFR. Closer inspection showed that patients with concordantly impaired global perfusion had significantly higher adjusted annualized event rates than patients with concordantly preserved perfusion (p=0.002) or patients with discordant perfusion with impaired CFR (p=0.01). However, no significant difference was observed between patients with concordantly impaired perfusion and patients with discordant perfusion and impaired hMBF (p=0.25). Similar results

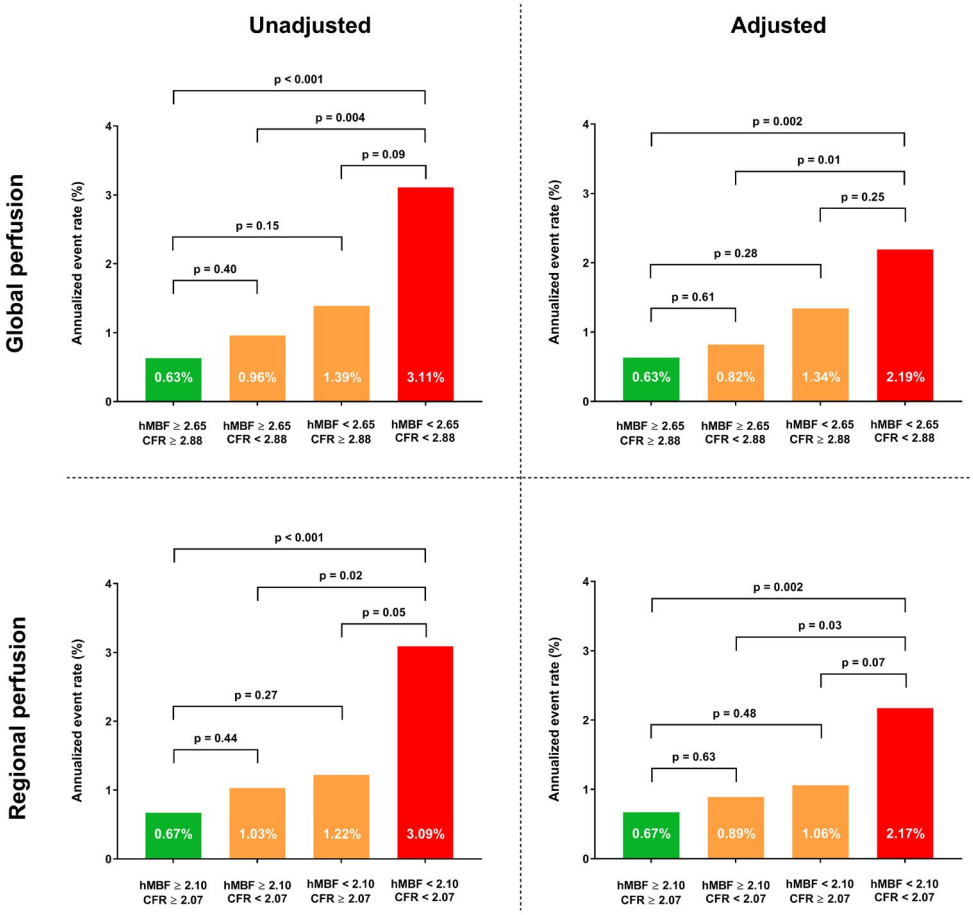

Figure 4. Annualized event rates according to global and regional PET perfusion
Unadjusted (left) and adjusted (right) annualized event rates for concordantly preserved perfusion (both hMBF and CFR preserved, green), discordantly impaired hMBF and CFR (orange) and concordantly impaired perfusion (both hMBF and CFR impaired, red), for global (top) and regional perfusion (bottom). Abbreviations as in figure 1.

were seen for regional perfusion, although a trend for higher adjusted annualized event rates was seen in patients with concordantly impaired perfusion than patients with discordant perfusion with impaired hMBF, this was not statistically significant (p=0.07). Again, patients with concordantly impaired regional perfusion had higher annualized event rates than patients with concordantly preserved perfusion (p=0.002) and patients with discordant perfusion with impaired CFR (p=0.03). For both global and regional perfusion, death and MI were thus driven by impairment of hMBF regardless of impairment in CFR.

The results of the analysis on univariable prognostic factors for the occurrence of death/MI are reported in Supplementary Table 2. Results of the multivariable Cox regression analysis on the independent prognostic value of global hMBF and CFR are shown in table 2. Both hMBF and CFR had significant prognostic value for death/MI after adjusting for clinical parameters (p=0.001 and p=0.016 respectively). Although a trend was observed, CFR did no longer have significant prognostic value for the occurrence of events after adjusting for the combined use of global hMBF and CFR (p=0.06). hMBF however was an independent prognostic factor for death and MI after adjusting for the combined use of hMBF and CFR (HR 2.87, p=0.006) and did even haveindependent prognostic value after adjusting for both clinical parameters and the combined use of hMBF and CFR (HR 2.13, p=0.04).

The results of the multivariable Cox regression for regional perfusion are depicted in table 3. Regional hMBF and CFR were significant prognostic factors for events after

Table 2. Prognostic value of global myocardial blood flow for the occurrence of death and MI

	Adjusted for clinical parameters *		Adjusted for combined use of hMBF and CFR †		Adjusted for clinical parameters + combined use of hMBF and CFR	
	HR (95% CI)	p-value	HR (95% CI)	p-value	HR (95% CI)	p-value
hMBF <2.65	3.03 (1.61 - 5.70)	0.001	2.87 (1.56 - 5.28)	0.001	2.55 (1.27 - 5.13)	0.008
CFR <2.88	2.12 (1.15 - 3.90)	0.016	1.85 (0.98 - 3.49)	0.06	1.44 (0.74 - 2.82)	0.29

* Clinical parameters included in the analysis were age, gender, BMI, diabetes, hypertension, smoking status, family history, and hyperlipidemia; † Hazard ratios represent the prognostic value of the parameters in a combined model where both hMBF and CFR were included. Abbreviations as in table 1.

adjusting for clinical parameters (p=0.001 and p=0.005 respectively) and after adjusting for the combined use of hMBF and CFR (HR 2.47, p=0.006 and HR: 1.99, p=0.04 respectively). However, CFR had no independent prognostic value after adjusting for both clinical parameters and the combined use of hMBF and CFR (p=0.16). Again, only hyperemic MBF had independent prognostic value for death and MI after adjusting for both clinical parameters and combined use of hMBF and CFR (HR 2.13, p=0.04).

Table 3. Prognostic value of regional myocardial blood flow for the occurrence of death and MI

	Adjusted for clinical parameters *		Adjusted for combined use of hMBF and CFR †		Adjusted for clinical parameters + combined use of hMBF and CFR	
	HR (95% CI)	p-value	HR (95% CI)	p-value	HR (95% CI)	p-value
hMBF <2.10	2.80 (1.49-5.25)	0.001	2.47 (1.30-4.70)	0.006	2.13 (1.03-4.37)	0.04
CFR <2.07	2.33 (1.30-4.18)	0.005	1.99 (1.05-3.78)	0.04	1.63 (0.83-3.18)	0.16

* Clinical parameters included in the analysis were age, gender, BMI, diabetes, hypertension, smoking status, and family history, hyperlipidemia; † Hazard ratios represent the prognostic value of the parameters in a combined model where both hMBF and CFR were included. Abbreviations as in table 1.

To account for the changes in resting flow caused by differences in hemodynamic conditions, additional analyses were performed to investigate the independent prognostic value of the corrected CFR in global (Supplementary Table 3) and regional perfusion (Supplementary Table 4). These analyses yielded comparable findings as the analysis using the uncorrected CFR. After adjusting for the combined use of hMBF and corrected CFR, corrected CFR did not have independent prognostic value (p=0.36 and p=0.11, for global and regional perfusion respectively). Furthermore, additional analyses were performed to correct for the occurrence of revascularization based on the initial diagnostic work-up (Supplementary Table 5 and S6). Although results were comparable to the results of the analysis without adjusting for imaging-based revascularization, only a trend was observed for the independent prognostic value of regional hMBF (p=0.06).

Prognostic value of the integration of global and regional PET perfusion

Strong correlations were found between global and regional hMBF (r=0.92, p<0.001) and between global and regional CFR (r=0.91, p<0.001). Mean regional hMBF and

CFR were significantly lower than mean global hMBF and CFR (table 1, p<0.001 for both). The analysis on the incremental prognostic value of the addition of global and regional PET perfusion to clinical variables is presented in Fig. 5. In a stepwise multivariable model, addition of global perfusion (hMBF and CFR) to clinical variables led to improved prognostic performance (p=0.001). Likewise, addition of regional perfusion (hMBF and CFR) to clinical characteristics also significantly improved prognostic performance (p=0.001). The addition of global perfusion to clinical characteristics resulted in similar increase in -2 log likelihood as the addition of regional perfusion, suggesting similar prognostic performance of the models. The combination of regional and global perfusion did not result in improved prognostic performance when compared to either global perfusion (p=0.55) or regional perfusion (p=0.37) alone.

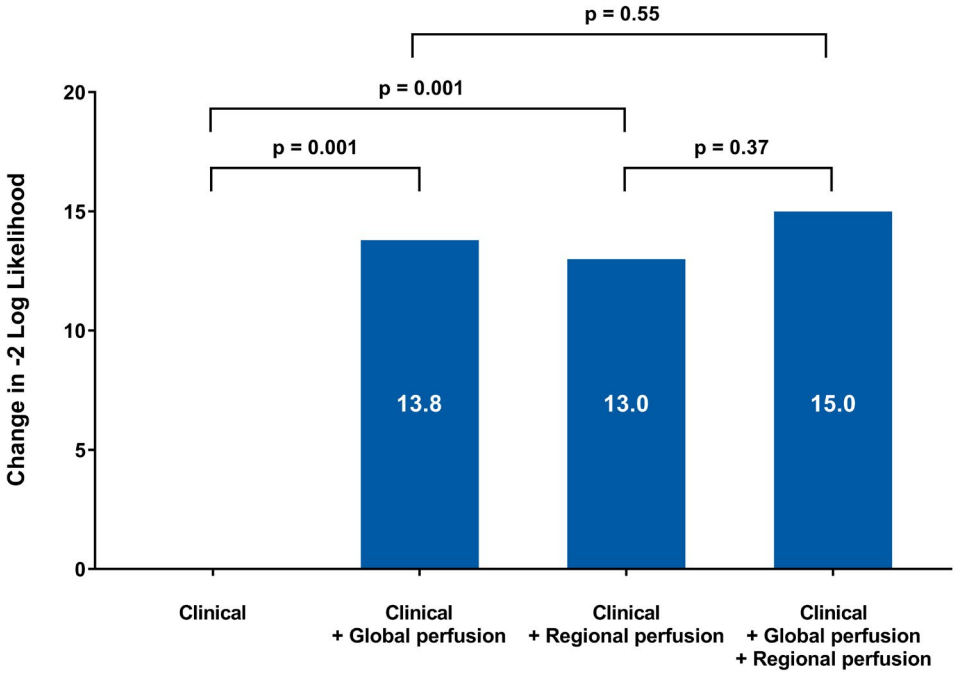

Figure 5. Incremental prognostic value of the combined use of global and regional PET perfusion
Incremental prognostic value for the occurrence of death/MI beyond clinical characterstics when adding global perfusion, regional perfusion and the combination of global and regional perfusion. Abbreviations as in figure 1.

Discussion

This study investigated the prognostic value of [^{15}O]H_2O PET-derived global and regional quantitative myocardial perfusion for the occurrence of death and MI. Both global hMBF and CFR demonstrated prognostic value for events, independent of clinical characteristics. Although a trend was observed for improved prognostic performance with the combined use of global hMBF and CFR, only hMBF remained an independent prognostic factor for the occurrence of events after adjusting for clinical variables and the combined use of hMBF and CFR. Similarly, impaired regional hMBF and CFR were associated with adverse prognosis, independent of clinical variables. Despite a trend for improved prognostic performance with the combined use of hMBF and CFR, only hMBF was an independent prognostic factor for the occurrence of events. Lastly, combining global and regional perfusion did not have incremental prognostic value over global or regional perfusion alone.

Prognostic value of global hyperemic MBF and CFR

The qualitative interpretation of PET perfusion imaging holds important prognostic information.(18) Additionally, quantification of absolute myocardial perfusion in PET imaging has been shown in numerous studies to further increase prognostic performance.(4-9) Most of these studies have focused on global perfusion parameters for the left ventricle as a whole and more specifically on global CFR and all have consistently shown independent prognostic value of global CFR to clinical characteristics.(4-7,9) Prognostic studies on the combined use of global hMBF and CFR however are scarce and have shown conflicting results.(3,6,8) Fukushima et al. investigated 275 patients with ^{82}Rb PET and reported that only CFR remained independently predictive for events after adjusting for age and the combined use of hMBF and CFR.(8) More recently, Gupta and colleagues reported similar findings in 4029 patients with ^{82}Rb or $^{13}NH_3$ PET imaging. CFR was again shown to be a stronger predictor than hMBF and the sole independent predictor for cardiovascular mortality. (3) Contrary, Farhad et al. have reported in a smaller ^{82}Rb PET study of 351 patients that hMBF was independently predictive for events, whereas CFR was not.(6) The present study is the first to determine optimal prognostic thresholds for [^{15}O]H_2O PET perfusion and to report on the prognostic value of global hMBF and CFR in

[^{15}O]H_2O PET. The optimal thresholds for global hMBF and CFR were 2.65 mL/min/g and 2.88 respectively. Using these thresholds, both hMBF and CFR were significant prognostic factors for death/MI and a trend was observed for improved prognostic performance with the use of combined hMBF and CFR. However, similar to the study by Farhad et al., hMBF was the only independent prognostic factor for the occurrence of events after adjusting for clinical characteristics and the combined use of hMBF and CFR. However, there are several important methodological differences between the studies. First, the identified thresholds for global hMBF and CFR in the current study are notably higher than thresholds used in previously published $^{13}NH_3$ and ^{82}Rb studies, which may be explained by fundamental differences in tracer kinetics.(6,8,19) PET imaging with [^{15}O]H_2O is characterized by a linear relationship between accumulation / clearance of the tracer and myocardial perfusion, rendering it the ideal for quantification of absolute MBF. Contrary, $^{13}NH_3$ and ^{82}Rb suffer from non-linearity in the relationship between MBF and tracer uptake, resulting in underestimation of MBF in higher flow rates.(2) This may in part explain the higher thresholds and the superior prognostic performance of hMBF in the present [^{15}O]H_2O PET study. Second, the sample size of the present study was relatively small. Since the incremental value of CFR after adjusting for the combined use of hMBF and CFR was borderline significant (p=0.06), the lack of incremental prognostic value of CFR might be caused by a lack of statistical power.

Prognostic value of regional hyperemic MBF and CFR

Although the majority of prognostic studies on quantitative PET perfusion imaging have focused on global perfusion, regional instead of global perfusion is used in clinical practice. To date only one study has investigated the prognostic value of [^{15}O]H_2O PET perfusion. In a hybrid PET-CT study in which CT angiography was selectively followed by PET imaging, impaired regional hMBF was associated with adverse prognosis in patients in whom CT angiography showed obstructive CAD.(20) Recently, the integration of regional hMBF and CFR, termed the coronary flow capacity, has been proposed as an alternative to using either hMBF or CFR alone as this enables a more comprehensive assessment of patients with suspected CAD.(10,12) Gould et al. recently investigated the prognostic value of combined regional hMBF and CFR using ^{82}Rb PET and reported that severely impaired coronary flow capacity,

defined by concordant severe impairment of hMBF and CFR, was independently associated with all-cause death.(11) In the current study optimal prognostic thresholds for regional [^{15}O]H_2O PET were identified, i.e. 2.10 mL/min/g for hMBF and 2.07 for CFR. Similar to Gould et al., both hMBF and CFR had significant prognostic value for the occurrence of death/MI after separately adjusting for clinical parameters and their combined use. However, after adjusting for both clinical parameters and the combined use of hMBF and CFR, only hMBF remained an independent prognostic factor for the occurrence of events. Importantly, Gould et al. have used a more elaborate approach to obtain regional coronary flow capacity, in which hMBF and CFR values were calculated for each of the 1344 pixel of the left ventricle and combined into a patient map of pixel-specific regional coronary flow capacities. In the present study, regional hMBF and CFR values were calculated per vascular territory by averaging the MBF values of two adjacent segments with the lowest MBF. These methodological differences in calculation of regional perfusion values, together with aforementioned differences in tracer kinetics may impair comparability between both studies. Furthermore, in the study by Gould et al. impaired coronary flow capacity was only independently associated with cardiovascular death when very low thresholds were used for hMBF (≤0.83 ml/min/g) and CFR (≤1.27). Since, the thresholds identified in the current study (<2.10 ml/min/g for hMBF and 2.07 for CFR) were notably higher, this may in part explain the apparent conflicting findings. Nonetheless, for both global and regional perfusion, only hMBF demonstrated independent prognostic value for the occurrence of events. Since CFR is inherently dependent on resting flow, which is known to be highly sensitive to hemodynamic conditions, impairment of CFR may be less specific for myocardial ischemia and subsequently for the occurrence of events. This is in accordance with previous diagnostic [^{15}O]H_2O PET studies, in which hMBF was shown to be superior to CFR for the detection of hemodynamically significant CAD. (15,21) Furthermore, to account for changes in resting flow caused by differences in hemodynamic conditions, the corrected CFR was calculated in which the resting flow was corrected for the rate pressure product. However, results were comparable when the corrected instead of the uncorrected CFR was used to investigate the prognostic value of global and regional PET perfusion parameters.

Prognostic value of combined global and regional perfusion

Combining global and regional PET perfusion might improve risk prediction over either of the two alone, since global and regional perfusion are proposed to provide incremental information on different aspects of myocardial perfusion. Impairment in global perfusion may be caused by either epicardial CAD or microcirculatory dysfunction. The addition of regional perfusion may enable the detection of small regional defects caused by epicardial CAD, which are not detected with global perfusion due to averaging of both ischemic and non-ischemic myocardium.(11) In the present study, global hMBF and CFR values were indeed significantly higher than regional hMBF and CFR ($p<0.001$ for both). Nonetheless there was an excellent correlation between global and regional hMBF ($r=0.92$) and between global and regional CFR ($r=0.91$). Given the close relationship between global and regional perfusion, it is not unexpected that the combined use of regional and global perfusion did not improve prognostic performance for death/MI when compared with either global ($p=0.55$) or regional perfusion ($p=0.37$) alone. Regional analysis of PET perfusion, used in clinical practice to guide treatment, can therefore be considered a feasible alternative to global perfusion for identifying patients at risk for adverse events.

Limitations

First, the retrospective single-center design of our study has inherent limitations. Most importantly, although care was taken to maximize follow-up data, a substantial amount of 10% of patients was lost to follow-up. This primarily affected the endpoint of myocardial infarction, given that national registry databases were consulted in all patients to establish all-cause mortality. Second, as mentioned previously, there are important differences in tracer kinetics between $[^{15}O]H_2O$ and other tracers. Caution must therefore be taken when extrapolating our results to perfusion imaging with other PET tracers. Third, elective revascularizations guided by the initial PET perfusion imaging results may have influenced the analysis on the prognostic value of global and regional PET perfusion. After adjusting for imaging-guided revascularization results for global perfusion were unaffected. However, for regional perfusion, only a trend was observed for independent prognostic value of hMBF after additional correction for imaging-guided revascularization. The results on the prognostic value for regional perfusion must therefore be interpreted with caution. Last, both sample size and event

rate in the current study were relatively limited. This may have hampered the analysis on the incremental prognostic value of different PET parameters. Additionally, external validation of the identified cut-off values was not possible in the current study and therefore overfitting might have substantially influenced our results. Larger prospective studies are warranted to validate the prognostic value of the identified thresholds for $[^{15}O]H_2O$ PET perfusion imaging.

Conclusion

Global hMBF and CFR both demonstrated prognostic value for the occurrence of the composite of death and MI, however global hMBF was the only independent prognostic factor after adjusting for clinical characteristics and the combined use of hMBF and CFR. Similarly, impaired regional hMBF and CFR were both associated with adverse prognosis, however only regional hMBF had independent prognostic value for the occurrence of events. Lastly, combining global and regional perfusion did not increase prognostic performance over either of the two alone.

References

1. Bourque JM, Beller GA. Stress myocardial perfusion imaging for assessing prognosis: an update. JACC Cardiovasc Imaging 2011;4:1305-19.
2. Driessen RS, Raijmakers PG, Stuijfzand WJ, Knaapen P. Myocardial perfusion imaging with PET. Int J Cardiovasc Imaging 2017;33:1021-1031.
3. Gupta A, Taqueti VR, van de Hoef TP et al. Integrated Non-invasive Physiological Assessment of Coronary Circulatory Function and Impact on Cardiovascular Mortality in Patients with Stable Coronary Artery Disease. Circulation 2017.
4. Ziadi MC, Dekemp RA, Williams KA et al. Impaired myocardial flow reserve on rubidium-82 positron emission tomography imaging predicts adverse outcomes in patients assessed for myocardial ischemia. J Am Coll Cardiol 2011;58:740-8.
5. Herzog BA, Husmann L, Valenta I et al. Long-term prognostic value of 13N-ammonia myocardial perfusion positron emission tomography added value of coronary flow reserve. J Am Coll Cardiol 2009;54:150-6.
6. Farhad H, Dunet V, Bachelard K, Allenbach G, Kaufmann PA, Prior JO. Added prognostic value of myocardial blood flow quantitation in rubidium-82 positron emission tomography imaging. Eur Heart J Cardiovasc Imaging 2013;14:1203-10.
7. Murthy VL, Naya M, Foster CR et al. Improved cardiac risk assessment with

noninvasive measures of coronary flow reserve. Circulation 2011;124:2215-24.
8. Fukushima K, Javadi MS, Higuchi T et al. Prediction of short-term cardiovascular events using quantification of global myocardial flow reserve in patients referred for clinical 82Rb PET perfusion imaging. J Nucl Med 2011;52:726-32.
9. Tio RA, Dabeshlim A, Siebelink HM et al. Comparison between the prognostic value of left ventricular function and myocardial perfusion reserve in patients with ischemic heart disease. J Nucl Med 2009;50:214-9.
10. Johnson NP, Gould KL. Integrating noninvasive absolute flow, coronary flow reserve, and ischemic thresholds into a comprehensive map of physiological severity. JACC Cardiovasc Imaging 2012;5:430-40.
11. Gould KL, Johnson NP, Roby A et al. Regional Artery Specific Thresholds Of Quantitative Myocardial Perfusion By PET Associated With Reduced MI and Death After Revascularization In Stable CAD. J Nucl Med 2018.
12. Gould KL, Johnson NP, Bateman TM et al. Anatomic versus physiologic assessment of coronary artery disease. Role of coronary flow reserve, fractional flow reserve, and positron emission tomography imaging in revascularization decision-making. J Am Coll Cardiol 2013;62:1639-1653.
13. Danad I, Raijmakers PG, Harms HJ et al. Impact of anatomical and functional severity of coronary atherosclerotic plaques on the transmural perfusion gradient: a [15O] H2O PET study. Eur Heart J 2014;35:2094-105.
14. Cerqueira MD, Weissman NJ, Dilsizian V et al. Standardized myocardial segmentation and nomenclature for tomographic imaging of the heart. A statement for healthcare professionals from the Cardiac Imaging Committee of the Council on Clinical Cardiology of the American Heart Association. Circulation 2002;105:539-42.
15. Danad I, Uusitalo V, Kero T et al. Quantitative assessment of myocardial perfusion in the detection of significant coronary artery disease: cutoff values and diagnostic accuracy of quantitative [(15)O]H2O PET imaging. J Am Coll Cardiol 2014;64:1464-75.
16. Neumann FJ, Sousa-Uva M, Ahlsson A et al. 2018 ESC/EACTS Guidelines on myocardial revascularization. Eur Heart J 2019;40:87-165.
17. Heagerty PJ, Lumley T, Pepe MS. Time-dependent ROC curves for censored survival data and a diagnostic marker. Biometrics 2000;56:337-44.
18. Dorbala S, Di Carli MF, Beanlands RS et al. Prognostic value of stress myocardial perfusion positron emission tomography: results from a multicenter observational registry. J Am Coll Cardiol 2013;61:176-84.
19. Juarez-Orozco LE, Tio RA, Alexanderson E et al. Quantitative myocardial perfusion

evaluation with positron emission tomography and the risk of cardiovascular events in patients with coronary artery disease: a systematic review of prognostic studies. Eur Heart J Cardiovasc Imaging 2018;19:1179-1187.

20. Maaniitty T, Stenstrom I, Bax JJ et al. Prognostic Value of Coronary CT Angiography With Selective PET Perfusion Imaging in Coronary Artery Disease. JACC Cardiovasc Imaging 2017;10:1361-1370.

21. Joutsiniemi E, Saraste A, Pietila M et al. Absolute flow or myocardial flow reserve for the detection of significant coronary artery disease? Eur Heart J Cardiovasc Imaging 2014;15:659-65.

Supplementary Data

Supplementary Table 1. Internal validation of the prognostic value of regional and global PET perfusion for the occurrence of death/MI

	Optimal cut-off (95% CI)	Hazard ratio (95% CI)		p-value *	Proportion of sets with p<0.05 *
	Training sets	Training sets	Validation sets		
Global perfusion					
Global hMBF	2.74 (2.47 - 3.17)	3.89 (2.36 - 6.70)	3.39 (1.99 - 6.53)	<0.01 (<0.01 - 0.07)	0.93
Global CFR	2.81 (2.39 - 3.37)	3.61 (2.43 - 6.79)	2.90 (1.87 - 5.41)	0.01 (<0.01 - 0.09)	0.90
Global corrected CFR	2.09 (1.89 - 2.57)	3.40 (1.94 - 5.83)	2.40 (1.70 - 5.27)	0.02 (<0.01 - 0.19)	0.76
Regional perfusion					
Regional hMBF	2.14 (1.78 - 2.50)	3.72 (2.26 - 6.08)	2.91 (1.98 - 4.68)	0.01 (<0.01 - 0.06)	0.92
Regional CFR	2.09 (1.89 - 2.57)	3.40 (1.94 - 5.83)	2.40 (1.70 - 5.27)	0.01 (<0.01 - 0.14)	0.87
Regional corrected CFR	1.64 (1.44 - 1.99)	3.28 (2.06 - 7.68)	2.75 (1.62 - 5.54)	0.01 (<0.01 - 0.21)	0.83

* p-value for hazard ratio in validation set. CFR = coronary flow reserve; hMBF = hyperemic myocardial bloodflow; MI = myocardial infarction; PET = positron emission tomography

Supplementary Table 2. Univariable analysis of prognostic factors for death/MI

	HR (95% CI)	p-value
Clinical characteristics		
Age, years	1.06 (1.03 – 1.08)	<0.001
Gender (male)	1.48 (0.89 – 2.46)	0.13
BMI, kg/m^2	0.99 (0.93 – 1.05)	0.69
Smoking	0.88 (0.52 – 1.48)	0.63
Diabetes	2.15 (1.26 – 3.67)	0.005
Hypertension	1.73 (1.03 – 2.92)	0.04
Dyslipidemia	1.57 (0.94 – 2.60)	0.08
Family history of CAD	0.67 (0.40 – 1.13)	0.13
PET imaging		
Regional hMBF	3.55 (2.04 – 6.19)	<0.001
Regional CFR	3.22 (1.85 – 5.61)	<0.001
Global hMBF	3.77 (2.14 – 6.51)	<0.001
Global CFR	2.99 (1.68 – 5.34)	<0.001

BMI = body mass index; CAD = coronary artery disease; other abbreviations as in Supplementary Table 1

Supplementary Table 3. Prognostic value of global perfusion using hyperemic myocardial blood flow and corrected coronary flow reserve for the occurrence of death and MI

	Adjusted for clinical parameters *		Adjusted for combined use of hMBF and CFR†		Adjusted for clinical parameters + combined use of hMBF and CFR	
	HR (95% CI)	p-value	HR (95% CI)	p-value	HR (95% CI)	p-value
hMBF <2.65	3.03 (1.61 - 5.70)	0.001	3.19 (1.67 - 6.11)	<0.001	2.95 (1.38 - 6.30)	0.005
Corrected CFR <2.10	1.81 (1.00 - 3.23)	0.047	1.35 (0.71 - 2.55)	0.36	1.02 (0.51 - 2.07)	0.95

* Clinical parameters included in the analysis were age, gender, BMI, diabetes, hypertension, smoking status, family history, and hyperlipidemia; † Hazard ratios represent the prognostic value of the parameters in a combined model where both hMBF and CFR were included. Abbreviations as in Supplementary Table 1.

Supplementary Table 4. Prognostic value of regional perfusion using hyperemic myocardial blood flow and corrected coronary flow reserve for the occurrence of death and MI

	Adjusted for clinical parameters *		Adjusted for combined use of hMBF and CFR †		Adjusted for clinical parameters + combined use of hMBF and CFR	
	HR (95% CI)	p-value	HR (95% CI)	p-value	HR (95% CI)	p-value
hMBF <2.10	2.80 (1.49 - 5.25)	0.001	2.56 (1.31 - 5.01)	0.006	2.17 (0.99 - 4.75)	0.05
Corrected CFR <1.60	2.27 (1.23 - 4.17)	0.009	1.77 (0.88 - 3.56)	0.11	1.45 (0.68 - 3.10)	0.34

* Clinical parameters included in the analysis were age, gender, BMI, diabetes, hypertension, smoking status, and family history, hyperlipidemia; † Hazard ratios represent the prognostic value of the parameters in a combined model where both hMBF and CFR were included. Abbreviations as in Supplementary Table 1.

Supplementary Table 5. Prognostic value of global myocardial blood flow for the occurrence of death and MI adjusting for revascularization based on initial diagnostic work-up

	Adjusted for clinical parameters including revascularization based on initial diagnostic work-up		Adjusted for clinical parameters including revascularization based on initial diagnostic work-up + combined use of hMBF and CFR †	
	HR (95% CI)	p-value	HR (95% CI)	p-value
hMBF <2.65	2.88 (1.49-5.56)	0.002	2.47 (1.21-5.05)	0.013
CFR <2.88	1.99 (1.07-3.70)	0.030	1.42 (0.72-2.79)	0.31

* Clinical parameters included in the analysis were age, gender, BMI, diabetes, hypertension, smoking status, family history, hyperlipidemia, and revascularization based on the initial diagnostic work-up; † Hazard ratios represent the prognostic value of the parameters in a combined model where clinical parameters and both hMBF and CFR were included. Abbreviations as in Supplementary Table 1.

Supplementary Table 6. Prognostic value of regional myocardial blood flow for the occurrence of death and MI adjusting for revascularization based on initial diagnostic work-up

	Adjusted for clinical parameters including revascularization based on initial diagnostic work-up		Adjusted for clinical parameters including revascularization based on initial diagnostic work-up + combined use of hMBF and CFR †	
	HR (95% CI)	p-value	HR (95% CI)	p-value
hMBF <2.10	2.67 (1.38-5.19)	0.004	2.06 (0.97-4.35)	0.06
CFR <2.07	2.19 (1.20-3.99)	0.01	1.61 (0.82-3.17)	0.17

* Clinical parameters included in the analysis were age, gender, BMI, diabetes, hypertension, smoking status, and family history, hyperlipidemia, and revascularization based on the initial diagnostic work-up; † Hazard ratios represent the prognostic value of the parameters in a combined model where clinical parameters and both hMBF and CFR were included. Abbreviations as in Supplementary Table 1.

PART III

Hybrid PET/CT imaging

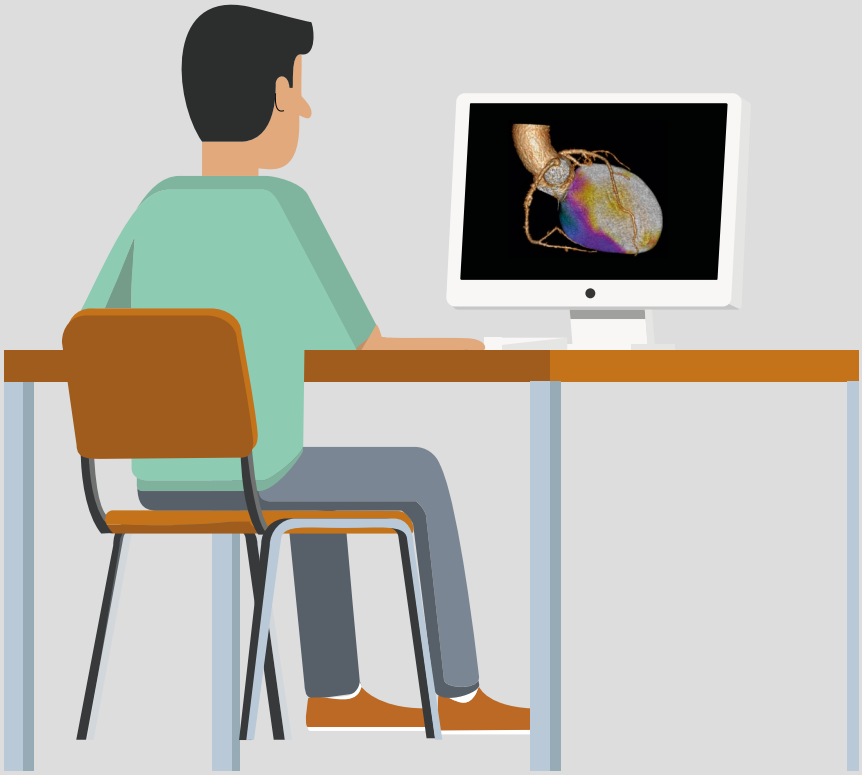

Chapter 12

Early Detection and Treatment of the Vulnerable Coronary Plaque: Can We Prevent Acute Coronary Syndromes?

Michiel J. Bom, Dirk J. van der Heijden, Elvin Kedhi, Jan van der Heyden, Martijn Meuwissen, Paul Knaapen, Stefan A.J. Timmer, and Niels van Royen

Circ Cardiovasc Imaging. 2017;10(5)

Abstract

Early identification and treatment of the vulnerable plaque, i.e. a coronary artery lesion with a high likelihood of rupture leading to an acute coronary syndrome, has gained great interest in the cardiovascular research field. Post-mortem studies have identified clear morphologic characteristics associated with plaque rupture. Recent advances in invasive and non-invasive coronary imaging techniques have empowered the clinician to identify suspected vulnerable plaques in vivo, and paved the way for the evaluation of therapeutic agents targeted at reducing plaque vulnerability. Local treatment of vulnerable plaques by percutaneous coronary intervention and systemic treatment with anti-inflammatory and LDL-lowering drugs are currently being investigated in large randomized clinical trials to assess their therapeutic potential for reducing adverse coronary events. Results from these studies may enable a more patient-tailored strategy for the treatment of coronary artery disease.

Introduction

Traditional strategies for the treatment of coronary artery disease (CAD) are aimed at restoring flow in coronary arteries with obstructive atherosclerotic lesions, and are the basis for millions of percutaneous coronary interventions (PCI) and coronary artery bypass grafting (CABG) procedures performed each year. Although this approach reduces ischemic burden and relieves angina symptoms, it does not prevent many acute coronary syndromes (ACS). ACS is frequently caused by plaque rupture of non-obstructive, eccentric coronary plaques, which initiates a thrombotic cascade leading to (near) total occlusion of the coronary lumen.(1) Consequently, an ACS with potentially devastating effects is frequently the initial presentation of CAD in previously asymptomatic patients. These observations have raised interest in the early identification and treatment of high-risk coronary artery lesions, or so-called 'vulnerable plaques', to prevent future ACS.(1-3) This review aims to give an update on the definition, detection and treatment of the vulnerable plaque.

Atherosclerosis and acute coronary syndrome

Plaque formation

Coronary artery disease is a chronic disease, in which over the course of decades inflammation of the coronary vessel wall can lead to the formation of complex atherosclerotic lesions.(1,4,5) Histological studies on the pathogenesis of atherosclerosis have provided clear insight into the various stages of coronary plaque formation. First, accumulation of low-density lipoprotein (LDL) particles in the intima of the arterial vessel wall lead to pathological intimal thickening, by acting as a chronic stimulator of the innate and adaptive immune response.(1) Histologically, this is characterized by the presence of smooth muscle cell remnants within an extracellular matrix composed of proteoglycans and collagen type 2, coinciding with small, extracellular lipid pools beneath layers of foam cells. Subsequently, macrophage infiltration within lipid pools and subsequent necrosis and apoptosis of these macrophages results in the formation of a demarcated acellular and lipid-rich necrotic core, which is encapsulated by surrounding fibrous tissue. This progressive type lesion is defined as a fibro-atheroma. Calcification can occur in all stages of progressive atherosclerosis.(1,4,5)

Mechanisms for acute coronary syndrome

In general, ACS is caused by the formation of an intracoronary thrombus superimposed on an atherosclerotic lesion, except for rare cases such as spontaneous coronary artery dissection and coronary vasospasm. Three distinct pathophysiological mechanisms have been described that may lead to intracoronary thrombus formation: plaque rupture, plaque erosion and calcified nodule.(2,4,6) Plaque rupture is defined as a defect or gap in the overlying cap of the fibroatheroma which leads to exposure of its highly thrombogenic contents to the blood and subsequently followed by rapid thrombus accumulation at the site of rupture.(2) The pathogenesis of ACS associated with plaque erosion is less well defined, but is characterized by the absence of plaque rupture. Histological examination of cases reveals absent endothelium at the site of erosion, leading to exposure of the proteoglycan and smooth muscle cell rich intima.(1,4) The exact mechanisms that induce thrombus formation at these sites remains unknown. Virmani et al. proposed a third mechanism in the formation of intracoronary thrombi, referred to as calcified nodule in which disruptive nodular calcifications protrude into the lumen and thereby cause thrombosis.(4) The role of calcified nodules in the pathogenesis of coronary events remains unclear.(7)

The vulnerable plaque

The term vulnerable plaque was introduced by Muller and colleagues in the late 1980s as a coronary plaque with a high susceptibility to rupture.(8) Nowadays the vulnerable plaque is commonly referred to as a lesion with a high likelihood of precipitating thrombosis.(9) Recently Stone et al. introduced an alternative, more clinically relevant definition of the vulnerable plaque, i.e. a plaque that places a patient at risk for future major adverse cardiac events (MACE).(10) However, historically most pathophysiological studies on plaque morphology predisposing to ACS have focused on plaque rupture. A plaque with a large necrotic core and a thin fibrous cap is suspected to be rupture-prone, and is frequently referred to as a thin-cap fibroatheroma (TCFA). Figure 1 depicts a schematic representation of a suspected vulnerable plaque, including the morphological aspects associated with rupture. These aspects are discussed in detail below.

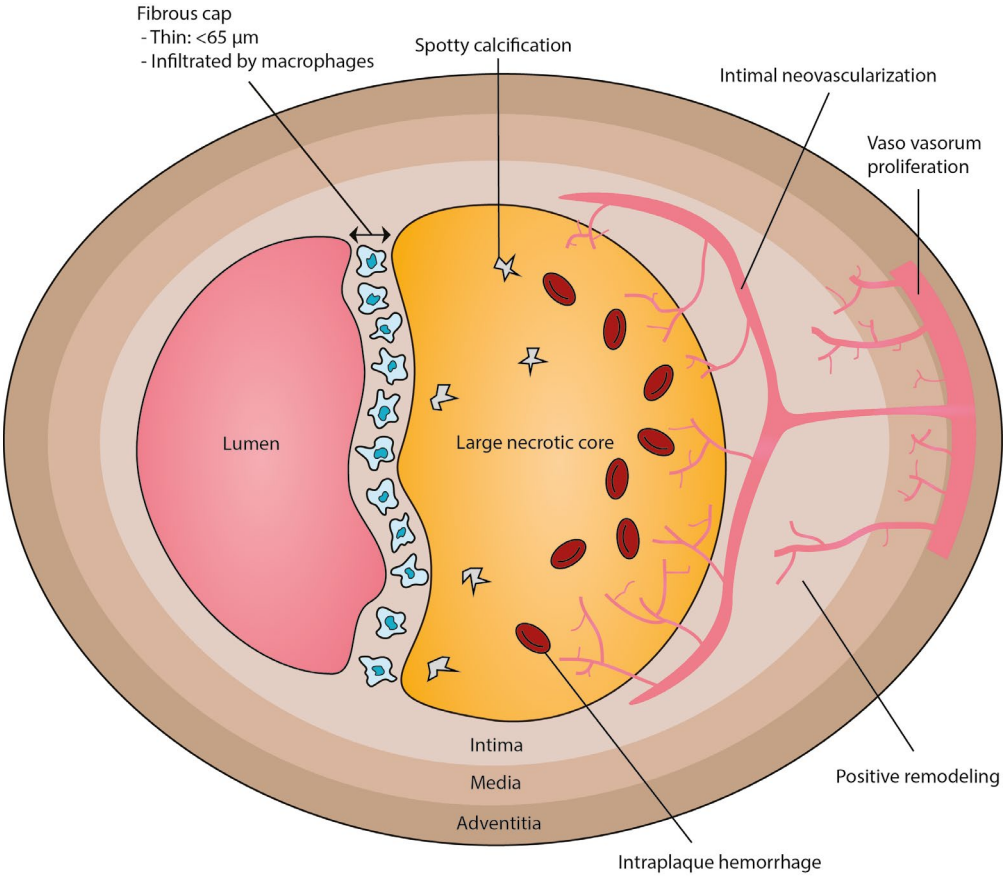

Figure 1. Schematic representation of a suspected vulnerable plaque
A large necrotic core is separated from the lumen by a thin fibrous cap (<65µm), infiltrated by macrophages. The proliferation of the vaso vasorum leads to intimal neovascularization. These immature neovessels tend to leak red blood cells and cause intraplaque bleeding. There is positive (outward) remodeling of the vessel and the necrotic core contains spotty calcification.

Morphology associated with plaque rupture

Autopsy studies have shown an inverse relationship between plaque cap thickness and risk of plaque rupture, with 95% of plaque ruptures occurring in lesions with a cap thickness <65 µm.(11) A post-mortem study by Narula et al. on 295 coronary atherosclerotic plaques analyzed the importance of various pathological characteristics to differentiate between TCFA and stable plaques and found that fibrous cap thickness was the most accurate discriminator.(12) A large plaque burden with central necrosis negatively affects plaque stability. Expansion of the necrotic core may lead to erosion

and subsequent thinning of the fibrous cap.(1) Indeed, autopsy studies have revealed that ruptured plaques are associated with a larger necrotic core as compared to non-ruptured plaques.(12,13) Ruptured caps are more frequently infiltrated by macrophage foam cells than caps of non-ruptured TCFA.(13,14) It is hypothesized that macrophages within the cap play a key role in thinning, and ultimately, cap rupture by secreting proteolytic enzymes such as matrix metalloproteinases.(1,6,14,15)

Coronary arteries may respond to plaque growth by expansion or shrinkage of the vessel wall, defined as positive and negative remodeling, respectively. Whereas vulnerable coronary plaques are generally associated with positive remodeling, stable plaques are characterized by negative remodeling of the vessel wall.(16) Although positive remodeling may spare the coronary lumen, continuous outward growth of the plaque will induce neovascularization by microvessels originating from the adventitial vasa vasorum.(17) Unfortunately, these microvessels are suspected to negatively affect plaque stability by causing intraplaque haemorrhage as a result of vascular immaturity and lack of supporting cells.(18-20)

Plaque calcification is associated with all stages of atherosclerosis, and can occur as early as during the intimal thickening phase. Microcalcification is believed to be triggered by apoptosis of smooth muscle cells in pathological intimal thickening lesions,(21) and by macrophage release of matrix vesicles or by apoptosis within the necrotic core in fibroatheroma lesions.(22) Microcalcification within the thin fibrous cap, or spotty calcification, may serve as a marker of plaque vulnerability.(23,24) In contrast, larger calcified sheets consisting of merged areas of microcalcification are associated with plaque stability. Whereas microcalcification within the thin fibrous cap and a specific calcification pattern called spotty calcification are reported to be associated with plaque rupture, predominantly calcified plaques with large calcific sheets are thought to be stable plaques.

Challenges to the vulnerable plaque concept

The concept of visualization and treatment of the vulnerable plaque has predominantly focused on plaque rupture, as this is the pathophysiological mechanism most frequently responsible for ACS.(6) A review of literature, which included 22 autopsy studies and a total of 1847 coronary arteries, reported that plaque rupture is observed in 73% of

all fatal coronary thrombi.(6) However, contemporary optical coherence tomography studies have provided preliminary evidence that the prevalence of plaque rupture in non-fatal ACS, and especially in NSTEMI, might be lower.(25-29) The prevalence of plaque rupture in these studies was reported to be 44-73%, whereas plaque erosion and calcified nodule were reported to be only 27-33% and 8% respectively. Although plaque rupture remains the most prominent cause of ACS, it should be noted that novel therapeutics aimed at preventing plaque rupture may have no effect on the incidence of ACS as a result of plaque erosion or calcified nodule.

Another challenge to the concept is the fact that not all cases of intracoronary thrombosis necessarily lead to a clinical event. A recent review by Arbab-Zadeh et al. examined the results of many clinical and pathological investigations and reported subclinical plaque rupture in 11.5% of patients with stable coronary artery disease (CAD) and 21.5% in patients who presented with ACS.(30) Subclinical plaque ruptures however are not without consequences, as they are considered an important mechanism responsible for increased plaque burden and subsequent lumen narrowing.(31) In line with this hypothesis, Park et al have recently shown that several suspected CCTA-derived vulnerable plaque features are correlated with ischemia-causing lesions as defined by an abnormal FFR.(32)

The focus on imaging and treatment of specific vulnerable plaques fails to address the fact that atherosclerosis is a systemic, multi-factorial disease, and optimal care likely consists of systemic and multi-focal diagnosis and therapy, of which local plaque therapy may be a component.(33) In addition, knowledge on the prevalence and natural history of suspected imaging-derived vulnerable features is limited. Longitudinal imaging studies have suggested that plaque morphology may change over time and many suspected vulnerable plaques may not progress over the course of years and may even regress to more stable lesions.(34-37) The results and limitations of these studies will be addressed in more detail in their respective sections. Although the identification of rupture prone plaques in vivo will certainly not be able to predict the occurrence of all coronary events, it could provide additional prognostic information to target novel therapeutics. Altogether, lack of clinical outcome studies proving that a suspected vulnerable plaque actually causes a coronary event hampers the clinical applicability of the concept.

Imaging of the vulnerable plaque

Invasive techniques

In the past decades, several intracoronary imaging techniques have been developed enabling analysis of in vivo plaque morphology, tissue composition and even inflammatory activity (table 1). The clinical potential of these invasive imaging techniques to identify vulnerable plaques will be discussed in this section.

Table 1. Intracoronary imaging of the vulnerable plaque

	VH-IVUS (40)	OCT (73)	NIRS (86)
Technical characteristics			
Energy source	Ultrasound	Infrared light	Near-infrared light
Pullback speed (mm/s)	0.5	10 - 40	0.5
Depth penetration (mm)	7 - 10	0.1 - 2.0 *	1 - 2
Spatial resolution (μm)	150 – 250	10	N/A
Vulnerable plaque features			
Remodelling	++ (40,53,54)	-	-
Lipid core	+ (40-44)	+ (46,47,73)	++ (87,88)
Plaque rupture	+ (40)	++ (73)	-
Thin fibrous cap	-	++ (46,68,73)	-
Macrophage infiltration	-	++ (73,76,77)	-
Neovascularization	-	+ (73)	-
Intra-plaque hemorraghe	-	-	-
Spotty calcification	++ (40-44)	+ (73)	-

*: Depth penetration of OCT is dependent on visualized tissue, i.e. depth penetration in lipid is limited, whereas penetration is greater in fibrous tissue. VH-IVUS = virtual histology intravascular ultrasound; OCT = optical coherence tomography; NIRS = near-infrared spectroscopy

Intravascular ultrasound (IVUS)

IVUS is performed by use of a catheter harboring a piezoelectric crystal at the distal end, attached to computerized ultrasound equipment. IVUS is based on the reflection of emitted ultrasound waves, according to the acoustic properties of the tissue.(38) Gray-scale IVUS is based only on the amplitude of sound waves backscattered from tissue (39) and results in relatively low spatial resolution which hampers detailed plaque characterization.(38) More recently, radiofrequency analysis IVUS has been introduced, of which virtual histology (VH-IVUS) is the most widely available. This

technology uses frequency in addition to echo-intensity information to compose an intra-luminal image of the coronary artery wall. VH-IVUS can visualize four distinct plaque components, i.e. fibrous plaque, fibro-fatty plaque, necrotic core, and calcium, as shown in figure 2.(40-42) Various ex-vivo studies have shown good correlation of these separate components with histology, with predictive accuracy of the various components ranging from 87% - 97%, in dissected coronary arteries during autopsy. (41-44). On the contrary, no significant correlation between in-vivo VH-IVUS derived necrotic core and histology was found in an atherosclerosis-prone micro pig model. (45) The accuracy of plaque morphology with in-vivo VH-IVUS therefore remains a matter of debate.

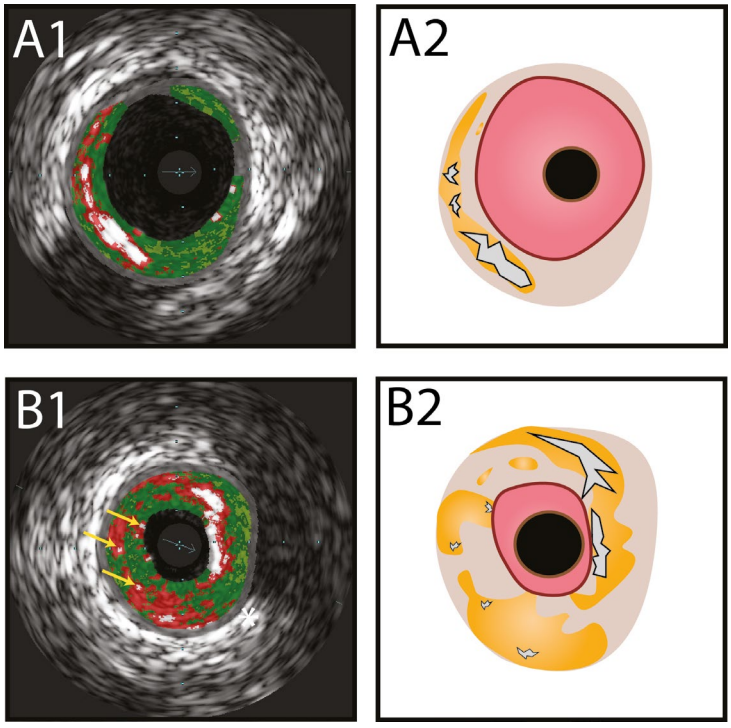

Figure 2. Plaque morphology with the use of VH-IVUS and corresponding illustrations
(A) VH-IVUS image showing a coronary plaque containing necrotic core (red colour), dense calcium (white area), fibrous tissue (green area) and fibrofatty tissue (yellow-green area). The plaque is classified as a thick cap fibroatheroma since there is a visible fibrous cap covering a confluent necrotic core of more than 10%. (B) VH-IVUS image showing of a thin-cap fibroatheroma. A confluent necrotic core of more than 10% lies in direct contact with the lumen. Spotty calcification can also be seen as small areas of dense calcium (yellow arrows).

TCFA can be identified by VH-IVUS in fair good correlation with histology, despite an axial resolution (100-200 μm) which limits the visualization of a thin fibrous cap (≤65 μm).(46-48) VH-derived TCFA (VH-TCFA) is defined as a lesion with a confluent necrotic core (≥10%) plaque in direct contact with the lumen.(46,49-51) Three relevant studies have been published on the prognostic value of VH-TCFA.(49-51) In the PROSPECT study, 697 patients with ACS underwent three-vessel gray-scale and VH-IVUS after PCI and were subsequently followed for MACE for a median of 3.4 years.(51) Independent predictors for the occurrence of MACE in non-culprit lesions were VH-TCFA, a small luminal area (≤4 mm2) and a large plaque burden (≥70%). Two other prognostic studies, the VIVA study and the ATHEROREMO-IVUS study, incorporating a combined endpoint of mortality, myocardial infarction and unplanned revascularization, have confirmed the independent prognostic value of VH-TCFA and a large plaque burden for the occurrence of MACE.(49,50) Although post-mortem studies have shown that large plaque burden is a common feature of ruptured plaques,(52) it should be noted that the combined endpoints of these studies were mainly driven by unstable or refractory angina, instead of myocardial infarction and death. Serial IVUS studies have reported conflicting data on the dynamic nature of VH-TCFA over time, with simultaneous development of new VH-TCFA and stabilization of existing lesions.(34,35) Kubo et al. reported that in predominantly stable CAD patients, after a mean follow-up of 12 months as many as 75% of all VH-TCFA regressed to more stable lesions, whereas only 6% of thick-cap fibroatheroma and 10% of pathological intimal thickening lesions evolved to VH-TCFA.(34) A substudy of the HORIZONS-AMI trial on the other hand showed that in non-culprit lesions in STEMI patients, VH-TCFA remained VH-TCFA in 78% after 13 months follow-up, whereas 49% of thick-cap fibroatheroma and 44% of pathological intimal thickening lesions progressed to VH-TCFA.(35) Patient vulnerability might play a role in the suspected dynamic nature of VH-TCFA. However, variability in the repeat measures of TCFA by VH-IVUS may also be playing a role and the results of VH-IVUS studies on the dynamic nature of TCFA have to be interpreted with caution.

Positive remodeling as defined by gray-scale IVUS has been reported to be more common in patients with ACS (53,54) and at sites with ruptured plaques.(55) However, positive remodeling was not an independent predictor for events in the three aforementioned

prognostic studies.(49-51) A recent substudy of the PROSPECT surprisingly reported that both positive and negative remodeling were associated with MACE in non-culprit lesions.(56) Because TCFA was more prevalent in lesions with negative remodeling, this may be presumed as a marker of more advanced atherosclerosis in which subclinical plaque rupture and healing leads to plaque progression. The authors also reported that lesions with positive remodeling more frequently had a large plaque burden (≥70%), when compared to lesions with intermediate or negative remodeling. It is possible that collinearity between a large plaque burden and positive remodeling is responsible for the fact that positive remodeling was not an independent predictor in the previously mentioned outcome studies.(49-51)

IVUS studies have identified a specific pattern of calcification, called spotty calcification, which is thought to be a marker of plaque vulnerability.(24,57-60) Spotty calcification on IVUS has been associated with ACS,(24) with ruptured plaques in autopsy studies,(57) and with VH-TCFA and a large necrotic core.(58) A recent comparison between IVUS and histology revealed that IVUS derived spotty calcification was more frequent in fibroatheroma than in fibrocalcific lesions.(59) Furthermore, a serial IVUS study reported that lesions with spotty calcification had a larger baseline plaque burden and accelerated progression of plaque burden as compared with non-calcified plaques.(60) Other prospective studies are needed to confirm these results.

Optical coherence tomography (OCT)

In OCT a low-coherence, infrared light source is directed at the vessel wall, using the backscattered light to produce an image of the tissue. The OCT catheter has an inner imaging core that rotates to provide cross-sectional images from distal to proximal, which can be simplified by an automated pullback system.(61) The resolution of OCT surpasses that of IVUS with an axial resolution of 10-20 μm (vs. 100-250 μm respectively), at the cost of a limited depth penetration 0.1-2.0 mm (vs. 7-10 mm respectively). OCT has been proposed as an alternative to IVUS in the guidance of PCI procedures, in the ILUMIEN studies,(62-64) and in the visualization of plaque morphology in vivo. Various post-mortem studies have indeed shown good correlation between OCT and histology for the characterization of different types of atherosclerotic plaques.(46,47,65,66) Studies that directly compare the ability of IVUS and OCT

to identify histopathological TCFA, have consistently shown better performance of OCT.(46,47) Recently hybrid catheters have been developed that combine the high resolution of OCT with the depth penetration of IVUS (67), with studies suggesting an increase in diagnostic performance.(46,47) An illustrative overview of the suspected OCT-derived vulnerable plaque features is shown in figure 3.

Due to its high spatial resolution OCT can be used to measure plaque cap thickness and to truly identify TCFA.(68) The identification of TCFA by OCT is in part hampered by the limited depth penetration of OCT and the consequent limitations in establishing lipid pools. Furthermore, light scattering in calcified and even fibrous plaques has been reported to cause misdiagnosis of lipid pools on OCT.(69) Although large prospective OCT studies with clinical follow-up are lacking, OCT-derived TCFA is shown to correlate with clinical presentation. Various studies have demonstrated that TCFA is more commonly found in patients presenting with ACS than in those presenting with stable angina pectoris(70,71) and cap thickness is thinner in culprit than in non-culprit lesions.(70,71) The definition of OCT-derived TCFA however is not unambiguous. Many studies have used 65 μm as cut-off for TCFA, based on post-mortem histology studies.(4,29,47,67,70,71) Nonetheless, both recent in and ex vivo OCT studies have shown that nearly all ruptured plaques have a cap thickness <80-85 μm (12,72) and in a direct post-mortem comparison of OCT and histology, Brown et al. identified a fibrous cap thickness ≤85 μm over 3 continuous frames to be the optimal definition for the identification of histopathological TCFA.(46) This discrepancy between OCT and post-mortem histology might be explained by tissue shrinkage occurring during tissue preparation.(73) Furthermore, some studies have used an additional parameter to define TCFA. The arc of the lipid pool has to be large, as a surrogate for a large necrotic core, with a frequently used cut-off of ≥90°.(71,74,75) The aforementioned study by Brown et al. reported a maximum arc of the lipid pool of ≥80 ° to be the optimal cut-off for the identification of TCFA.(46) The latest OCT consensus statement stated that the cut-offs for cap thickness should be related to histopathology and should be adjusted to account for tissue shrinkage and that the number of quadrants of the arc of the lipid pool defining a TCFA remains an unanswered question.(73) Prospective OCT studies with clinical follow-up to validate the definition of OCT-derived TCFA are warranted.

Macrophage infiltration of the thin fibrous cap is thought to be an important feature of

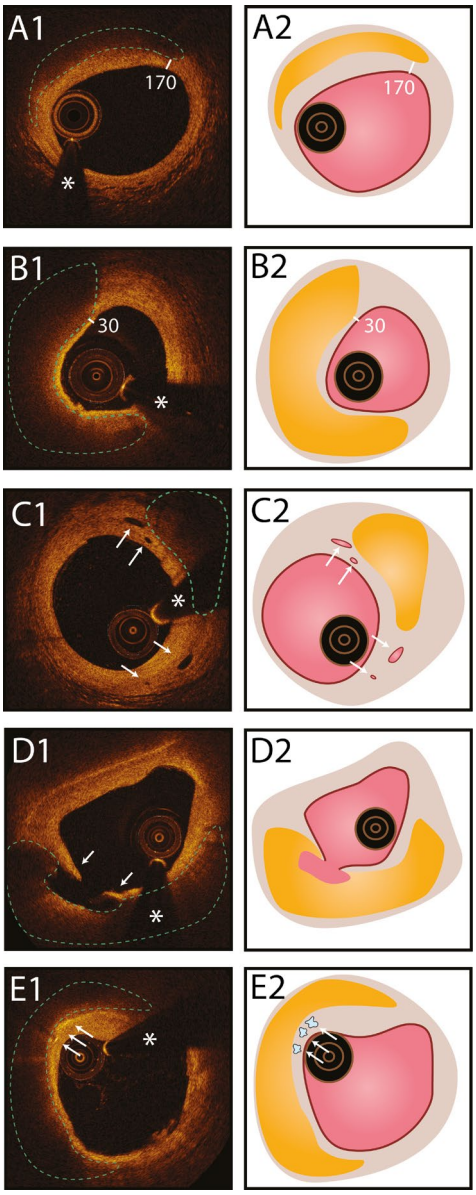

Figure 3. Vulnerable plaque features visualized by OCT with corresponding illustrations
(A) OCT image showing a signal poor region with a poorly delineated border (green dashed line) (A1) which corresponds with a lipid pool (A2). Since the thickness of the overlying fibrous cap (white line) is 170µm, this lesion is called a thick-cap fibroatheroma. The asterisk in the image represents a guidewire artifact. (B) Another lesion with a larger lipid pool is depicted in this OCT frame (B1), however the thickness of the fibrous cap is below 65µm in this lesion. The lesion is thus termed a thin-cap fibroatheroma (B2). (C) An OCT image of intimal microchannels (white arrows) (C1), which represents neo-vascularization within the intimal wall (C2). (D) A ruptured fibrous cap (white arrows) is seen in this OCT image. The contents of the ruptured plaque are washed away leaving behind a cavity filled with contrast agent. (E) Macrophage infiltration can be seen on OCT as signal rich distinct regions; so called “bright spots”.

the vulnerable plaque.(12) Macrophages appear on OCT as so-called 'bright spots' with a high signal attenuation behind it.(73) Tearney et al. reported excellent correlation between quantification of bright spots and macrophage density in carotid artery plaques. (76) This was confirmed in coronary artery plaques by a recent post-mortem study on coronary artery plaques by Di Vito et al.(77) Further studies showed that macrophage density is greater in TCFA as compared to non-TCFA (78), greater in culprit versus non-culprit plaques (79), and greater in ST-elevation myocardial infarction (STEMI) patients versus stable angina patients.(80) It should be noted however, that to a lesser degree other structures such as cellular fibrous tissue and cholesterol clefts may also appear as bright spots on OCT, thereby mimicking macrophage infiltrates.(81)

Vaso vasorum and micro vessels within coronary atherosclerotic plaques can be visualized by OCT, appearing as micro channels.(82,83) Several reports have shown a correlation between the density of micro channels in OCT and plaque vulnerability (defined as TCFA) (74,75,84) as well as increase in plaque volume.(85)

Near-infrared spectroscopy (NIRS)

In NIRS, a scanning laser delivers near-infrared light to the tissue of interest and the proportion of light reflected back is measured over the range of optical wavelength by a detector. Cholesterol has specific features in the wavelength region of NIRS, allowing distinct imaging of a lipid core plaque (LCP).(86) The measured data is displayed as a chemogram, a two-dimensional visualization of the probability of the presence of a LCP per millimeter. NIRS data can also be used to calculate a lipid core burden index (LCBI), which is the amount of lipid in a scanned artery. $LCBI_{4mm}$ is commonly used to represent the amount of lipid in a coronary segment of 4mm length. Gardner et al. confirmed the ability of NIRS signals to visualize LCP in coronary arteries in a post-mortem study showing good correlation with histology.(87) A comparison by Waxman et al. showed similar NIRS results in and ex-vivo.(88) Another in-vivo study reported that culprit lesions in ACS are more frequently LCP and patients with an ACS have more non-culprit LCP as compared to stable angina patients, supporting the feasibility of NIRS to visualize LCP.(89) A typical example of NIRS findings in a STEMI culprit lesion is depicted in figure 4.

NIRS alone however is limited by its inability to provide information about the lumen

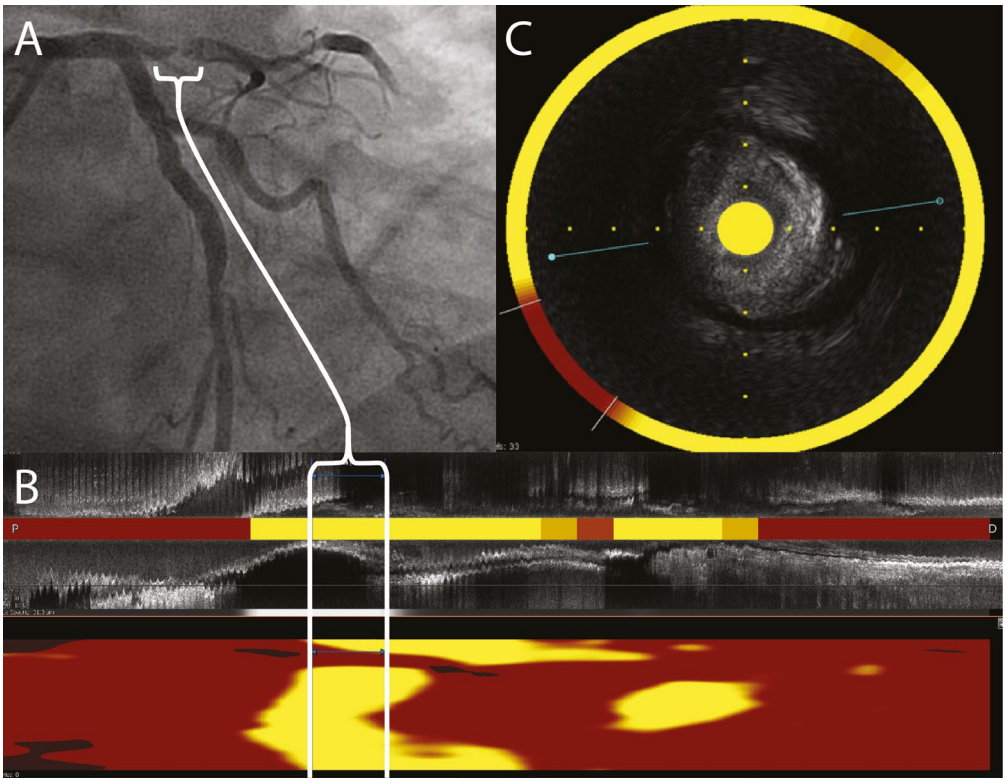

Figure 4. NIRS findings in a 62 year old male presenting with an anterior STEMI
(A) Initial angiogram shows a culprit lesion in the proximal LAD with a filling defect consistent with thrombus (white brackets) resulting in TIMI 1 flow. NIRS-IVUS was obtained after angioplasty using an undersized balloon to establish TIMI 3 flow and automatically co-registered longitudinal and cross-sectional images are represented in (B) and (C) respectively. The white brackets in the longitudinal images indicate the location of the culprit lesion. (B) NIRS chemogram demonstrates a large lipid-rich plaque (maxLCBI4mm = 880) at the site of the culprit lesion. (C) Cross-sectional NIRS-IVUS image of the culprit lesion confirms a large stenotic lipid-rich plaque. Courtesy of Ryan Madder, MD, Spectrum Health, Grand Rapids, Michigan, USA

and plaque depth. Therefore NIRS is commonly combined with IVUS in a combined NIRS-IVUS catheter, in which both techniques can be acquired simultaneously in one pullback. Multiple post-mortem studies have compared the ability of NIRS and gray-scale IVUS alone versus combined NIRS-IVUS to identify fibroatheroma and showed that combined NIRS-IVUS was superior to NIRS or IVUS alone.(90,91) In vivo studies have shown that with NIRS-IVUS, $LCBI_{4mm}$ with a cut-off of >400 was able to identify culprit lesions in patients with STEMI,(92) non-STEMI and unstable angina.(93) A recent prospective observational study investigated the prognostic value of NIRS in non-culprit vessels in patients with ACS or stable angina referred for PCI. The authors found that LCBI above the median was a significant predictor for the

occurrence of mortality, non-fatal ACS, stroke and unplanned revascularization within 1 year follow-up.(94) Although analysis was done on a patient-level, a high LCBI might be an important feature of the suspected vulnerable plaque. Two prospective trials examining the natural history of non-culprit lesions with high LCBI at NIRS are currently enrolling patients, i.e. the PROSPECT II trial (NCT02171065) and the LRP study (NCT02033694).

Non-invasive imaging

Next to invasive imaging modalities, coronary computed tomography angiography (CCTA), positron emission tomography (PET) and magnetic resonance imaging (MRI) have emerged as possible non-invasive alternatives to visualize the vulnerable plaque. The characteristics of these imaging modalities are summarized in table 2 and will be discussed in this section.

Coronary computed tomography angiography (CCTA)

CCTA is a widely available non-invasive imaging tool with a relatively high spatial resolution that allows visualization of different components of the vulnerable plaque,(95) as is illustrated in figure 5.

In accordance with autopsy and IVUS, positive remodeling is a suspected feature of CCTA-derived plaque vulnerability.(16,53-56,96-99) In a direct comparison between CCTA and VH-IVUS, Kröner et al. reported that plaques with positive remodeling had larger necrotic cores and were more frequent VH-TCFA than plaques without positive remodeling.(96) Furthermore, a recent meta-analysis by Thomsen at al. showed that the remodeling index was higher in patients with ACS than in patients with stable angina and in culprit lesions versus non-culprit lesions.(99)

CCTA uses CT-attenuation, expressed in Hounsfield Units, to differentiate between calcified plaques with higher attenuation and partially- and non-calcified plaques with lower attenuation. Low-attenuation plaques (LAP) have been shown to correlate with lipid rich plaques assessed by VH-IVUS.(100-102) Furthermore, studies that compare CCTA with OCT have reported that both positive remodeling and LAP were associated with OCT-derived TCFA (98) and OCT-derived TCFA with macrophage infiltration.

Table 2. Non-invasive imaging modalities and vulnerable plaque features

	CCTA (95)	FDG-PET (117)	NaF-PET (117)	MRI (135)
Technical characteristics				
Iodine contrast agent	Yes	No	No	No
Radionuclide tracer	No	^{18}F-fluoro-deoxyglucose	^{18}F-sodium fluoride	No
Use of CT	High-dose CT	Low-dose AC CT	Low-dose AC CT	No
Radiation burden	+	++	++	-
Spatial resolution (mm)	~ 0.4	~ 4 - 5	~ 4 - 5	~ 0,5 - 1
Patient preparation	Nitroglycerin sl and heartrate reduction with beta-blockers	Low-carbohydrate diet and/or fasting	-	-
Vulnerable plaque features				
Remodelling	++ (96,97,188)	-	-	-
Lipid core	+ (97,98, 101,102)	-	-	+ (130)
Plaque rupture	-	-	-	-
Thin fibrous cap	-	-	-	-
Inflammation	-	+ (120)	-	-
Neovascularization	-	-	-	-
Intra-plaque hemorraghe	-	-	-	+ (130)
Microcalcification	-	-	++ (124)	-
Spotty calcification	++ (106,107)	-	-	-

CCTA = Coronary Computed Tomography Angiography; Positron Emission Tomography; MRI = Magnetic Resonance Imaging; AC = Attenuation Correction; sl = sublingual

(97) However, many studies report important overlap in CT densities between lipid-rich and fibrous plaques, thus somewhat limiting the ability of CT attenuation to reliably identify lipid-rich plaques.(100-102)

As in IVUS studies,(24,57-60) some CCTA studies have suggested that not only LAP, but also plaques with spotty calcification might be considered vulnerable.(103-105) The aforementioned meta-analysis by Thomsen at al. reported that plaques with spotty calcification were associated with ACS rather than stable angina and with culprit rather than non-culprit lesions.(99) Furthermore CCTA-derived spotty calcification has been shown to correlate well with IVUS-derived spotty calcification (106) and is shown to correlate with VH-TCFA and a large necrotic core on IVUS.(107)

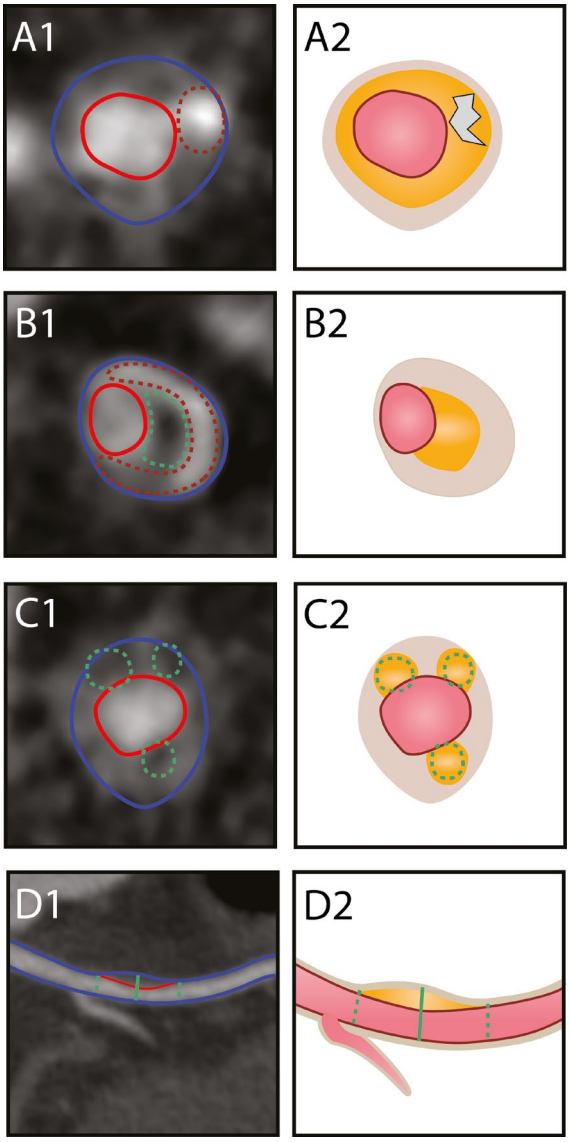

Figure 5. Vulnerable plaque features visualized by CCTA with corresponding illustrations
(A) Short axis CT view of a coronary plaque with spotty calcification. (B) Cross-sectional CT image showing a center of low attenuation in contact with the lumen (green dashed line) surrounded by a ring-like area of higher attenuation (red dashed line): a napkin ring sign (B1). The center of low-attenuation corresponds with a lipid core, whereas the higher attenuation area represents fibrous tissue (B2). (C) Cross-sectional CT image of a coronary plaque with areas with low CT attenuation (green dashed line), defined by less than 30 Hounsfield Units (C1). The corresponding illustration (C2) shows that a low-attenuation area represents a lipid-rich core. (D) Curved multi-planar reconstruction showing a moderate stenosis with positive (outward) remodeling of the vessel wall (D1). The maximal vessel diameter (solid green line) is greater than the proximal and distal reference diameter (dashed green lines).

The napkin-ring sign is an additional suspected CT feature of plaque vulnerability and represents a necrotic core with low attenuation surrounded by a ring-like area of higher attenuation.(108-112) Recent autopsy studies on human donor hearts confirmed the presence of a large necrotic core in plaques with a napkin-ring sign (108) and showed excellent diagnostic accuracy of the napkin-ring sign for TCFA. (109) Studies comparing OCT and CCTA have reported conflicting results on the value of the CCTA napkin-ring sign.(97,110,112) Some studies reported a correlation between napkin-ring sign and OCT-derived TCFA,(110,112) whereas a recent study by Nakazato et al. showed no correlation between the napkin-ring sign and TCFA with macrophage infiltration.(97)

To evaluate the prognostic value of the suspected CT features of the vulnerable plaque, studies on the natural history of these components are needed. The first prospective observational study by Motoyama et al. studying the prognostic value of LAP, positive remodeling and spotty calcification, reported that both LAP and positive remodeling at CCTA were independent predictors for the occurrence of MACE in short term follow up, whereas spotty calcification was not.(113) Motoyama and colleagues recently confirmed the prognostic value of LAP and positive remodeling in the same cohort for the mid-term follow-up (3.9 ± 2.4 years).(36) Furthermore, a prospective study with 895 patients and a mean follow-up of 2.3 years, reported that the napkin-ring sign in addition to LAP and positive remodeling, was independently associated with a composite endpoint of ACS and cardiac death.(111) However, because these studies used MACE on a patient-level as outcome, the events did not necessarily correlate with the specific CCTA-derived vulnerable plaque. While LAP, positive remodeling and the napkin-ring sign appear as important features of CT-derived plaque vulnerability, the impact of spotty calcification remains somewhat unclear.

Limited studies with serial CCTA imaging have evaluated the natural history of the suspected CCTA-derived vulnerable plaque.(36,37) In the previously mentioned study by Motoyama et al., 423 patient with serial CCTA imaging after a median of 4.1 years were included for analysis.(36) The authors reported that of all patients with high-risk plaques at baseline, which was defined by either positive remodeling or LAP, 93% had high-risk plaques at follow-up and 7% of non-high risk plaques progressed to high risk plaques at follow-up. Furthermore, patients with serial CCTA imaging in the

PROSPECT study showed an increase in plaque volume over time accommodated by expansive remodeling.(37) The ongoing multi-centre PARADIGM study will include 5000 patients and perform serial CCTA after 2 years to assess the natural history of coronary plaques on CCTA over time (NCT02803411).

The added value of CCTA imaging of suspected vulnerable plaques has also been demonstrated in patients presenting with acute chest pain.(104,114) Kristensen et al. reported that in patients with NSTEMI the amount of non-calcified plaque volume in non-obstructive lesions was an independent predictor for the occurrence of MACE during follow-up.(114) The ROMICAT-II trial investigated patients presenting to the emergency room with acute chest pain but negative initial electrocardiography and troponin by CCTA imaging. The presence of any of the suspected vulnerable plaque features was an independent predictor for the presence of ACS.(104) CCTA might have a role in establishing both the diagnosis and the prognosis in patients with ACS.

Plaque quantification and characterization by automated software has been proposed to increase prognostic value of CCTA in recent years and studies have shown good correlation with VH-IVUS quantitative measures.(101,102) Furthermore, coronary plaques labeled lipid-rich and/or positive remodeled by automated software are reported to be more frequent in NSTEMI than in patients with stable angina.(115) Versteylen et al. have recently demonstrated that a semi-automated approach in which plaques are manually identified followed by automatic characterization and quantification, provided incremental prognostic value to conventional CT reading for the occurrence of MACE.(116)

Positron Emission Tomography (PET)

Although widely used in oncology for several decades, 18F-fluorodeoxyglucose (18F-FDG) and 18F-sodium fluoride (18F-NaF) have only recently been proposed in the imaging of atherosclerosis.

18F-FDG is a radiolabeled glucose analogue and its uptake determined by PET imaging can be used as a surrogate for metabolic activity.(117) 18F-FDG uptake has been linked with increased plaque macrophage density in animal models (118,119) and in human carotid arteries after endarterectomy (120) and is considered to be a

marker of plaque inflammation and vulnerability. The use of 18F-FDG imaging in coronary artery disease is, however, limited by the high background 18F-FDG uptake caused by the glucose metabolism of the myocardium. Studies regarding FDG imaging of the coronary arteries have therefore shown conflicting results.(121-123) Rogers and colleagues reported that in a group of 25 patients FDG uptake was significantly higher in culprit lesions in ACS than in lesions stented for stable CAD. (121) Although the results were in line with findings from Cheng et al. in a similar population,(123) a more recent study on 40 patients with acute myocardial infarction showed no difference in uptake between culprit lesions and non-culprit lesions.(122)

18F-NaF is a PET tracer that detects areas of microcalcification by binding to hydroxyapatite, and is not hampered by uptake in the myocardium.(124) Unlike macrocalcification which can be visualized by CT, these microcalcifications are considered an important feature of the vulnerable plaque.(22) The prognostic value of 18F-NaF uptake was recently confirmed in a prospective study that showed that 18F-NaF uptake was higher in culprit lesions than in non-culprit lesions in patients after myocardial infarction and in patients with symptomatic carotid artery disease. (122) Furthermore, 18F-NaF uptake showed a trend for the identification of TCFA on intravascular ultrasound (p=0.068). 18F-NaF PET imaging appears a promising imaging technique for the non-invasive identification of vulnerable plaques. The PREFFIR study was designed to investigate the natural history of coronary plaques with high 18F-NaF uptake in patients after myocardial infarction and results are expected in 2019. (NCT02278211)

Recently, pre-clinical and early clinical data have proposed the use of several PET tracers that target macrophages for the imaging of atherosclerosis. 68Ga-DOTATATE is a PET tracer that targets up-regulated somatostatine receptor 2 in macrophages and its uptake is reported to be co-localized with macrophage-rich plaques in an atherosclerotic mouse model.(125) In humans, the uptake of 68Ga-DOTATATE has been associated with coronary calcification and clinical risk profile.(126) Another macrophage targeted tracer 11C-PK11195, a selective ligand of the translocator protein highly expressed on macrophages, has been reported to have increased uptake in carotid plaques in patients with symptomatic carotid artery disease.(127) Furthermore, 18F-Galacto-RGD is a PET tracer that specifically binds integrin alpha(v)beta(3),

which is expressed by macrophages and endothelial cells in atherosclerotic lesions. An early clinical study reported accumulation of this tracer in obstructive carotid atherosclerosis.(128) Further translational studies are needed to clarify the ability of these tracers to target suspected vulnerable plaques.

Magnetic Resonance Imaging (MRI)

Magnetic Resonance Imaging (MRI) has been widely used in carotid artery disease to differentiate between plaque components and to study high-risk plaque features.(129) The identification of intra-plaque hemorrhage, lipid core, fibrous tissue components and calcification can be achieved by the use of several MRI image techniques, i.e. pre and post contrast T1-weighted, T2-weighted, proton-density and time-of-flight (TOF) imaging, The use of MRI in coronary arteries however is limited by its relatively low spatial resolution and by cardiac and respiratory motion. Despite these limitations, the use of MRI, has shown some potential in coronary artery disease.(130) A post-mortem study on 28 plaques obtained from human donor hearts has reported an excellent correlation of ex-vivo T1-, T2-weighted and ultrashort echo time MRI with histology for the identification of calcified and lipid-rich coronary plaques.(130) Several studies have investigated the potential of T1-weighted imaging co-registered with Magnetic Resonance Angiography (MRA) in patients with coronary artery disease.(131-134) High signal intensity on T1-weighted images is reported to be a marker for intra-plaque hemorrhage and intra-coronary thrombus and is shown to be associated with IVUS-derived positive remodeling(131), with low CT-attenuation(131) and with OCT-derived intracoronary thrombus (132,134), macrophage accumulation(133), lipid-rich plaque, plaque rupture, and TCFA,(134) Noguchi and colleagues prospectively studied 650 patients with suspected or known CAD and showed that high-intensity plaques on T1-weighted images were associated with a worse MACE-free survival on a patient-level.(135) There is currently no data on the ability of T1-weighted MRI imaging to identify lesion-specific MACE.

As mentioned previously T2-weighted, proton-density and time-of-flight (TOF) imaging are used next to T1-weighted images in carotid artery disease to differentiate between plaque components. Studies that report on the value of these techniques in coronary artery disease are limited to animal studies and case reports. In a porchine

model of coronary balloon injury T2-weighted imaging enabled detection of coronary vessel wall edema in good correlation with histology.(136) Further studies are needed to evaluate the role of the various MRI techniques in the visualization of the suspected vulnerable plaque.

Treatment of vulnerable plaques

Local therapy

Current management guidelines focus on identifying and revascularizing obstructive coronary stenoses that cause a haemodynamically significant reduction in coronary blood flow,(137,138) Despite extensive validation of this flow-limiting guided revascularization strategy in large prospective randomized trials, such as the FAME and DEFER trial,(139,140) the event rate after complete revascularization remains relatively high with MACE occurring in approximately 30% of patients after 5 years (FAME trial)(139). Serial angiography studies have shown that, although plaques leading to ACS are frequently flow-limiting, coronary lesions with initially mild stenosis often rapidly progress in the weeks to months prior to an ACS.(141) As discussed in the previous section different aspects of plaque vulnerability are shown to have independent prognostic value for the occurrence of MACE and might be used to improve risk stratification and guide personalized therapy.

The PRAMI study reported a reduced risk of adverse cardiovascular events after revascularization of residual coronary artery disease in STEMI patients after primary PCI of infarct-artery.(142) Given that approximately 35% of intermediate lesions are haemodynamically significant,(143) sealing of non-obstructive vulnerable plaques is a potential explanation of improved outcome in the PRAMI study. However, no definite evidence exists that this is indeed the mechanism responsible for the improved outcome. The first-in-human trial of attempted sealing of non-obstructive high-risk plaques was the SECRITT trial. In this trial a nitinol self-expanding stent was implanted in a non-obstructive VH-TCFA with thin-cap at OCT in 13 patients and revealed recovery of neo-cap thickness without complications at 6 months follow up.(144) Instead of placing a traditional bare metal stent (BMS), the use of a bioabsorbable vascular scaffold (BVS) may avoid long-term detrimental effects such as late stent thrombosis,

by dissolving ultimately and facilitating restoration of normal coronary physiology. Implantation of an everolimus-eluting BVS in a porcine coronary artery model showed complete dissolution of the struts after 3 years by both OCT and histology and showed a fibromuscular neointima covering the plaque.(145) In an in-human study, Brugaletta et al revealed formation of a thick neointima in 58 patients who received an ABSORB BVS, with a mean neo-intima thickness of 210 μm after 6 months and 220μm after 12 months.(146) A recent post-hoc analysis, using data from the ABSORB cohort B trial, the SECRITT trial and the Svelte first-in-man trial, evaluated changes in plaque morphology after BVS and BMS implantation.(147) Serial OCT showed development of a neo-intima over TCFA, both after BVS and BMS implantation, thus sealing the plaque and transforming the TCFA to a thick-cap fibroatheroma. Furthermore after BVS implantation the neointima development continued after short-term follow-up without compromising luminal dimensions, whereas neo-intima formation following BMS placement caused reduction in luminal dimensions and ceased after 6 months. Although evidence is limited these findings suggest the feasibility of BVS to seal non-obstructive vulnerable plaques. Currently, three randomized trials that address this issue are including patients (table 3).

The PROSPECT-ABSORB, will randomize patients after STEMI/NSTEMI with residual non-obstructive lesions and vulnerability as assessed by IVUS to either BVS implantation with optimal medical therapy or optimal medical therapy only (NCT02171065). The PECTUS trial has a similar study design, although it will incorporate OCT as a gatekeeper for the detection of plaque vulnerability (NTR5590). The PREVENT study will use both IVUS, NIRS and OCT to assess plaque vulnerability and guide BVS implantation (NCT02316886). These trials will likely shed light on this much-debated topic. Potentially, future coronary revascularization strategies may not solely be dictated by hemodynamic significance of coronary stenoses, but also by plaque composition and subsequent risk of rupturing.

Systemic therapy

Although local treatment of an individual vulnerable plaque is appealing, it fails to address the fact that atherosclerosis is a systemic disease. Various systemic therapies have been proposed to reduce plaque vulnerability (table 4).

Table 3. On-going clinical trial on the preventive local treatment of vulnerable plaques.

	PROSPECT-ABSORB	PECTUS	PREVENT
Number of patients	300	500	1600
Date of start inclusion	06-2014	03-2016	10-2015
Planned primary completion date	12-2019	03-2020	01-2019
Imaging modality	IVUS	OCT	IVUS, NIRS and/or OCT
Definition for plaque vulnerability	Plaque burden ≥70%	2 of the following: - Thin fibrous cap (<65µm) - Large arc of the lipid pool (>90 degrees) - Intra-coronary thrombus or plaque disruption	2 of the following: - IVUS MLA <4mm^2 - IVUS plaque burden >70% - Lipid rich plaque on NIRS - TCFA defined by OCT or VH-IVUS
Intervention	PCI with BVS placement (ABSORB)	PCI with BVS placement (ABSORB)	PCI with BVS placement
Control	OMT	OMT	OMT
Primary endpoint	Minimal luminal area at randomized non-culprit lesion site	Composite of all-cause mortality, non-fatal MI, or unplanned revascularization at one year FU	Composite of cardiovascular death, non-fatal MI, unplanned hospitalization due to unstable angina after 24 months FU
Powered for reduction in clinical endpoints	No	Yes	Yes

BVS = bioabsorbable vascular scaffold; FU = follow-up; IVUS = intravascular ultrasound; IVUS-NIRS = intravascular ultrasound – near-infrared spectroscopy; MI = myocardial infarction; NIRS = near-infrared spectroscopy; OCT = optical coherence tomography; OMT = optimal medical therapy; PCI = percutaneous coronary intervention; TCFA = thin-cap fibroatheroma; VH-IVUS = virtual-histology intravascular ultrasound

LDL-lowering drugs

The mortality benefit of LDL-lowering therapy by use of statins is well established (148) and its use in patients with CAD is advocated by current guidelines.(137,138) In addition to their lipid-lowering properties statins are reported to possess pleotropic effects, i.e. enhancement of endothelial function and decrease of oxidative stress and inflammation.(149) The effects of statins on coronary plaque progression in vivo have been investigated by various imaging modalities. Serial CCTA studies have shown that initiation of statin therapy reduces progression of non-calcified plaque volume (150-152) and even progression in LAP volume.(150) Furthermore, a recent trial randomized

Table 4. Systemic treatment proposed to reduce plaque vulnerability

Drug	Method of action	Imaging studies	Clinical endpoint trials
LDL-lowering drugs			
Statin	HMG-CoA reductase inhibition	↑ OCT-derived fibrous cap thickness (159,160) ↓ IVUS-derived high-risk plaque features (157,159)	↓ Major vascular events (RR 0.78) (148) *
Ezetimibe	NPC1L1 protein blockage	↓ IVUS-derived plaque burden and ↑ negative remodelling (162) ↑ OCT-derived fibrous cap thickness (163)	↓ MACE (HR 0.94) (161) †
Alirocumab, bococizumab, evolocumab	PCSK9 inhibition	↓ IVUS-derived plaque burden (167)	Pending (169-171)
Anti-inflammatory drugs			
Darapladib, varespladib	Lp-PLA2 inhibition	↓ IVUS-derived necrotic core (176)	No reduction in MACE (178,179) ‡ ↑ MI (HR 1.66) (177) §
Methotrexate	Antagonization of folic acid	N/A	Pending (181)
Colchicine	Disruption of microtubule formation	N/A	↓ MACE (HR 0.33) (184) ‖
Canakinumab	Neutralization of IL-1β	N/A	Pending (187)

* Meta-analysis of 26 randomized trials showing reduction in major vascular events. † Reduction in primary composite endpoint of death from cardiovascular causes, major coronary event, or nonfatal stroke. ‡ Darapladib: no reduction in composite endpoint of cardiovascular death, myocardial infarction, (urgent revascularization) or stroke. § Varespladib: increase in the secondary endpoint of myocardial infarction at interim analysis. ‖ Reduction in composite endpoint of acute coronary syndrome, out-of-hospital cardiac arrest, or noncardioembolic ischemic stroke. HMG-CoA = 3-hydroxy-3-methylglutaryl-coenzyme A; OCT = optical coherence tomography; IVUS = intravascular ultrasound; NPC1L1 = Niemann-Pick C1-Like 1; MACE = major adverse cardiac events; PCSK9 = Proprotein convertase subtilisin/kexin type 9; Lp-PLA2 = Lipoprotein-associated phospholipase A2; MI = myocardial infarction; IL-1β = Interleukine-1 beta

patients between high intensity and standard statin therapy and showed increase in dense calcium volume, implicating possible plaque stabilization.(153) Several serial IVUS studies have shown that high-intensity statin therapy induces regression in plaque burden.(154-156) This was recently confirmed by a post hoc analysis including data from 3495 patients.(157) In addition to reduction of plaque burden, the authors reported that statin therapy induces plaque calcification, which is associated with plaque stabilization.(157) Kataoka et al. published pooled data from 8 clinical trials on the beneficial effect of statins in IVUS-derived high-risk plaques (large atheroma

volume, positive remodeling and spotty calcification).(158) The authors reported that atheroma regression was highest in patients with high-risk plaques, suggesting a plaque stabilizing effect of statin therapy. This is supported by findings from OCT studies.(159,160) Kataoka and colleagues reported that high intensity statin therapy in patients with stable CAD is associated with less vulnerable plaque features on OCT, i.e. thicker fibrous cap and smaller lipid arc.(159) Furthermore, the EASY-FIT study showed that in patients with unstable angina high intensity statin therapy provided greater increase in fibrous cap thickness than low intensity statin therapy.(160) Since this increase in cap thickness was associated with decrease in inflammatory biomarkers, it is believed that in addition to the LDL-lowering action, anti-inflammatory effects of statin therapy may influence plaque vulnerability.

The IMPROVE-IT trial(161) with a total number of 18144 patients showed a reduction in adverse cardiac events in patients on ezetimibe and simvastatin versus simvastatin only and paved the way for the introduction of ezetimibe into treatment guidelines.(138) A randomized clinical trial with serial IVUS imaging showed that combination therapy of ezetimibe and statin was correlated with negative vessel remodelling and produced stronger coronary plaque regression than statin therapy alone.(162) A small single center randomized study showed that addition of ezetimibe to fluvastatin resulted in a larger increase in fibrous cap thickness measured by OCT.(163)

Recently, a novel class of LDL-lowering drugs called proprotein convertase subtilisin–kexin type 9 (PCSK9) inhibitors has emerged. PCSK9 binds to the LDL receptor leading to destruction of the receptor and thereby preventing the recirculation of LDL receptor to the hepatocyte cell surface. Through the inhibition of PCKS9, these novel drugs significantly reduce LDL cholesterol levels when added to statin therapy.(164) PCKS9 levels are linearly associated with necrotic core size of plaques in non-culprit coronary arteries.(165) The impact of PCSK9 inhibition on plaque vulnerability remains to be elucidated, but one PCKS9 inhibtor, alirocumab, is reported to reduce plaque macrophage and necrotic core content in a mouse model of atherosclerosis.(166) The recently published GLAGOV trial, reported a reduction in IVUS-derived plaque atheroma volume in patients treated with evolocumab for 78 weeks.(167) In a post-hoc analysis of the ODYSSEY LONG TERM study, addition of a PCKS9 inhibitor to statin therapy resulted in better MACE-free survival (defined as death from coronary

heart disease, nonfatal myocardial infarction, ischemic stroke, or unstable angina requiring hospitalization).(168) Larger prospective clinical trials with hard clinical endpoints are currently enrolling and will provide more information on the added value of PCSK9 inhibition.(169-171)

Anti-inflammatory drugs

Inflammation plays a key role in plaque formation and vulnerability.(172,173) Several anti-inflammatory therapies have been proposed to reduce atherosclerotic burden and stabilize coronary plaques.(174)

Lipoprotein-associated phospholipase A2 (Lp-PLA2) is an enzyme produced and secreted by inflammatory cells centrally involved in atherosclerosis and is highly expressed in the necrotic core of atherosclerotic plaques.(175) Lp-PLA2 inhibition has been proposed as a therapeutic agent targeting the vulnerable plaque. While a randomized placebo controlled trial reported a reduction in IVUS-derived necrotic core development,(176) large randomized trials on the benefit of Lp-PLA2 inhibitors on clinical endpoints have so far been negative.(177-179)

Methotrexate is a folic acid antagonist with anti-inflammatory actions and is used for the treatment of several autoimmune disorders. A large meta-analysis of observational studies in patients receiving low-dose methotrexate for psoriasis and rheumatoid arthritis showed a reduction in cardiovascular events.(180) The CIRT trial was designed to investigate the ability of low dose methotrexate to prevent future coronary events in patients after myocardial infarction.(181)

The anti-inflammatory activity of colchicine is used in the treatment of inflammatory conditions such as gout, pericarditis and familial Mediterranean fever. Retrospective studies have shown indirect support for the use of colchicine in atherosclerosis by reporting lower prevalence of myocardial infarction in colchicine-treated patients suffering from gout(182) and familial Mediterranean fever(183). This was confirmed by the LoDoCo trial, a randomized placebo controlled trial with 532 patients with stable CAD and median follow-up of 3 years, showing improved MACE-free survival in patients treated with colchicine.(184) The LoDoCo-2 trial will investigate the effects of colchicine in 3000 patients over 3 years and is scheduled to be completed in 2019

(ACTRN12614000093684).

Canakinumab is a monoclonal antibody that selectively neutralizes IL-1β, a pro-inflammatory cytokine that plays multiple roles in atherosclerosis and rupture prone plaques.(185) A recent phase IIb trial with 556 patients, has shown that subcutaneous injection of canakinumab is well tolerated and reduces different biomarkers of inflammation, i.e. CRP, IL-6 and fibrinogen.(186) The CANTOS trial has finalized enrollment of 10120 patients and is awaiting follow-up to report on the possible reduction of recurrent MACE by canakinumab in patients after myocardial infarction. (187)

Conclusions and future perspectives

Recent advances in invasive as well as non-invasive imaging modalities have improved the potential for early and accurate identification of vulnerable coronary plaques. Although several imaging studies have been published on the natural history of suspected vulnerable coronary plaques, more evidence is warranted to establish the prognostic value of the various invasive and non-invasive plaque characteristics. Novel applications of invasive imaging modalities such as IVUS, OCT and NIRS have paved the way for the evaluation of therapeutic agents specifically targeted at reducing plaque vulnerability. In the future, reliable non-invasive imaging modalities are crucial for the detection and treatment of vulnerable plaque in larger and lower risk populations. Preliminary data have shown potential for pre-emptive local treatment of vulnerable coronary plaques with PCI and this strategy is currently being investigated in the PROSPECT ABSORB, the PECTUS trial and the PREVENT. Statin therapy has been shown to induce plaque stabilization and lead to a significant reduction in cardiovascular events. The effects of other systemic, mostly anti-inflammatory, drug therapies on cardiovascular outcome are currently being studied in large clinical trials. Results from these studies may guide in proper decision making pertaining the management of vulnerable plaques in patients with myocardial infarction to prevent future ACS. Nonetheless, an era of personalized treatment for patients with CAD seems both inevitable and indispensable.

References

1. Bentzon J.F., Otsuka F., Virmani R., Falk E. Mechanisms of plaque formation and rupture. Circ Res 2014;114:1852-1866
2. Schaar J.A., Muller J.E., Falk E., et al. Terminology for high-risk and vulnerable coronary artery plaques. Report of a meeting on the vulnerable plaque, June 17 and 18, 2003, Santorini, Greece. Eur Heart J 2004;25:1077-1082
3. Waxman S., Ishibashi F., Muller J.E. Detection and treatment of vulnerable plaques and vulnerable patients: novel approaches to prevention of coronary events. Circulation 2006;114:2390-2411
4. Virmani R., Kolodgie F.D., Burke A.P., Farb A., Schwartz S.M. Lessons from sudden coronary death: a comprehensive morphological classification scheme for atherosclerotic lesions. Arterioscler Thromb Vasc Biol 2000;20:1262-1275
5. Yahagi K., Kolodgie F.D., Otsuka F., et al. Pathophysiology of native coronary, vein graft, and in-stent atherosclerosis. Nat Rev Cardiol 2016;13:79-98
6. Falk E., Nakano M., Bentzon J.F., Finn A.V., Virmani R. Update on acute coronary syndromes: the pathologists' view. Eur Heart J 2013;34:719-728
7. Xu Y., Mintz G.S., Tam A., et al. Prevalence, distribution, predictors, and outcomes of patients with calcified nodules in native coronary arteries: a 3-vessel intravascular ultrasound analysis from Providing Regional Observations to Study Predictors of Events in the Coronary Tree (PROSPECT). Circulation 2012;126:537-545
8. Muller J.E., Tofler G.H., Stone P.H. Circadian variation and triggers of onset of acute cardiovascular disease. Circulation 1989;79:733-743
9. Davies M.J. The pathophysiology of acute coronary syndromes. Heart 2000;83:361-366
10. Stone G.W., Maehara A., Mintz G.S. The reality of vulnerable plaque detection. JACC Cardiovasc Imaging 2011;4:902-904
11. Burke A.P., Farb A., Malcom G.T., Liang Y.H., Smialek J., Virmani R. Coronary risk factors and plaque morphology in men with coronary disease who died suddenly. N Engl J Med 1997;336:1276-1282
12. Narula J., Nakano M., Virmani R., et al. Histopathologic characteristics of atherosclerotic coronary disease and implications of the findings for the invasive and noninvasive detection of vulnerable plaques. J Am Coll Cardiol 2013;61:1041-1051
13. Virmani R., Burke A.P., Farb A., Kolodgie F.D. Pathology of the vulnerable plaque. J Am Coll Cardiol 2006;47:C13-C18
14. Kolodgie F.D., Burke A.P., Farb A., et al. The thin-cap fibroatheroma: a type of vulnerable plaque: the major precursor lesion to acute coronary syndromes. Curr Opin Cardiol

2001;16:285-292
15. Libby P., Geng Y.J., Aikawa M., et al. Macrophages and atherosclerotic plaque stability. Curr Opin Lipidol 1996;7:330-335
16. Varnava A.M., Mills P.G., Davies M.J. Relationship between coronary artery remodeling and plaque vulnerability. Circulation 2002;105:939-943
17. Narula J., Strauss H.W. The popcorn plaques. Nat Med 2007;13:532-534
18. Sluimer J.C., Kolodgie F.D., Bijnens A.P., et al. Thin-walled microvessels in human coronary atherosclerotic plaques show incomplete endothelial junctions relevance of compromised structural integrity for intraplaque microvascular leakage. J Am Coll Cardiol 2009;53:1517-1527
19. Virmani R., Kolodgie F.D., Burke A.P., et al. Atherosclerotic plaque progression and vulnerability to rupture: angiogenesis as a source of intraplaque hemorrhage. Arterioscler Thromb Vasc Biol 2005;25:2054-2061
20. Kolodgie F.D., Gold H.K., Burke A.P., et al. Intraplaque hemorrhage and progression of coronary atheroma. N Engl J Med 2003;349:2316-2325
21. Kockx M.M., De Meyer G.R., Muhring J., Jacob W., Bult H., Herman A.G. Apoptosis and related proteins in different stages of human atherosclerotic plaques. Circulation 1998;97:2307-2315
22. Joshi N.V., Vesey A., Newby D.E., Dweck M.R. Will 18F-sodium fluoride PET-CT imaging be the magic bullet for identifying vulnerable coronary atherosclerotic plaques? Curr Cardiol Rep 2014;16:521
23. Vengrenyuk Y., Carlier S., Xanthos S., et al. A hypothesis for vulnerable plaque rupture due to stress-induced debonding around cellular microcalcifications in thin fibrous caps. Proc Natl Acad Sci U S A 2006;103:14678-14683
24. Ehara S., Kobayashi Y., Yoshiyama M., et al. Spotty calcification typifies the culprit plaque in patients with acute myocardial infarction: an intravascular ultrasound study. Circulation 2004;110:3424-3429
25. Saia F., Komukai K., Capodanno D., et al. Eroded Versus Ruptured Plaques at the Culprit Site of STEMI: In Vivo Pathophysiological Features and Response to Primary PCI. JACC Cardiovasc Imaging 2015;8:566-575
26. Jia H., Abtahian F., Aguirre A.D., et al. In vivo diagnosis of plaque erosion and calcified nodule in patients with acute coronary syndrome by intravascular optical coherence tomography. J Am Coll Cardiol 2013;62:1748-1758
27. Higuma T., Soeda T., Abe N., et al. A Combined Optical Coherence Tomography and Intravascular Ultrasound Study on Plaque Rupture, Plaque Erosion, and Calcified Nodule in Patients With ST-Segment Elevation Myocardial Infarction: Incidence,

Morphologic Characteristics, and Outcomes After Percutaneous Coronary Intervention. JACC Cardiovasc Interv 2015;8:1166-1176

28. Ino Y., Kubo T., Tanaka A., et al. Difference of culprit lesion morphologies between ST-segment elevation myocardial infarction and non-ST-segment elevation acute coronary syndrome: an optical coherence tomography study. JACC Cardiovasc Interv 2011;4:76-82
29. Kubo T., Imanishi T., Takarada S., et al. Assessment of culprit lesion morphology in acute myocardial infarction: ability of optical coherence tomography compared with intravascular ultrasound and coronary angioscopy. J Am Coll Cardiol 2007;50:933-939
30. Arbab-Zadeh A., Fuster V. The myth of the "vulnerable plaque": transitioning from a focus on individual lesions to atherosclerotic disease burden for coronary artery disease risk assessment. J Am Coll Cardiol 2015;65:846-855
31. Burke A.P., Kolodgie F.D., Farb A., et al. Healed plaque ruptures and sudden coronary death: evidence that subclinical rupture has a role in plaque progression. Circulation 2001;103:934-940
32. Park H.B., Heo R., Hartaigh B., et al. Atherosclerotic plaque characteristics by CT angiography identify coronary lesions that cause ischemia: a direct comparison to fractional flow reserve. JACC Cardiovasc Imaging 2015;8:1-10
33. Naghavi M., Libby P., Falk E., et al. From vulnerable plaque to vulnerable patient: a call for new definitions and risk assessment strategies: Part I. Circulation 2003;108:1664-1672
34. Kubo T., Maehara A., Mintz G.S., et al. The dynamic nature of coronary artery lesion morphology assessed by serial virtual histology intravascular ultrasound tissue characterization. J Am Coll Cardiol 2010;55:1590-1597
35. Zhao Z., Witzenbichler B., Mintz G.S., et al. Dynamic nature of nonculprit coronary artery lesion morphology in STEMI: a serial IVUS analysis from the HORIZONS-AMI trial. JACC Cardiovasc Imaging 2013;6:86-95
36. Motoyama S., Ito H., Sarai M., et al. Plaque Characterization by Coronary Computed Tomography Angiography and the Likelihood of Acute Coronary Events in Mid-Term Follow-Up. J Am Coll Cardiol 2015;66:337-346
37. Papadopoulou S.L., Neefjes L.A., Garcia-Garcia H.M., et al. Natural history of coronary atherosclerosis by multislice computed tomography. JACC Cardiovasc Imaging 2012;5:S28-S37
38. Garcia-Garcia H.M., Gogas B.D., Serruys P.W., Bruining N. IVUS-based imaging modalities for tissue characterization: similarities and differences. Int J Cardiovasc Imaging 2011;27:215-224

39. Sangiorgi G.M., Clementi F., Cola C., Biondi-Zoccai G. Plaque vulnerability and related coronary event prediction by intravascular ultrasound with virtual histology: "it's a long way to tipperary"? Catheter Cardiovasc Interv 2007;70:203-210
40. Garcia-Garcia H.M., Mintz G.S., Lerman A., et al. Tissue characterisation using intravascular radiofrequency data analysis: recommendations for acquisition, analysis, interpretation and reporting. EuroIntervention 2009;5:177-189
41. Nair A., Kuban B.D., Tuzcu E.M., Schoenhagen P., Nissen S.E., Vince D.G. Coronary plaque classification with intravascular ultrasound radiofrequency data analysis. Circulation 2002;106:2200-2206
42. Nair A., Margolis M.P., Kuban B.D., Vince D.G. Automated coronary plaque characterisation with intravascular ultrasound backscatter: ex vivo validation. EuroIntervention 2007;3:113-120
43. Campos C.M., Fedewa R.J., Garcia-Garcia H.M., et al. Ex vivo validation of 45 MHz intravascular ultrasound backscatter tissue characterization. Eur Heart J Cardiovasc Imaging 2015;16:1112-1119
44. Nasu K., Tsuchikane E., Katoh O., et al. Accuracy of in vivo coronary plaque morphology assessment: a validation study of in vivo virtual histology compared with in vitro histopathology. J Am Coll Cardiol 2006;47:2405-2412
45. Thim T., Hagensen M.K., Wallace-Bradley D., et al. Unreliable assessment of necrotic core by virtual histology intravascular ultrasound in porcine coronary artery disease. Circ Cardiovasc Imaging 2010;3:384-391
46. Brown A.J., Obaid D.R., Costopoulos C., et al. Direct Comparison of Virtual-Histology Intravascular Ultrasound and Optical Coherence Tomography Imaging for Identification of Thin-Cap Fibroatheroma. Circ Cardiovasc Imaging 2015;8:e003487
47. Fujii K., Hao H., Shibuya M., et al. Accuracy of OCT, grayscale IVUS, and their combination for the diagnosis of coronary TCFA: an ex vivo validation study. JACC Cardiovasc Imaging 2015;8:451-460
48. Garcia-Garcia H.M., Costa M.A., Serruys P.W. Imaging of coronary atherosclerosis: intravascular ultrasound. Eur Heart J 2010;31:2456-2469
49. Calvert P.A., Obaid D.R., O'Sullivan M., et al. Association between IVUS findings and adverse outcomes in patients with coronary artery disease: the VIVA (VH-IVUS in Vulnerable Atherosclerosis) Study. JACC Cardiovasc Imaging 2011;4:894-901
50. Cheng J.M., Garcia-Garcia H.M., de Boer S.P., et al. In vivo detection of high-risk coronary plaques by radiofrequency intravascular ultrasound and cardiovascular outcome: results of the ATHEROREMO-IVUS study. Eur Heart J 2014;35:639-647
51. Stone G.W., Maehara A., Lansky A.J., et al. A prospective natural-history study of

coronary atherosclerosis. N Engl J Med 2011;364:226-235
52. Fujii K., Mintz G.S., Carlier S.G., et al. Intravascular ultrasound profile analysis of ruptured coronary plaques. Am J Cardiol 2006;98:429-435
53. Schoenhagen P., Ziada K.M., Kapadia S.R., Crowe T.D., Nissen S.E., Tuzcu E.M. Extent and direction of arterial remodeling in stable versus unstable coronary syndromes : an intravascular ultrasound study. Circulation 2000;101:598-603
54. Nakamura M., Nishikawa H., Mukai S., et al. Impact of coronary artery remodeling on clinical presentation of coronary artery disease: an intravascular ultrasound study. J Am Coll Cardiol 2001;37:63-69
55. Maehara A., Mintz G.S., Bui A.B., et al. Morphologic and angiographic features of coronary plaque rupture detected by intravascular ultrasound. J Am Coll Cardiol 2002;40:904-910
56. Inaba S., Mintz G.S., Farhat N.Z., et al. Impact of positive and negative lesion site remodeling on clinical outcomes: insights from PROSPECT. JACC Cardiovasc Imaging 2014;7:70-78
57. Fujii K., Carlier S.G., Mintz G.S., et al. Intravascular ultrasound study of patterns of calcium in ruptured coronary plaques. Am J Cardiol 2005;96:352-357
58. Amano H., Ikeda T., Toda M., et al. Assessment of angiographic coronary calcification and plaque composition in virtual histology intravascular ultrasound. J Interv Cardiol 2015;28:205-214
59. Pu J., Mintz G.S., Biro S., et al. Insights into echo-attenuated plaques, echolucent plaques, and plaques with spotty calcification: novel findings from comparisons among intravascular ultrasound, near-infrared spectroscopy, and pathological histology in 2,294 human coronary artery segments. J Am Coll Cardiol 2014;63:2220-2233
60. Kataoka Y., Wolski K., Uno K., et al. Spotty calcification as a marker of accelerated progression of coronary atherosclerosis: insights from serial intravascular ultrasound. J Am Coll Cardiol 2012;59:1592-1597
61. Honda Y., Fitzgerald P.J. Frontiers in intravascular imaging technologies. Circulation 2008;117:2024-2037
62. Wijns W., Shite J., Jones M.R., et al. Optical coherence tomography imaging during percutaneous coronary intervention impacts physician decision-making: ILUMIEN I study. Eur Heart J 2015;36:3346-3355
63. Maehara A., Ben-Yehuda O., Ali Z., et al. Comparison of Stent Expansion Guided by Optical Coherence Tomography Versus Intravascular Ultrasound: The ILUMIEN II Study (Observational Study of Optical Coherence Tomography [OCT] in Patients Undergoing Fractional Flow Reserve [FFR] and Percutaneous Coronary Intervention).

JACC Cardiovasc Interv 2015;8:1704-1714

64. Ali Z.A., Maehara A., Genereux P., et al. Optical coherence tomography compared with intravascular ultrasound and with angiography to guide coronary stent implantation (ILUMIEN III: OPTIMIZE PCI): a randomised controlled trial. Lancet 2016;388:2618-2628
65. Kume T., Akasaka T., Kawamoto T., et al. Assessment of coronary arterial plaque by optical coherence tomography. Am J Cardiol 2006;97:1172-1175
66. Yabushita H., Bouma B.E., Houser S.L., et al. Characterization of human atherosclerosis by optical coherence tomography. Circulation 2002;106:1640-1645
67. Tian J., Ren X., Vergallo R., et al. Distinct morphological features of ruptured culprit plaque for acute coronary events compared to those with silent rupture and thin-cap fibroatheroma: a combined optical coherence tomography and intravascular ultrasound study. J Am Coll Cardiol 2014;63:2209-2216
68. Kume T., Akasaka T., Kawamoto T., et al. Measurement of the thickness of the fibrous cap by optical coherence tomography. Am Heart J 2006;152:755-4
69. Phipps J.E., Hoyt T., Vela D., et al. Diagnosis of Thin-Capped Fibroatheromas in Intravascular Optical Coherence Tomography Images: Effects of Light Scattering. Circ Cardiovasc Interv 2016;9
70. Kato K., Yonetsu T., Kim S.J., et al. Nonculprit plaques in patients with acute coronary syndromes have more vulnerable features compared with those with non-acute coronary syndromes: a 3-vessel optical coherence tomography study. Circ Cardiovasc Imaging 2012;5:433-440
71. Maejima N., Hibi K., Saka K., et al. Morphological features of non-culprit plaques on optical coherence tomography and integrated backscatter intravascular ultrasound in patients with acute coronary syndromes. Eur Heart J Cardiovasc Imaging 2015;16:190-197
72. Yonetsu T., Kakuta T., Lee T., et al. In vivo critical fibrous cap thickness for rupture-prone coronary plaques assessed by optical coherence tomography. Eur Heart J 2011;32:1251-1259
73. Tearney G.J., Regar E., Akasaka T., et al. Consensus standards for acquisition, measurement, and reporting of intravascular optical coherence tomography studies: a report from the International Working Group for Intravascular Optical Coherence Tomography Standardization and Validation. J Am Coll Cardiol 2012;59:1058-1072
74. Uemura S., Ishigami K., Soeda T., et al. Thin-cap fibroatheroma and microchannel findings in optical coherence tomography correlate with subsequent progression of coronary atheromatous plaques. Eur Heart J 2012;33:78-85

75. Tian J., Hou J., Xing L., et al. Significance of intraplaque neovascularisation for vulnerability: optical coherence tomography study. Heart 2012;98:1504-1509
76. Tearney G.J., Yabushita H., Houser S.L., et al. Quantification of macrophage content in atherosclerotic plaques by optical coherence tomography. Circulation 2003;107:113-119
77. Di Vito L., Agozzino M., Marco V., et al. Identification and quantification of macrophage presence in coronary atherosclerotic plaques by optical coherence tomography. Eur Heart J Cardiovasc Imaging 2015;16:807-813
78. Raffel O.C., Tearney G.J., Gauthier D.D., Halpern E.F., Bouma B.E., Jang I.K. Relationship between a systemic inflammatory marker, plaque inflammation, and plaque characteristics determined by intravascular optical coherence tomography. Arterioscler Thromb Vasc Biol 2007;27:1820-1827
79. MacNeill B.D., Jang I.K., Bouma B.E., et al. Focal and multi-focal plaque macrophage distributions in patients with acute and stable presentations of coronary artery disease. J Am Coll Cardiol 2004;44:972-979
80. Galon M.Z., Wang Z., Bezerra H.G., et al. Differences determined by optical coherence tomography volumetric analysis in non-culprit lesion morphology and inflammation in ST-segment elevation myocardial infarction and stable angina pectoris patients. Catheter Cardiovasc Interv 2015;85:E108-E115
81. Phipps J.E., Vela D., Hoyt T., et al. Macrophages and intravascular OCT bright spots: a quantitative study. JACC Cardiovasc Imaging 2015;8:63-72
82. Nishimiya K., Matsumoto Y., Takahashi J., et al. In vivo visualization of adventitial vasa vasorum of the human coronary artery on optical frequency domain imaging. Validation study. Circ J 2014;78:2516-2518
83. Vorpahl M., Nakano M., Virmani R. Small black holes in optical frequency domain imaging matches intravascular neoangiogenesis formation in histology. Eur Heart J 2010;31:1889
84. Kitabata H., Tanaka A., Kubo T., et al. Relation of microchannel structure identified by optical coherence tomography to plaque vulnerability in patients with coronary artery disease. Am J Cardiol 2010;105:1673-1678
85. Taruya A., Tanaka A., Nishiguchi T., et al. Vasa Vasorum Restructuring in Human Atherosclerotic Plaque Vulnerability: A Clinical Optical Coherence Tomography Study. J Am Coll Cardiol 2015;65:2469-2477
86. Kilic I.D., Caiazzo G., Fabris E., et al. Near-infrared spectroscopy-intravascular ultrasound: scientific basis and clinical applications. Eur Heart J Cardiovasc Imaging 2015;16:1299-1306
87. Gardner C.M., Tan H., Hull E.L., et al. Detection of lipid core coronary plaques in

autopsy specimens with a novel catheter-based near-infrared spectroscopy system. JACC Cardiovasc Imaging 2008;1:638-648

88. Waxman S., Dixon S.R., L'Allier P., et al. In vivo validation of a catheter-based near-infrared spectroscopy system for detection of lipid core coronary plaques: initial results of the SPECTACL study. JACC Cardiovasc Imaging 2009;2:858-868
89. Madder R.D., Smith J.L., Dixon S.R., Goldstein J.A. Composition of target lesions by near-infrared spectroscopy in patients with acute coronary syndrome versus stable angina. Circ Cardiovasc Interv 2012;5:55-61
90. Kang S.J., Mintz G.S., Pu J., et al. Combined IVUS and NIRS detection of fibroatheromas: histopathological validation in human coronary arteries. JACC Cardiovasc Imaging 2015;8:184-194
91. Puri R., Madder R.D., Madden S.P., et al. Near-Infrared Spectroscopy Enhances Intravascular Ultrasound Assessment of Vulnerable Coronary Plaque: A Combined Pathological and In Vivo Study. Arterioscler Thromb Vasc Biol 2015;35:2423-2431
92. Madder R.D., Goldstein J.A., Madden S.P., et al. Detection by near-infrared spectroscopy of large lipid core plaques at culprit sites in patients with acute ST-segment elevation myocardial infarction. JACC Cardiovasc Interv 2013;6:838-846
93. Madder R.D., Husaini M., Davis A.T., et al. Detection by near-infrared spectroscopy of large lipid cores at culprit sites in patients with non-st-segment elevation myocardial infarction and unstable angina. Catheter Cardiovasc Interv 2015;86:1014-1021
94. Oemrawsingh R.M., Cheng J.M., Garcia-Garcia H.M., et al. Near-infrared spectroscopy predicts cardiovascular outcome in patients with coronary artery disease. J Am Coll Cardiol 2014;64:2510-2518
95. Leipsic J., Abbara S., Achenbach S., et al. SCCT guidelines for the interpretation and reporting of coronary CT angiography: a report of the Society of Cardiovascular Computed Tomography Guidelines Committee. J Cardiovasc Comput Tomogr 2014;8:342-358
96. Kroner E.S., van Velzen J.E., Boogers M.J., et al. Positive remodeling on coronary computed tomography as a marker for plaque vulnerability on virtual histology intravascular ultrasound. Am J Cardiol 2011;107:1725-1729
97. Nakazato R., Otake H., Konishi A., et al. Atherosclerotic plaque characterization by CT angiography for identification of high-risk coronary artery lesions: a comparison to optical coherence tomography. Eur Heart J Cardiovasc Imaging 2015;16:373-379
98. Sato A., Hoshi T., Kakefuda Y., et al. In vivo evaluation of fibrous cap thickness by optical coherence tomography for positive remodeling and low-attenuation plaques assessed by computed tomography angiography. Int J Cardiol 2015;182:419-425

99. Thomsen C., Abdulla J. Characteristics of high-risk coronary plaques identified by computed tomographic angiography and associated prognosis: a systematic review and meta-analysis. Eur Heart J Cardiovasc Imaging 2016;17:120-129
100. Benedek T., Jako B., Benedek I. Plaque quantification by coronary CT and intravascular ultrasound identifies a low CT density core as a marker of plaque instability in acute coronary syndromes. Int Heart J 2014;55:22-28
101. Voros S., Rinehart S., Qian Z., et al. Prospective validation of standardized, 3-dimensional, quantitative coronary computed tomographic plaque measurements using radiofrequency backscatter intravascular ultrasound as reference standard in intermediate coronary arterial lesions: results from the ATLANTA (assessment of tissue characteristics, lesion morphology, and hemodynamics by angiography with fractional flow reserve, intravascular ultrasound and virtual histology, and noninvasive computed tomography in atherosclerotic plaques) I study. JACC Cardiovasc Interv 2011;4:198-208
102. Marwan M., Taher M.A., El M.K., et al. In vivo CT detection of lipid-rich coronary artery atherosclerotic plaques using quantitative histogram analysis: a head to head comparison with IVUS. Atherosclerosis 2011;215:110-115
103. Motoyama S., Kondo T., Sarai M., et al. Multislice computed tomographic characteristics of coronary lesions in acute coronary syndromes. J Am Coll Cardiol 2007;50:319-326
104. Puchner S.B., Liu T., Mayrhofer T., et al. High-risk plaque detected on coronary CT angiography predicts acute coronary syndromes independent of significant stenosis in acute chest pain: results from the ROMICAT-II trial. J Am Coll Cardiol 2014;64:684-692
105. Yang X., Gai L., Dong W., et al. Characterization of culprit lesions in acute coronary syndromes compared with stable angina pectoris by dual-source computed tomography. Int J Cardiovasc Imaging 2013;29:945-953
106. Nakazato R., Shalev A., Doh J.H., et al. Quantification and characterisation of coronary artery plaque volume and adverse plaque features by coronary computed tomographic angiography: a direct comparison to intravascular ultrasound. Eur Radiol 2013;23:2109-2117
107. van Velzen J.E., de Graaf F.R., de Graaf M.A., et al. Comprehensive assessment of spotty calcifications on computed tomography angiography: comparison to plaque characteristics on intravascular ultrasound with radiofrequency backscatter analysis. J Nucl Cardiol 2011;18:893-903
108. Seifarth H., Schlett C.L., Nakano M., et al. Histopathological correlates of the napkin-ring sign plaque in coronary CT angiography. Atherosclerosis 2012;224:90-96
109. Maurovich-Horvat P., Schlett C.L., Alkadhi H., et al. The napkin-ring sign indicates

advanced atherosclerotic lesions in coronary CT angiography. JACC Cardiovasc Imaging 2012;5:1243-1252

110. Ito T., Terashima M., Kaneda H., et al. Comparison of in vivo assessment of vulnerable plaque by 64-slice multislice computed tomography versus optical coherence tomography. Am J Cardiol 2011;107:1270-1277
111. Otsuka K., Fukuda S., Tanaka A., et al. Napkin-ring sign on coronary CT angiography for the prediction of acute coronary syndrome. JACC Cardiovasc Imaging 2013;6:448-457
112. Kashiwagi M., Tanaka A., Kitabata H., et al. Feasibility of noninvasive assessment of thin-cap fibroatheroma by multidetector computed tomography. JACC Cardiovasc Imaging 2009;2:1412-1419
113. Motoyama S., Sarai M., Harigaya H., et al. Computed tomographic angiography characteristics of atherosclerotic plaques subsequently resulting in acute coronary syndrome. J Am Coll Cardiol 2009;54:49-57
114. Kristensen T.S., Kofoed K.F., Kuhl J.T., Nielsen W.B., Nielsen M.B., Kelbaek H. Prognostic implications of nonobstructive coronary plaques in patients with non-ST-segment elevation myocardial infarction: a multidetector computed tomography study. J Am Coll Cardiol 2011;58:502-509
115. Hammer-Hansen S., Kofoed K.F., Kelbaek H., et al. Volumetric evaluation of coronary plaque in patients presenting with acute myocardial infarction or stable angina pectoris-a multislice computerized tomography study. Am Heart J 2009;157:481-487
116. Versteylen M.O., Kietselaer B.L., Dagnelie P.C., et al. Additive value of semiautomated quantification of coronary artery disease using cardiac computed tomographic angiography to predict future acute coronary syndrome. J Am Coll Cardiol 2013;61:2296-2305
117. Tarkin J.M., Joshi F.R., Rudd J.H. PET imaging of inflammation in atherosclerosis. Nat Rev Cardiol 2014;11:443-457
118. Zhang Z., Machac J., Helft G., et al. Non-invasive imaging of atherosclerotic plaque macrophage in a rabbit model with F-18 FDG PET: a histopathological correlation. BMC Nucl Med 2006;6:3
119. Tawakol A., Migrino R.Q., Hoffmann U., et al. Noninvasive in vivo measurement of vascular inflammation with F-18 fluorodeoxyglucose positron emission tomography. J Nucl Cardiol 2005;12:294-301
120. Tawakol A., Migrino R.Q., Bashian G.G., et al. In vivo 18F-fluorodeoxyglucose positron emission tomography imaging provides a noninvasive measure of carotid plaque inflammation in patients. J Am Coll Cardiol 2006;48:1818-1824

121. Rogers I.S., Nasir K., Figueroa A.L., et al. Feasibility of FDG imaging of the coronary arteries: comparison between acute coronary syndrome and stable angina. JACC Cardiovasc Imaging 2010;3:388-397
122. Joshi N.V., Vesey A.T., Williams M.C., et al. 18F-fluoride positron emission tomography for identification of ruptured and high-risk coronary atherosclerotic plaques: a prospective clinical trial. Lancet 2014;383:705-713
123. Cheng V.Y., Slomka P.J., Le M.L., et al. Coronary arterial 18F-FDG uptake by fusion of PET and coronary CT angiography at sites of percutaneous stenting for acute myocardial infarction and stable coronary artery disease. J Nucl Med 2012;53:575-583
124. Irkle A., Vesey A.T., Lewis D.Y., et al. Identifying active vascular microcalcification by (18)F-sodium fluoride positron emission tomography. Nat Commun 2015;6:7495
125. Li X., Bauer W., Kreissl M.C., et al. Specific somatostatin receptor II expression in arterial plaque: (68)Ga-DOTATATE autoradiographic, immunohistochemical and flow cytometric studies in apoE-deficient mice. Atherosclerosis 2013;230:33-39
126. Rominger A., Saam T., Vogl E., et al. In vivo imaging of macrophage activity in the coronary arteries using 68Ga-DOTATATE PET/CT: correlation with coronary calcium burden and risk factors. J Nucl Med 2010;51:193-197
127. Gaemperli O., Shalhoub J., Owen D.R., et al. Imaging intraplaque inflammation in carotid atherosclerosis with 11C-PK11195 positron emission tomography/computed tomography. Eur Heart J 2012;33:1902-1910
128. Beer A.J., Pelisek J., Heider P., et al. PET/CT imaging of integrin alphavbeta3 expression in human carotid atherosclerosis. JACC Cardiovasc Imaging 2014;7:178-187
129. den Hartog A.G., Bovens S.M., Koning W., et al. Current status of clinical magnetic resonance imaging for plaque characterisation in patients with carotid artery stenosis. Eur J Vasc Endovasc Surg 2013;45:7-21
130. Karolyi M., Seifarth H., Liew G., et al. Classification of coronary atherosclerotic plaques ex vivo with T1, T2, and ultrashort echo time CMR. JACC Cardiovasc Imaging 2013;6:466-474
131. Kawasaki T., Koga S., Koga N., et al. Characterization of hyperintense plaque with noncontrast T(1)-weighted cardiac magnetic resonance coronary plaque imaging: comparison with multislice computed tomography and intravascular ultrasound. JACC Cardiovasc Imaging 2009;2:720-728
132. Ehara S., Hasegawa T., Nakata S., et al. Hyperintense plaque identified by magnetic resonance imaging relates to intracoronary thrombus as detected by optical coherence tomography in patients with angina pectoris. Eur Heart J Cardiovasc Imaging 2012;13:394-399

133. Matsumoto K., Ehara S., Hasegawa T., et al. Localization of Coronary High-Intensity Signals on T1-Weighted MR Imaging: Relation to Plaque Morphology and Clinical Severity of Angina Pectoris. JACC Cardiovasc Imaging 2015;8:1143-1152
134. Matsumoto K., Ehara S., Hasegawa T., Nishimura S., Shimada K. The signal intensity of coronary culprit lesions on T1-weighted magnetic resonance imaging is directly correlated with the accumulation of vulnerable morphologies. Int J Cardiol 2017;231:284-286
135. Noguchi T., Kawasaki T., Tanaka A., et al. High-intensity signals in coronary plaques on noncontrast T1-weighted magnetic resonance imaging as a novel determinant of coronary events. J Am Coll Cardiol 2014;63:989-999
136. Pedersen S.F., Thrysoe S.A., Paaske W.P., et al. Determination of edema in porcine coronary arteries by T2 weighted cardiovascular magnetic resonance. J Cardiovasc Magn Reson 2011;13:52
137. Montalescot G., Sechtem U., Achenbach S., et al. 2013 ESC guidelines on the management of stable coronary artery disease: the Task Force on the management of stable coronary artery disease of the European Society of Cardiology. Eur Heart J 2013;34:2949-3003
138. Roffi M., Patrono C., Collet J.P., et al. 2015 ESC Guidelines for the management of acute coronary syndromes in patients presenting without persistent ST-segment elevation: Task Force for the Management of Acute Coronary Syndromes in Patients Presenting without Persistent ST-Segment Elevation of the European Society of Cardiology (ESC). Eur Heart J 2016;37:267-315
139. van Nunen L.X., Zimmermann F.M., Tonino P.A., et al. Fractional flow reserve versus angiography for guidance of PCI in patients with multivessel coronary artery disease (FAME): 5-year follow-up of a randomised controlled trial. Lancet 2015;386:1853-1860
140. Zimmermann F.M., Ferrara A., Johnson N.P., et al. Deferral vs. performance of percutaneous coronary intervention of functionally non-significant coronary stenosis: 15-year follow-up of the DEFER trial. Eur Heart J 2015;36:3182-3188
141. Ahmadi A., Leipsic J., Blankstein R., et al. Do plaques rapidly progress prior to myocardial infarction? The interplay between plaque vulnerability and progression. Circ Res 2015;117:99-104
142. Wald D.S., Morris J.K., Wald N.J., et al. Randomized trial of preventive angioplasty in myocardial infarction. N Engl J Med 2013;369:1115-1123
143. Pijls N.H., van S.P., Manoharan G., et al. Percutaneous coronary intervention of functionally nonsignificant stenosis: 5-year follow-up of the DEFER Study. J Am Coll Cardiol 2007;49:2105-2111
144. Wykrzykowska J.J., Diletti R., Gutierrez-Chico J.L., et al. Plaque sealing and passivation

with a mechanical self-expanding low outward force nitinol vShield device for the treatment of IVUS and OCT-derived thin cap fibroatheromas (TCFAs) in native coronary arteries: report of the pilot study vShield Evaluated at Cardiac hospital in Rotterdam for Investigation and Treatment of TCFA (SECRITT). EuroIntervention 2012;8:945-954

145. Onuma Y., Serruys P.W., Perkins L.E., et al. Intracoronary optical coherence tomography and histology at 1 month and 2, 3, and 4 years after implantation of everolimus-eluting bioresorbable vascular scaffolds in a porcine coronary artery model: an attempt to decipher the human optical coherence tomography images in the ABSORB trial. Circulation 2010;122:2288-2300
146. Brugaletta S., Radu M.D., Garcia-Garcia H.M., et al. Circumferential evaluation of the neointima by optical coherence tomography after ABSORB bioresorbable vascular scaffold implantation: can the scaffold cap the plaque? Atherosclerosis 2012;221:106-112
147. Bourantas C.V., Serruys P.W., Nakatani S., et al. Bioresorbable vascular scaffold treatment induces the formation of neointimal cap that seals the underlying plaque without compromising the luminal dimensions: a concept based on serial optical coherence tomography data. EuroIntervention 2015;11:746-756
148. Baigent C., Blackwell L., Emberson J., et al. Efficacy and safety of more intensive lowering of LDL cholesterol: a meta-analysis of data from 170,000 participants in 26 randomised trials. Lancet 2010;376:1670-1681
149. Rosenson R.S., Brown A.S. Statin use in acute coronary syndromes: cellular mechanisms and clinical evidence. Curr Opin Lipidol 2002;13:625-630
150. Zeb I., Li D., Nasir K., et al. Effect of statin treatment on coronary plaque progression - a serial coronary CT angiography study. Atherosclerosis 2013;231:198-204
151. Burgstahler C., Reimann A., Beck T., et al. Influence of a lipid-lowering therapy on calcified and noncalcified coronary plaques monitored by multislice detector computed tomography: results of the New Age II Pilot Study. Invest Radiol 2007;42:189-195
152. Hoffmann H., Frieler K., Schlattmann P., Hamm B., Dewey M. Influence of statin treatment on coronary atherosclerosis visualised using multidetector computed tomography. Eur Radiol 2010;20:2824-2833
153. Auscher S., Heinsen L., Nieman K., et al. Effects of intensive lipid-lowering therapy on coronary plaques composition in patients with acute myocardial infarction: Assessment with serial coronary CT angiography. Atherosclerosis 2015;241:579-587
154. Nicholls S.J., Ballantyne C.M., Barter P.J., et al. Effect of two intensive statin regimens on progression of coronary disease. N Engl J Med 2011;365:2078-2087

155. Nissen S.E., Tuzcu E.M., Schoenhagen P., et al. Effect of intensive compared with moderate lipid-lowering therapy on progression of coronary atherosclerosis: a randomized controlled trial. JAMA 2004;291:1071-1080
156. Nissen S.E., Nicholls S.J., Sipahi I., et al. Effect of very high-intensity statin therapy on regression of coronary atherosclerosis: the ASTEROID trial. JAMA 2006;295:1556-1565
157. Puri R., Nicholls S.J., Shao M., et al. Impact of statins on serial coronary calcification during atheroma progression and regression. J Am Coll Cardiol 2015;65:1273-1282
158. Kataoka Y., Wolski K., Balog C., et al. Progression of coronary atherosclerosis in stable patients with ultrasonic features of high-risk plaques. Eur Heart J Cardiovasc Imaging 2014;15:1035-1041
159. Kataoka Y., Puri R., Hammadah M., et al. Frequency-domain optical coherence tomographic analysis of plaque microstructures at nonculprit narrowings in patients receiving potent statin therapy. Am J Cardiol 2014;114:549-554
160. Komukai K., Kubo T., Kitabata H., et al. Effect of atorvastatin therapy on fibrous cap thickness in coronary atherosclerotic plaque as assessed by optical coherence tomography: the EASY-FIT study. J Am Coll Cardiol 2014;64:2207-2217
161. Cannon C.P., Blazing M.A., Giugliano R.P., et al. Ezetimibe Added to Statin Therapy after Acute Coronary Syndromes. N Engl J Med 2015;372:2387-2397
162. Tsujita K., Sugiyama S., Sumida H., et al. Impact of Dual Lipid-Lowering Strategy With Ezetimibe and Atorvastatin on Coronary Plaque Regression in Patients With Percutaneous Coronary Intervention: The Multicenter Randomized Controlled PRECISE-IVUS Trial. J Am Coll Cardiol 2015;66:495-507
163. Habara M., Nasu K., Terashima M., et al. Impact on optical coherence tomographic coronary findings of fluvastatin alone versus fluvastatin + ezetimibe. Am J Cardiol 2014;113:580-587
164. Giugliano R.P., Sabatine M.S. Are PCSK9 Inhibitors the Next Breakthrough in the Cardiovascular Field? J Am Coll Cardiol 2015;65:2638-2651
165. Cheng J.M., Oemrawsingh R.M., Garcia-Garcia H.M., et al. PCSK9 in relation to coronary plaque inflammation: Results of the ATHEROREMO-IVUS study. Atherosclerosis 2016;248:117-122
166. Kuhnast S., van der Hoorn J.W., Pieterman E.J., et al. Alirocumab inhibits atherosclerosis, improves the plaque morphology, and enhances the effects of a statin. J Lipid Res 2014;55:2103-2112
167. Nicholls S.J., Puri R., Anderson T., et al. Effect of Evolocumab on Progression of Coronary Disease in Statin-Treated Patients: The GLAGOV Randomized Clinical Trial. JAMA 2016;316:2373-2384

168. Robinson J.G., Farnier M., Krempf M., et al. Efficacy and safety of alirocumab in reducing lipids and cardiovascular events. N Engl J Med 2015;372:1489-1499
169. Sabatine M.S., Giugliano R.P., Keech A., et al. Rationale and design of the Further cardiovascular OUtcomes Research with PCSK9 Inhibition in subjects with Elevated Risk trial. Am Heart J 2016;173:94-101
170. Schwartz G.G., Bessac L., Berdan L.G., et al. Effect of alirocumab, a monoclonal antibody to PCSK9, on long-term cardiovascular outcomes following acute coronary syndromes: rationale and design of the ODYSSEY outcomes trial. Am Heart J 2014;168:682-689
171. Ridker P.M., Amarenco P., Brunell R., et al. Evaluating bococizumab, a monoclonal antibody to PCSK9, on lipid levels and clinical events in broad patient groups with and without prior cardiovascular events: Rationale and design of the Studies of PCSK9 Inhibition and the Reduction of vascular Events (SPIRE) Lipid Lowering and SPIRE Cardiovascular Outcomes Trials. Am Heart J 2016;178:135-144
172. Arbab-Zadeh A., Nakano M., Virmani R., Fuster V. Acute coronary events. Circulation 2012;125:1147-1156
173. Libby P. Inflammation in atherosclerosis. Nature 2002;420:868-874
174. Back M., Hansson G.K. Anti-inflammatory therapies for atherosclerosis. Nat Rev Cardiol 2015;12:199-211
175. Rosenson R.S., Hurt-Camejo E. Phospholipase A2 enzymes and the risk of atherosclerosis. Eur Heart J 2012;33:2899-2909
176. Serruys P.W., Garcia-Garcia H.M., Buszman P., et al. Effects of the direct lipoprotein-associated phospholipase A(2) inhibitor darapladib on human coronary atherosclerotic plaque. Circulation 2008;118:1172-1182
177. Nicholls S.J., Kastelein J.J., Schwartz G.G., et al. Varespladib and cardiovascular events in patients with an acute coronary syndrome: the VISTA-16 randomized clinical trial. JAMA 2014;311:252-262
178. White H.D., Held C., Stewart R., et al. Darapladib for preventing ischemic events in stable coronary heart disease. N Engl J Med 2014;370:1702-1711
179. O'Donoghue M.L., Braunwald E., White H.D., et al. Effect of darapladib on major coronary events after an acute coronary syndrome: the SOLID-TIMI 52 randomized clinical trial. JAMA 2014;312:1006-1015
180. Micha R., Imamura F., Wyler von B.M., et al. Systematic review and meta-analysis of methotrexate use and risk of cardiovascular disease. Am J Cardiol 2011;108:1362-1370
181. Everett B.M., Pradhan A.D., Solomon D.H., et al. Rationale and design of the Cardiovascular Inflammation Reduction Trial: a test of the inflammatory hypothesis of atherothrombosis. Am Heart J 2013;166:199-207

182. Crittenden D.B., Lehmann R.A., Schneck L., et al. Colchicine use is associated with decreased prevalence of myocardial infarction in patients with gout. J Rheumatol 2012;39:1458-1464
183. Langevitz P., Livneh A., Neumann L., et al. Prevalence of ischemic heart disease in patients with familial Mediterranean fever. Isr Med Assoc J 2001;3:9-12
184. Nidorf S.M., Eikelboom J.W., Budgeon C.A., Thompson P.L. Low-dose colchicine for secondary prevention of cardiovascular disease. J Am Coll Cardiol 2013;61:404-410
185. Ridker P.M., Luscher T.F. Anti-inflammatory therapies for cardiovascular disease. Eur Heart J 2014;35:1782-1791
186. Ridker P.M., Howard C.P., Walter V., et al. Effects of interleukin-1beta inhibition with canakinumab on hemoglobin A1c, lipids, C-reactive protein, interleukin-6, and fibrinogen: a phase IIb randomized, placebo-controlled trial. Circulation 2012;126:2739-2748
187. Ridker P.M., Thuren T., Zalewski A., Libby P. Interleukin-1beta inhibition and the prevention of recurrent cardiovascular events: rationale and design of the Canakinumab Anti-inflammatory Thrombosis Outcomes Study (CANTOS). Am Heart J 2011;162:597-605
188. Thomsen C., Abdulla J. Characteristics of high-risk coronary plaques identified by computed tomographic angiography and associated prognosis: a systematic review and meta-analysis. Eur Heart J Cardiovasc Imaging 2015

Chapter 13

Impact of individualized segmentation on diagnostic performance of quantitative positron emission tomography for haemodynamically significant coronary artery disease

Michiel J. Bom, Stefan P. Schumacher, Roel S. Driessen, Pieter G. Raijmakers, Henk Everaars, Pepijn A. van Diemen, Adriaan A. Lammertsma, Peter M. van de Ven, Albert C. van Rossum, Juhani Knuuti, Maija Mäki, Ibrahim Danad, and Paul Knaapen

Eur Heart J Cardiovasc Imaging. 2019;20(5):525-532

Abstract

Aims: Despite high variability in coronary anatomy, quantitative positron emission tomography (PET) perfusion in coronary territories is traditionally calculated according to the American Heart Association (AHA) 17-segments model. This study aimed to assess the impact of individualized segmentation of myocardial segments on the diagnostic accuracy of hyperemic MBF values for hemodynamically significant coronary artery disease (CAD).

Methods and results: Patients with suspected CAD (n=204) underwent coronary computed tomography angiography (CCTA) and [^{15}O]H_2O PET followed by invasive coronary angiography with fractional flow reserve assessment of all major coronary arteries. Hyperemic MBF per vascular territory was calculated using both standard segmentation according to the AHA model and individualized segmentation, in which CCTA was used to assign coronary arteries to PET perfusion territories. In 122 (59.8%) patients one or more segments were redistributed after individualized segmentation. No differences in mean MBF values were seen between segmentation methods, except for a minor difference in hyperemic MBF in the LCX territory (p=0.001). These minor changes resulted in discordant PET-defined hemodynamically significant CAD between the two methods in only 5 (0.8%) vessels. The diagnostic value for detecting hemodynamically significant CAD did not differ between individualized and standard segmentation, with area under the curves of 0.79 and 0.78 respectively (p=0.34).

Conclusions: Individualized segmentation using CCTA-derived coronary anatomy led to redistribution of standard myocardial segments in 60% of patients. However, this had little impact on [^{15}O]H_2O PET MBF values and diagnostic value for detecting hemodynamically significant CAD did not change. Therefore, clinical impact of individualized segmentation seems limited.

Introduction

Positron emission tomography (PET) is a radionuclide imaging modality that allows for noninvasive quantification of myocardial blood flow (MBF).(1) Among the myriad of available imaging techniques, quantitative PET currently yields the highest diagnostic accuracy for detecting obstructive coronary artery disease.(2) In the assessment of MBF in specific vascular territories, the standard 17-segments American Heart Association (AHA) model is used to divide the left ventricular (LV) wall into the vascular territories of the LAD, LCX and RCA.(3) This standard model, however, is an oversimplification of the actual vascular architecture in a specific patient, since there is great variability in coronary anatomy. Variability in coronary anatomy is most frequently seen in difference in coronary dominance in which the RDP is supplied by either the LCX or RCA and in second or third order vessels such as the anterolateral wall which may be supplied by diagonal or obtuse marginal branches. Individualized segmentation of the LV wall based on actual coronary anatomy would potentially lead to a more accurate assessment of vessel-specific MBF with a subsequent increase in diagnostic performance. Although several small studies have shown the feasibility of using coronary computed tomography angiography (CCTA) to obtain individualized segmentation in perfusion imaging, data on the diagnostic performance of this individualized method in quantitative PET perfusion imaging for detecting hemodynamically significant coronary artery disease (CAD) are scarce.(4-7) The purpose of this study was, therefore, to assess diagnostic accuracy of quantitative $[^{15}O]H_2O$ PET perfusion measurements to detect hemodynamically significant CAD, as defined by fractional flow reserve (FFR), using both standard and individualized segmentations.

Methods

Study population

The current report is a substudy of the PACIFIC trial and details regarding the study design are described previously.(2) The study population consisted of 208 patients with stable new-onset chest pain and suspected CAD. All patients were aged 40 years and above and had intermediate pre-test probability for CAD as defined by Diamond and Forrester criteria. Major exclusion criteria were renal failure (i.e. eGFR < 45 mL/

min), a left ventricular ejection fraction <50%, history of COPD or chronic asthma, a prior history of CAD, atrial fibrillation, and second or third degree AV block. In brief, 208 patients with suspected CAD underwent CCTA, single photon emission computed tomography, and [^{15}O]H_2O PET imaging, followed by invasive coronary angiography with FFR measurement in all major coronary vessels. For the present substudy all patients with PET imaging were included (n=204). The study protocol was approved by the Medical Ethics Committee of the VU University Medical Center and written informed consent was obtained from all participants.

Invasive coronary angiography and FFR

Invasive coronary angiography and FFR measurements were performed as described previously.(2) In brief, all major coronary arteries were routinely interrogated by FFR except for occluded or subtotal lesions with a diameter stenosis ≥90%. Maximal hyperemia was induced by intracoronary (150 μg) or intravenous (140 $\mu g \cdot kg^{-1} \cdot min^{-1}$) administration of adenosine. An FFR of ≤0.80 was considered hemodynamically significant. In case FFR measurement was not performed, a stenosis of ≥ 90% was deemed significant, whereas a stenosis of ≤30% (obtained with Quantitative Coronary Analysis, QCA) was deemed non-significant.(8)

[^{15}O]H_2O PET acquisition

PET imaging was performed on the same day as CCTA imaging. Patients were scanned using a hybrid PET-CT device (Philips Gemini TF 64, Philips Healthcare, Best, The Netherlands). The scanning protocol has been described in detail previously.(9) In summary, a dynamic PET perfusion scan was performed during resting conditions using 370 MBq of [^{15}O]H_2O. A 6 min emission scan was started simultaneously with the administration of [^{15}O]H_2O. This dynamic scan sequence was followed immediately by a low dose CT scan for attenuation correction. After a 10 min interval to allow for decay of radioactivity, an identical PET sequence was performed during hyperemic conditions induced by intravenous adenosine infusion (140 $\mu g \cdot kg^{-1} \cdot min^{-1}$), initiated 2 min before the hyperemic scan to ensure maximal vasodilation.

CCTA acquisition

Patient preparation and image acquisition were performed as described previously.(2)

In short, patients underwent CCTA on a 256-slice CT-scanner (Brilliance iCT, Philips Healthcare, Best, the Netherlands) with a collimation of 128 x 0.625 mm and a tube rotation time of 270 ms. Tube current was set between 200 and 360 mAs at 120 kV, adjusting primarily the mAs based on body habitus. Axial scanning was performed with prospective ECG-gating (Step & Shoot Cardiac, Philips Healthcare) at 75% of the R-R interval. A bolus of 100 mL iobitidol (Xenetix 350) was injected intravenously (5.7 mL/s) followed by a 50 mL saline flush. The scan was triggered using an automatic bolus tracking technique, with a region of interest placed in the descending thoracic aorta with a threshold of 150 Hounsfield Units (HU). In patients with a prescan heart rate of ≥ 65 beats per minute, metoprolol 50 to 150 mg was administered orally one hour before the start of the CT protocol. If necessary, 5 to 25 mg metoprolol was given intravenously just before the scan to achieve a heart rate < 65 bpm. All patients received 800 mcg of sublingual nitroglycerine immediately before scanning.

PET/CT analysis

PET images were reconstructed using the 3D row action maximum likelihood algorithm and applying all appropriate corrections. Parametric MBF images were generated and quantitatively analyzed using in-house developed software (Cardiac VUer).(10) Myocardial blood flow was expressed in mL / min / g and both resting and hyperemic MBF were calculated for the LV as a whole. Calculation of MBF values in the vascular territories of the LAD, LCX, and RCA was performed using two different segmentation methods (figure 1). First, segmentation of the three vascular territories was derived from the 17-segment standard AHA model (standard segmentation). Second, CCTA was used to define the vascular territories of the three coronary arteries (individualized segmentation). For the individualized segmentation, short axis projections of the LV were used. Four maximum intensity projection slices of equal thickness were used to assign each of the 17 myocardial segments to one of the three major coronary arteries (LAD, LCx, and RCA), hereby creating individualized polar maps.(4) These individualized polar maps were then used to generate mean MBF values for the corresponding vascular territories. In both the standard and the individualized segmentation, PET-defined hemodynamically significant CAD was defined by a perfusion defect of at least 2 adjacent myocardial segments with hyperemic MBF ≤ 2.30 mL/min/g.(2,11) In vascular territories in which a perfusion defect was present,

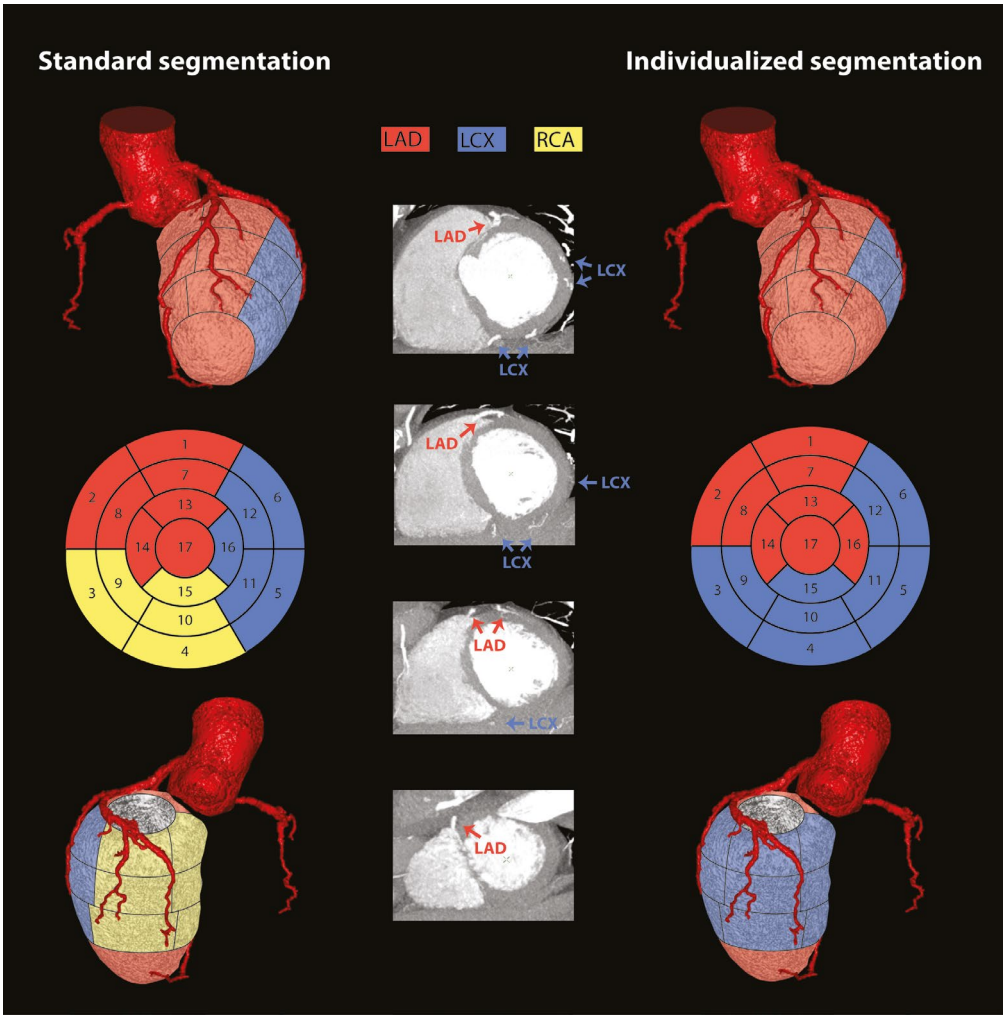

Figure 1. Case example of myocardial segmentation analysis
CCTA images of a 61-year old male presented with atypical chest pain. Standard segmentation was performed according to the American Heart Association (AHA) model (left panel). In this model the left ventricle was divided into 17 segments and the LAD vascular territory was comprised of 7 segments, whereas the LCx and RCA vascular territories were comprised of 5 segments. For the individualized method, four maximum intensity projection slices of equal thickness were generated to visualize the four short-axis views of the left ventricle (middle panel). These images were used to assign each of the 17 myocardial segments to one of the three major coronary arteries (LAD, LCx, and RCA), hereby creating an individualized segmentation of the left ventricle wall (right panel). In this case, there is a left dominant coronary circulation in which the RCA was not subtending any left ventricle mass. Therefore segments 3, 4, 9, 10, and 15 were reassigned to the LCx. Furthermore, there was a large second diagonal branch which supplied the apical lateral segment of the left ventricle (segment 16) and therefore this segment was reassigned to the LAD.

MBF and MFR were defined by the mean of all segments with a perfusion defect. In vascular territories where no perfusion defect was present the MBF and MFR were calculated by the mean of all myocardial segments in that territory. Myocardial flow reserve (MFR) was defined as the ratio between hyperemic and resting MBF.

In patients in which CCTA showed a left dominant coronary anatomy in which the RCA did not subtend any LV myocardium, the RCA vessel was excluded from the comparative analysis of the two segmentations methods for diagnostic value for FFR-defined hemodynamically significant CAD. The myocardial segments subtended by the PDA were attributed to the LCX territory in these cases.

Statistical analyses

All statistical analyses were performed using the SPSS software package (version 20.0.0, IBM SPSS Statistics, Armonk, New York), except for receiver operating characteristics (ROC) curve analyses which were performed with MedCalc for Windows (version 12.7.8.0, MedCalc Software, Oostende, Belgium). Continuous variables were tested for normal distribution. Normal distributed continuous variables are presented as mean ± SD. Non-normal distributed variables are presented as median with interquartile range. Categorical variables are presented as frequencies with percentages and compared with the chi-square test. For the separate vessels, the mean rest MBF, hyperemic MBF, and MFR were compared between standard and individualized segmentation using a linear mixed model with a fixed effect for method of segmentation and random effects for patient. Sensitivity, specificity, accuracy, NPV and PPV for the presence of FFR-defined hemodynamically significant CAD averaged over all LAD, RCA and RCx vessels were estimated and compared between the two segmentation methods using Generalized Estimating Equations for dichotomous outcome with an unstructured correlation structure to account for correlation of observations made on vessels from the same patient. Vessel-type specific sensitivity, specificity and accuracy were compared using the McNemar test and vessel-type specific NPV and PPV using Generalized Estimating Equations an independent correlation structure.(12) Furthermore, the respective areas under the receiver-operating characteristic (ROC) curves were compared using the method of DeLong for both per-vessel and per-patient analyses. A p-value <0.05 was considered statistically significant.

Results

Study population and LV segmentation

The baseline characteristics of all 204 included patients are shown in table 1. Individualized segmentation of the LV wall resulted in redistribution of 287/3468 (8.3%) myocardial segments as compared with standard segmentation. In 122 (59.8%) patients one or more segments were redistributed after individualized segmentation. A schematic overview of the distribution of specific myocardial segments supplied by each individual coronary artery (LAD, LCx, and RCA) according to the individualized segmentation is provided in figure 2A. The relative occurrence of redistribution with the individualized method for each myocardial segment is depicted in figure 2B. Redistribution of segments occurred in up to 29% in segments of the standard RCA and LCX territory. In contrast, redistribution did not occur in the standard LAD territory, except for one case of coronary anomaly (hypoplastic LAD) and in 5 (2.5%) cases in which the apex which was supplied by a different coronary. Redistribution occurred most often in the inferior (segments 4, 10, and 15) and lateral wall (segments 12 and 16).

Table 1. Baseline characteristics

Demographics	**N = 204**
Age, years	58 ± 9
Male	129 (63%)
Body mass index	27 ± 4
Cardiovascular risk factors – no (%)	
Diabetes Mellitus type II	32 (16%)
Hypertension	96 (47%)
Hyperlipidaemia	81 (40%)
Current tobacco use	40 (20%)
History of tobacco use	99 (49%)
Family history of CAD	104 (51%)
Type of chest-pain – no (%)	
Typical angina	71 (35%)
Atypical angina	77 (38%)
Non-specific chest discomfort	56 (28%)

CAD: coronary artery disease

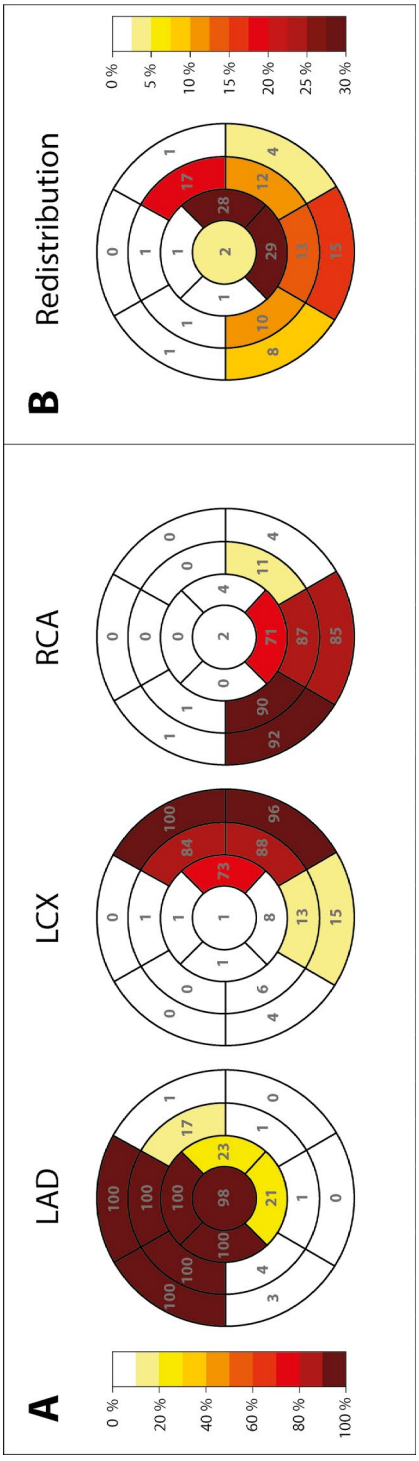

Figure 2. Individualized segmentation per vessel and redistribution between standard and individualized segmentation
(A) Polar maps of the left ventricle visualizing the distribution of specific LV segments supplied by each individual coronary artery (respectively LAD, LCx, and RCA). The colours indicate the proportion of cases in which the segment was supplied by that particular coronary artery (0 - 100%). (B) Polar map depicting the relative occurrence of redistribution of coronary segments with the individualized segmentation model. The colours indicate the frequency of redistribution of a particular segment (0 - 30%).

[^{15}O]H_2O PET

An overview of mean rest MBF, mean hyperemic MBF and mean MFR values based on standard and individualized segmentation methods on a per-vessel level is shown in table 2. There were no significant differences in mean rest MBF and MFR values between the two segmentation methods. Hyperemic MBF values were only significantly different in the LCX (p<0.001), no differences in hyperemic MBF were observed in

Table 2. PET-derived myocardial blood flow parameters based on both standard and individualized segmentation methods

	Standard segmentation	Individualized segmentation	p-value
Mean rest MBF			
LAD territory	0.96 ± 0.27	0.97 ± 0.31	0.58
LCX territory	0.94 ± 0.25	0.94 ± 0.31	0.84
RCA territory	0.86 ± 0.24	0.87 ± 0.30*	0.73
Mean hyperemic MBF			
LAD territory	2.73 ± 1.25	2.73 ± 1.26	0.75
LCX territory	2.88 ± 1.19	2.83 ± 1.14	0.001
RCA territory	2.63 ± 1.17	2.64 ± 1.20*	0.82
Mean MFR			
LAD territory	2.98 ± 1.24	2.98 ± 1.23	0.73
LCX territory	3.14 ± 1.22	3.12 ± 1.16	0.52
RCA territory	3.18 ± 1.41	3.18 ± 1.44*	0.34

The rest and stress MBF and MFR values represent the mean values of all 204 vessels in that particular vascular territory. The RCA territories in the individualized segmentation (*) contained only 190 vessels instead of 204 vessels, due to the presence of a left dominant coronary system in 14 cases in which the RCA did not subtend any LV myocardium. In these cases the myocardial segments subtended by the PDA were attributed to the LCX territory. Abbreviations: PET: positron emission tomography; MBF: myocardial blood flow; MFR: myocardial flow reserve

the LAD (p=0.75) and RCA (p=0.82). In 14 patients, CCTA showed a left-dominant coronary anatomy in which the RCA did not subtend the left ventricular myocardium. In these patients, calculation of hyperemic MBF in the RCA territory based on individualized segmentation method was not possible and therefore these vessels were excluded from further analysis. Therefore, the total number of vessels included for further analysis of PET perfusion was 598 (97.7%).The relationship between hyperemic MBF values calculated using standard and individualized segmentation methods is illustrated in figure 3. There was a strong correlation between hyperemic MBF calculated with the two segmentation methods (r=0.98, p<0.001; figure 3A) and

excellent agreement (ICC=0.99, p<0.001; figure 3B). Bland-Altman plots showed an overall bias of 0.015±0.15 mL/min/g (figure 3B). Despite these minimal differences in MBF values, the presence of PET-defined hemodynamically significant CAD (hyperemic MBF ≤ 2.3 mL/min/g in two adjacent myocardial segments) did not differ between the two segmentation methods. PET-defined hemodynamically significant CAD was present in 252 (42.1%) vessels in the standard method and 253 (42.3%) vessels in the individualized method (p=0.95). PET-defined hemodynamically significant CAD results based on both segmentation methods were concordant in 593 (99.2%) vessels (figure 3A). Discordance in PET-defined hemodynamically significant CAD between the two methods occurred in only 5 (0.8%) vessels: two vessels changed from hemodynamically significant to non-hemodynamically significant (left upper quadrant figure 3A) and 3 changed from non-hemodynamically significant to hemodynamically significant CAD with the use of the individualized segmentation (right lower quadrant figure 3A).

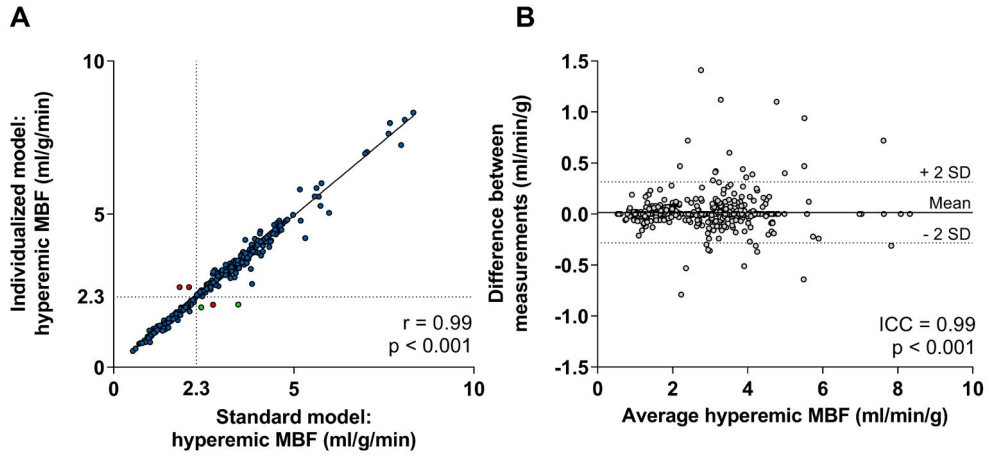

Figure 3. Relationship between hyperemic MBF derived from standard and individualized segmentation methods
(A) Scatterplot demonstrating a strong correlation between hyperemic MBF values calculated using both standard and individualized segmentation methods (r=0.99, p<0.001). Concordance in MBF results between both methods (concordant negative result, right upper quadrant; corcondant positive result, left lower quadrant) are depicted in blue. Discordant MBF measurements with a corresponding negative FFR measurement are depicted in green, whereas discordant measurements with a positive FFR measurement are depicted in red. (B) Bland-Altman plot demonstrating excellent agreement between hyperemic MBF calculated with both segmentation methods (ICC=0.99, p<0.001).

Diagnostic accuracy of both segmentation methods for hemodynamically significant CAD

FFR measurements were performed in 537 (89.8%) vessels. In 58 (9.6%) vessels FFR was not performed due to a total or sub-total lesion. These vessels all showed >90% diameter stenosis and were deemed hemodynamically obstructed. Additionally, FFR measurement was not possible in 3 (0.5%) vessels because of severe tortuosity. None of these vessels showed a coronary lesion of ≥30% diameter stenosis and all were deemed non-obstructed. The total number of vessels with hemodynamically significant CAD was 160 (26.8%). Based on FFR results, 4 out of 5 vessels with discordance in PET-defined hemodynamically significant CAD between the two segmentation methods, were falsely reclassified by the individualized segmentation: two vessels changed from true positive to false negative (figure 3A, left upper quadrant) and two vessels changed from true negative to false positive (figure 3A, right lower quadrant). Only one vessel was adequately reclassified with the individualized method, from false negative to true positive (figure 3A, right lower quadrant). The diagnostic performance of hyperemic MBF with standard and individualized segmentation methods for detecting presence of hemodynamically significant CAD are provided in table 3 on a per-vessel and per-patient basis. No differences in sensitivity, specificity, NPV, PPV and diagnostic accuracy were noted between the two groups. Furthermore, ROC curve analysis showed no significant difference in diagnostic value of hyperemic MBF between standard and individualized segmentation methods, with AUCs of 0.79 in both methods in per-vessel analysis (p=0.34) and AUCs of 0.82 and 0.83 respectively in per-patient analysis (p=0.33). The results of the impact of the two segmentation methods on the diagnostic performance of hyperemic MBF in the subgroups of the individual coronary arteries (LAD, LCX, and RCA) are shown in the supplementary material online (Supplementary Table 1). There were no significant differences in diagnostic value between the two segmentation methods in any of the individual coronary arteries.

Discussion

Our study evaluated the effect of individualized LV wall segmentation on the diagnostic value of quantitative $[^{15}O]H_2O$ PET. Results show that although redistribution

Table 3. Diagnostic accuracy of hyperemic MBF for detecting hemodynamically significant CAD using both standard and individualized segmentation methods.

	Standard segmentation	Individualized segmentation	p-value
Per-vessel			
Sensitivity (%)	84 (76-90)	83 (75-89)	0.38
Specificity (%)	69 (62-75)	69 (62-75)	0.20
NPV (%)	94 (90-96)	93 (89-95)	0.60
PPV (%)	54 (46-61)	54 (47-61)	0.73
Accuracy (%)	77 (72-81)	76 (71-80)	0.34
AUC	0.79 (0.76-0.82)	0.79 (0.75-0.82)	0.34
Per-patient			
Sensitivity (%)	87 (78-93)	88 (80-94)	1.00
Specificity (%)	78 (69-85)	78 (69-85)	1.00
NPV (%)	88 (80-94)	89 (81-94)	1.00
PPV (%)	76 (67-84)	76 (67-84)	0.32
Accuracy (%)	82 (76-87)	82 (76-87)	0.32
AUC	0.82 (0.76-0.87)	0.83 (0.77-0.88)	0.32

All values except AUC are % (95% confidence interval). AUC, area under the curve; NPV, negative predictive value; PPV, positive predictive value

of myocardial segments from standard to individualized segmentation occurred in 60% of patients, impact on MBF values was small. Discordance in PET-defined hemodynamically significant CAD between standard and individualized segmentation occurred in only 0.8% of vessels. As a result, the diagnostic value for the presence of hemodynamically significant CAD did not change with the use of individualized segmentation. Therefore, there is no need to use coronary anatomy from CCTA to define vascular territories in clinical PET perfusion imaging.

Correspondence of myocardial segments with coronary anatomy

Since no information on coronary anatomy and lesion location is obtained with PET, the standard AHA 17-segments model is commonly used to assign individual LV perfusion segments to specific coronary arteries.(3) This model is based on SPECT data obtained during transient coronary occlusion.(13) Although widely adopted, the AHA model ignores the tremendous variability in coronary anatomy. An individualized segmentation method in which information on coronary anatomy is used to assign coronary arteries to perfusion territories has been proposed to overcome this

shortcoming.(4-7) In the current report, CCTA-based individualized segmentation resulted in redistribution of LV segments in 60% of patients and in 8% of segments. Segments in the LAD territory were almost completely specific for the LAD, whereas redistribution was frequent in the LCX and RCA territories. Redistribution occurred most often in the inferior (segments 4, 10, and 15) and lateral wall (segments 12 and 16). In general, these results are in line with prior findings..(4-7,14-16) Most studies, like the present, have used anatomical information from CCTA to match myocardial segments with their feeding coronary artery.(4-7) Pereztol-Valdés et al. and Ortiz-Pérez et al., however, matched angiographic occlusion sites with respectively SPECT perfusion defects and cardiac magnetic resonance hyperenhancement.(15,16) All prior studies, except Javadi et al., corroborate the present findings that segments of the standard LAD territory are almost exclusively attributed to the LAD. Furthermore, in line with the present findings, variability of coronary anatomy was largest in lateral myocardial segments (12 and 16). To some extent, variability in the inferior segments was also reported in all aforementioned studies. Interestingly, studies that used invasive angiography to obtain anatomic information noted high variability in the septal segments.(15,16) This was not seen in our study, nor in most other CCTA studies.(4,6) A possible explanation for this discrepancy is the fact that visualization of small intramural arteries to septal segments with CCTA is challenging. This may have led to underestimation of the arterial supply of the inferoseptal segments by the LAD. Another explanation could be that in invasive angiography the push of dye into a coronary artery may lead to visualization of vessels in watershed regions. Differences in the force of dye injection could therefore lead to under or overestimation of the vascular supply to the inferoseptal segments.

Diagnostic value of quantitative PET with individualized segmentation

Data on the impact of CCTA-defined individualized segmentation on the diagnostic value of PET perfusion imaging are scarce. Liga et al. reported on the diagnostic value of hybrid imaging with fusion of CCTA and perfusion images in 252 patients.(7) In this predominantly SPECT/CT study individualized segmentation resulted in a change in SPECT/PET-defined hemodynamically significant CAD in 18% of patients and an increased diagnostic accuracy of hybrid versus stand-alone imaging. The validity of these results for PET imaging however are unclear, as only 29% of patients underwent

PET/CT and no data on the PET/CT subgroup were presented. Furthermore, the increased diagnostic value may not solely be the result of differences in segmentation, as the addition of CCTA-derived stenosis grade may have also augmented diagnostic performance. Therefore, no reliable conclusion on the sole effect of individualized segmentation can be drawn from this study. To date, only one study has investigated the effect of individualized segmentation on the diagnostic value of quantitative PET perfusion. Thomassen et al. reported no difference in hyperemic MBF values between standard and individualized segmentation, in a small population of 44 patients undergoing [^{15}O]H_2O PET and CCTA.(4) As a consequence, individualized segmentation of myocardial segments had little effect on PET-defined hemodynamically significant CAD results with discordance in PET-defined hemodynamically significant CAD between segmentation methods in only 1 patient. Using QCA stenosis ≥50% as reference standard, no difference in diagnostic performance between the segmentation methods was noted.

In contrast with Thomassen et al., redistribution of segments by the individualized method led to minimal changes in hyperemic MBF values in the current study. These changes, however, were very small with and there was excellent agreement of MBF values between the two methods (ICC=0.99). In concordance with Thomassen et al., discordance in PET-defined hemodynamically significant CAD between the segmentation methods was very infrequent and occurred in only 5 (0.8%) vessels. Only one of these discordant vessels was correctly reclassified according to FFR. As a result, the diagnostic value of [^{15}O]H_2O PET for detecting obstructive CAD did not change with the use of individualized segmentation. Although similar to Thomassen et al., our results expand on their findings in three ways. First, Thomassen et al. reported almost no redistribution of inferior myocardial segments. Since this is likely an effect of the relatively small patient population,(17) the influence of individualized segmentation on the diagnostic value reported in their study may not adequately reflect the effect in larger patient populations. Second, the reference standard for hemodynamically significant CAD of QCA-defined stenosis is considered suboptimal, since several studies have shown that angiographic stenosis severity does not adequately predict the functional consequences of a stenosis.(8) Therefore, FFR was used as reference for hemodynamically significant CAD in our study. Third, Thomassen et al. used mean

hyperemic MBF value in the entire perfusion territory to define hemodynamically significant CAD. Since perfusion defects seldom cover the whole perfusion territory, MBF values will be averaged over both ischemic and non-ischemic segments. This may lead to underestimation of hemodynamically significant CAD. Therefore, we used the previously validated and commonly used definition of two adjacent myocardial segments with a hyperemic MBF ≤2.3 for PET-defined hemodynamically significant CAD.(2,11) Using these definitions for PET and FFR, diagnostic accuracy of [^{15}O] H_2O PET was not altered by the individualized segmentation of myocardial segments. Therefore there is no need to perform the time-consuming procedure of matching CCTA-defined coronary anatomy with PET perfusion territories in clinical PET perfusion imaging.

Nevertheless, it is important to note that standard myocardial segments are an oversimplification of perfusion territories since single myocardial segments can be supplied by multiple coronary arteries. MBF values per segment may therefore be averaged over both ischemic and non-ischemic myocardium. Recent advances in CCTA analysis might enable more accurate delineation of perfusion defects. The Voronoi-algorithm is a mathematical algorithm which enables estimation of subtending myocardial mass from CCTA data.(18-20) Prior studies have reported excellent correlation between the Voronoi-algorithm segmentation and both SPECT-based myocardial mass at risk in humans and histological myocardial mass in animal models.(18-20) Furthermore, recent developments have enabled CT-perfusion-based MBF quantification in the vascular territory of a specific coronary stenosis using the Voronoi-algorithm.(21) However, fusion of PET perfusion data with Voronoi-algorithm segmentation is not yet available. These technical advances in PET perfusion imaging have the potential to improve diagnostic performance and are eagerly awaited.

Limitations

This study has several limitations. First, as already mentioned, it is likely that arterial supply of septal segments by the LAD has been underestimated by the present CCTA-based segmentation method. This may have affected the diagnostic value of the individualized method. Second, FFR was not available in 61 (10.2%) vessels. In these vessels assumptions on hemodynamically significant CAD were made. Although prior

data has shown FFR to be positive in almost all vessels with a subtotal stenosis and negative in all vessels without ≥30% stenosis, these assumptions may have affected our results.(8) Third, according to the AHA 17-segments model, the apex (segment 17) is defined as the area of myocardium beyond the end of the left ventricular cavity.(3) Instead we used the methodology of Thomassen et al. in which the LV myocardium is divided into 4 slices of equal thickness.(4) Although the differences between these segmentation methodologies are small, minor influence on our results may have occurred. Fourth, $[^{15}O]H_2O$ was used as tracer in the current study. Since $[^{15}O]H_2O$ is metabolically inert and freely diffusible across myocyte membrane and subsequently uptake in/and clearance from the myocardium is linear to perfusion, it is considered the optimal tracer for perfusion imaging.(1) Although one should be cautious to directly extrapolated our results to PET perfusion imaging with other tracers, such as $^{13}NH_3$ and ^{82}Rb, it seems plausible that our conclusion may also hold true for imaging with other tracers. Fifth, several studies have reported on the clinical impact of hybrid imaging with fusion of CCTA and perfusion images which enables co-localization of myocardial perfusion abnormalities and subtending coronary arteries.(22,23) This might result in more precise adjudication of perfusion territories than with separate interpretation of CT and PET/SPECT. In our study, CCTA and PET analysis were performed in a blinded fashion to evaluate the sole effect of myocardial segmentation on the diagnostic value of quantitative PET perfusion. Individualized segmentation with image fusion might have yielded different results. Sixth, the impact of individualized segmentation may be influenced by knowledge of the complexity of disease. Since analysis of PET data was performed blinded for CCTA and angiographic data, this will not have affected our results. Last, the added value of the use of CCTA for segmentation of myocardial segments might theoretically be larger in inexperienced readers. Since PET imaging analysis in the current study was performed by an experienced core laboratory, our results may not be extrapolated to the diagnostic value of PET when evaluated by inexperienced readers.

Conclusion

Individualized segmentation of myocardial segments using CCTA-derived coronary anatomy led to redistribution of standard myocardial segments in 60% of patients. However, the impact on $[^{15}O]H_2O$ PET derived MBF values was small, with

discordance in PET-defined hemodynamically significant CAD between standard and individualized segmentation in only 0.8% of vessels. As a result, the diagnostic value of [^{15}O]H_2O PET in detecting presence of hemodynamically significant CAD did not change with the use of individualized segmentation. Therefore, there is no need to use CCTA to allocate vascular territories to their corresponding coronary arteries in clinical PET perfusion imaging.

References

1. Driessen RS, Raijmakers PG, Stuijfzand WJ, Knaapen P. Myocardial perfusion imaging with PET. Int J Cardiovasc Imaging 2017;33:1021-1031.
2. Danad I, Raijmakers PG, Driessen RS et al. Comparison of Coronary CT Angiography, SPECT, PET, and Hybrid Imaging for Diagnosis of Ischemic Heart Disease Determined by Fractional Flow Reserve. JAMA Cardiol 2017;2:1100-1107.
3. Cerqueira MD, Weissman NJ, Dilsizian V et al. Standardized myocardial segmentation and nomenclature for tomographic imaging of the heart. A statement for healthcare professionals from the Cardiac Imaging Committee of the Council on Clinical Cardiology of the American Heart Association. Circulation 2002;105:539-42.
4. Thomassen A, Petersen H, Johansen A et al. Quantitative myocardial perfusion by O-15-water PET: individualized vs. standardized vascular territories. Eur Heart J Cardiovasc Imaging 2015;16:970-6.
5. Javadi MS, Lautamaki R, Merrill J et al. Definition of vascular territories on myocardial perfusion images by integration with true coronary anatomy: a hybrid PET/CT analysis. J Nucl Med 2010;51:198-203.
6. Setser RM, O'Donnell TP, Smedira NG et al. Coregistered MR imaging myocardial viability maps and multi-detector row CT coronary angiography displays for surgical revascularization planning: initial experience. Radiology 2005;237:465-73.
7. Liga R, Vontobel J, Rovai D et al. Multicentre multi-device hybrid imaging study of coronary artery disease: results from the EValuation of INtegrated Cardiac Imaging for the Detection and Characterization of Ischaemic Heart Disease (EVINCI) hybrid imaging population. Eur Heart J Cardiovasc Imaging 2016;17:951-60.
8. Tonino PA, Fearon WF, De Bruyne B et al. Angiographic versus functional severity of coronary artery stenoses in the FAME study fractional flow reserve versus angiography in multivessel evaluation. J Am Coll Cardiol 2010;55:2816-21.
9. Danad I, Raijmakers PG, Harms HJ et al. Impact of anatomical and functional severity of coronary atherosclerotic plaques on the transmural perfusion gradient: a [15O]H2O

PET study. Eur Heart J 2014;35:2094-105.
10. Harms HJ, Knaapen P, de Haan S, Halbmeijer R, Lammertsma AA, Lubberink M. Automatic generation of absolute myocardial blood flow images using [15O]H2O and a clinical PET/CT scanner. Eur J Nucl Med Mol Imaging 2011;38:930-9.
11. Danad I, Uusitalo V, Kero T et al. Quantitative assessment of myocardial perfusion in the detection of significant coronary artery disease: cutoff values and diagnostic accuracy of quantitative [(15)O]H2O PET imaging. J Am Coll Cardiol 2014;64:1464-75.
12. Leisenring W, Alonzo T, Pepe MS. Comparisons of predictive values of binary medical diagnostic tests for paired designs. Biometrics 2000;56:345-51.
13. Gallik DM, Obermueller SD, Swarna US, Guidry GW, Mahmarian JJ, Verani MS. Simultaneous assessment of myocardial perfusion and left ventricular function during transient coronary occlusion. J Am Coll Cardiol 1995;25:1529-38.
14. Aepfelbacher FC, Johnson RB, Schwartz JG et al. Validation of a model of left ventricular segmentation for interpretation of SPET myocardial perfusion images. Eur J Nucl Med 2001;28:1624-9.
15. Ortiz-Perez JT, Rodriguez J, Meyers SN, Lee DC, Davidson C, Wu E. Correspondence between the 17-segment model and coronary arterial anatomy using contrast-enhanced cardiac magnetic resonance imaging. JACC Cardiovasc Imaging 2008;1:282-93.
16. Pereztol-Valdes O, Candell-Riera J, Santana-Boado C et al. Correspondence between left ventricular 17 myocardial segments and coronary arteries. Eur Heart J 2005;26:2637-43.
17. Knuuti J, Saraste A. Perfusion imaging and coronary anatomy. Eur Heart J Cardiovasc Imaging 2015;16:966-7.
18. Kurata A, Kono A, Sakamoto T et al. Quantification of the myocardial area at risk using coronary CT angiography and Voronoi algorithm-based myocardial segmentation. Eur Radiol 2015;25:49-57.
19. Ide S, Sumitsuji S, Yamaguchi O, Sakata Y. Cardiac computed tomography-derived myocardial mass at risk using the Voronoi-based segmentation algorithm: A histological validation study. J Cardiovasc Comput Tomogr 2017;11:179-182.
20. Chung MS, Yang DH, Kim YH et al. Myocardial segmentation based on coronary anatomy using coronary computed tomography angiography: Development and validation in a pig model. Eur Radiol 2017;27:4044-4053.
21. Tomizawa N, Fujino Y, Kamitani M et al. Longer diabetes duration reduces myocardial blood flow in remote myocardium assessed by dynamic myocardial CT perfusion. J Diabetes Complications 2018;32:609-615.
22. Gaemperli O, Schepis T, Valenta I et al. Cardiac image fusion from stand-alone SPECT and CT: clinical experience. J Nucl Med 2007;48:696-703.

23. Santana CA, Garcia EV, Faber TL et al. Diagnostic performance of fusion of myocardial perfusion imaging (MPI) and computed tomography coronary angiography. J Nucl Cardiol 2009;16:201-11.

Supplementary data

Supplementary Table 1. Diagnostic accuracy of hyperemic MBF for detecting hemodynamically significant CAD using both standard and individualized segmentation methods for individual coronary arteries.

	Standard segmentation	Individualized segmentation	p-value
LAD			
Sensitivity (%)	80 (69-88)	81 (71-89)	1.00
Specificity (%)	78 (69-85)	78 (69-85)	1.00
NPV (%)	85 (78-90)	86 (79-90)	0.32
PPV (%)	71 (63-78)	71 (64-78)	0.32
Accuracy (%)	78 (72-84)	79 (73-84)	1.00
AUC	0.79 (0.72-0.84)	0.79 (0.73-0.85)	0.32
LCX			
Sensitivity (%)	87 (73-96)	85 (69-94)	1.00
Specificity (%)	76 (69-83)	75 (68-82)	0.50
NPV (%)	96 (92-98)	95 (91-98)	0.28
PPV (%)	47 (39-54)	45 (37-52)	0.08
Accuracy (%)	78 (72-84)	77 (71-83)	0.25
AUC	0.82 (0.76-0.87)	0.80 (0.74-0.85)	0.17
RCA			
Sensitivity (%)	95 (82-99)	92 (79-98)	1.00
Specificity (%)	67 (59-75)	67 (59-75)	1.00
NPV (%)	98 (93-100)	97 (92-99)	0.27
PPV (%)	42 (36-48)	41 (35-47)	0.78
Accuracy (%)	73 (66-79)	72 (65-78)	1.00
AUC	0.81 (0.75-0.86)	0.80 (0.73-0.85)	0.32

All values except AUC are % (95% confidence interval). AUC = area under the curve; NPV = negative predictive value; PPV = positive predictive value

Chapter 14

Incremental prognostic value of hybrid PET-CT: combining myocardial blood flow, coronary stenosis severity and high-risk plaque morphology

Michiel J. Bom*, Roel S. Driessen*, Pepijn A. van Diemen, Stefan P. Schumacher, Remi M. Leonora, Henk Everaars, Albert C. van Rossum, Pieter G. Raijmakers, Peter M. van de Ven, Cornelis C. van Kuijk, Adriaan A. Lammertsma, Juhani Knuuti, Amir Ahmadi, James K. Min, Jonathon A. Leipsic, Jagat Narula, Ibrahim Danad, and Paul Knaapen

* Both authors contributed equally

Eur Heart J Cardiovasc Imaging. 2020;21(10):1105-1113

Abstract

Aims: The present study sought to determine the prognostic value of combined functional testing using positron emission tomography (PET) perfusion imaging and anatomical testing using coronary computed tomography angiography (CCTA)-derived stenosis severity and plaque morphology in patients with suspected coronary artery disease (CAD).

Methods and results: In this retrospective study, 539 patients referred for hybrid [^{15}O] H_2O PET–CT imaging because of suspected CAD were investigated. PET was used to determine myocardial blood flow (MBF), whereas CCTA images were evaluated for obstructive stenoses and high-risk plaque morphology. Patients were followed up for the occurrence of all-cause death and non-fatal myocardial infarction (MI). During a median follow-up of 6.8 [interquartile range 4.8-7.8] years, 42 (7.8%) patients experienced events, including 23 (4.3%) deaths and 19 (3.5%) MIs. Annualized event rates for normal vs. abnormal results of PET MBF, CCTA-derived stenosis and high-risk plaque morphology were 0.6 vs 2.1%, 0.4 vs 2.1% and 0.8 vs 2.8%, respectively ($p<0.001$ for all). Cox regression analysis demonstrated prognostic values of PET perfusion imaging (Hazard ratio [HR] 3.75 [1.84–7.63], $p<0.001$), CCTA-derived stenosis (HR 5.61 [2.36–13.34], $p<0.001$) and high-risk plaques (HR 3.37 [1.83–6.18], $p<0.001$) for the occurrence of death or MI. However, only stenosis severity (HR 3.01 [1.06–8.54], $p=0.039$) and high-risk plaques (HR 1.93 [1.00–3.71], $p=0.049$) remained independently associated.

Conclusions: PET-derived MBF, CCTA-derived stenosis severity and high-risk plaque morphology were univariably associated with death and MI, whereas only stenosis severity and high-risk plaque morphology provided independent prognostic value.

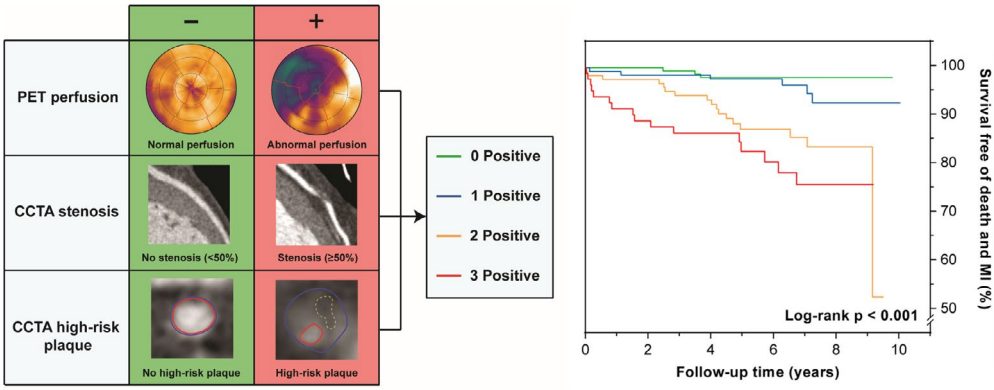

Graphical abstract. Incremental prognostic value by hybrid PET-CT findings.
Combined use of hybrid imaging with positron emission tomography perfusion imaging (≤2.30 mL·min-1·g-1), coronary computed tomography angiography-derived stenosis (≥50%) and high-risk plaque (≥2 adverse plaque characteristics) enables strong and incremental risk prediction for clinical outcome.

Introduction

Traditionally, angiographic severity of coronary artery disease (CAD) has been used to guide patient management with either revascularization or optimal medical treatment. Stenosis severity is now increasingly assessed non-invasively with coronary computed tomography angiography (CCTA), which was shown to be a powerful prognostic tool (1, 2). Next to luminal stenosis severity, CCTA allows for non-invasive evaluation of atherosclerotic plaque morphology, including adverse plaque characteristics (APCs) such as positive remodelling and low attenuation. The presence of these characteristics have been described to represent an elevated risk for future cardiac events(3, 4). CCTA's moderate specificity, however, might cause increased downstream diagnostic and treatment costs (5). Moreover, in recent years the clinical arena has shifted from anatomically to physiologically guided management as a result of various trials (6) which is reflected by recommendations in current revascularization guidelines (7). In this regard, positron emission tomography (PET) is considered the non-invasive reference standard for quantitative myocardial perfusion analysis and showed incremental prognostic value over traditional clinical predictors (8, 9). Combining PET with CCTA (so-called hybrid PET-CT) allows for functional as well as anatomical evaluation of CAD, which is suggested to enhance prognostic value over either one modality alone (10). While PET derived myocardial perfusion as well as CCTA derived stenosis severity and plaque morphology all have their established individual value, the incremental prognostic value of these combined entities derived from hybrid PET-CT is currently unknown. Therefore, the present study investigated the prognostic value of comprehensive hybrid PET-CT imaging in patients with suspected CAD.

Methods

Patient population

A total of 650 consecutive patients, who underwent PET-CT imaging because of suspected stable CAD at the VU University Medical Center in Amsterdam between 2008 and 2014, were initially evaluated for inclusion. In all patients, PET and CT imaging was performed, regardless of the result of either one of the imaging tests. Exclusion criteria for PET-CT imaging performance were atrial fibrillation, high degree atrioventricular block, impaired renal function, symptomatic asthma, and

pregnancy. No cardiovascular events occurred between the two tests. Post-imaging treatment strategy was left to the discretion of the referring physician. Among these patients, 32 (5%) were excluded because of a documented history of CAD (MI, PCI, or CABG), whereas 25 (4%) patients were excluded due to uninterpretable imaging results. Of the remaining 593 patients, 54 (10%) were lost to follow up, resulting in a final study population of 539 patients. This study complied with the Declaration of Helsinki and was approved by the Medical Ethics Review Committee of the VU University Medical Center with waiver of informed consent.

Positron emission tomography and coronary computed tomography angiography assessment

All patients underwent hybrid PET-CT imaging. PET perfusion images were acquired on a Gemini TF 64 PET-CT scanner (Philips Healthcare, Best, The Netherlands). CCTA images were acquired on the same Gemini TF 64 PET-CT scanner in 352 patients and on a 256-slice Brilliance iCT scanner (Philips Healthcare, Best, The Netherlands) in the remaining 187 patients. The hybrid PET-CT imaging procedures have been described in detail previously (11, 12).

With regard to the PET imaging protocol, a dynamic perfusion scan was performed using 370 MBq of $[^{15}O]H_2O$ both during resting and adenosine (140 $\mu g \cdot kg^{-1} \cdot min^{-1}$) induced hyperaemic conditions. Low dose CT scans were used for attenuation correction. Quantitative parametric myocardial blood flow (MBF) images were generated using in-house developed software.(13) Hyperaemic MBF, expressed in $mL \cdot min^{-1} \cdot g^{-1}$ of perfusable myocardial tissue, was calculated for all three vascular territories derived from standard segmentation: left anterior descending (LAD), left circumflex (LCX), and right coronary artery (RCA). Hyperaemic MBF ≤2.30 $mL \cdot min^{-1} \cdot g^{-1}$ in any of the vascular territories was defined as abnormal.(14) PET and CCTA images were evaluated separately.

Prior to the CCTA scanning protocol, sublingual nitroglycerine spray was administered to all patients and metoprolol when necessary, aiming for a heart rate of <65 beats·min^{-1}. Coronary artery calcium scoring (CACS) was obtained during a single breath-hold on a non-contrast CT and expressed in Agatston units. ECG-gated prospective acquisition was then applied when feasible, triggered at 75% of the R-R interval. For visualization

of the coronary artery lumen a bolus of 100 mL iobitidol (Xenetix 350) was injected intravenously. Scans were triggered using an automatic bolus tracking technique, with a region of interest in the descending thoracic aorta. All coronary segments with a diameter ≥2 mm were assessed for stenosis severity and plaque morphology as previously described (15). The coronary tree was evaluated according to a 17-segment coronary artery model using axial, multiplanar reformation, maximum intensity projection, and cross-sectional images. Stenosis severity was graded visually and a diameter stenosis ≥50% was considered significantly obstructive. In addition, coronary lesions were analysed for APCs. The remodelling index was computed as the ratio of vessel area at the site of the maximal lesion to that of a proximal reference point, with an index >1.1 representing positive remodelling (PR) (16). Low attenuation plaque (LAP) was defined as a plaque containing any voxel <30 HU (16). Spotty calcification (SC) was characterized by a calcified plaque comprising <90° of the vessel circumference and <3 mm in length (16). The napkin ring sign (NRS) was defined by a plaque core with low CT attenuation surrounded by a rim-like area of higher CT attenuation (17). A high-risk plaque was defined by the presence of at least two plaque characteristics (16).

Follow-up

Patients were retrospectively followed-up by observers blinded to the imaging results using national registry databases, electronic medical records, and standardized telephone interviews. Individual follow-up intervals ranged from the imaging acquisition until April 2018. Follow-up was censored at the time of the endpoint or at the time patients were last contacted. The study endpoint was a composite of all-cause death and non-fatal myocardial infarction (MI). Identified events were scored in accordance with the criteria provided in the European Society of Cardiology guidelines (7).

Statistical analysis

Continuous variables are shown as mean ± SD or median (interquartile range [25th to 75th percentile]). Categorical variables are presented as percentages. Continuous variables were tested for normal distribution and compared using Student's t-test or Mann-Whitney U test where applicable. Categorical variables were compared using

chi-square test. Annualized event rates were expressed as a proportion of the number of patients experiencing events divided by the number of patient-years follow-up and compared between groups using Poisson regression analysis. The cumulative event free survival in subgroups of patients defined by results of PET, CCTA stenosis and presence of high-risk plaques were visualized with Kaplan–Meier curves and compared using the log-rank test. Univariable Cox regression was used to assess associations of patient and imaging characteristics with death and MI. Significant covariates on univariable regression analysis were included in a multivariable analysis. The assumption of proportional hazard was tested by obtaining and reviewing the log-minus-log plots and deemed appropriate in all categories. A two-sided $p<0.05$ was considered statistically significant. Statistical analyses were conducted with IBM SPSS Statistics version 22.0 (IBM Corporation, Armonk, New York).

Results

Study population

Detailed baseline and imaging characteristics of the 539 study patients, with and without adverse events, are presented in table 1. Mean age was 58.6±9.2 years and 297 (55%) were male. Patients who suffered from an event were older, featured a higher coronary risk profile and were taking more medications.

Imaging findings

PET showed abnormal quantitative myocardial perfusion in 259 (48.1%) patients. According to CCTA, atherosclerotic plaques were present in 422 (78.1%) patients, whereas 302 (56.0%) patients showed obstructive stenosis (≥50%). In patients with a significant stenosis on CCTA, abnormal perfusion on PET was found in 202 (66.9%) cases. Among patients with abnormal PET perfusion, 21 (9%) showed normal coronary arteries on CCTA. CCTA-derived APCs were present in 303 (56.2%) patients. Among these characteristics, PR (n = 270, 50.1%) and LAP (n = 131, 24.3%) were most prevalent, followed by SC (n = 53, 9.8%) and NRS (n = 47, 8.7%). High-risk plaques (defined by presence of ≥2 APCs) were present in 127 (23.6%) of patients. APCs were most commonly present in patients with significant stenosis (n = 230, 76.2%) as opposed to non-significant stenosis (n = 72, 23.8%). 94 (74%) Patients with high-risk

plaques also showed abnormal PET. Median CACS was 52.9 [0–312.0], whereas high levels (>1000) were observed in 52 (9.6%) patients. An overview of the distribution of the imaging findings within groups is provided in figure 1.

Table 1. Patient baseline and imaging characteristics

	Overall (N=539)	Death/MI (n=42)	No death/MI (n=497)	P-value
Demographics				
Age, years	58.6±9.2	64.2±8.5	58.1±9.1	<0.001
Male	297 (55%)	27 (64%)	270 (54%)	0.14
Body mass index (kg/m^2)	27.0±4.1	26.6±3.4	27.0±4.2	0.49
CAD risk factors (n=532)				
Hypertension	251 (47%)	25 (60%)	226 (46%)	0.06
Hyperlipidemia	196 (37%)	22 (52%)	174 (36%)	0.02
Diabetes	93 (17%)	15 (36%)	78 (16%)	0.002
Smoking	184 (35%)	17 (41%)	167 (34%)	0.24
Family history of CAD	286 (54%)	21 (50%)	265 (54%)	0.36
Medication (n=534)				
Aspirin	404 (76%)	38 (91%)	366 (74%)	0.01
Statin	356 (67%)	35 (83%)	321 (65%)	0.01
Beta-blocker	325 (61%)	32 (76%)	293 (60%)	0.02
ACE inhibitor / ARB	190 (36%)	23 (55%)	167 (34%)	0.01
Calcium-channel blocker	141 (26%)	17 (41%)	124 (25%)	0.03
Type of chest pain (n=533)				0.06
Typical angina	165 (31%)	16 (39%)	149 (30%)	-
Atypical angina	188 (35%)	17 (42%)	171 (35%)	-
Non-specific chest pain	180 (34%)	8 (20%)	172 (35%)	-
PET perfusion imaging				
Abnormal hyperaemic MBF	259 (48%)	32 (76%)	227 (46%)	<0.001
CCTA findings				
CACS (n=535)	52.9 [0-312]	320.9 [87.2-1365.9]	39.0 [0.0-281.4]	<0.001
Normal coronary arteries	118 (22%)	0 (0%)	118 (24%)	<0.001
Non-obstructive CAD	119 (22%)	6 (14%)	113 (23%)	0.14
Obstructive CAD	302 (56%)	36 (86%)	266 (54%)	<0.001
High-risk plaque	127 (24%)	20 (48%)	107 (22%)	<0.001

Values are mean ± SD, median [IQR] or n (%). ACE: angiotensin-converting enzyme; ARB: angiotensin receptor blocker; CACS: coronary artery calcium score; CAD: coronary artery disease; CCTA: coronary computed tomography angiography; IQR: interquartile range; MBF: myocardial blood flow; MI: myocardial infarction; PET: positron emission tomography

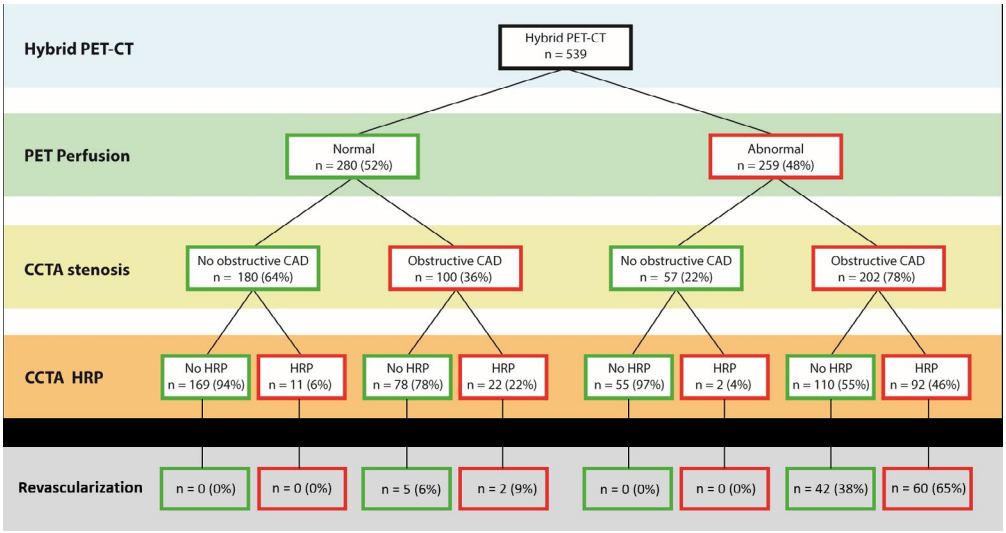

Figure 1. Distribution of hybrid PET-CT findings
Flowchart demonstrating the distribution of the hybrid PET-CT findings and revascularization performance among the three imaging parameters, i.e. PET perfusion abnormalities, CCTA-derived obstructive CAD, CCTA-derived HRP. CAD = coronary artery disease; CCTA = coronary computed tomography angiography; CT = computed tomography; HRP = high-risk plaque; PET = positron emission tomography

Follow-up results

During the median follow-up period of 6.8 years (IQR 4.8-7.8 years), an event occurred in 42 (7.8%) patients, including 23 (4.3%) deaths, 19 (3.5%) MIs. A total of 109 (20.2%) early, 38 (7.1%) late non-urgent, and 20 (3.7%) urgent revascularizations were performed during follow-up. These revascularizations were not regarded as adverse events. Annual rates of all-cause mortality and MI were 0.68% and 0.60%, respectively.

Survival analysis

Figures 2 depicts the Kaplan-Meier survival curves of individual PET perfusion, CCTA stenosis severity, and CT high-risk plaque for the combined endpoint of death and MI (log-rank P<0.001 for all). Annualized event rates were 2.1 and 0.6% (p<0.001) for patients with and without abnormal PET perfusion, respectively. Similarly, for patients with and without a obstructive stenosis on CCTA, the annual rates of death or MI were 2.1 and 0.4% (p<0.001), respectively. Respective annual rates for patients with and without high-risk plaques were 2.8 and 0.8% (p<0.001) respectively.

Furthermore, the combined use of PET and CCTA parameters resulted in a significantly

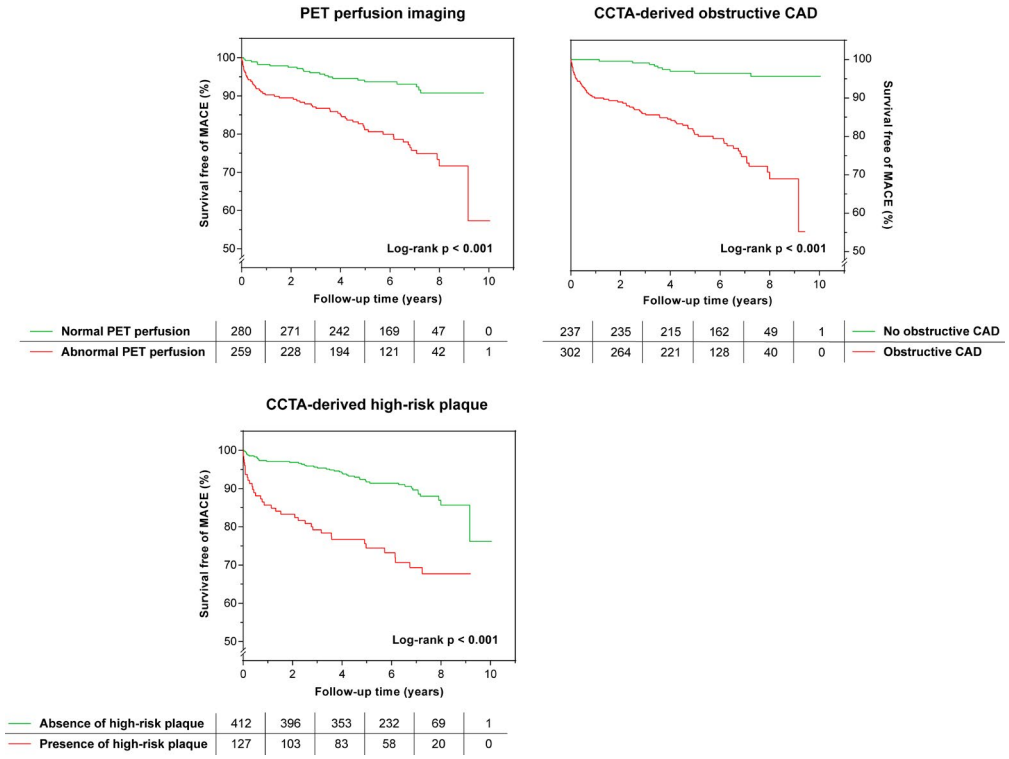

Figure 2. Survival analyses for death and MI according to imaging findings.
Kaplan-Meier curves for survival free from myocardial infarction and all cause death according to PET perfusion, CCTA-derived stenosis grade, and CCTA-derived high-risk plaque. MI = myocardial infarction; other abbreviations as in Figure 1

improved prediction of detrimental outcome (log-rank P<0.001) as shown in the survival curves in Figure 3. In patients without positive imaging findings (i.e. normal PET perfusion, CCTA stenosis <50%, no high-risk plaque, n=169), the annualized event rate was 0.3%. This resulted in a total event free survival during follow-up (median 6.8 years) of 98.2% in our cohort. Accordingly, for patients with 1 (n=144), 2 (n=134), and 3 (n=92) positive PET-CT findings, the annualized event rate was 0.7%, 2.2%, and 3.3%, respectively, with a total event free survival of 95.8%, 87.3%, and 82.6%, respectively, during follow-up in our cohort.

Among patients who reached the combined endpoint of death or MI, patients with high-risk plaques showed the shortest median time to event of 566 days (IQR 79-1810 days), as compared with obstructive stenosis 1037 days (IQR 224-1814 days) and abnormal perfusion 1231 (IQR 290-1806 days). Accordingly, landmark analysis with

pairwise log-rank comparisons showed very low risk of events for patients without high-risk plaques at 4 years and no significant differences, regardless of obstructive stenosis (p=0.21) or impaired myocardial blood flow (p=0.11) (figure 4).

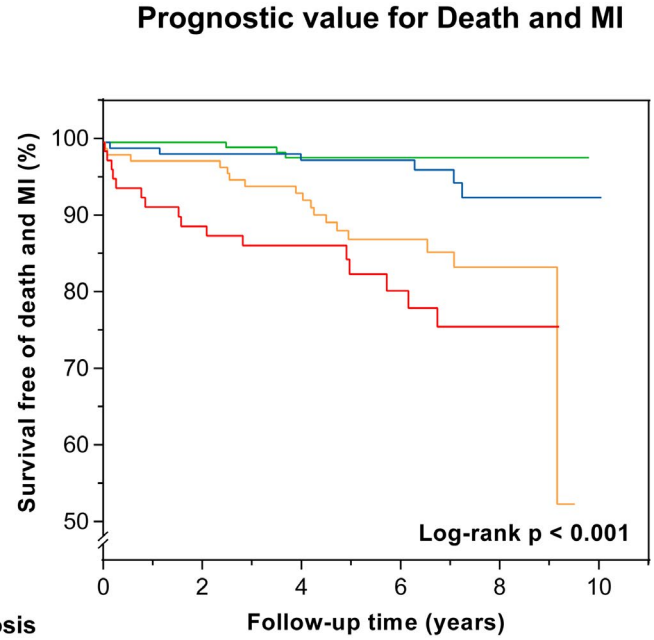

Combined PET-CT stenosis and CCTA-derived HRP						
0 Positive findings	169	168	153	115	32	0
1 Positive finding	144	140	129	86	26	1
2 Positive findings	134	130	112	62	26	0
3 Positive findings	92	79	64	40	14	0

Figure 3. Survival analyses according to combined imaging findings.
Kaplan-Meier curves demonstrating cumulative survival for death and MI according to combined hybrid PET-CT imaging findings. Abbreviations as in Figure 1 and 2.

Univariable and multivariable analysis

Baseline univariable and multivariable prognostic factors and corresponding hazard ratios are listed in table 2. Among baseline patient characteristics, age and presence of diabetes and dyslipidaemia were univariably associated with death and MI. Accordingly, all imaging results (PET-derived MBF, CT-derived CACS, stenosis, and high-risk plaque) were univariably associated with future events. Among the univariable parameters, the largest hazard ratio was observed for a significant CCTA

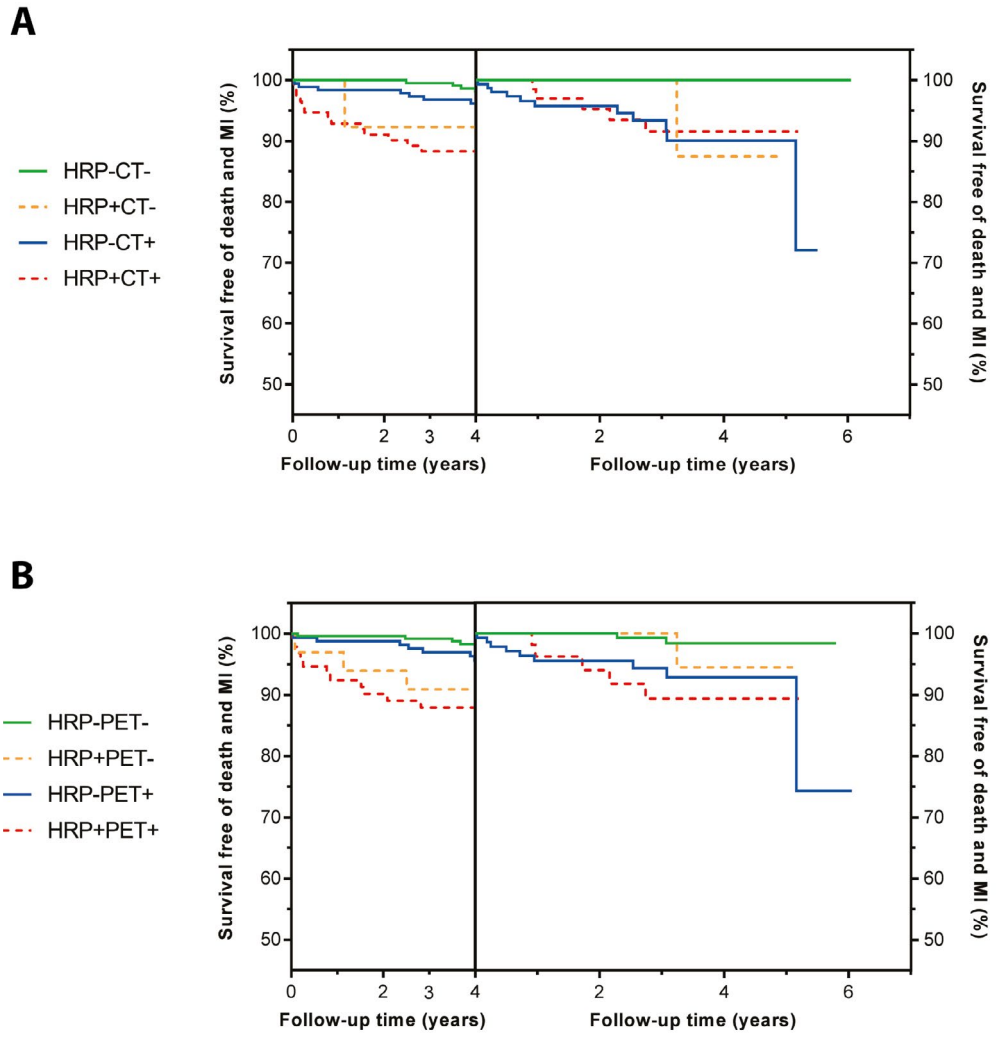

Figure 4. Short term and long term survival analyses according to combined imaging stratified by high-risk plaques
Landmark analysis with Kaplan-Meier curves demonstrating cumulative survival of death and MI for short term (4 years) and long term follow-up, according to combined high-risk plaque with obstructive stenosis (A) and with abnormal flow (B). Survival was not significantly different at 4 years for patients without high-risk plaques (HRP-), regardless of obstructive stenosis (CT, p=0.21) or impaired myocardial blood flow (PET, p=0.11). Abbreviations as in figure 1.

stenosis (≥50%) (hazard ratio: 5.61, p<0.001). Univariably significant prognostic factors were included in a subsequent multivariable Cox regression analysis, on which only age, CCTA stenosis and high-risk plaques remained independently associated. Abnormal PET perfusion and higher CACS did not reach independent prognostic

Table 2. Univariable and multivariable prognostic value for death and MI

Characteristic	Univariable		Multivariable	
	Hazard ratio (95% CI)	p-value	Hazard ratio (95% CI)	p-value
Baseline characteristics				
Age, years	1.07 (1.03 – 1.10)	**<0.001**	1.04 (1.01 – 1.08)	**0.022**
Gender (male)	1.57 (0.83 – 2.95)	0.16		
BMI, kg/m^2	0.97 (0.89 – 1.04)	0.36		
Smoking	0.87 (0.47 – 1.62)	0.67		
Diabetes	2.49 (1.32 – 4.71)	**0.005**	1.85 (0.94 – 3.66)	0.077
Hypertension	1.65 (0.89 – 3.05)	0.11		
Dyslipidemia	1.88 (1.02 – 3.45)	**0.04**	1.22 (0.65 – 2.30)	0.530
Family history of CAD	0.87 (0.48 – 1.60)	0.66		
Imaging results				
CACS	1.00 (1.00 – 1.00)	**<0.001**	1.00 (1.00 – 1.00)	0.778
CCTA stenosis (≥50%)	5.61 (2.36 – 13.34)	**<0.001**	3.01 (1.06 – 8.54)	**0.039**
High risk plaque (≥2 features)	3.37 (1.83 – 6.18)	**<0.001**	1.93 (1.00 – 3.71)	**0.049**
PET (MBF≤2.30ml/min/g)	3.75 (1.84 – 7.63)	**<0.001**	1.91 (0.84 – 4.31)	0.121

Abbreviations as in Table 1

value. Regarding the prognostic value of the PET-CT imaging measures, the largest hazard ratio was again observed for CCTA obstructive stenosis (3.01, p=0.039).

Discussion

The present study of hybrid PET-CT imaging in patients with suspected stable CAD explored the prognostic value of PET-derived MBF, CCTA-derived stenosis severity and plaque morphology. All three imaging parameters were associated with the combined endpoint death and MI. Moreover, an incremental prognostic value of comprehensive hybrid PET-CT assessment was found (Graphical abstract). In this cohort, CCTA stenosis severity showed an independent and the strongest prognostic value among all parameters. Also adverse plaque morphology provided independent prognostic value. PET-derived MBF, which is strongly related to stenosis severity and plaque morphology, did not. Still, the current findings also suggest that comprehensive imaging assessment could result in an improved risk stratification as compared to any of the separate assessments alone.

Previous studies have described the prognostic value of both myocardial perfusion imaging with PET as well as stenosis severity assessment with CCTA and seem to improve risk stratification and patient management (1, 8, 9, 11). Both a normal perfusion with MPI (8) and no luminal stenosis on CCTA (18) confer a favourable prognosis. This is in line with the present study, which revealed a good long-term prognosis with very limited adverse events in case of normal PET MBF or no obstructive stenosis on CCTA. In recent years, attention grew on combining functional and anatomical assessment with hybrid devices like PET-CT. Although this promising technique was of incremental diagnostic value in some studies, others found only limited additional value.(11, 19, 20) Only few studies, however, assessed the prognostic value of hybrid SPECT-CT, whilst prognostic data of PET-CT is even more scarce (10, 21-23). The present findings add to these previous studies that hybrid imaging has indeed some incremental prognostic value as compared to one of the stand-alone imaging techniques.

Apart from traditional stenosis severity, CCTA also allows for a non-invasive evaluation of atherosclerotic plaque morphology. Previous studies identified specific morphological features that could be linked to so-called vulnerable plaques with pathology studies (24). These CCTA-derived high-risk plaque features have been associated with a poorer clinical outcome, even independent of stenosis severity (3, 4) and CACS (25). A recent substudy of the SCOT-HEART trial, however, reported that high-risk plaques did not provide independent prognostic value when CACS was taken into account as a measure of total atherosclerotic plaque burden (26). Our results differ from these findings, as high-risk plaque morphology in the present analysis did clearly improve prognostic value over quantitative CACS. Interestingly, patients with high-risk plaques who suffered from an event, had the shortest median time-to-event as compared to obstructive stenosis and abnormal myocardial perfusion (566 vs. 1037 vs. 1231 days, respectively). This is underlined by the finding that absence of high-risk plaques conferred a very low risk of death and MI at short term follow-up, regardless of CT stenosis or abnormal perfusion (figure 4). This suggests that patients with such plaques may be more vulnerable for plaque progression or rupture resulting in adverse events in a relative short term. Our findings represent the first evaluation of the prognostic value of high-risk plaques in a comprehensive assessment with myocardial

perfusion and coronary stenosis severity and evidently demonstrated incremental value of plaque morphology over clinical variables, perfusion, CACS and stenosis severity. A possible explanation could be that patients having such plaques benefit from statin therapy which might slow plaque progression and induce phenotypic plaque transformation into more calcified and less vulnerable plaques(27).

There has been a long debate about the comparative prognostic value of anatomical versus physiological findings, but until recently most argued for an advantage of physiology over anatomy. Some recent studies, however, reported a superior prognostic value of anatomical testing such as a substudy from the PROMISE trial showing a significantly better discriminatory ability of CCTA in predicting events than functional testing and also the EVINCI trial hinted in that direction (2, 28). Furthermore, the SCOT-HEART trial showed a lower rate of MI when using CCTA as compared to standard care (1, 2). Considering the largest hazard ratios in our multivariable analysis (Table 2), more diverging Kaplan-Meier curves (Figure 2) and annualized event rates, the present study seems to agree that CCTA-derived stenosis might have the greatest prognostic value among the findings which can be derived from a hybrid imaging modality. More specifically, normal coronary arteries on CCTA resulted in no events during follow-up and absence of obstructive lesions showed a greater event-free survival than normal MBF on PET or no high-risk plaque morphology on CCTA (figure 2). This is also in line with the recent ISCHEMIA trial, which did not proof that in patients with moderate or severe ischemia an initial invasive strategy reduced the risk of ischemic cardiovascular events or death(29). Possible explanations for those and our results are that obstructive stenoses might act as a more effective surrogate of plaque burden than ischaemia(30). Alternatively, patients with obstructive disease received more and possibly benefitted the most from revascularization (Figure 1).

Altogether, the current study urges for a prospective trial with comprehensive imaging including anatomy, function and morphology, in order to answer the question whether the present findings could indeed improve patient clinical outcome.

Limitations

The present retrospective study with a moderate sample size and limited number of events, has some limitations. First, current results may not be generalizable due to

the single centre setup of the study, such as inherent centre specific CCTA scanning techniques and specific PET tracers and thresholds for abnormal perfusion. Accordingly, current results derived from $[^{15}O]H_2O$ PET cannot be extrapolated to the more commonly used tracers $[^{13}N]NH_3$ and Rubidium-82. As per protocol in our tertiary referral centre, all study patients underwent both PET and CCTA imaging. This might hamper the generalizability of our results to an approach of performing CCTA and PET selectively. Finally, pragmatic dichotomous definitions of abnormal MBF, obstructive CAD and high-risk plaques were defined based on accepted standards and make current findings most useful for clinical practice. This simplification, however, disregards the potential extent of ischemia, such as quantitative global and regional absolute hyperaemic flow or flow reserve on a continuous scale, as well as quantitative high-risk plaque burden, such as low-attenuation or noncalcified plaque volume, which are of prognostic validity (8, 25, 30). A recent study, however, did not find incremental value of (adding) flow reserve over maximal flow(31). Still, future studies are to be undertaken to examine the anticipated incremental prognostic value of quantification of atherosclerotic disease and myocardial perfusion.

Conclusion

Hybrid PET-CT allowed for an integrated evaluation of myocardial blood flow, coronary stenosis severity and atherosclerotic plaque morphology. Such a comprehensive assessment showed an incremental prognostic value in patients suspected of stable CAD for a combined hard endpoint of death and MI. Among these imaging parameters, CCTA-derived stenosis severity might have the greatest independent predictive value for adverse events overall. High-risk plaque morphology, specifically, might have the strongest short-term negative predictive value. Future prospective trials are, however, warranted to test whether comprehensive assessment with hybrid PET-CT or CCTA alone could indeed improve patient outcome.

References

1. Newby DE, Adamson PD, Berry C, et al. Coronary CT Angiography and 5-Year Risk of Myocardial Infarction. N Engl J Med 2018;379(10):924-933.
2. Hoffmann U, Ferencik M, Udelson JE, et al. Prognostic Value of Noninvasive Cardiovascular Testing in Patients With Stable Chest Pain: Insights From the PROMISE

Trial (Prospective Multicenter Imaging Study for Evaluation of Chest Pain). Circulation 2017;135(24):2320-2332.

3. Motoyama S, Ito H, Sarai M, et al. Plaque Characterization by Coronary Computed Tomography Angiography and the Likelihood of Acute Coronary Events in Mid-Term Follow-Up. J Am Coll Cardiol 2015;66(4):337-346.
4. Ferencik M, Mayrhofer T, Bittner DO, et al. Use of High-Risk Coronary Atherosclerotic Plaque Detection for Risk Stratification of Patients With Stable Chest Pain: A Secondary Analysis of the PROMISE Randomized Clinical Trial. JAMA Cardiol 2018;3(2):144-152.
5. Foy AJ, Dhruva SS, Peterson B, Mandrola JM, Morgan DJ, Redberg RF. Coronary Computed Tomography Angiography vs Functional Stress Testing for Patients With Suspected Coronary Artery Disease: A Systematic Review and Meta-analysis. JAMA Intern Med 2017;177(11):1623-1631.
6. Zimmermann FM, Omerovic E, Fournier S, et al. Fractional flow reserve-guided percutaneous coronary intervention vs. medical therapy for patients with stable coronary lesions: meta-analysis of individual patient data. Eur Heart J 2019;40(2):180-186.
7. Neumann FJ, Sousa-Uva M, Ahlsson A, et al. 2018 ESC/EACTS Guidelines on myocardial revascularization. Eur Heart J 2019;40(2):87-165.
8. Murthy VL, Naya M, Foster CR, et al. Improved cardiac risk assessment with noninvasive measures of coronary flow reserve. Circulation 2011;124(20):2215-2224.
9. Patel KK, Spertus JA, Chan PS, et al. Myocardial blood flow reserve assessed by positron emission tomography myocardial perfusion imaging identifies patients with a survival benefit from early revascularization. Eur Heart J 2020;41(6):759-768.
10. Maaniitty T, Stenstrom I, Bax JJ, et al. Prognostic Value of Coronary CT Angiography With Selective PET Perfusion Imaging in Coronary Artery Disease. JACC Cardiovasc Imaging 2017;10(11):1361-1370.
11. Danad I, Raijmakers PG, Driessen RS, et al. Comparison of Coronary CT Angiography, SPECT, PET, and Hybrid Imaging for Diagnosis of Ischemic Heart Disease Determined by Fractional Flow Reserve. JAMA Cardiol 2017;2(10):1100-1107.
12. Danad I, Raijmakers PG, Appelman YE, et al. Coronary risk factors and myocardial blood flow in patients evaluated for coronary artery disease: a quantitative [15O]H2O PET/CT study. Eur J Nucl Med Mol Imaging 2012;39(1):102-112.
13. Harms HJ, Knaapen P, de Haan S, Halbmeijer R, Lammertsma AA, Lubberink M. Automatic generation of absolute myocardial blood flow images using [15O]H2O and a clinical PET/CT scanner. Eur J Nucl Med Mol Imaging 2011;38(5):930-939.

14. Danad I, Uusitalo V, Kero T, et al. Quantitative assessment of myocardial perfusion in the detection of significant coronary artery disease: cutoff values and diagnostic accuracy of quantitative [(15)O]H2O PET imaging. J Am Coll Cardiol 2014;64(14):1464-1475.
15. Driessen RS, Stuijfzand WJ, Raijmakers PG, et al. Effect of Plaque Burden and Morphology on Myocardial Blood Flow and Fractional Flow Reserve. J Am Coll Cardiol 2018;71(5):499-509.
16. Nerlekar N, Ha FJ, Cheshire C, et al. Computed Tomographic Coronary Angiography-Derived Plaque Characteristics Predict Major Adverse Cardiovascular Events: A Systematic Review and Meta-Analysis. Circ Cardiovasc Imaging 2018;11(1):e006973.
17. Maurovich-Horvat P, Hoffmann U, Vorpahl M, Nakano M, Virmani R, Alkadhi H. The napkin-ring sign: CT signature of high-risk coronary plaques? JACC Cardiovasc Imaging 2010;3(4):440-444.
18. Shaw LJ, Hausleiter J, Achenbach S, et al. Coronary computed tomographic angiography as a gatekeeper to invasive diagnostic and surgical procedures: results from the multicenter CONFIRM (Coronary CT Angiography Evaluation for Clinical Outcomes: an International Multicenter) registry. J Am Coll Cardiol 2012;60(20):2103-2114.
19. Rizvi A, Han D, Danad I, et al. Diagnostic Performance of Hybrid Cardiac Imaging Methods for Assessment of Obstructive Coronary Artery Disease Compared With Stand-Alone Coronary Computed Tomography Angiography: A Meta-Analysis. JACC Cardiovasc Imaging 2018;11(4):589-599.
20. Liga R, Vontobel J, Rovai D, et al. Multicentre multi-device hybrid imaging study of coronary artery disease: results from the EValuation of INtegrated Cardiac Imaging for the Detection and Characterization of Ischaemic Heart Disease (EVINCI) hybrid imaging population. Eur Heart J Cardiovasc Imaging 2016;17(9):951-960.
21. van Werkhoven JM, Schuijf JD, Gaemperli O, et al. Prognostic value of multislice computed tomography and gated single-photon emission computed tomography in patients with suspected coronary artery disease. J Am Coll Cardiol 2009;53(7):623-632.
22. Pazhenkottil AP, Benz DC, Grani C, et al. Hybrid SPECT Perfusion Imaging and Coronary CT Angiography: Long-term Prognostic Value for Cardiovascular Outcomes. Radiology 2018;288(3):694-702.
23. Kim HL, Kim YJ, Lee SP, et al. Incremental prognostic value of sequential imaging of single-photon emission computed tomography and coronary computed tomography angiography in patients with suspected coronary artery disease. Eur Heart J Cardiovasc Imaging 2014;15(8):878-885.
24. Han D, Torii S, Yahagi K, et al. Quantitative measurement of lipid rich plaque by coronary computed tomography angiography: A correlation of histology in sudden

cardiac death. Atherosclerosis 2018;275:426-433.

25. Versteylen MO, Kietselaer BL, Dagnelie PC, et al. Additive value of semiautomated quantification of coronary artery disease using cardiac computed tomographic angiography to predict future acute coronary syndrome. J Am Coll Cardiol 2013;61(22):2296-2305.
26. Williams MC, Moss AJ, Dweck M, et al Coronary Artery Plaque Characteristics Associated With Adverse Outcomes in the SCOT-HEART Study. J Am Coll Cardiol 2019;73(3):291-301.
27. Lee SE, Chang HJ, Sung JM, et al. Effects of Statins on Coronary Atherosclerotic Plaques: The PARADIGM Study. JACC Cardiovasc Imaging 2018;11(10):1475-1484.
28. Neglia D, Liga R, Caselli C, et al. Anatomical and functional coronary imaging to predict long-term outcome in patients with suspected coronary artery disease: the EVINCI-outcome study. Eur Heart J Cardiovasc Imaging 2019[epub].
29. Maron DJ, Hochman JS, Reynolds HR, et al. Initial Invasive or Conservative Strategy for Stable Coronary Disease. N Engl J Med 2020;382(15):1395-1407.
30. Williams MC, Kwiecinski J, Doris M, et al. Low-Attenuation Noncalcified Plaque on Coronary Computed Tomography Angiography Predicts Myocardial Infarction: Results From the Multicenter SCOT-HEART Trial (Scottish Computed Tomography of the HEART). Circulation 2020;141(18):1452-1462.
31. Bom MJ, van Diemen PA, Driessen RS, et al. Prognostic value of [15O]H2O positron emission tomography-derived global and regional myocardial perfusion. Eur Heart J Cardiovasc Imaging 2019[epub].

Chapter 15

General summary and future perspectives

General summary

The detection of hemodynamically obstructive coronary stenoses is a cornerstone in the management of patients with suspected CAD. Since the current gold standard for detection of hemodynamically obstructive CAD, invasively measured fractional flow reserve (FFR), entails a non-negligible risk of serious complications such as stroke, myocardial infarction and death, current guidelines advocate the use of non-invasive imaging modalities for the initial diagnostic work-up of patients with suspected CAD. The aim of this thesis was to improve the diagnostic work-up of patients with suspected CAD through the investigation of advances in CCTA, quantitative PET perfusion and hybrid imaging.

Part I Coronary Computed Tomography Angiography

The initial diagnostic work-up of patients with suspected CAD starts with a clinical assessment of the probability of obstructive CAD, the pre-test probability (PTP). This clinical assessment is followed by a non-invasive imaging test such as CCTA. **Chapter 2** aimed to investigate to what extent CCTA leads to reclassification of patients and which impact CCTA results have on patient management in patients with a low to intermediate PTP. In a routine cohort of 1560 patients, CCTA resulted in reclassification in the majority of patients. Furthermore, medication changes (aspirin and/or statin therapy) occurred in 41% of patients. Interestingly, the Duke Clinical Score, a score used to define PTP, was shown to overestimate the probability of obstructive CAD as compared with CCTA findings.

Although diagnostic accuracy of stenosis grading using CCTA is high, with an excellent sensitivity and negative predictive value, specificity for hemodynamically obstructive CAD is relatively low. Several functional CCTA parameters have been proposed in an attempt to increase specificity of CCTA. One of these novel CCTA indices is the transluminal attenuation gradient (TAG), a CCTA derived measure of intracoronary luminal attenuation along the course of the vessels. In **Chapter 3**, the incremental diagnostic value of TAG and TAG with corrected contrast opacification (TAG-CCO) for the identification of ischemia as defined by both the invasive reference standard FFR and the noninvasive reference standard quantitative $[^{15}O]H_2O$ PET perfusion was evaluated. Additionally, the influence of the decrease in luminal diameter along the

course of the vessel (TDG) on these contrast-based flow estimations. Results show that TAG and TAG-CCO did not provide incremental diagnostic value of CCTA alone. Because TAG was significantly correlated with TDG, the lack of diagnostic value of TAG may be a result of interrelation with differences in coronary luminal diameter.

In addition to TAG, several other CCTA indices have been proposed to increase diagnostic performance of CCTA, i.e. qualitative and quantitative stenosis (visual grading and minimal lumen area, MLA) and plaque measures (characteristics and volumes), and more recently subtended myocardial mass (V_{sub}). Additionally, V_{sub}/MLA^2, a mathematical coronary CTA index based on the Hagen-Poiseuille law, has been proposed to increase diagnostic performance of standard coronary CTA assessment. In addition to these on-site coronary CTA parameters, remotely performed CT-derived FFR (FFR_{CT}) has emerged as a promising tool for the functional assessment of stenoses. **Chapter 4** reports on the diagnostic value of contemporary on and off-site CCTA assessment for FFR-defined hemodynamically obstructive CAD in 132 patients from the PACIFIC trial with ≥30% angiographic stenosis. Results show that in on-site coronary CTA assessment, MLA, plaque measures and Vsub were all independently predictive for hemodynamically obstructive CAD. Furthermore, the addition of off-site FFR_{CT} to on-site CTA analysis including V_{sub} significantly yet only minimally increased diagnostic performance for the identification of hemodynamically obstructive CAD. These results demonstrate that on-site CCTA assessment is a reasonable alternative to FFR_{CT}.

The HEART-score is a recently developed risk score that stratifies risk of major adverse cardiac events (MACE) in patients presenting to the emergency department with chest pain. In **Chapter 5**, we evaluated the ability of a low HEART score to predict the presence of CAD defined by CCTA and the occurrence of MACE. In a cohort of 713 consecutive patients presenting to the emergency department and subsequently referred for CCTA imaging, a low HEART score was shown to be a significant predictor of MACE-free survival. However, there was no difference in CCTA-defined obstructive CAD in patients with a low vs. intermediate/high HEART score and the ability of the HEART score to identify CCTA-defined obstructive CAD was poor. The results of this study demonstrate that although the HEART score is able to predict the occurrence of MACE, it does not adequately identify patients with obstructive CAD at

CCTA. Excluding patients from additional testing based on a low HEART score may lead to suboptimal patient management.

Risk assessment is a crucial aspect in the management of patients with suspected CAD. However, traditional risk stratification models using generally available clinical risk factors and plasma lipid levels have only modest predictive value for the presence of CAD and the occurrence of events. Recent technological advances have enabled the simultaneous measurement of large amounts of proteins using only one microliter of plasma, paving the way for the use of proteomics in large populations. **Chapter 6** investigated the predictive ability of targeted proteomics (332 proteins) for coronary plaque morphology in 203 patients from the PACIFIC trial with CCTA imaging and available plasma samples. Using machine learning models, trained on targeted proteomics, we defined two complementary protein signatures: one for identification of patients with high-risk plaques and one for identification of patients with absence of CAD. Both biomarker subsets were superior to generally available clinical characteristics and conventional biomarkers in predicting presence of high-risk plaque or absence of coronary atherosclerosis. These promising findings warrant external validation of the value of targeted proteomics to identify cardiovascular risk in outcome studies.

In **Chapter 7**, the incremental prognostic performance of coronary artery calcium scoring (CACS) and CCTA was evaluated in an single-center cohort of 1551 patients with suspected CAD and low to intermediate pre-test probability of obstructive CAD. Both CACS and CCTA were shown to have independent prognostic value for the occurrence of MACE. Additionally, a non-negligible amount of patients with a CACS of zero had obstructive CAD at CCTA. CCTA can be utilized in these patients to stratify risk for future MACE. Given the relatively low radiation burden in our study, the excellent prognostic value reported in our study supports the use of an initial CCTA strategy in patients with low to intermediate pre-test probability of obstructive CAD.

Coronary inflammation can be assessed on CCTA by determining pericoronary adipose tissue CT-attenuation (PCATa), which has been proposed as prognostic biomarker. **Chapter 8** investigated the prognostic value of PCTa beyond CCTA-derived atherosclerotic burden and PET-derived ischemia in a retrospective cohort

of 539 patients with suspected CAD. Results showed that PCTa of the RCA was an independent predictor for the occurrence of death or myocardial infarct beyond clinical characteristics, CT-derived plaque and stenosis measures, and PET-derived ischemia. Although promising, these findings warrant external validation in large prospective studies.

In addition to its role in the diagnostic work-up of patients with suspected CAD, the use of CCTA has recently been proposed for PCI procedural planning. Recent advances in FFR_{CT} technology have enabled the simulation of hyperemic pressure changes after virtual removal of stenoses, predicting the hemodynamic benefits of PCI using the FFR_{CT} planner tool. In **Chapter 9**, the accuracy of this novel FFR_{CT} planner tool referenced by invasive FFR measurements was investigated in a cohort of 56 patients with FFR measurements before and after PCI. FFR_{CT} planner demonstrated significant agreement with post-PCI FFR and with change in FFR values after PCI. These results indicate that the FFR_{CT} planner tool may hold promise for the non-invasive prediction of the hemodynamic benefits of PCI and for PCI procedural planning.

Part II Positron Emission Tomography

Contrary to the anatomical testing with CCTA, PET perfusion imaging is a functional imaging modality that measures the physiological consequences of coronary artery disease by quantifying absolute myocardial perfusion. In the diagnostic work-up of patients with suspected CAD, hyperemic myocardial blood flow (MBF) and coronary flow reserve (CFR) are the most commonly used PET parameters. However, recently the longitudinal MBF gradient, a decrease in hyperemic MBF from the base to the apex of the left ventricle, has been proposed as a more specific index for hemodynamically obstructive CAD. **Chapter 10** investigates the diagnostic value of the PET-derived longitudinal flow gradient for the presence of hemodynamically obstructive CAD defined by FFR. Results show lower diagnostic value of the longitudinal flow gradient as compared with hyperemic MBF. Furthermore, lesion location was found to affect the correlation of the longitudinal flow gradient and FFR. The presence of a longitudinal flow gradient may therefore be partly caused by normalization to a relatively normal perfused area, rather than by a distinct physiological phenomenon.

Quantification of myocardial blood flow, both hyperemic MFB and CFR, can be

performed on a global level for the left ventricle as a whole or on a regional level for the two adjacent segments with the lowest MBF per vascular territory. **Chapter 11** reports the results of a retrospective cohort study investigating the prognostic value of $[^{15}O]H_2O$ PET derived global and regional myocardial perfusion. Global and regional hyperemic MBF and CFR were all predictive of death and MI. However, for both global and regional perfusion, hyperemic MBF remained the only independent predictor after adjusting for the combined use of hyperemic MBF and CFR. Additionally, integrating global and regional perfusion did not increase prognostic performance compared to either regional or global perfusion alone. Regional analysis of PET perfusion, used in clinical practice to guide treatment, can therefore be considered a feasible alternative to global perfusion for identifying patients at risk for adverse events.

Part III Hybrid PET/CT Imaging

Chapter 12 gives a detailed overview of the detection and treatment of vulnerable coronary plaques, i.e. plaques with a high susceptibility to rupture. Recent advances in invasive and noninvasive coronary imaging techniques have empowered the clinician to identify suspected vulnerable plaques in vivo and paved the way for the evaluation of therapeutic agents targeted at reducing plaque vulnerability. Local treatment of vulnerable plaques by PCI and systemic treatment with anti-inflammatory and low-density lipoprotein–lowering drugs are currently being investigated in large randomized clinical trials to assess their therapeutic potential for reducing adverse coronary events. Results from these studies may enable a more patient-tailored strategy for the treatment of coronary artery disease.

Despite high variability in coronary anatomy, quantitative PET perfusion in coronary territories is traditionally calculated according to the American Heart Association 17-segments model. **Chapter 13** aimed to investigate the impact of individualized segmentation of myocardial segments using CCTA derived coronary anatomy on the diagnostic accuracy of quantitative $[^{15}O]H_2O$ PET perfusion for hemodynamically significant coronary artery disease. In this substudy of the PACIFIC trial, individualized segmentation using CCTA-derived coronary anatomy led to redistribution of standard myocardial segments in the majority of patients. However, this had little impact on $[^{15}O]H_2O$ PET MBF values and diagnostic value for detecting hemodynamically

significant CAD did not change. Therefore, there is no need to perform the time-consuming procedure of matching CCTA-defined coronary anatomy with PET perfusion territories in clinical PET perfusion imaging.

Although the prognostic value of both CCTA and PET perfusion imaging has been demonstrated by several large prospective studies, the independent prognostic value of combined PET/CT imaging remains largely unknown. **Chapter 14** describes the results of a retrospective cohort study on the prognostic value of hybrid PET/CT, allowing an integrated evaluation of myocardial blood flow, coronary stenosis severity and atherosclerotic plaque morphology. PET-derived MBF, CCTA-derived stenosis severity and high-risk plaque morphology were all long-term predictors of adverse cardiac events. However, only stenosis severity and high-risk plaque morphology provided independent prognostic value. Nonetheless, the findings of this study suggest that comprehensive imaging assessment could result in an improved risk stratification as compared to any of the separate assessments alone.

Future perspectives

Non-invasive imaging is an important aspect of the diagnostic work-up of patients with suspected CAD. Anatomical imaging using CCTA has emerged as one of the most widely used imaging modalities and both previous studies and studies from this thesis have demonstrated great diagnostic and prognostic performance of stenosis grading using CCTA. Studies from this thesis and other studies have also shown that novel parameters obtained through post-processing of standard CCTA data, such as plaque measures, subtended myocardial mass, FFR_{CT} and pericoronary fat attenuation may improve diagnostic and prognostic performance of CCTA. Ideally, future research efforts should focus on the development of a comprehensive tool that incorporates all valuable information obtained from CCTA to estimate the patient specific probability of hemodynamically obstructive CAD and patient risk for future events. Such tools will help in optimizing the diagnostic and prognostic abilities of CCTA. Subsequently, further randomized trials investigating the prognostic value of comprehensive CCTA-guided management are warranted to establish its role in management of patients with suspected CAD. These efforts will eventually facilitate the introduction of true comprehensive CCTA assessment to clinical practice.

In addition to its role in the diagnostic work-up of patients with suspected CAD, the use of CCTA has recently been proposed for PCI procedural planning. Data from this thesis confirms the potential of using CCTA for PCI procedural planning. However, given the small sample size and the novelty of the technology, these data should be considered hypothesis generating. Technological advances are warranted to improve the current status of the technology. Eventually the true value of PCI procedural planning using FFR_{CT} planner should be confirmed in large comparative trials. CCTA may become a valuable tool in patients undergoing percutaneous revascularization through proper patient selection and adequate procedural planning, minimizing procedural complication and optimizing treatment effect.

Quantitative perfusion imaging using $[^{15}O]H_2O$ PET has also gained great interest in the last decades. Previous studies and studies from this thesis have shown excellent diagnostic and prognostic performance of $[^{15}O]H_2O$ PET-derived absolute quantification of myocardial blood flow. Nonetheless, contrary to the widespread availability of CCTA, $[^{15}O]H_2O$ PET imaging is still limited to only a few centers worldwide given the short physical half-life $[^{15}O]H_2O$ and the subsequent need for an on-site cyclotron. Additionally, FDA approval for $[^{15}O]H_2O$ is still pending on the completion of a large international multi-center trial confirming the diagnostic performance. Future FDA approval and the recent development of a small cyclotron with subsequent lower costs for producing $[^{15}O]H_2O$ may facilitate the wide-spread availability of $[^{15}O]H_2O$ PET.

Hybrid imaging with PET/CT has been proposed to combine the strengths and overcome the limitations of both separate techniques. Although recent studies have questioned the diagnostic potential of hybrid PET/CT imaging, data from this thesis suggest that comprehensive imaging incorporating PET-derived myocardial blood flow, CCTA-derived stenosis severity, and high-risk plaque morphology might result in an improved risk stratification. These promising findings urge for a prospective clinical trial with interventions based on hybrid imaging including anatomy, function and morphology. Hypothetically, combined anatomical and functional information from hybrid PET/CT may improve patient outcome by guiding the use of invasive coronary angiography and expensive medication to the highest risk groups and conversely avoiding overtreatment in patients without coronary atherosclerosis.

Prospective clinical trials testing this hypothesis are eagerly awaited.

Appendices

Nederlandse samenvatting

Het detecteren van hemodynamisch belangrijk coronaire stenoses is een hoeksteen in de behandeling van patiënten met de verdenking op coronairlijden. De gouden standaard, invasief gemeten fractionele flow reserve (FFR), brengt echter niet-verwaarloosbare risico's op ernstige complicaties zoals een beroerte, myocard infarct en overlijden met zich mee. Derhalve adviseren de huidige richtlijnen het gebruik van non-invasieve beeldvormende technieken voor het initiële diagnostische traject bij patiënten met de verdenking op coronairlijden. Het doel van dit proefschrift is dan ook het verbeteren van dit diagnostische traject door het onderzoeken van verbeteringen in coronaire CT angiografie (CCTA), kwantitatieve positron emissie tomografie (PET) perfusie en hybride beeldvorming.

Deel I Coronaire Computed Tomografie Angiografie

Het initiële diagnostische traject bij patiënten waarbij een verdenking op coronairlijden bestaat, begint met een klinische inschatting van de waarschijnlijkheid op obstructief coronairlijden, de zogenaamde "pre-test probability" (PTP). Na deze klinische inschatting wordt een non-invasieve beeldvormende techniek zoals CCTA aanbevolen. **Hoofdstuk 2** had als doel het onderzoeken in welke mate CCTA tot reclassificatie van patiënten leidt en welke impact CCTA resultaten hebben op de behandeling van patiënten met een lage tot intermediaire PTP. In een klinisch cohort van 1560 patiënten, leidde CCTA tot reclassificatie in de meerderheid van de patiënten. Daarnaast traden medicatie veranderingen (aspirine en/of statine) op in 41% van de patiënten. Tot slot toonde het onderzoek dat de Duke Clinical Score, een score die vaak gebruikt wordt voor het definiëren van de PTP, de waarschijnlijkheid op obstructief coronairlijden overschat in vergelijking met de CCTA bevindingen.

De diagnostische waarde van de visuele beoordeling van stenose graad middels CCTA is erg hoog, met een uitstekende sensitiviteit en negatief voorspellende waarde. De specificiteit voor het vaststellen van hemodynamisch obstructief coronairlijden is echter relatief laag. Om de specificiteit van CCTA te verhogen is het gebruik van verschillende functionele CCTA parameters voorgesteld. Een van deze parameters is de transluminale attenuatie gradient (TAG), een CTA-gederiveerde maat van de intracoronaire luminale attenuatie in het beloop van het vat. In **hoofdstuk 3** werd de

diagnostische waarde van de TAG en de TAG met gecorrigeerde contrast opacificatie (TAG-CCO) voor de identificatie van ischemie, gedefinieerd door zowel de invasieve referentie standaard FFR als de non-invasieve referentie standaard [^{15}O]H_2O PET perfusie, onderzocht. Daarnaast werd onderzocht welke invloed de afname in luminale diameter in het beloop van het vat (TDG) had op deze contrast-gebaseerde schattingen van de bloeddoorstroming. De resultaten van de studie tonen dat TAG en TAG-CCO geen toegevoegde diagnostische waarde hadden bovenop CCTA. Aangezien er een significante correlatie was tussen TAG en TDG, kan het ontbreken van diagnostische waarde van de TAG mogelijk verklaard worden door een relatie met verschillen in coronaire luminale diameter.

Naast TAG zijn er verschillende andere CCTA indices waarvan verondersteld wordt dat ze mogelijk de diagnostische waarde van CCTA kunnen vergroten, zoals kwalitatieve en kwantitatieve stenose (visuele beoordeling van stenose graad en minimale luminale oppervlakte, MLA) en plaque maten (plaque karakteristieken en volume), en recentelijk de achterliggende myocardiale massa (V_{sub}). Daarnaast heeft een recente studie het gebruik van de V_{sub}/MLA^2, een wiskundige CCTA index gebaseerd op de wet van Hagen-Poiseuille, voorgesteld voor het vergroten van de diagnostische waarde van CCTA. Naast deze intern verrichte analyses, wordt de extern verrichte analyse van de CT-gederiveerde FFR (FFR_{CT}) genoemd in recente studies als veelbelovend instrument voor de functionele beoordeling van coronaire stenoses. **Hoofdstuk 4** beschrijft de diagnostische waarde van state-of-the-art intern en extern verrichte CCTA analyse voor FFR-gedefinieerd hemodynamisch belangrijk coronairlijden in 132 patiënten van de PACIFIC trial met een ≥30% angiografische stenose. De resultaten tonen dat van de intern verrichte analyses, de MLA, plaque maten en V_{sub} allen onafhankelijke voorspellers waren voor hemodynamisch belangrijk coronairlijden. De toevoeging van de externe analyse van FFR_{CT} aan deze interne analyses leidde tot een significante, echter slechts minimale, verbetering van de diagnostische waarde. Deze resultaten tonen dat de state-of-the-art intern verrichte CT analyse een redelijk alternatief is voor FFR_{CT}.

De HEART-score is een recent ontwikkelde risico score die gebruikt wordt voor risico-stratificatie bij patiënten die zich presenteren op de eerste hulp met pijn op de borst. In **hoofdstuk 5** onderzochten we de waarde van een lage HEART score voor

het voorspellen van de aanwezigheid van coronairlijden zoals gezien op CCTA en het optreden van op ernstige cardiale events (MACE). In een cohort van 713 patiënten die zich presenteerden op de eerste hulp en aansluitend een CCTA ondergingen, bleek een lage HEART score een significante voorspeller voor het uitblijven van MACE. Er werd echter geen verschil gevonden in CCTA-gedefinieerd coronairlijden tussen patiënten met een laag of intermediare/hoge HEART score en de HEART score bleek slecht te zijn in het identificeren van obstructief coronairlijden. De resultaten van deze studie laten zien dat de HEART score niet goed kan identificeren welke patiënten obstructief coronairlijden hebben, ondanks het feit dat de HEART score het optreden van MACE wel goed kan voorspellen. Het excluderen van patiënten voor aanvullend onderzoek op basis van de HEART-score kan daarom leiden tot suboptimale behandeling van patiënten.

Risico-inschatting is een cruciaal onderdeel van de behandeling van patiënten met mogelijk coronairlijden. De traditionele risicostratificatie modellen die algemeen beschikbare klinische risicofactoren en plasma lipiden spiegels gebruiken hebben echter slechts matige voorspellende waarde voor de aanwezigheid van coronairlijden en voor het optreden van cardiale events. Recente technologische ontwikkelingen hebben ervoor gezorgd dat grote hoeveelheden eiwitten bepaald kunnen worden met slechts een microliter plasma. Deze ontwikkelingen hebben de deur geopend voor het gebruik van proteomica in grote klinische populaties. **Hoofdstuk 6** beschrijft de resultaten van een onderzoek naar de voorspellende waarde van proteomica (332 eiwitten) voor coronaire plaque morfologie in 203 patiënten uit de PACIFIC trial met beschikbare CCTA beelden en plasma monsters. Middels machine learning modelering identificeerde wij twee complementaire eiwit sets: een voor de identificatie van patiënten met hoog-risico plaques en een voor de identificatie van patiënten met afwezigheid van coronairlijden. Beide eiwit sets waren superieur ten opzichte van algemeen beschikbare klinische karakteristieken en conventionele biomarkers voor het voorspellen van de aanwezigheid van high-risico plaques of de afwezigheid van coronaire atherosclerose. Deze veelbelovende bevindingen vragen om externe validatie van de waarde van proteomica voor het identificeren van cardiovasculair risico in studies met cardiovasculaire events als uitkomstmaat.

In **hoofdstuk 7** werd de toegevoegde prognostische waarde van de coronairarterie

calcium score (CACS) en CCTA onderzocht in een single-center cohort van 1551 patiënten met de verdenking op coronairlijden en een lage tot intermediaire PTP. De resultaten van het onderzoek tonen dat zowel CACS als CCTA onafhankelijke voorspellende waarde hebben voor het optreden van MACE. Daarnaast toonde de CCTA toch obstructief coronairlijden bij een niet-verwaarloosbaar gedeelte van de patiënten met een CACS van nul. CCTA kan gebruikt worden in deze patiënten om het risico op MACE in te schatten. De relatief lage stralingsdosis en de uitstekende prognostische waarde in onze studie ondersteunen het gebruik van een initiële CCTA strategie bij patiënten met een laag tot matige PTP voor obstructief coronairlijden.

Coronaire inflammatie kan in beeld gebracht worden middels CCTA door het meten van de pericoronaire vet CT-attenuatie (PCATa), welke door verschillende studies wordt gezien als prognostische biomarker. **Hoofdstuk 8** onderzoekt de prognostische waarde van PCATa bovenop CCTA-afgeleide atherosclerose parameters en PET-afgeleide ischemie in een retrospectief cohort van 539 patiënten met mogelijk coronairlijden. De resultaten van het onderzoek tonen dat PCATa van de RCA een onafhankelijke voorspeller was voor het optreden van overlijden of myocard infarct in aanvulling op klinische karaketeristieken, CT-afgeleide stenose en plaque maten en PET-afgeleide ischemie. Hoewel deze bevindingen veelbelovend zijn, dienen ze extern gevalideerd te worden in grote prospectieve studies.

Naast het gebruik van CCTA in het diagnostische traject van patiënten met mogelijk coronairlijden, hebben sommige onderzoekers gesuggereerd dat CCTA ook gebruikt kan worden voor het plannen van PCI procedures. Recente technologische ontwikkelingen op het gebied van FFR_{CT} hebben namelijk het simuleren van hyperemische druk veranderingen na het virtueel verwijderen van stenoses mogelijk gemaakt. Met de FFR_{CT} planner tool wordt beoogd de hemodynamische effecten van PCI te voorspellen. In **hoofdstuk 9**, werd de nauwkeurigheid van deze FFR_{CT} planner tool voor invasieve FFR metingen onderzocht in een cohort van 56 patiënten met FFR metingen voor en na PCI. FFR_{CT} planner waarden toonden een significante overeenkomst met post-PCI FFR waarden en met veranderingen in FFR waarden na PCI. Deze resultaten tonen aan dat de FFR_{CT} planner tool een veelbelovende techniek is voor de non-invasieve voorspelling van de hemodynamische effecten van PCI en voor het plannen van een PCI procedure.

Deel II Positron Emissie Tomografie

In tegenstelling tot anatomische beeldvorming middels CCTA, is PET perfusie beeldvorming een functionele beeldvormende modaliteit die de fysiologische consequenties van coronairlijden meet middels de kwantificatie van de absolute myocardiale perfusie. De hyperemische myocardiale bloeddoorstroming (MBF) en de coronaire flow reserve (CFR) zijn de PET parameters die het meest gebruikt worden in het diagnostische traject van patiënten met een verdenking op coronairlijden. Recentelijk is er echter een aanvullende parameter voorgesteld als een mogelijk specifiekere index voor hemodynamisch significant coronairlijden, genaamd de longitudinale MBF gradiënt. Deze gradiënt wordt gedefinieerd als een geleidelijke afname in hyperemische MBF van de basis naar de apex van de linker ventrikel. **Hoofdstuk 10** beschrijft een onderzoek naar de diagnostische waarde van de PET-gederiveerde longitudinale MBF gradiënt voor de aanwezigheid van hemodynamisch obstructief coronairlijden gedefinieerd door FFR. De resultaten van het onderzoek tonen een lagere diagnostische waarde van de longitudinale flow gradiënt in vergelijking met hyperemische MBF. Daarnaast toont het onderzoek dat de laesie locatie een belangrijke invloed heeft op de correlatie tussen de longitudinale MBF gradiënt en de FFR. De aanwezigheid van een longitudinale MBF gradiënt kan derhalve deels veroorzaakt worden door normalisatie met een relatief normaal geperfundeerd gebied, in plaats van door een specifiek fysiologisch fenomeen.

De kwantificatie van de myocardiale perfusie, zowel middels hyperemische MBF als CFR, kan verricht worden op globaal niveau voor de gehele linker ventrikel of op regionaal niveau voor twee aaneengrenzende segmenten met de laagste MBF per vasculair stroomgebied. **Hoofdstuk 11** beschrijft de resultaten van een retrospectieve cohort studie naar de prognostische waarde van $[^{15}O]H_2O$ PET gederiveerde globale en regionale myocardiale perfusie. Globale en regionale hyperemische MBF en CFR waren allen voorspellend voor het optreden van dood en myocard infarct. Echter, hyperemische MBF was de enige onafhankelijke voorspeller na correctie voor het gecombineerd gebruik van hyperemische MBF en CFR, voor zowel globale als regionale perfusie. Tot slot toonde het onderzoek dat het integreren van globale en regionale perfusie de prognostische waarde niet verhoogde ten opzichte van het apart gebruiken van regionale dan wel globale perfusie. Deze resultaten suggereren dat de

regionale analyses van PET perfusie, zoals gangbaar in de klinische praktijk voor het sturen van behandeling, als redelijk alternatief voor globale perfusie gebruikt kan worden om patiënten te identificeren die verhoogd risico hebben op cardiale events.

Deel III Hybride beeldvorming

Hoofdstuk 12 geeft een gedetailleerd overzicht van de detectie en behandeling van vulnerabele coronaire plaques, te weten plaques met een hoge kans om te ruptureren. Recente ontwikkelingen in invasieve en non-invasieve beeldvormende technieken hebben er toe geleid dat clinici verdachte vulnerabele plaques in vivo kunnen identificeren en hebben de deur geopend voor de evaluatie van therapeutische middelen gericht op het reduceren van plaque vulnerabiliteit. Lokale behandeling van vulnerabele plaques middels PCI en systemische behandeling met anti-inflammatoire en lipide verlagende middelen worden momenteel onderzocht in grote gerandomiseerde klinische onderzoeken om vast te stellen wat de therapeutische effecten voor het reduceren van klinische events is. De resultaten van deze studies kunnen mogelijk leiden tot een meer gepersonaliseerde behandel strategie voor de behandeling van coronairlijden.

Kwantitatieve PET perfusie in coronaire stroomgebieden wordt traditioneel berekend aan de hand van het American Heart Association 17-segmenten model, ondanks de bekende grote variabiliteit in de coronaire anatomie. **Hoofdstuk 13** had als doel te onderzoeken welke impact een geïndividualiseerde segmentatie van myocardiale segmenten middels CCTA heeft op de diagnostische waarde van kwantitatieve [^{15}O]H_2O PET perfusie. In deze substudie van de PACIFIC trial leidde geïndividualiseerde segmentatie middels CCTA-gederiveerde coronaire anatomie tot redistributie van myocardiale segmenten in de meerderheid van de patiënten. Echter, de impact op [^{15}O]H_2O PET MBF waardes was klein en de diagnostische waarde voor het detecteren van hemodynamisch belangrijk coronairlijden veranderde niet. Dit hoofdstuk toont derhalve aan dat er bij klinische PET perfusie beeldvorming geen noodzaak is voor het verrichten van de tijdrovende procedure van het matchen van CCTA-gederiveerde coronaire anatomie en PET perfusie gebieden.

Meerdere grote prospectieve studies hebben de prognostische waarde van zowel CCTA als PET perfusie beeldvorming aangetoond. De onafhankelijk voorspellende

waarde van gecombineerde PET/CT beeldvorming is echter nauwelijks onderzocht. **Hoofdstuk 14** beschrijft de resultaten van een retrospectieve cohort studie naar de prognostische waarde van hybride PET/CT, waarmee een geïntegreerde evaluatie van myocardiale bloed flow, coronaire stenose ernst en atherosclerotische plaque morfologie mogelijk is. PET-afgeleide MBF, CCTA-afgeleide stenose ernst en hoog-risico plaque morfologie waren allen lange termijn voorspellers voor cardiale events. Echter, alleen stenose ernst en hoog-risico plaque morfologie bleken onafhankelijke prognostische waarde te hebben. Desalniettemin suggereren de bevindingen van dit onderzoek dat gecombineerde analyse van de twee beeldvormende technieken kan leiden tot een verbeterde risico stratificatie dan de op zichzelf staande technieken.

Toekomstperspectieven

Non-invasieve beeldvormende technieken hebben een belangrijke plek in het diagnostisch traject van patiënten met de verdenking op coronairlijden. Anatomische beeldvorming met CCTA is de afgelopen decennia uitgegroeid tot een van de meest gebruikte technieken en zowel eerdere studies als studies uit dit proefschrift hebben de uitstekende diagnostische en prognostische waarde van CCTA aangetoond. Daarnaast hebben eerdere studies en studies uit dit proefschrift laten zien dat nieuwe indices, verkregen door post-processing van standaard CCTA data, zoals plaque maten, achterliggende myocardiale massa, FFR_{CT} en pericoronaire vet attenuatie de diagnostische en prognostische waarde van CCTA kunnen verbeteren. Toekomstig onderzoek dient zich dan ook te focussen op het ontwikkelen van een tool die al deze waardevolle CCTA informatie combineert om de patiënt-specifieke kans op hemodynamisch belangrijk coronairlijden en op toekomstige cardiale events te voorspellen. Zulke toepassingen kunnen ervoor zorgen dat de diagnostische en prognostische mogelijkheden van CCTA worden geoptimaliseerd. Aanvullende gerandomiseerde studies naar de prognostische waarde van state-of-the-art CCTA zijn nodig om te onderzoeken wat de plaats is van CCTA in de behandeling van patiënten met verdenking op coronairlijden. Deze inspanningen zullen uiteindelijk de introductie van een ware uitgebreide CCTA analyse in de klinische praktijk faciliteren.

Naast het gebruik van CCTA in het diagnostische traject van patiënten met verdenking op coronairlijden, wordt het gebruik van CCTA recent suggereert voor het plannen

van PCI procedures. Data uit dit proefschrift bevestigt de potentie van CCTA voor het plannen van PCI procedures. Echter, gezien de kleine studie populatie en het feit dat de techniek relatief nieuw is moeten onze resultaten gezien worden als hypothese genererend. Technologische vooruitgang is nodig om de huidige technieken te verbeteren. Uiteindelijk zal de waarde van het CCTA-geleid plannen van PCI procedures met de FFR_{CT} planner bevestigd moeten worden in grote vergelijkende studies. CCTA kan een belangrijke tool worden voor patiënten die een PCI ondergaan door het mogelijk maken van adequate patiënt selectie en adequate procedure planning, het minimaliseren van procedurele complicaties en optimaliseren van het behandel effect.

Kwantitatieve perfusie imaging middels $[^{15}O]H_2O$ PET heeft ook veel aandacht gekregen in de afgelopen decennia. Eerdere studies en studies uit dit proefschrift hebben de uitstekende diagnostische en prognostische waarde van $[^{15}O]H_2O$ PET-gederiveerde absolute myocardiale perfusie kwantificatie aangetoond. In tegenstelling tot de wijdverspreide beschikbaarheid van CCTA, is $[^{15}O]H_2O$ PET beeldvorming helaas nog steeds gelimiteerd tot slechts een paar centra wereldwijd, gezien de korte half waarde tijd van $[^{15}O]H_2O$ en de hierdoor benodigde aanwezigheid van een cyclotron in het ziekenhuis. Daarnaast is FDA-goedkeuring van $[^{15}O]H_2O$ afhankelijk van de resultaten van een momenteel lopende grote internationale multi-center studie. Toekomstige FDA-goedkeuring en de recente ontwikkeling van een kleine cyclotron met daaruit voortvloeiende lagere kosten voor het produceren van $[^{15}O]H_2O$ zullen mogelijk bijdragen aan het wijdverspreid beschikbaar worden van $[^{15}O]H_2O$ PET.

Van hybride beeldvorming middels PET/CT wordt gezegd dat het mogelijk de kracht van beide technieken combineert en de zwaktes van beide technieken verkleint. Hoewel recente studies en een studie uit dit proefschrift de diagnostische waarde van hybride PET/CT imaging in twijfel trekken, laat een ander onderzoek uit dit proefschrift zien dat hybride PET/CT door het combineren van PET-gederiveerde myocardiale bloed flow, CCTA-gederiveerde stenose graad en hoog-risico plaque morfologie tot een verbeterde risico stratificatie kan leiden. Deze veelbelovende bevindingen vragen om een prospectief klinisch onderzoek met interventies gebaseerd op hybride beeldvormingsbevindingen zoals anatomie, functie en morfologie. Hypothetisch zou het combineren van anatomische en functionele informatie van PET/CT leiden tot een verbetering van prognose bij patiënten door het beter inzetten van invasieve coronair

angiografie en dure medicatie en omgekeerd het voorkomen van overbehandeling in patiënten zonder coronairlijden. Prospectieve klinische onderzoeken die deze hypothese testen zullen mogelijk een meer patiënt-specifieke behandeling mogelijk maken.

Curriculum Vitae

Michiel Bom was born on April 6th 1989 in Almelo, the Netherlands. After finishing his pre-university eduction (VWO) at the Pius X College in Almelo, he moved to Groningen to study Medicine at the University of Groningen. During his master thesis and internships at the Deventer Hospital he developed an interest in cardiology. After obtaining his master's degree he started working as a resident at the cardiology department of the Medical Center Alkmaar. During this residency, he was involved in several research projects on the diagnostic and prognostic implications of coronary CT angiography. Afterwards, he started his PhD project at the cardiology department of the VU University Medical Center under supervision of prof. P. Knaapen and prof. A.C. van Rossum, which resulted in this thesis. In December 2019 he started his training to become a cardiologist at the cardiology department of the VU University Medical Center under supervision of dr. G.Veen. Michiel lives together with his girlfriend, Annefleur Koopen, and their son, Boris, in Amsterdam.

List of publications

Included in this thesis

- **Bom MJ***, van Diemen PA*, Driessen RS, Schumacher SP, Everaars H, de Winter RW, van de Ven PM, Freiman M, Goshen L, Heijtel D, Langzam E, Min JK, Leipsic JA, Raijmakers PG, van Rossum AC, Danad I, Knaapen P. Prognostic Value of RCA Pericoronary Adipose Tissue CT-Attenuation Beyond High-Risk Plaques, Plaque Volume, and Ischemia. JACC Cardiovasc Imaging. 2021;14(8):1598-1610.

- **Bom MJ***, Driessen RS*, van Diemen PA, Schumacher SP, Leonora RM, Everaars H, van Rossum AC, Raijmakers PG, van de Ven PM, van Kuijk CC, Lammertsma AA, Knuuti J, Ahmadi A, Min JK, Leipsic JA, Narula J, Danad I, Knaapen P. Incremental prognostic value of hybrid [15O]H2O positron emission tomography-computed tomography: combining myocardial blood flow, coronary stenosis severity, and high-risk plaque morphology. Eur Heart J Cardiovasc Imaging 2020;21:1105-1113.

- **Bom MJ**, Schumacher SP, Driessen RS, van Diemen PA, Everaars H, de Winter RW, van de Ven PM, van Rossum AC, Sprengers RW, Verouden NJW, Nap A, Opolski MP, Leipsic JA, Danad I, Taylor CA, Knaapen P. Non-invasive procedural planning using computed tomography-derived fractional flow reserve. Catheter Cardiovasc Interv 2021;97:614-622.

- **Bom MJ**, Driessen RS, Kurata A, van Diemen PA, Everaars H, Schumacher SP, de Winter RW, van de Ven PM, van Rossum AC, Taylor CA, Min JK, Leipsic JA, Danad I, Knaapen P. Diagnostic value of comprehensive on-site and off-site coronary CT angiography for identifying hemodynamically obstructive coronary artery disease. J Cardiovasc Comput Tomogr 2021;15:37-45

- **Bom MJ**, van Diemen PA, Driessen RS, Everaars H, Schumacher SP, Wijmenga JT, Raijmakers PG, van de Ven PM, Lammertsma AA, van Rossum AC, Knuuti J, Danad I, Knaapen P. Prognostic value of [15O]H2O positron emission tomography-derived global and regional myocardial perfusion. Eur Heart J

Cardiovasc Imaging 2020;21:777-786.

- **Bom MJ**, Schumacher SP, Driessen RS, Raijmakers PG, Everaars H, van Diemen PA, Lammertsma AA, van de Ven PM, van Rossum AC, Knuuti J, Maki M, Danad I, Knaapen P. Impact of individualized segmentation on diagnostic performance of quantitative positron emission tomography for haemodynamically significant coronary artery disease. Eur Heart J Cardiovasc Imaging 2019;20:525-532.

- **Bom MJ**, Driessen RS, Raijmakers PG, Everaars H, Lammertsma AA, van Rossum AC, van Royen N, Knuuti J, Maki M, Danad I, Knaapen P. Diagnostic value of longitudinal flow gradient for the presence of haemodynamically significant coronary artery disease. Eur Heart J Cardiovasc Imaging 2019;20:21-30.

- **Bom MJ**, Levin E, Driessen RS, Danad I, Van Kuijk CC, van Rossum AC, Narula J, Min JK, Leipsic JA, Belo Pereira JP, Taylor CA, Nieuwdorp M, Raijmakers PG, Koenig W, Groen AK, Stroes ESG, Knaapen P. Predictive value of targeted proteomics for coronary plaque morphology in patients with suspected coronary artery disease. EBioMedicine 2019;39:109-117.

- **Bom MJ**, Driessen RS, Stuijfzand WJ, Raijmakers PG, Van Kuijk CC, Lammertsma AA, van Rossum AC, van Royen N, Knuuti J, Maki M, Nieman K, Min JK, Leipsic JA, Danad I, Knaapen P. Diagnostic Value of Transluminal Attenuation Gradient for the Presence of Ischemia as Defined by Fractional Flow Reserve and Quantitative Positron Emission Tomography. JACC Cardiovasc Imaging 2019;12:323-333.

- **Bom MJ**, van der Heijden DJ, Kedhi E, van der Heyden J, Meuwissen M, Knaapen P, Timmer SAJ, van Royen N. Early Detection and Treatment of the Vulnerable Coronary Plaque: Can We Prevent Acute Coronary Syndromes? Circ Cardiovasc Imaging 2017;10.

- **Bom MJ***, Kolff AQ*, Knol RJ, van de Zant FM, van der Zee PM, Cornel JH. Discriminative Power of the HEART Score for Obstructive Coronary Artery Disease in Acute Chest Pain Patients Referred for CCTA. Crit Pathw Cardiol

2016;15:6-10.

- **Bom MJ**, Van der Zee PM, Van der Zant FM, Knol RJ, Cornel JH. Independent prognostic value of coronary artery calcium score and coronary computed tomography angiography in an outpatient cohort of low to intermediate risk chest pain patients. Neth Heart J 2016;24:332-42.

- **Bom MJ**, van der Zee PM, Cornel JH. Anatomical versus Functional Testing for Coronary Artery Disease. N Engl J Med 2015;373:89.

- **Bom MJ**, van der Zee PM, Cornel JH, van der Zant FM, Knol RJ. Diagnostic and Therapeutic Usefulness of Coronary Computed Tomography Angiography in Out-Clinic Patients Referred for Chest Pain. Am J Cardiol 2015;116:30-6.

* Both authors contributed equally

Other publications

- van Diemen PA, de Winter RW, Schumacher SP, **Bom MJ**, Driessen RS, Everaars H, Jukema RA, Somsen YB, Popelkova L, van de Ven PM, van Rossum AC, van de Hoef TP, de Haan S, Marques KM, Lemkes JS, Appelman Y, Nap A, Verouden NJ, Opolski MP, Danad I, Knaapen P. Residual Quantitative Flow Ratio to Estimate Post-Percutaneous Coronary Intervention Fractional Flow Reserve. J Interv Cardiol. 2021;2021:4339451.

- Everaars H, Schumacher SP, Stuijfzand WJ, van Basten Batenburg M, Huynh J, van Diemen PA, **Bom MJ**, de Winter RW, van de Ven PM, van Loon RB, van Rossum AC, Opolski MP, Nap A, Knaapen P. Functional recovery after percutaneous revascularization of coronary chronic total occlusions: insights from cardiac magnetic resonance tissue tracking. Int J Cardiovasc Imaging 2021;37:3057-3068

- Schumacher SP, Everaars H, Stuijfzand WJ, van Diemen PA, Driessen RS, **Bom MJ**, de Winter RW, Somsen YBO, Huynh JW, van Loon RB, van de Ven PM, van Rossum AC, Opolski MP, Nap A, Knaapen P. Viability and functional recovery after chronic total occlusion percutaneous coronary intervention. Catheter

Cardiovasc Interv 2021; Online ahead of print

- Schumacher SP, Stuijfzand WJ, de Winter RW, van Diemen PA, **Bom MJ**, Everaars H, Driessen RS, Kamperman L, Kockx M, Hagen BSH, Raijmakers PG, van de Ven PM, van Rossum AC, Opolski MP, Nap A, Knaapen P. Ischemic Burden Reduction and Long-Term Clinical Outcomes After Chronic Total Occlusion Percutaneous Coronary Intervention. JACC Cardiovasc Interv 2021;14:1407-1418

- Reeskamp LF, Nurmohamed NS, Bom MJ, Planken RN, Driessen RS, van Diemen PA, Luirink IK, Groothoff JW, Kuipers IM, Knaapen P, Stroes ESG, Wiegman A, Hovingh GK. Marked plaque regression in homozygous familial hypercholesterolemia. Atherosclerosis 2021;327:13-17

- Everaars H, van Diemen PA, Biesbroek PS, Hopman LHGA, **Bom MJ**, Schumacher SP, de Winter RW, van de Ven PM, Raijmakers PG, Lammertsma AA, Hofman MBM, Nijveldt R, Götte MJ, van Rossum AC, Danad I, Driessen RS, Knaapen P. Comparison between cardiac magnetic resonance stress T1 mapping and [15O]H2O positron emission tomography in patients with suspected obstructive coronary artery disease. Eur Heart J Cardiovasc Imaging 2021; Online ahead of print

- de Winter RW, Schumacher SP, Stuijfzand WJ, van Diemen PA, Everaars H, **Bom MJ**, van Rossum AC, van de Ven PM, Appelman Y, Lemkes JS, Verouden NJ, Nap A, Raijmakers PG, Knaapen P. Evolution of coronary artery calcium and absolute myocardial perfusion after percutaneous revascularization: A 3-year serial hybrid [15 O]H 2 O PET/CT imaging study. Atherosclerosis. 2021;318:22-31

- Mol JQ, **Bom MJ**, Damman P, Knaapen P, van Royen N. Pre-Emptive OCT-Guided Angioplasty of Vulnerable Intermediate Coronary Lesions: Results from the Prematurely Halted PECTUS-Trial J Interv Cardiol 2020:8821525.

- van Diemen PA, Wijmenga JT, Driessen RS, **Bom MJ**, Schumacher SP, Stuijfzand WJ, Everaars H, de Winter RW, Raijmakers PG, van de Ven PM, van Rossum

AC, Danad I, Knaapen P. Defining the prognostic value of [15O]H2O positron emission tomography-derived myocardial ischaemic burden. Eur Heart J Cardiovasc Imaging 2020;21:1105-1113.

- Opolski MP, Schumacher SP, Verouden NJW, van Diemen PA, Borucki BA, Sprengers R, Everaars H, de Winter RW, van Rossum AC, Nap A, **Bom MJ**, Knaapen P. On-Site Computed Tomography Versus Angiography Alone to Guide Coronary Stent Implantation: A Prospective Randomized Study. J Invasive Cardiol 2020;32:E268-E276.

- Stuijfzand WJ, van Rosendael AR, Lin FY, Chang HJ, van den Hoogen IJ, Gianni U, Choi JH, Doh JH, Her AY, Koo BK, Nam CW, Park HB, Shin SH, Cole J, Gimelli A, Khan MA, Lu B, Gao Y, Nabi F, Nakazato R, Schoepf UJ, Driessen RS, **Bom MJ**, Thompson R, Jang JJ, Ridner M, Rowan C, Avelar E, Genereux P, Knaapen P, de Waard GA, Pontone G, Andreini D, Al-Mallah MH, Lu Y, Berman DS, Narula J, Min JK, Bax JJ, Shaw LJ, Investigators C. Stress Myocardial Perfusion Imaging vs Coronary Computed Tomographic Angiography for Diagnosis of Invasive Vessel-Specific Coronary Physiology: Predictive Modeling Results From the Computed Tomographic Evaluation of Atherosclerotic Determinants of Myocardial Ischemia (CREDENCE) Trial. JAMA Cardiol 2020;5(12):1338-1348

- Hoogeveen RM, Pereira JPB, Nurmohamed NS, Zampoleri V, **Bom MJ**, Baragetti A, Boekholdt SM, Knaapen P, Khaw KT, Wareham NJ, Groen AK, Catapano AL, Koenig W, Levin E, Stroes ESG. Improved cardiovascular risk prediction using targeted plasma proteomics in primary prevention. Eur Heart J 2020;41:3998-4007.

- van Diemen PA, Schumacher SP, Driessen RS, **Bom MJ**, Stuijfzand WJ, Everaars H, de Winter RW, Raijmakers PG, van Rossum AC, Hirsch A, Danad I, Knaapen P. Coronary computed tomography angiography and [(15)O]H2O positron emission tomography perfusion imaging for the assessment of coronary artery disease. Neth Heart J 2020;28:57-65.

- van Diemen PA, Driessen RS, Kooistra RA, Stuijfzand WJ, Raijmakers PG,

Boellaard R, Schumacher SP, **Bom MJ**, Everaars H, de Winter RW, van de Ven PM, Reiber JH, Min JK, Leipsic JA, Knuuti J, Underwood RS, van Rossum AC, Danad I, Knaapen P. Comparison Between the Performance of Quantitative Flow Ratio and Perfusion Imaging for Diagnosing Myocardial Ischemia. JACC Cardiovasc Imaging 2020.

- Schumacher SP, Everaars H, Stuijfzand WJ, Huynh JW, van Diemen PA, **Bom MJ**, de Winter RW, van Loon RB, van de Ven PM, van Rossum AC, Opolski MP, Nap A, Knaapen P. Coronary collaterals and myocardial viability in patients with chronic total occlusions. EuroIntervention 2020;16:e453-e461.

- Everaars H, van Diemen PA, **Bom MJ**, Schumacher SP, de Winter RW, van de Ven PM, Raijmakers PG, Lammertsma AA, Hofman MBM, van der Geest RJ, Gotte MJ, van Rossum AC, Nijveldt R, Danad I, Driessen RS, Knaapen P. Comparison between quantitative cardiac magnetic resonance perfusion imaging and [(15)O]H2O positron emission tomography. Eur J Nucl Med Mol Imaging 2020;47:1688-1697.

- Bruikman CS, Vreeken D, Hoogeveen RM, **Bom MJ**, Danad I, Pinto-Sietsma SJ, van Zonneveld AJ, Knaapen P, Hovingh GK, Stroes ESG, van Gils JM. Netrin-1 and the Grade of Atherosclerosis Are Inversely Correlated in Humans. Arterioscler Thromb Vasc Biol 2020;40:462-472.

- van Diemen PA, Driessen RS, Stuijfzand WJ, Raijmakers PG, Schumacher SP, **Bom MJ**, Everaars H, Min JK, Leipsic JA, Knuuti J, Underwood SR, van de Ven PM, van Rossum AC, Danad I, Knaapen P. Data on the impact of scan quality on the diagnostic performance of CCTA, SPECT, and PET for diagnosing myocardial ischemia defined by fractional flow reserve on a per vessel level. Data Brief 2019;27:104584.

- Schumacher SP, Stuijfzand WJ, Driessen RS, van Diemen PA, **Bom MJ**, Everaars H, Kockx M, Raijmakers PG, Boellaard R, van de Ven PM, van Rossum AC, Opolski MP, Nap A, Knaapen P. Impact of Specific Crossing Techniques in Chronic Total Occlusion Percutaneous Coronary Intervention on Recovery of Absolute Myocardial Perfusion. Circ Cardiovasc Interv 2019;12:e008064.

- Schumacher SP, Kockx M, Stuijfzand WJ, Driessen RS, van Diemen PA, **Bom MJ**, Everaars H, Raijmakers PG, Boellaard R, van Rossum AC, Opolski MP, Nap A, Knaapen P. Ischaemic burden and changes in absolute myocardial perfusion after chronic total occlusion percutaneous coronary intervention. EuroIntervention 2020;16:e462-e471.

- Driessen RS, de Waard GA, Stuijfzand WJ, Raijmakers PG, Danad I, **Bom MJ**, Min JK, Leipsic JA, Ahmadi A, van de Ven PM, Knuuti J, van Rossum AC, Davies JE, van Royen N, Narula J, Knaapen P. Adverse Plaque Characteristics Relate More Strongly With Hyperemic Fractional Flow Reserve and Instantaneous Wave-Free Ratio Than With Resting Instantaneous Wave-Free Ratio. JACC Cardiovasc Imaging 2019.

- Everaars H, de Waard GA, Schumacher SP, Zimmermann FM, **Bom MJ**, van de Ven PM, Raijmakers PG, Lammertsma AA, Gotte MJ, van Rossum AC, Kurata A, Marques KMJ, Pijls NHJ, van Royen N, Knaapen P. Continuous thermodilution to assess absolute flow and microvascular resistance: validation in humans using [15O]H2O positron emission tomography. Eur Heart J 2019;40:2350-2359.

- van Diemen PA, Schumacher SP, **Bom MJ**, Driessen RS, Everaars H, Stuijfzand WJ, Raijmakers PG, van de Ven PM, Min JK, Leipsic JA, Knuuti J, Boellaard PR, Taylor CA, van Rossum AC, Danad I, Knaapen P. The association of coronary lumen volume to left ventricle mass ratio with myocardial blood flow and fractional flow reserve. J Cardiovasc Comput Tomogr 2019.

- van Diemen PA, Driessen RS, Stuijfzand WJ, Raijmakers PG, Schumacher SP, **Bom MJ**, Everaars H, Min JK, Leipsic JA, Knuuti J, Underwood SR, van de Ven PM, van Rossum AC, Danad I, Knaapen P. Impact of scan quality on the diagnostic performance of CCTA, SPECT, and PET for diagnosing myocardial ischemia defined by fractional flow reserve. J Cardiovasc Comput Tomogr 2019.

- Demirkiran A, Everaars H, Amier RP, Beijnink C, **Bom MJ**, Gotte MJW, van Loon RB, Selder JL, van Rossum AC, Nijveldt R. Cardiovascular magnetic resonance techniques for tissue characterization after acute myocardial injury. Eur Heart J Cardiovasc Imaging 2019;20:723-734.

- IJsselmuiden AJJ, Zwaan EM, Oemrawsingh RM, **Bom MJ**, Dankers F, de Boer MJ, Camaro C, van Geuns RJM, Daemen J, van der Heijden DJ, Jukema JW, Kraaijeveld AO, Meuwissen M, Scholzel BE, Pundziute G, van der Harst P, van Ramshorst J, Dirksen MT, Zivelonghi C, Agostoni P, van der Heyden JAS, Wykrzykowska JJ, Scholte MJ, Nef HM, Kofflard MJM, van Royen N, Alings M, Kedhi E. Appropriate use criteria for optical coherence tomography guidance in percutaneous coronary interventions : Recommendations of the working group of interventional cardiology of the Netherlands Society of Cardiology. Neth Heart J 2018;26:473-483.

- **Bom MJ**, Manders JM, Uijlings R, Badings EA, Martens FM. Negative predictive value of SPECT for the occurrence of MACE in a medium-sized clinic in the Netherlands. Neth Heart J 2014;22:151-7.

* Both authors contributed equally

Dankwoord

Dit proefschrift was er nooit geweest zonder de hulp van velen. Allereerst wil ik alle patiënten bedanken die deel hebben genomen aan de verschillende studies in dit proefschrift. Daarnaast wil ik mijn dank uitspreken naar de vele collega's, vrienden en familie die mij hebben geholpen tijdens mijn promotie onderzoek en daarmee een groot aandeel hebben gehad in de totstandkoming van dit proefschrift.

Prof. dr. P. Knaapen: Beste Paul, ik wil je bedanken voor het feit dat je mij onder je hoede hebt genomen toen de PECTUS on-hold werd gezet. Hoewel we elkaar niet goed kenden gaf je mij de kans onderdeel te worden van jouw onderzoeksgroep. De ruimte en het vertrouwen dat je mij hebt gegeven stel ik zeer op prijs. Je kritische en scherpe blik evenals je eerlijke en directe manier van communiceren ("John Wick style!") hebben me veel geleerd. Ondanks het feit dat je vaker in Japan, Finland of Polen bent dan in de VU, was je altijd bereikbaar wanneer ik je nodig had. Ik denk dat we beiden trots kunnen zijn op de artikelen die we in de laatste 2.5 jaar van mijn promotie tijd samen hebben afgeleverd.

Prof. dr. A.C. van Rossum: Beste Bert, als afdelingshoofd ben jij verantwoordelijk voor de uitstekende sfeer op de afdeling cardiologie. Ook in rumoerige tijden heb je laten zien er te zijn voor alle onderzoekers en heb je de rust weten te bewaren. Ik wil je hartelijk bedanken voor jouw ondersteuning in de afhandeling van de PECTUS studie en de daaruit voortvloeiende zaken. In deze periode heb ik ervaren dat de afdeling staat voor zijn mensen en hier heb jij een groot aandeel in.

Dr. I. Danad: Beste Ibrahim, ik ben je veel dank verschuldigd voor het opzetten en uitvoeren van de PACIFIC trial. Zonder deze prachtig opgezette studie had het grootste gedeelte van dit proefschrift niet geschreven kunnen worden. Je bent een wetenschappelijk genie en het is een kwestie van tijd tot we je met professor Danad moeten aanspreken.

Graag wil ik alle leden van de beoordelingscommissie, prof. dr. S.A.J. Chamuleau, prof. dr. J. Knuuti, prof. N. van Royen, prof. J.W. Jukema, prof. dr. C. van Kuijk en dr. P.G.H.M. Raijmakers bedanken voor hun bereidheid dit proefschrift te lezen en te beoordelen.

Daarnaast wil ik in het bijzonder prof. dr. N. van Royen bedanken. Beste Niels, bedankt voor de begeleiding gedurende de eerste helft van mijn promotie onderzoek. Helaas voor mij kreeg jij een fantastische kans in Nijmegen om afdelingshoofd te worden in het Radboud UMC. Je hebt mij de kneepjes van het onderzoeksvak geleerd en hiervoor wil ik je hartelijk bedanken.

Ik wil mijn dank uitspreken aan alle stafleden van de vakgroep cardiologie in het VUmc voor de prettige werksfeer op de afdeling en voor hun hulp bij het verrichten van de vele studiehandelingen. In het bijzonder wil ik de interventie cardiologen, Maarten van Leeuwen, Yolande Appelman, Koen Marques, Jorrit Lemkes, Alexander Nap, Niels Verouden en de (voormalig) interventie fellows Stefan de Haan en Dirk van der Heijden bedanken voor het verrichten van talloze metingen bij studie patiënten op het cathlab. Dirk, jouw hulp met de PECTUS studie was fantastisch. Helaas kreeg je halverwege mijn promotie traject een top baan in Den Haag. Ik wens je alle geluk in je verdere carrière. Niels en Alex, ik weet dat jullie soms moe werden van al die metingen in de AR-PCI studie en vurig hoopten op een angio-guided strategy in plaats van naar ons te luisteren met een bril op jullie hoofd, maar zonder jullie was dit project nooit van de grond gekomen! Ik wil ook alle cathlab verpleegkundigen bedanken voor hun hulp bij het verrichten van de vele metingen voor de PACIFIC, de PECTUS en de AR-PCI studie. De research verpleegkundigen, Ellen, Debby, Iris, Yvonne, Britt en Hanneke, mogen uiteraard niet ontbreken in dit dankwoord. Bedankt voor jullie ondersteuning bij alle projecten.

Beste Stefan Timmer, door jou ben ik terecht gekomen in de VU. Door een goed woordje voor mij te doen bij Niels, heb je ervoor gezorgd dat ik aangenomen werd op het project dat jij zelf hebt opgezet. Ik wil je heel erg bedanken voor je hulp tijdens mijn begintijd als onderzoeker. Zowel wetenschappelijk als persoonlijk heb je me fantastisch begeleid en geholpen. Helaas was onze samenwerking door omstandigheden van korte duur. Ik wens je alle geluk in het leven en heel veel succes in je verdere (waarschijnlijk briljante) carrière.

Het begin van mijn wetenschappelijke carrière heb ik te danken aan de maatschap cardiologie in het Deventer Ziekenhuis en in het bijzonder Fabrice Martens. Beste Fabrice, bedankt dat je mij als student onder je hoede nam en kennis hebt laten maken

met de cardiologie. Mede door jouw enthousiasme voor het vak ben ik verder gegaan met onderzoek binnen de cardiologie.

Het eerste gedeelte van dit proefschrift is tot stand gekomen tijdens mijn tijd in het Medisch Centrum Alkmaar (nu Noord West Ziekenhuisgroep, NWZ). Hiervoor ben ik de maatschap cardiologie en de afdeling nucleaire geneeskunde in het NWZ dank verschuldigd. In het bijzonder wil ik Jan-Hein Cornel, Mark van der Zee, Friso van der Zant en Remco Knol bedanken voor het feit dat jullie mij als ANIOS zonder noemenswaardige wetenschappelijke ervaring de kans hebben gegeven om te werken met jullie fantastische dataset. Ik heb heel veel geleerd tijdens mijn tijd in Alkmaar en mede dankzij jullie is dit proefschrift tot stand gekomen.

Ik wil graag de betrokkenen van de afdeling radiologie en nucleaire geneeskunde bedanken voor hun bijdrage aan dit proefschrift. In het bijzonder Lilian Meijboom, Ralf Sprengers, Pieter Raijmakers en Adriaan Lammertsma. Beste Lilian, bedankt voor je tijd en energie tijdens de talloze scans die we samen voor PECTUS studie hebben doorgespit op zoek naar vulnerable plaques. Beste Ralf, bedankt voor de ondersteuning bij de AR-PCI studie en het opzetten van de PROCTOR trial en de VALIDATE-HRP. Beste Pieter en Adriaan, mijn dank gaat uit naar jullie voor het opzetten en uitvoeren van de PACIFIC trial, zonder dit belangrijke werk had dit proefschrift niet tot stand kunnen komen.

Zonder de vele nationale en internationale samenwerkingsverbanden was dit proefschrift er niet geweest. Beste Erik Stroes, toen we contact met je opnamen over de biomarkers van de PACIFIC trial hadden we geen idee waar we het over hadden. Gelukkig voor ons wist jij samen met Evgeni Levin en Bert Groen precies welke kant we op moesten om dit project tot een succes te maken. Jouw enthousiasme en knowhow hebben mij enorm geholpen. Heel erg bedankt voor al je hulp. Ik kijk uit naar alle nieuwe projecten die we samen gaan verrichten. Dear Maksimylian Opolski, the AR-glasses guy, thank you for letting me be part of the AR-PCI trial and for being such a great mentor in coronary CT angiography guided revascularization. Despite some minor setbacks in the medical ethics review process (hence the nickname, Maks "Bad news again" Opolski), our collaboration went very smoothly. I sincerely hope we can continue to work together on shared projects in the future. Dear Akira Kurata, thank

you for your assistance in the subtended myocardial mass analyses. We could not have performed this interesting sub study without your help. I would also like to thank Charley Taylor and Campbell Rodgers for the opportunity to work with the HeartFlow FFR_{CT} and FFR_{CT} planner technology. Hopefully we can continue our collaboration in the future.

Grote dank gaat natuurlijk uit naar alle arts-onderzoekers van de afdeling cardiologie in de VU. Hoe zou ik het ooit volgehouden hebben zonder jullie? Vanaf de eerste dag dat ik begon als arts-onderzoeker heb ik me helemaal op mijn plek gevoeld in deze fijne groep. De vrijdagmiddag borrels in de Basket, de wintersport, onderzoekersuitjes, bruiloften, kerstdiners, junior kamerdagen, afscheidsdiners en prachtige congressen maakten mijn promotie tijd tot een groot feest. Allereerst wil ik natuurlijk mijn kamergenoten, Henk, Maurits, Guus, Nina, Ahmet en Pien, bedanken. Vanaf het begin was het feest op de kamer, waar iedereen elkaar in de zeik nam en niemand werd gespaard. Onder het genot van een kop vers gemalen koffie uit de onvolprezen Saeco machine met profi cappuccinatore (Maurits wist hier uiteraard alles van), hebben we heel wat afgelachen. Ik heb ontzettend veel van jullie geleerd en als ik jullie nodig had waren jullie er voor me. Hiervoor heel veel dank. Ik ben er van overtuigd dat jullie allemaal prachtige carrières in het vooruitzicht hebben! Ik wil ook de boys van de Knaapen groep apart noemen: Schumi, Pep, Roel, Wynand, Henk en Ruben. Naast de relaxte sfeer en de eindeloze gesprekken over voetbal en andere belangrijke onbelangrijke zaken onder het genot van een biertje, hebben jullie een groot aandeel gehad in al mijn papers. De vele brainstorm sessies over non-invasieve imaging en coronaire fysiologie hebben me vele nieuwe inzichten gegeven ("60% of the time, it works everytime"). Schumi, we waren een top team in het opzetten van de PROCTOR, het organiseren van de wintersport en het uitvoeren van de AR-PCI trial! Uiteraard verdienen ook Roel en Ibrahim een speciale vermelding: door jullie harde werk hebben we allemaal kunnen profiteren van de PACIFIC data. Hiervoor heel veel dank! Ook de andere arts-onderzoekers wil ik van harte bedanken: Alwin, Raquel, Stefan Biesbroek, Rahana, Paul, Monique, Gladys, Anne-Lotte, Marthe, Arno, Mark, Klaske, Amaya, Luuk en Nick. Bedankt voor de mooie tijd en heel veel succes met jullie promotie en verdere carrière!

Mijn vrienden mogen ook niet ontbreken in dit dankwoord. De boys van DEVO '58

zaterdag 2 en in het bijzonder Wessel, Tom Meijer, Tom Kelder, Evert, Niels, Philip, Khalid, Paul en Lars wil ik graag bedanken. Als ik even helemaal klaar was met mijn onderzoek kon ik altijd bij jullie terecht om van de mooie dingen in het leven te genieten, zoals de derde helft op Devonello, festivals, avonden in de Treffers, oud en nieuw huisfeestjes, bruiloften, wintersport en wielertripjes. Thanks! Ook de jongens van PKC uit Groningen, de "Drinken app" (Jelle, Thijs, Bram, Nick, Wouter, Maarten en Ruben), verdienen een eervolle vermelding. Ik vind het te gek dat we elkaar na al die tijd nog zoveel zien, al ben ik er weleens niet bij ("Ben je nu alweer op congres?"). Eindeloze discussies over de zin van het leven afgewisseld met slap geouwehoer over precies niets maken de avonden met jullie onvergetelijk. Jullie zijn toppers! Mijn studiemaatjes uit Groningen, Arne de Niet en Erik van Bommel, mogen ook niet ontbreken. Wie had gedacht dat we nog wat van ons leven zouden maken toen we in de Joffer stonden om 3 uur 's nachts.

Paranimfen, Wouter en Henk, prachtig dat jullie tijdens de verdediging naast mijn zijde zullen staan. Wouter, "Eddy" voor intimi, we kennen elkaar al meer dan 14 jaar en hebben mooie dingen meegemaakt: van flaneren over de Karelsbrug in Praag en koersen door Slovenië tot op zondagmiddag rode wijn drinken bij de Coffee and Coconuts en filosoferen over hobbies. Je bent een fantastische vriend. Henk, we hebben van het begin tot het eind van mijn promotie traject samen op een kamer gezeten en lief en leed gedeeld. We zaten samen in de shit, maar zoals Kendrick Lamar ooit heeft gezegd: "We gon' be alright!". We mogen allebei trots zijn dat we er iets moois van hebben gemaakt.

Lieve bonusfamilie, Karen, Michiel, Marlot, Cat en natuurlijk Jesse en Rens, bedankt voor jullie support. Wat hebben we mooie dingen meegemaakt sinds ik samen ben met Fleurtje: weekendjes in de Veluwe, Ardennen en Valencia maar ook top avonden in de kroeg in Amsterdam en op bezoek bij Cat en Rens in Boston. Het blijf niet te bevatten dat we nu nieuwe herinneringen maken zonder Karen, maar gelukkig zijn we er voor elkaar. Ik ben blij dat ik onderdeel van jullie gezin ben.

Lieve pap en mam, bedankt voor jullie liefde. Ik voel me altijd voor de volle 100% gesteund door jullie in alles wat ik doe. Ik heb super veel bewondering voor jullie en hoe jullie ons hebben opgevoed. Het is af en toe niet makkelijk geweest de afgelopen

jaren, maar ik ben trots op hoe jullie je erdoor heen slaan en altijd het positieve van alles blijven zien. Freek en Luuk, broertjes, bedankt voor jullie steun. Hoewel we alle drie totaal verschillend zijn, begrijpen we elkaar heel erg goed. Ik weet dat jullie er altijd voor me zullen zijn.

Tot slot, lieve Fleurtje, wat zou ik zonder jou moeten! De afgelopen jaren zijn fantastisch geweest en dat komt grotendeels door jou. Ik verbaas me nog elke dag over hoe attent, lief, vrolijk en grappig je bent. Toen we elkaar leerden kennen in Alkmaar dacht ik in eerste instantie dat je "out of my league" was en dat denk ik eigenlijk nog steeds. Je bent een doorpakker, mega slim en super scherp. Je kan de hele wereld aan! Tijdens mijn tijd als onderzoeker is er een hoop gebeurd, maar jij was er altijd om me erdoor heen te slepen. Weet dat ik er ook altijd voor jou zal zijn. Ik ben super blij met je en kan niet wachten op de rest van ons leven samen met onze geweldige zoon Boris. Ik hou van je!

Boris, kleine man, wat super fijn dat je er bent!